USZ Universitäts Spital Zürich

22nd Day of Clinical Research

Innovationen in der Interventionellen Medizin

Donnerstag, 25. Mai 2023, 8.15 – 18.00 Uhr
Grosser Hörsaal OST, Universitätsspital Zürich

Verleihung Day of Clinical Research Preis 2023
Georg-Friedrich-Götz-Preisverleihung 2023

Wir wissen weiter.

Committee Day of Clinical Research

Aguzzi Adriano, Prof. Dr.
Cinelli Paolo, PD Dr.
Distler Oliver, Prof. Dr.
Moch Holger, Prof. Dr.
Schneider Robin, MBA
Senti Gabriela, Prof. Dr.
Speck Roberto, Prof. Dr
Van den Broek Maries, Prof. Dr.
von Eckardstein Arnold, Prof. Dr.
Weller Michael, Prof. Dr.
Zinkernagel Annelies, Prof. Dr.

Table of contents

Cover Figure:

Programm

Donnerstag, 25. Mai 2023

Grosser Hörsaal Ost

Live-Übertragung

08.15 **Begrüssung**
Prof. Dr. Gabriela Senti
Direktorin Forschung und Lehre, Universitätsspital Zürich

08.20 **Begrüssung**
Prof. Dr. Maries van den Broek
Vizedekanin Forschung, Medizinische Fakultät der Universität Zürich

08.25 **Einführung und Moderation durch**
Prof. Dr. Gabriela Senti und Chairman PD Dr. Paolo Cinelli

Block 1: Historische Einführung

08.35 **Innovationen in Medizinischen Kulturen: Chancen und Risiken in historischer Perspektive**
Prof. Dr. Flurin Condrau, Zentrum für Medical Humanities, Universität Zürich

Block 2: Roboterunterstützte Chirurgie

08.50 **Roboterunterstützte Thoraxchirurgie**
Prof. Dr. Isabelle Schmitt-Opitz, Klinik für Thoraxchirurgie

09.10 **Roboterunterstütze Chirurgie in Gynäkologie - neue Einsatzgebiete**
Prof. Dr. Isabell Witzel, Klinik für Gynäkologie

09.30 **Roboter-assistierte Mikro- und Supermikrochirurgie (IP)**
Prof. Dr. Nicole Lindenblatt, Klinik für Plastische und Handchirurgie

09.50 **Coffee Break**

Block 3: Minimalinvasive Techniken

10.10 **Minimal-invasive Operationen für das Ungeborene**
Prof. Dr. Nicole Ochsenbein-Kölble, Klinik für Geburtshilfe

10.30 **Innovationen in der Lungenbildgebung: von Röntgen bis KI**
Prof. Dr. Thomas Frauenfelder, Institut für diagnostische und Interventionelle Radiologie

10.50 **Kammertachykardien– über Ursachen, Diagnose und innovative Behandlungsverfahren**
PD Dr. Ardan Saguner, Klinik für Kardiologie

11.10 **Ist die minimalinvasive Herzchirurgie die Zukunft?**
Prof. Dr. Dr. h. c. Omer Dzemali, Klinik für Herzchirurgie

11.30 **Minimal invasive Techniken in der Pneumologie**
Dr. Carolin Steinack, Klinik für Pneumologie

Block 4: «Modern Technologies» Innovationspool Projekte

11.50 **Kathetergestützte mechanische Thrombektomie bei akuter «Hochrisiko-Lungenembolie» – erste Erfahrungen am USZ**
PD Dr. Erik Holy, Klinik für Angeologie

Live-Übertragung

12.00 Clinical proof of concept of innovative surgical planning with more efficient operating room usage through 3D printing and augmented reality technologies
Prof. Dr. Valentin Neuhaus, Klinik für Traumatologie

12.10 Effect of hypoxia on patients with pulmonary vascular diseases
Prof. Dr. Silvia Ulrich, Klinik für Pneumologie

12.30 Lunch / Poster viewing

14.00 Verleihung Day of Clinical Research Preis
Prof. Dr. Gabriela Senti, Direktorin Forschung und Lehre, Universitätsspital Zürich

14.10 Session 1: Cardiovascular/Metabolism/Endocrinology
Effect of alkali therapy on kidney function in kidney transplant recipients with metabolic acidosis (Preserve-Transplant Study)
Dr. Alexander Ritter, Division of Nephrology

14.20 Session 2: Hematology/Oncology
Functional Screening to Unravel Novel Therapeutic Vulnerabilities in Soft Tissue Sarcoma
Yanjiang Chen, Institute of Pathology and Molecular Pathology

14.30 Session 3: Head Region/Neuroscience
SPTLC1 variants associated with ALS produce distinct sphingolipid signatures through impaired interaction with ORMDL proteins
Museer Lone, PhD, Institute for Clinical Chemistry

14.40 Session 4: Infection/Immunity/Inflammation/Systemic Diseases
Increase of infective endocarditis due to viridans Streptococci among patients at moderate risk after change of guidance on antibiotic prophylaxis to prevent infective endocarditis: Results from a tertiary care referral centre in Switzerland
Dr. Jana Epprecht, Department of Infectious Disease and Hospital Epidemiology

14.50 Session 5: Mixed Topics
Endometriosis and Fibrosis: Reduction of deep endometriosis lesions through a novel immunotherapy treatment
Daniel Rodriguez Gutierrez PhD, Department of Reproductive Endocrinology

15.00 Coffee Break / Pause

Verleihung Georg Friedrich Götz-Preis 2023

15.30 Begrüssung der Gäste durch Prof. Dr. Beatrice Beck Schimmer
Direktorin Universitäre Medizin Zürich

15.35 Einführung und Würdigung der Preisträgerin
Prof. Ana Guerreiro Stücklin
durch Prof. Dr. Maries van den Broek, Vizedekanin Forschung, Universität Zürich

15.40 Kurzreferat von Frau Prof. Ana Guerreiro Stücklin
«Hirntumore bei Kleinkindern: Der Weg von der Entdeckung neuer Tumorentitäten zu gezielteren Therapien»
Universitäts-Kinderspital Zürich

15.55 Preisverleihung durch Prof. Dr. Beatrice Beck Schimmer Direktorin Universitäre Medizin Zürich

16.00 Einführung und Würdigung des Preisträgers
Dr. Carlo Cervia durch Prof. Dr. Maries van den Broek, Vizedekanin Forschung, Universität Zürich

16.05 Kurzreferat von Dr. Carlo Cervia

«Klinische und wissenschaftliche Forschung auf dem Gebiet der postinfektiösen immunologischen Erkrankungen»
Klinik für Immunologie, Universitätsspital Zürich

16.20 Preisverleihung durch Prof. Dr. Beatrice Beck Schimmer Direktorin Universitäre Medizin Zürich

16.25 Einführung und Würdigung der Preisträgerin
Dr. Florentia Dimitriou
durch Prof. Dr. Maries van den Broek, Vizedekanin Forschung, Universität Zürich

16.30 Kurzreferat von Dr. Florentia Dimitriou
«Immuntherapie bei fortgeschrittenem mukosalen Melanom»
Dermatologische Klinik, Universitätsspital Zürich

16.45 Preisverleihung durch Prof. Dr. Beatrice Beck Schimmer Direktorin Universitäre Medizin Zürich

17.00 Apéro Götzstiftung

Cardiovascular / Metabolism / Endocrinology

Basic Research

560
IS. Martinez Lopez, T. Papasotiropoulos, F. Schläpfer, S. Ulrich, I. Opitz, MB. Kirschner
MicroRNA expression correlates with clinical presentation of Chronic Thromboembolic Pulmonary Hypertension

566
G. Panteloglou, P. Zanoni, A. Othman, J. Haas, R. Meier, S. Radosavljevic, E. Schlumpf, M. Futema, S. Humphries, W. März, B. Staels, B. van de Sluis, J. Kuivenhoven, J. Robert, A. von Eckardstein
Genome-wide siRNA screen unravels novel potential Familial Hypercholesterolemia (FH) causing genes

567
S. Graf, G. Rathmes, R. Lehmann, C. Cavelti-Weder
Real-World Evidence Supporting The Use Of Advanced Hybrid Closed Loop In Poorly Controlled Type 1 Diabetic Patients

576
A. Majcher, H. Aleš, P. Bjorkund, T. Hornemann
Type 2 diabetes causes an elevation of neurotoxic 1-deoxysphingolipids in skin and plasma: A cause for diabetic neuropathy?

596
A. Joachimbauer, N. Cadosch, C. Gil-Cruz, C. Perez-Shibayama, K. Frischmann, F. Tanner, D. Schmidt, B. Ludewig
Treatment of autoimmune myocarditis-associated heart failure through restoration of bone morphogenic protein signalling

603
A. Mengozzi, S. Costantino, S. Mohammed, E. Gorica, A. Mongelli, E. Duranti, S. Taddei, S. Masi, A. Virdis, F. Paneni
BRD4 inhibition Attenuates obesity-related microvascular dysfunction: role of endothelium and perivascular adipose tissue

607
E. Gorica, S. Mohammed, S. Ambrosini, A. Mengozzi, A. Mongelli, F. Wenzl, F. Ruschitzka, N. Hamdani, S. Costantino, F. Paneni
Pro-inflammatory Macrophage Role in the Heart Failure with Preserved Ejection Fraction

608
S. Tashi, M. Hermann
Real-life data about lipid-lowering therapy in very elderly patients at very high cardiovascular risk

Clinical Trials

500
J. Müller, L. Mayer, S. Schneider, A. Titz, E. Schwarz, S. Saxer, M. Furian, E. Grünig, S. Ulrich, M. Lichtblau
Pulmonary arterial wedge pressure increase during exercise in patients with pulmonary vascular disease

506
E. SAMARA, L. Sazgary, A. Stüssi, M. Guckenberger, A. SAGUNER
Preliminary study on the impact of clinical audits in patient radiation exposure

512
N. Winkler, S. Anwer, P. Rumpf, G. Tsiourantani, TG. Donati, J. Michel, AM. Kasel, FC. Tanner
Left atrial pump strain predicts long-term mortality in patients undergoing transcatheter aortic valve implantation

520
A. Ritter, A. Wiegand, N. Graf, S. Dahdal, D. Sidler, S. Arampatzis, K. Hadaya, T. Müller, C. Wagner, R. Wüthrich, N. Mohebbi
Effect of alkali therapy on kidney function in kidney transplant recipients with metabolic acidosis (Preserve-Transplant Study)

536
R. Fumagalli, A. Fürbringer-Schwarz, F. Catalani, N. Kucher, S. Konstantinides, S. Barco
CAtheter-directed Thrombolysis for Acute PULmonary Thromboembolism (CATAPULT) study: interim analysis of individual patient-level data

546
R. Fumagalli, F. Catalani, A. Fürbringer-Schwarz, I. Farmakis, L. Valerio, K. Christodoulou, K. Keller, L. Hobohm, N. Kucher, S. Konstantinides, S. Barco
Effectiveness and safety of catheter-directed thrombolysis for acute pulmonary embolism:
A systematic review and meta-analysis

561
M. Ahmadsei, J. von Spiczak, B. Kovacs, R. Manka, A. SAGUNER, M. Guckenberger, N. Andratschke, M. Mayinger
Structural cardiac changes detected by MRI after stereotactic body radiotherapy for targets in close proximity to the heart

597
S. Anwer, g. Miriam, AU. Marchetti, NE. Winkler, V. Wilzeck, C. Gruner, FC. Tanner
Left ventricular early diastolic strain rate and cardiovascular outcome in patients with left ventricular non-compaction phenotype

598
S. Anwer, D. Zuercher, DC. Benz, NE. Winkler, TG. Donati, G. Tsiourantani, V. Wilzeck, J. Michel, AM. Kasel, FC. Tanner
Left ventricular early diastolic strain rate predicts mortality after transcatheter aortic valve implantation

Hematology / Oncology

Basic Research

475
J. Buschmann, D. Heuberger, F. Kivrak Pfiffner, P. Wolint, J. Jang, W. Jungraithmayr, P. Giovanoli, M. Calcagni, C. Waschkies
Probing Vasoreactivity and Hypoxic Phenotype in Different Tumor Grafts Grown on the Chorioallantoic Membrane of the Chicken Embryo In Ovo Using MRI

476
D. Heuberger, P. Wolint, J. Jang, S. Itani, W. Jungraithmayr, C. Waschkies, G. Meier Bürgisser, S. Andreoli, K. Spanaus, R. Schuepbach, M. Calcagni, C. Fahrni, J. Buschmann
High-Affinity Cu(I)-Chelator with Potential Anti-Tumorigenic Action – a Proof-of-Principle Experimental Study of Human H460 Tumors in the CAM Assay

477
A. Tastanova, G. Restivo, Z. Balazs, F. Panebianco, M. Diepenbruck, C. Ercan, B. Preca, J. Hafner, W. Weber, C. Beisel, M. Bentires-Alj, M. Krauthammer, M. Levesque
Live slow-frozen human tumor tissues viable for 2D, 3D, ex vivo cultures and single-cell RNAseq

478
E. Topcu, J. Fullin, S. Boettcher
Elucidating the effect of inflammation for clonal expansion of TP-53-mutant clonal hematopoiesis

489
MB. Kirschner, V. Orlowski, F. Schläpfer, I. Opitz, G. Reid
Association of novel microRNAs with diagnosis and histology of malignant pleural mesothelioma

494
L. Heeb, L. Russo, E. Breuer, PA. Clavien, A. Gupta
Perioperative immunotherapy controls tumor growth in the regenerating liver

495
jJ. Hench, D. Mihic-Probst, A. Agaimy, M. Massi, M. Mandala
Comprehensive molecular profiling of dedifferentiated cutaneous melanomas reveals extensive epigenetic reprogramming

497
R. Staeger, A. Tastanova, A. Ghosh, E. Ramelyte, N. Winkelbeiner, V. Haunerdinger, P. Shukla, P. Cheng, P. Turko, I. Kolm-Djamei, MP. Levesque, R. Dummer, B. Meier-Schiesser
Tebentafusp induces activation and proliferation of cytotoxic T cells and downregulation of melanin synthesis in the skin of uveal melanoma patients

504
J. Pfister, T. Stein, S. Shllaku, N. Gölz, M. Schmugge, F. Franzoso
Molecular Insights Into the Apoptosis and Autophagy Pathway Mechanisms Underlying the Pathogenesis of Pediatric Immune Thrombocytopenia

507
L.P. Leuenberger, L. Isenegger, E. Zaninotto, C. Pauli, P.K. Bode, U. Camenisch, C. Matter, H. Moch, C. Britschgi
Targeting PI3K signaling is a potential therapeutic strategy in Clear Cell Sarcoma

513
A. Roggo, A. Tastanova, E. Ramelyte, M. Levesque, R. Dummer
Exploring ‘Immunologic Itch’ in Sézary Syndrome and Atopic Dermatitis using targeted spatial Transcriptomics

518
L. Dietsche, K. Stirm, C. Schneidawind, A. Müller, A. Theocharides
SMAD1 is a silenced tumor suppressor in AML with MLL rearrangement

527
A. Kraft, M. Meerang, MB. Kirschner, V. Boeva, I. Opitz
Transcriptomic Characterization of Extracellular Vesicles Secreted In Pleural Mesothelioma

528
J. Mengers, M. Haberecker, M. Kirschner, N. Bosbach, O. Lauk, I. Opitz, M. Meerang
Low Ki-67 Positive Index is Prognostic Factor for Better Survival Outcomes of Patients Treated with Intracavitary Cisplatin-Fibrin

540
H. Bolck, A. Kriston, E. Migh, D. Rutishauser, S. Kreutzer, P. Leary, P. Schraml, N. Rupp, P. Horvath, h. Moch
Addressing the challenges of intra-tumor heterogeneity in clear cell renal cell carcinoma (ccRCC)

541
L. Russo, L. Heeb, S. Ulugöl, L. Roth, L. Scherer, A. Gupta, K. Lehmann
Improving treatment of peritoneal metastasis originating from metastatic colorectal cancer

543
N. Desboeufs, G. Semere, C. Pauli, P. Leary, J. Jetzer, LK. Chan, AE. Kremer, L. Planas-Paz, LA. Clerbaux, M. Lopes, A. Weber
DNA replication stress as molecular driver and potential therapeutic target in hepatocellular carcinoma

544
J. Fullin, E. Topcu, N. Klemm, R. Schimmer, C. Koch, S. Boettcher
The divergent roles of mono- and biallelic TP53 mutations in leukemogenesis

549
ME. Healy, P. Leary, LK. Chan, S. Gabriel, R. Parrotta, R. Jackson, A. Weber
Identification of protein-encoding lncRNA as potential new targets for HCC

554
L. Chan, M. Healy, G. Semere, N. Desboeufs, J. Jetzer, R. Parrotta, A. Leblond, A. Weber
STING-independent function of cGAS reduces liver apoptosis and tumorigenesis in Mcl-1Dhep mice

569
H. Lakshminarayanan, K. Yim, S. Pfammatter, A. Banaei-Esfahani, D. Rutishauser, P. Schraml, R. Chahwan, H. Bolck, H. Moch
Exploring extracellular vesicles as liquid biopsy biomarkers for clear cell renal cell carcinoma

578
M. Lapaeva, A. Agustina, P. Wallimann, M. Günther, E. Konukoglu, N. Andratschke, M. Guckenberger, S. Tanadini-Lang, R. Dal Bello
Synthetic computed tomographies for low-field magnetic resonance-guided radiotherapy in the abdomen

580
G. Azzarito, L. Kurmann, B. Leeners, RK. Dubey
Micro-RNA193a-3p Inhibits Breast Cancer Cell Driven Growth of Vascular Endothelial Cells by Altering Secretome and Inhibiting Mitogenesis: Transcriptomic and Functional Evidence

581
N. Klemm, N. Konrad, J. Fullin, R. Schimmer, E. Topcu, S. Stolz, S. Böttcher
Elucidating the molecular mechanism of the dominant-negative effect of the p53 missense variant R248Q

582
G. Azzarito, M. Henry, T. Rotshteyn, B. Leeners, RK. Dubey
Transcriptomic and Functional Evidence That miRNA193a-3p Inhibits Lymphatic Endothelial Cell (LEC) and LEC + MCF-7 Spheroid Growth Directly and by Altering MCF-7 Secretome

601
S. Steiner, S. Hussung, A. Pliego, M. Haberecker, F. Arnold, D. Lenggenhager, R. Fritsch, C. Pauli
Ex vivo patient-derived pancreatic cancer organoids to uncover individual therapeutic vulnerabilities and model acquired resistance

602
Y. Chen, A. Pliego-Mendieta, M. Herzog, L. Planas-Paz, c. Pauli
Functional Screening to Unravel Novel Therapeutic Vulnerabilities in Soft Tissue Sarcoma

Clinical Trials

563
M. Ahmadsei, V. Jegarajah, R. Dal Bello, L. Stark, P. Balermpas, N. Andratschke, S. Tanadini-Lang, M. Guckenberger
Dosimetric analysis of proximal bronchial tree sub-segments to assess the risk of severe toxicity after stereotactic body radiation therapy of ultra-central lung tumors

585
P. Bellstedt
A prove-of-concept study to identify a first Aprataxin inhibitor for sensitizing cancer cells

Head Region / Neuroscience

Basic Research

485
S. Sridhar, A. Ibrahim, I. Tassi, A. Keller
Agonistic Anti-TREM2 administration as a potential therapy for Primary Familial Brain Calcification

514
E. Köksal, L. Madrigal, A. Levin, S. Cai, I. Condado-Morales, A. Aguzzi, T. Knowles, S. Hornemann
Digital microfluidics for absolute quantification of α-synuclein propagons for Parkinson disease diagnosis

539
M. Lone, M. Aaltonen, A. Zidell, P. Helio, S. Saute, S. Mathew, P. Mohassel, C. Bonnemann, T. Hornemann
SPTLC1 variants associated with ALS produce distinct sphingolipid signatures through impaired interaction with ORMDL proteins

542
A. Hülsmeier, S. Toelle, C. Wentzel, T. Hornemann
The sphingolipid C18SOΔ14Z is a potential biomarker for DEGS1 related hypomyelinating leukodystrophy

547
CG. Moreira, A. Müllner, P. Hofmann, M. Gönel, CR. Baumann, D. Noain
Reduced axonal injury, demyelination and cognitive decline upon enhancement of slow waves by closed-loop auditory stimulation in traumatic brain injury rats

551
I. Dias, M. Lopez, S. Kollarik, C. G. Moreira, C. R. Baumann, D. Noain
Establishing up-phase closed-loop auditory stimulation of slow-waves in mouse models of neurodegeneration

575
U. Maheshwari, J. Melero, R. Ni, U. Weber, A. Keller
Microangiopathy and arteriole-associated calcifications in the brain of Xpr1 heterozygous mice

592
F. Costa, G. Indiveri, J. Sarnthein
Real-time and low-power framework to detect epilepsy biomarkers in electrocorticography with a neuromorphic hardware.

593
O. Gallou, J. Sarnthein, G. Indiveri, D. Ledergerber, L. Imbach
Detection of electrographic seizures with a low-power neuromorphic hardware in real-time

Clinical Trials

505
v. Dimakopoulos, G. Selmin, L. Regli, J. Sarnthein
Varying the stimulus repetition rate affects amplitude and noise of the somatosensory evoked potential.

570
AF. Taner, JVM. Hanson, C. Weber, D. Bassler, DL. McCulloch, C. Gerth-Kahlert
Flicker electroretinogram in preterm infants

594
V. Dimakopoulos, J. Gotman, W. Stacey, N. von Ellenrieder, J. Jacobs, C. Papadelis, J. Cimbalnik, G. Worrell, MR. Sperling, M. Zijlmans, L. Imbach, B. Frauscher, J. Sarnthein
Multicenter comparison of interictal high frequency oscillations as a predictor of seizure freedom

Infection / Immunity / Inflammation / Systemic Diseases

Basic Research

479
N-J. Lu, H. Koliwer-Brandl, A. Egli, F. Hafezi
High-fluence accelerated photoactivated chromophore for keratitis cross-linking (PACK-CXL) to treat porcine corneas infected with Staphylococcus aureus or Pseudomonas aeruginosa

480
H. Koliwer-Brandl, A. Nil, J. Birri, M. Sachs, R. Zimmermann, A. Egli, R. Zbinden, D. Balsyte
Evaluation of two rapid commercial assays for detection of Streptococcus agalactiae from vaginal samples

482
L. Šošić, D. Melillo, A. Duda, Y. Wäckerle-Men, A. Streuli, K. Eyer, T. Kündig, P. Johansen
Mapping of IgG-binding epitopes in major birch pollen allergen Bet v 1 for identification of hypoallergenic peptides with potential therapeutic application

488
V. Schmidt, S. Lalevée, S. Traidl, M. Ameri, R. Ziadlou, S. Ingen-Housz-Oro, C. Barau, N. de Prost, M. Nägeli, Y. Mitamura, B. Meier-Schiesser, A. Navarini, L. French, E. Contassot, M. Brüggen
Intravenous immunoglobulins, cyclosporine and best supportive care in Epidermal Necrolysis: Diverse effects on systemic inflammation

493
H. Seth-Smith, E. Badell, A. Berger, M. Blaschitz, J. D'Aeth, A. Dangel, K. Fabiánová, N. Fry, F. Imkamp, V. Hinic, A. Indra, G. Jost, N. Liassine, K. Lippert, D. Litt, G. Martinetti, T. Roloff, S. Schindler, S. Seiffert, A. Sprenger, J. Zavadilová, O. Nolte, S. Brisse, S. Pleininger, A. Sing, A. Egli
Ongoing European outbreak of Corynebacterium diphtheriae among asylum seekers: situational report illuminated through whole genome sequencing

498
SN. Hobbie, S. Radmer Almind, JU. Hansen, M. Plattner, K. Haldimann, C. Vingsbo Lundberg, N. Frimodt-Møller
Susceptibility of blood-culture isolates to apramycin and in-vivo efficacy against nine Escherichia coli and Klebsiella pneumoniae isolates in a mouse peritonitis model

499
E. Parietti, A. Gomez Mejia, C. Chun-Chi, S. Mairpady Shambat, A. Zinkernagel
Investigating the effect of rifampicin on macrophage response during Staphylococcus aureus infection

501
M. Houtman, R. Micheroli, K. Bürki, S. Edalat, M. Frank Bertoncelj, C. Pauli, O. Distler, c. ospelt, M. Elhai
Deciphering the synovial tissue and fibroblast subsets in systemic sclerosis

502
D. Voci, A. Götschi, U. Held, R. Bingisser, G. Colucci, D. Duerschmied, R.M. Fumagalli, B. Gerber, B. Hasse, D.I. Keller, S.V. Konstantinides, F. Mach, S.K. Rampini, M. Righini, H. Robert-Ebadi, T. Rosemann, S. Roth-Zetzsche, T. Sebastian, N.R. Simon, D. Spirk, S. Stortecky, L. Vaisnora, N. Kucher, S. Barco
Enoxaparin for outpatients with COVID-19: 90-day results from the randomised, open-label, parallel-group, multinational, phase III OVID trial

509
Y. Gütlin, D. Albertos Torres, A. Gensch, AK. Schlotterbeck, L. Stöger, S. Heller, L. Infanti, K. Leuzinger, HH. Hirsch, A. Buser, A. Egli
Total anti-SARS-CoV-2 Immunoglobulin and neutralising antibody responses in healthy blood donors over the course of the pandemic - a single city experience

511
F. Wegner, B. Cabrera Gil, A. Neves, A. Egli
How much should we sequence? An analysis of the Swiss SARS-CoV-2 genomic surveillance effort

519
A. Hukara, T. Tabib, M. Rudnik, O. Distler, P. Blyszczuk, R. Lafyatis, G. Kania
FOSL-2 transcription factor as a driver of pro-phagocytic macrophages in patients with systemic sclerosis

524
J. Epprecht, B. Ledergerber, M. Frank, M. Greutmann, M. Van Hemelrijck, L. Ilcheva, M. Padrutt, B. Stadlinger, MÖ. Özcan, TC. Carrel, BH. Hasse
Increase of infective endocarditis due to viridans Streptococci among patients at moderate risk after change of guidance on antibiotic prophylaxis to prevent infective endocarditis: Results from a tertiary care referral centre in Switzerland

525
A. Tarnutzer, V. Haunreiter Dengler, M. von Matt, J. Bär, S. Hertegonne, F. Andreoni, C. Vulin, L. Künzi, C. Menzi, P. Kiefer, J.A. Vorholt, A.S. Zinkernagel
C-di-AMP levels influence Staphylococcus aureus cell wall thickness and virulence

526
L. Luise, V. Matus, R. Sánchez Álvarez, A. Montalban-Arques, M. Scharl, M. Spalinger
The role of PTPN23 in intestinal epithelial cells and macrophages in acute colitis

533
A. Zbinden, H. Seth-Smith, v. beltrami, S. Mancini, A. Egli, S. Droz, U. Bürgi, J. Barben, N. Müller, F. Imkamp
Characterization of Burkholderia cenocepacia ST-250 isolates in patients with cystic fibrosis (CF) in Switzerland

555
S. Hertegonne, T.A. Schweizer, S. Mairpady Shambat, A. Zinkernagel
Neutrophil and Staphyloccus aureus infection dynamics and interactions

558
Z K. Kotkowska, Y. Waeckerle Men, I. Kolm, A. Duda, F. Sella, H. Fischer, L. Hausamann, J. Rust, A. Høgset, T M. Kündig, C. Halin Winter, P. Johansen
Photochemical internalization (PCI): when photodynamic therapy (PDT) becomes an integral of potential cancer vaccines

562
J. Tschumi, L. Jörimann, K. Neumann, M. Zeeb, D. Braun, R. Kouyos, KJ. Metzner, HF. Günthard, S. Swiss HIV Cohort Study
Investigating the origins of intermittent viremia in individuals who initiate therapy during primary HIV-1 infection

564
L. Jörimann, J. Tschumi, M. Zeeb, C. Leemann, C. Schenkel, K. Neumann, S. Chaudron, M. Zaheri, P. Frischknecht, N. Neuner-Jehle, H. Kuster, D. Braun, C. Grube, R. Kouyos, K. Metzner, H. Günthard, S. SHCS
Absence of HIV-1 evolution in early treated individuals switching to Dolutegravir monotherapy for 48 weeks

571
O. Hasan Ali, T. Sinnberg, C. Lichtensteiger, O. Pop, A. Jochum, L. Risch, SD. Brugger, A. Velic, D. Bomze, P. Kohler, P. Vernazza, WC. Albrich, C. Kahlert, M. Abdou, N. Wyss, K. Hofmeister, H. Niessner, C. Zinner, M. Gilardi, A. Tzankov, R. Martin, A. Dulovic, . Shambat, N. Ruetalo, P. Buehler, T. Scheier, W. Jochum, L. Kern, S. Henz, T. Schneider, G. Kuster, M. Lampart, M. Siegemund, R. Bingisser, M. Schindler, N. Schneiderhan-Marra, H. Kalbacher, C. McCoy, W. Spengler, M. Brutsche, B. Maček, R. Twerenbold, J. Penninger, M. Matter, L. Flatz
Pulmonary surfactant proteins are inhibited by immunoglobulin A autoantibodies in severe COVID-19

579
Y. Achermann, T C. Scheier, C. Quiblier, N K. Kuleta, D. Albertos-Torres, T. Roloff-Handschin, M. Meola, F. Imkamp, R. Zbinden, S D. Brugger, A. Egli, I. Frey-Wagner
C. difficile abundance and gut microbiota composition in the first three weeks after antimicrobial treatment for C. difficile infection

Clinical Trials

474
S. Klinnert, C. Schenkel, P. Freitag, H. Günthard, A. Plückthun, K. Metzner
Targeted shock-and-kill HIV-1 gene therapy approach combining CRISPR activation, suicide gene tBid and retargeted adenovirus delivery

483
N. Schmid, L. Weidmann, S. von Moos, B. Helmchen, A. Gaspert, T. Müller, T. Schachtner
Isolated glomerulitis is strongly associated with the absence of antibody-mediated rejection by molecular diagnostics

484
N. Schmid, L. Weidmann, s. von Moos, B. Helmchen, a. Gaspert, t. Müller, T. Schachtner
Prospective assessment of the need for and added value of molecular diagnostics of kidney allograft biopsies – An evaluation in clinical practice

584
J. Scherer, M. Held, R. Dunn, F. Thienemann
Clinical, radiological and histological findings of spinal tuberculosis: Results of the Cape Town Spinal TB cohort study

590
DM. Heuberger, PD. Wendel-Garcia, O. Sazpinar, M. Mueller, H. Klein, BS. Kim, R. Andermatt, R. Erlebach, RA. Schuepbach, PK. Buehler, S. David, DA. Hofmaenner
Role of circulating Angiopoietin-2 in severely burned patients

Mixed Topics

Basic Research

490
D. Schibler, A. Landsmann, P. Wolint, F. Starsich, I. Hermann, M. Calcagni, J. Buschmann, A. Boss
Biodistribution of iron carbide nanoparticles in the living developing chicken embryo using magnetic resonance imaging

491
J. Rieber, M. Gabriella, I. Miescher, F. Weber, P. Wolint, M. Zenobi-Wong, Y. Yang, E. Ongini, J. Snedeker, M. Calcagni, J. Buschmann
Bioactive electrospun polymer tubes releasing IGF-1 for tendon repair

492
S. Shim, B. Karol, A. Ciritsis, C. Rossi, C. Ruppert, A. Boss
Radiation dose prediction for spiral breast CT using Monte Carlo simulation and machine learning model

503
A. Balic, D. Perver, P. Pagella, H. Rehrauer, B. Stadlinger, V. Vogel, TA. Mitsiadis
Extracellular matrix remodelling in dental pulp upon carious lesion through the prism of single-cell analysis

515
N. Jarzebska, J. Frei, M. Mellett, S. Pascolo, M. Tusup
RNA with chemotherapeutic base analogues as a superlative dual-functional anti-cancer drug

516
J. Baum, C. Boggon, N. Ranzoni, L. Isa, S. Brugger
Microbiota engineering for the erradication of Staphylococcus aureus

521
T. Roloff Handschin, H. Seth-Smith, F. Imkamp, A. Egli
Optimizing the whole genome sequencing workflow in a diagnostic microbiology lab to improve the utility for clinical customers

529
B.M. Carrara, Q. Vallmajo-Martin, M. Ehrbar
Mesenchymal Stromal Cells Characterized Through In Vivo Bone Marrow Organoids

530
F. Xiu, M. Visentin
The Effect of 7-ketocholesterol on the Function of Organic Cation Transporter 2 (OCT2)

531
C. Perez-Shibayama, C. Gil-Cruz, N. Cadosch, M. Lütge, H. Cheng, K. Frischmann, A. Joachimbauer, L. Onder, I. Papadopoulou, C. Papadopoulou, S. Ring, P. Krebs, V. Vu, M. Nägele, V. Rossi, D. Parianos, V. Zsilavecz, L. Cooper, A. Flammer, F. Ruschitzka, P. Rainer, D. Schmidt, B. Ludewig
Bone morphogenic protein-4 availability in the cardiac microenvironment controls myocardial inflammation and fibrosis

532
P. Wallimann, B. Pouymayou, M. Mayinger, S. Nowakowska, A. Boss, M. Guckenberger, S. Tanadini-Lang, N. Andratschke
Phantom measurements of apparent diffusion coefficient on a 0.35T MR-Linac

535
L. Moser, K. Gegenschatz-Schmid, N. Ochsenbein-Kölble, M. Ehrbar
A 3D printed device for the in vitro investigation of novel healing strategies for fetoscopic interventions sites in fetal membrane

538
N. Schmid, T. Schachtner
Isolated glomerulitis is strongly associated with the absence of antibody-mediated rejection by molecular diagnostics

548
S. Salemi, L. Schori, T. Gerwinn, M. Horst, D. Eberli
Inhibition of myostatin/Smad pathway signalling in smooth muscle cells

550
V. Baumgartner, S. Salemi, d. Eberli
Targeting metabolic vulnerabilities in androgen-mediated reprogramming of prostate cancer

552
S. Pravato, L A. Krattiger, D V. Deshmukh, M. Ehrbar, M. Tibbitt
Tunable patterning of vascular networks for tissue engineering

557
K. Sun, D. Bochicchio, F. Seehusen, E. Breuer, S. Da Silva Guerra, P. Dutkowski, B. Humar, P. Clavien
Novel animal model for donation after circulatory death in rat uterine transplantation - a new tool for assessing ischaemia and reperfusion (I/R) injury?

565
E. Müller, K. Gegenschatz-Schmid, L. Moser, N. Ochsenbein-Kölble, M. Ehrbar
The Effect of WNT Signalling and External Cues on Migration of Isolated Fetal Membrane Cells

572
M. Jacobs, M. Ehrbar
Development of an in vitro ovary model for the sustained culture of primary follicles

573
D. Rodriguez Gutierrez, A. Astourian, M. Hartmann, I. Dedes, P. Imesch, J. Metzler, G. Schär, M. Shilaih, V. Valentina, B. Leeners
Endometriosis and Fibrosis: Reduction of deep endometriosis lesions through a novel immunotherapy treatment

574
A. Plüss, A. Korczak, M. Ehrbar
3D bioprinted, perfused and vascularized bone organoids to study extravasation and metastasis of cancer

577
AA. Korczak, BM. Carrara, Q. Vallmajó Martín, K. Gegenschatz-Schmid, M. Ehrbar
High efficiency functional elucidation of human bone marrow stromal cells in vivo

583
S. Guerra, DL. Birrer, P. A. Clavien, B. Humar
Macroscopic division of tasks: a basis for accelerated regeneration after ALPPS surgery

586
D. Spiess, V. Abegg, S. Kuoni, A. Chauveau, M. Reinehr, O. Potterat, M. Hamburger, AP. Simões-Wüst
Transplacental passage of compounds from St. John’s wort

587
LA. Krattiger, R. Odabasi, B. Simona, MW. Tibbitt, M. Ehrbar
An in vitro platform to study the recovery of therapeutically ablated vascular networks

588
M. Sachs, S. Makieva, M. Xie, A. Velasco, F. Ille, M. Schmidhauser, M. Saenz-de-Juanco, S. Ulbrich, B. Leeners
Biomarker for Embryo Selection: Transcriptomic signature of live birth revealed in luteinised cumulus cells of women undergoing an ICSI cycle for infertility treatment

589
L. Zurfluh, S. Santos, M. Mennet, O. Potterat, U. von Mandach, M. Hamburger, AP. Simões-Wüst
Bryophyllum pinnatum Attenuates Oxytocin-Induced Pro-inflammatory Signalling Pathways in Human Myometrial Cells

591
S. Kakava, E. Schlumpf, A. von Eckardstein, J. Robert
Apolipoprotein E defines the trafficking of High-density lipoprotein (HDL) particles in brain endothelial cells

604
SA. Mohammed, E. Gorica, G. Karsay, M. Albiero, GP. Fadini, S. Costantino, F. Ruschitzka, F. Paneni
A Chromatin Signature by the Methyltransferase SETD7 Orchestrates Angiogenic Response in Diabetic Limb Ischemia

Clinical Trials

487
D. Fehr, L. Maintz, N. Herrmann, S. Müller, R. Havenith, C. Lang, E. Bersuch, Y. Mitamura, A. Dreher, G. Hammel, M. Reiger, D. Luschkova, E. Renner, C. Akdis, R. Lauener, C. Rhyner, P. Schmid-Grendelmeier, C. Traidl-Hoffmann, T. Bieber, M. Brüggen
Association between atopic dermatitis and cardiovascular diseases: A large multicenter observational study (ProRaD)

508
KH. Huebel, FT. Fehr, TM. Müller, US. Schanz, PC. Cippa
Donor-specific tolerance induction by combined kidney and hematopoetic stem cell transplantation

517
JM. Boss, J. Willms, E. Keller
Bringing an AI Solution for Delayed Cerebral Ischemia Prediction Closer to Clinics through Intermediate Silent Validation

522
JM. Hoffmann, R. Grossmann, A. Widmann
Academic clinical trials: Publication of study results on an international registry – we can do better!

523
JM. Hoffmann, A. Blümle, R. Grossmann, H. Yau, B. Lang, C. Bradbury
The Importance of international Harmonization for Clinical Research – a global survey on quality standards and services of academic Clinical Trial Units

534
N. Hermann, L. Maul, M. Ameri, S. Traidl, R. Ziadlou, K. Papageorgiou, I. Kolm, M. Levesque, J. Maul, M. Brüggen
Vitiligo-like-depigmentation in patients with melanoma under immunotherapy: Clinical presentation and prognostic features - A monocentric prospective observational study

599
Z. Khodabakhshi, Y. Huang, F. Rainer, S. Tanadini-Lang, F. Putz, N. Andratschke
Fully Automated Detection and Segmentation of Brain Metastasis Using a Deep Continual Learning Approach: A Multicentric Study

474

S. Klinnert[2, 3], C. Schenkel[2, 3], P. Freitag[1], H. Günthard[2, 3], A. Plückthun[1], K. Metzner[2, 3]

Targeted shock-and-kill HIV-1 gene therapy approach combining CRISPR activation, suicide gene tBid and retargeted adenovirus delivery

Department of Biochemistry, University of Zurich, Zurich, Switzerland[1], Department of Infectious Diseases and Hospital Epidemiology, University Hospital Zurich, University of Zurich, Zurich, Switzerland[2], Institute of Medical Virology, University of Zurich, Zurich, Switzerland[3]

Introduction:
Infections with the human immunodeficiency virus type 1 (HIV-1) are incurable due the long-lasting, latent viral reservoir. The shock-and-kill cure approach aims to activate latent proviruses in HIV-1 infected cells and subsequently kill these cells with strategies such as therapeutic vaccines or immune enhancement.

Methods:
Here, we combined the dCas9-VPR CRISPR activation (CRISPRa) system with gRNA-V (shock), the truncated Bid (tBid)-based suicide gene strategy (kill) and CD3-retargeted adenovirus (Ad) delivery vectors (targeted), in an all-in-one targeted shock-and-kill gene therapy approach to achieve specific elimination of latently HIV-1 infected cells

Results:
Simultaneous transduction of latently HIV-1 infected J-Lat 10.6 cells with a CD3-retargeted Ad-CRISPRa-V and Ad-tBid led to a 57.7±17.0% reduction of productively HIV-1 infected cells and 2.4-fold ±0.25 increase in cell death. The effective activation of latent HIV-1 provirus by Ad-CRISPRa-V was similar to the activation control TNF-α. The strictly HIV-1 dependent and non-leaky killing by tBid could be demonstrated. Furthermore, the high transduction efficiency of 56.6±1.0% to 87.1±0.2% by the CD3-retargeting technology in HIV-1 latently infected cell lines was the basis of successful shock and kill.

Conclusion:
This novel targeted shock-and-kill all-in-one gene therapy approach has the potential to safely and effectively eliminate HIV-1 infected cells in a highly HIV-1- and T cell specific manner.

475

J. Buschmann[3], D. Heuberger[4], F. Kivrak Pfiffner[6], P. Wolint[3], J. Jang[2], W. Jungraithmayr[5], P. Giovanoli[3], M. Calcagni[3], C. Waschkies[1]

Probing Vasoreactivity and Hypoxic Phenotype in Different Tumor Grafts Grown on the Chorioallantoic Membrane of the Chicken Embryo In Ovo Using MRI

University Hospital Zurich, Center for Surgical Research[1], University Hospital Zurich, Department of Thoracic Surgery,[2], University Hospital Zurich, Plastic Surgery and Hand Surgery[3], University Hospital Zurich,, Institute of Intensive Care Medicine[4], University of Freiburg, Department of Thoracic Surgery, Medical Center-University of Freiburg, Faculty of Medicine[5], University of Zurich, Institute of Medical Molecular Genetics[6]

Introduction:
Cancer is a burden worldwide, leading to high economical costs. The pre-clinical study of tumors is manifold, including characterization of vascular and oxygenation phenotypes, and currently produces a plethora of data; not only with respect to screening novel anti-cancer strategies, but also with regards to different types of preclinical animal models. Rodent models are related to high costs and the need to apply for veterinary licences, which is often time-consuming. In order to spare animals and costs, the chorioallantoic membrane (CAM) of the living chicken embryo provides a viable option to study angiogenesis in tumor-related questions. Moreover, it serves as an efficient and validated 3R (replace, reduce, refine) model, and no veterinary licence is needed until embryonic day 14 (Swiss animal care guidelines). The CAM assay can be easily imaged by MRI and functional gas challenge is feasible on the CAM.

Methods:
Different tumor phenotypes were characterized with MRI, using quantitative T1 and T2* as readouts on a 4.7 T cm Bruker PharmaScan system (Bruker BioSpin, Ettlingen, Germany). Quantitative T1 and T2* are considered as MRI markers associated with vascular functionality and oxygenation status when compared between periods of exposure to medical air, hypercapnia HC (5% CO2, 21% O2, balanced with N2) and hypercapnic hyperoxia HCHO (5% CO2, 95% O2, i.e. carbogen), respectively. Gases were delivered through a plastic tubing at 200ml/ min flow rate directed onto the CAM, which serves as a breathing organ during chicken embryo development. We explored the response of MC-38 colon, A549 and H460 adeno-carcinoma cell grafts, respectively, to hypercapnic (HC) and hypercapnic-hyperoxic (HCHO) gas challenges, pertaining to the grafts vascular and oxygenation phenotypes. We compared medetomidine and a cooling (4 °C) sedation protocol for HCHO gas challenge. The hypotheses were that HC and HCHO gas challenges would evoke different responses in different tumor types. With MC-38 colon and H460 lung adeno-carcinoma, densely packed and less vascularized tumor types were chosen, in contrast to the more vascularized, granular and patchy A549 lung adeno-carcinoma.

Results:
Quantitative T1 and T2* maps were obtained from all graft types displaying distinct spatial distribution patterns within the graft and functional response. Interestingly, though of similar origin as the A549, H460 grafts resembled more the characteristics of MC-38 grafts in terms of graft size (~3.8 mm compared to ~4.0 mm in MC-38 grafts; and ~2.0 mm in A459 grafts) and spatial distribution of T1 and T2* (larger within graft center for MC-38 and H460; and lower within the center for A459 grafts) and response to gas challenge.

Region of interest analysis within the graft revealed a significant decrease in T1 ($p < 0.01$, Wilcoxon test) and increase in T2* ($p < 0.005$ Wilcoxon test) in the A549 grafts under hypercapnic hyperoxia (HCHO). Hypercapnia (HC) alone did otherwise not produce significant response in T1 and T2* in any of the three tumor types. Neither were H460 or MC-38 grafts responsive to HCHO, consistent with their more hypoxic phenotype that was previously corroborated with HIF-1a immunohistochemical staining for MC-grafts and was accordingly found for H460 tumors here.

Conclusion:
Different tumor grafts are characterized by a differential response to hypercapnic and hypercapnic-hyperoxic functional gas challenge. It is shown that in A549 tumor grafts a significant response in T1 was revealed during HCHO, but not HC, which is consistent with the normoxic phenotype of the graft in comparison to the other rather hypoxic graft types. Furthermore, response of A459 grafts under HC and HCHO in T2* pertains to its vascular reactivity and therefore demonstrates the capability to use functional gas challenge to study vascular functional and oxygenation phenotypes of grafts in the CAM model noninvasively.

476

D. Heuberger[6], P. Wolint[5], J. Jang[4], S. Itani[4], W. Jungraithmayr[7], C. Waschkies[2], G. Meier Bürgisser[5], S. Andreoli[5], K. Spanaus[3], R. Schuepbach[6], M. Calcagni[5], C. Fahrni[1], J. Buschmann[5]

High-Affinity Cu(I)-Chelator with Potential Anti-Tumorigenic Action – a Proof-of-Principle Experimental Study of Human H460 Tumors in the CAM Assay

Georgia Institute of Technology, School of Chemistry and Biochemistry and Petit Institute for Bioengineering and Bioscience[1], University Hospital Zurich, Center for Surgical Research[2], University Hospital Zurich, Clinical Chemistry[3], University Hospital Zurich, Department of Thoracic Surgery,[4], University Hospital Zurich, Plastic Surgery and Hand Surgery[5], University Hospital Zurich,, Institute of Intensive Care Medicine[6], University of Freiburg, Department of Thoracic Surgery, Medical Center-University of Freiburg, Faculty of Medicine[7]

Introduction:
Copper plays a critical role in activating and supporting tumorigenesis by stimulating angiogenesis. It is involved in all steps of the angiogenic process covering initiation, endothelial cell proliferation, migration and morphogenesis, as well as ECM remodeling and tube formation. Excessive angiogenesis can arise from an imbalanced activity of pro- and anti-angiogenic cues, including increased copper levels, which may support the progression of malignant tumors. Cancer patients not only exhibit elevated copper levels in tumors but generally also display higher copper serum levels. Therefore, the anti-angiogenic potential of copper starvation is an important strategy in clinical oncology.

Recently, our research team evaluated a new high-affinity Cu(I) chelator, PSP-2, for its potential anti-angiogenic activity in vitro and in ovo, i.e., in the chorioallantoic membrane assay of the chicken embryo (CAM assay). We were able to show a significant reduction in angiogenic activity when PSP-2 was applied. In the present study, we go a step further and test the anti-tumorigenic impact of PSP-2.

Methods:
Six established lung cancer cell lines were tested for their viability upon treatment with PSP-2, a novel high-affinity Cu(I) chelator. Among these cell lines, H460 cells responded with the most significant reduction in viability and thus were chosen for experiments in the CAM assay. Specifically, H460 cells were seeded in Matrigel onto the CAM assay for one week, resulting in small tumors that grew on the membrane. The tumors were then treated with PSP-2 at two different concentrations, and the tumor weight, vessel density, copper content, percentages of ki67+ proliferating cells and HIF-1-alpha+ hypoxic cells were quantitatively assessed.

Results:
The main findings of this study point towards a significant decrease in tumor vessel density under PSP-2 treatment, accompanied by a decrease in tumor weight when PSP-2 was applied. Although the high-dose PSP-2 and the control groups were not significantly different for the fraction of HIF-1a+ cells, the low-dose PSP-2 group revealed a significantly lower fraction of HIF-1alpha+ cells compared to both other groups, even though that the total cell counts were similar for all three groups. Moreover, the ki67+ cell fraction was higher for high-dose PSP-2 compared to control and low-dose PSP-2 but similar for low-dose PSP-2 and control.

Conclusion:
The observed decrease of the H460 tumor weight under low and high-dose PSP-2 treatment with concurrent significant angiosuppression points towards an anti-cancer potential of PSP-2 via an anti-angiogenesis mechanism. Before clinical trials can be considered, however, PSP-2 should be tested with other types of tumors and in preclinical animal models that allow for an observation period longer than 1-week, which was imposed by the CAM assay used in this study.

477

A. Tastanova[3], G. Restivo[3], Z. Balazs[4], F. Panebianco[1], M. Diepenbruck[1], C. Ercan[6], B. Preca[1], J. Hafner[3], W. Weber[5], C. Beisel[2], M. Bentires-Alj[1], M. Krauthammer[4], M. Levesque[3]

Live slow-frozen human tumor tissues viable for 2D, 3D, ex vivo cultures and single-cell RNAseq

Department of Biomedicine, Department of Surgery, University Hospital Basel, University of Basel, Basel, Switzerland[1], Department of Biosystems Science and Engineering, ETH Zurich, Basel, Switzerland[2], Department of Dermatology, University Hospital Zurich, University of Zurich, Zurich, Switzerland[3], Department of Quantitative Biomedicine, University Hospital Zurich, Zurich, Switzerland[4], Department of Surgery, Breast Center, University Hospital Basel, Basel, Switzerland[5], Institute of Medical Genetics and Pathology, University Hospital Basel, Basel, Switzerland[6]

Introduction:
Biobanking of surplus human healthy and disease-derived tissues is essential for diagnostics and translational research. An enormous amount of formalin-fixed and paraffin-embedded (FFPE), Tissue-Tek OCT embedded or snap-frozen tissues are preserved in many biobanks worldwide and have been the basis of translational studies. However, their usage is limited to assays that do not require viable cells. The access to intact and viable human material is a prerequisite for translational validation of basic research, for novel therapeutic target discovery, and functional testing.

Methods:
Here we show that surplus tissues from multiple solid human cancers directly slow-frozen after resection can subsequently be used for different types of methods including the establishment of 2D, 3D, and ex vivo cultures as well as single-cell RNA sequencing with similar results when compared to freshly analyzed material.

Results:
We demonstrate the suitability of live-frozen tissue by comparing it to the fresh counterpart for various in vitro and ex vivo applications including cell line and organoids establishment, drug testing and high dimensional single-cell RNA sequencing on a range of tumor samples, including melanoma, colorectal cancer and liver metastasis, basal cell carcinoma, and breast cancer. Furthermore, we have shown in slow-frozen breast cancer samples that scRNAseq can detect important clinically relevant markers and validate their presence with conventional IHC at the protein level. The storage duration of slow-frozen samples paired to freshly processed samples in this study was between 1 week to 14 months for scRNAseq, < 1 month to 7 months for samples processed for 2D (with no significant difference in time of storage between successful and not-successful cultures) and 1 week for 3D and ex vivo cultures. Based on our results we can conclude that tumor pieces can be stored for up to one year as slow-frozen samples for future downstream analysis.

Conclusion:
In conclusion, this work opens up a broad spectrum of applications for surplus clinical material from different solid cancers that cannot be used immediately after collection with a direct impact in biomarker discovery, drug testing and other translational cancer research applications.

478

E. Topcu[1], J. Fullin[1], S. Boettcher[1]

Elucidating the effect of inflammation for clonal expansion of TP-53-mutant clonal hematopoiesis

University Hospital Zurich[1]

Introduction:
Clonal hematopoiesis of indeterminate potential (CHIP) is characterized by the presence of expanded somatic blood cell clones bearing mutations in leukemia driver genes. TP53 encodes the fundamental tumor suppressor p53 and is one of the recurrently mutated genes in CHIP. The factors driving clonal expansion and malignant transformation of mutated hematopoietic stem and progenitor cells (HSPCs), including environmental factors, are incompletely understood. In this context, inflammation has been hypothesized to play an essential role in Tet2-mutant CHIP. In this study, we investigate the role of inflammation for the clonal expansion and malignant transformation of TP53-mutant clonal hematopoiesis.

Methods:
To test the effect of inflammation of TP53 clonal expansion, we use immortalized murine HSPCs lines derived from a conditional knock-in Trp53.loxP-245W-GFP mouse, which has inducible expression of the murine equivalent of one the most common TP53 missense mutations (TP53.R248W in humans) linked via a T2A self-cleaving peptide to green fluorescent protein (GFP). Briefly, immortalization is achieved by retroviral beta-estradiol-driven Hoxb8 expression. Upon doxycycline treatment, Tet-inducible-Cre-recombinase is expressed, and as a result, mono- or biallelic Trp53 mutations can be induced at a desired level. This in vitro model system enables us to test various inflammatory factors and ensuing molecular mechanisms in a high-throughput manner. In order to validate our findings from in vitro model system, we tested the effect of inflammation on Trp53-mutant clonal expansion and malignant transformation of pre-leukemic HSPCs in vivo. To achieve this, Trp53.R245W-GFP mice described above are bred to Scl-CreERT2 mice, which allows tamoxifen-inducible expression of Trp53.R245W-GFP specifically in the hematopoietic system.

Results:
In order to test if inflammatory stimuli drive TP53 mutant clonal expansion, we conducted competitive cell growth assays with particular pathogen-associated molecular patterns (PAMPs), which are recognized by pattern recognition receptors such as Toll-like receptors (TLRs). Among the tested TLR agonists, both mono- and biallelic TP53 mutations gained a significant competitive advantage over their uninduced, functionally wild-type counterparts upon lipopolysaccharide (LPS, TLR4 agonist) exposure. To understand how LPS stimulates clonal expansion of Trp53-mutant, but not wild-type HSPCs, we performed functional assays. We observed that cells bearing biallelic Trp53 mutations were resistant to LPS-induced apoptosis relative to their functionally wild-type counterparts.

Conclusion:
Our preliminary data suggest that inflammation plays an important role in the pathogenesis of TP53-mutant clonal hematopoiesis by conferring a competitive advantage to mono- and biallelic Trp53-mutant cells over their wild type counterparts upon LPS treatment. We will further dissect the underlying molecular mechanisms.

479

N-J. Lu[2], H. Koliwer-Brandl[1], A. Egli[1], F. Hafezi[2]

High-fluence accelerated photoactivated chromophore for keratitis cross-linking (PACK-CXL) to treat porcine corneas infected with Staphylococcus aureus or Pseudomonas aeruginosa

Institute of Medical Microbiology, UZH[1], Ocular Cell Biology Group, Center for Applied Biotechnology and Molecular Medicine, UZH[2]

Introduction:
Infectious keratitis results from micro-damage to the cornea structure e.g., via contact lenses and a subsequent superinfection with bacterial or fungal pathogen. Infectious keratitis can be a therapeutic challenge. We aimed to investigate whether high-fluence accelerated PACK-CXL can effectively treat porcine corneas infected with *Staphylococcus aureus* or *Pseudomonas aeruginosa*.

Methods:
We prepared and cultured fresh porcine corneas, and established the bacterial keratitis model on porcine corneas using *S. aureus* and *P. aeruginosa*, respectively. After we successfully established the models for 24 hours, we randomly applied two high-fluence accelerated PACK-CXL protocols with different chromophores (riboflavin, exposed to 365 nm UV-A light: 30 mW/cm^2, 8 min 20 secs, 15 J/cm^2; rose bengal exposed to 522 nm green light: 15 mW/cm^2, 16 min 40 secs, 15 J/cm^2) to one quarter of infected corneas. We incubated all corneas for another 24 hours, and we applied 8 mm corneal trephine to all corneas to get corneal buttons. We vortexed the corneal buttons in 0.9% saline solution to release the bacterial cells. Next, we diluted, plated and inoculated the irradiated and unirradiated solutions on Columbia agar + 5% sheep blood (bioMérieux, Marcy l'Étoile, France) for quantification. We calculated bacterial killing ratios (BKR) from at least 3 biological replicates with at least 3 technical replicates for each condition.

Results:
In this ex-vivo porcine infectious keratitis model, we successfully applied PACK-CXL with riboflavin plus UV-A light and observed an average BKR for S. aureus and P. aeruginosa of 55.5% and 54.3%, respectively. When we applied PACK-CXL with rose bengal plus green light, the average BKR for *S. aureus* and *P. aeruginosa* was 83.0% and 73.3%, respectively. The BKR is significantly increased by applying rose bengal as compared to riboflavin.

Conclusion:
Both types of high-fluence accelerated PACK-CXL can significantly decrease the bacterial load of *S. aureus* and *P. aeruginosa* in a porcine cornea model. The results are promising to further optimize the treatment and have a high translation potential for treatment in humans.

480

H. Koliwer-Brandl[2], A. Nil[2], J. Birri[1], M. Sachs[1], R. Zimmermann[1], A. Egli[2], R. Zbinden[2], D. Balsyte[1]

Evaluation of two rapid commercial assays for detection of Streptococcus agalactiae from vaginal samples

Division of Obstetrics, USZ[1], Institute of Medical Microbiology, UZH[2]

Introduction:
Streptococcus agalactiae, also known as group B streptococci (GBS), is associated with invasive infections in neonates. Identification of GBS vaginal colonization of pregnant women before delivery is essential for treatment with antibiotics to prevent intrapartum vertical transmission to the newborn. We aimed to compare two PCR based assays against our culture-based reference standard in samples of pregnant women.

Methods:
This study was designed to evaluate applicability of the rapid real-time PCR Xpert® GBS (Xpert; Cepheid, Sunnyvale, California, U.S.). The test was compared with GenomEra® GBS PCR (GenomEra; Abacus Diagnostica, Turku, Finland). Culture-based detection served as reference standard. Culture was performed on CNA agar (bioMérieux, Marcy l'Étoile, France), GBS agar (Brilliance GBS, Thermo Scientific, Waltham, MA, USA) and GBS enrichment bouillon containing casein and starch (Merck, Darmstadt, Germany) at 37°C for 24h. Identification was done with MALDI-TOF MS.

Results:
We analyzed vaginal samples of 260 pregnant women; 42 (16.2%) samples were tested GBS-positive by culture, 30 (11.5%) by Xpert, and 37 (14.2%) by GenomEra. Xpert and GenomEra assays performed with sensitivities of 71.4% and 88.1%, as well as specificities of 98.6% and 99.1%, respectively. Twelve vaginal samples were false-negative by Xpert and 5 samples by GenomEra. Interestingly, three Xpert-negative samples (according to the manufacturer) exhibited high Ct-values (> 42) and were positive by culture. By inclusion of higher Ct-values, the sensitivity of Xpert increases up to 78.6%. Moreover, only three Xpert PCRs had to be repeated due to not interpretable results, compared to 15 repetitions of the GenomEra PCR.

Conclusion:
The GenomEra assay showed a higher sensitivity (88.1%) than the Xpert PCR (71.4%). However, the Xpert assay needed less hands-on-time for a sample preparation and required substantially less repetitions compared to the GenomEra assay. The Xpert assay showed an overall acceptable sensitivity and high specificity, which make it applicable as rapid intrapartum point-of-care test.

482

L. Šošić[2], D. Melillo[2], A. Duda[1], Y. Wäckerle-Men[1, 2], A. Streuli[3], K. Eyer[3], T. Kündig[1, 2], P. Johansen[1, 2]

Mapping of IgG-binding epitopes in major birch pollen allergen Bet v 1 for identification of hypoallergenic peptides with potential therapeutic application

Department of Dermatology, University Hospital Zürich, Zürich, 8091, Switzerland[1], Department of Dermatology, University of Zürich, Zürich, 8091, Switzerland[2], Laboratory for Functional Immune Repertoire Analysis, Institute of Pharmaceutical Sciences, D-CHAB, ETH, Zürich, Zürich, 8093, Switzerland[3]

Introduction:
Allergy is an important socio-economic health problem currently estimated to affect one billion people worldwide. Allergen immunotherapy (AIT), as the only curative approach, is associated with the stimulation of allergen-specific neutralising IgG4 antibodies and allergen tolerance. While IgE epitope mapping has been important to identify and characterise major allergens, IgG epitope mapping has not yet been a major focus of allergy research. In this project, we aim to define IgG-binding epitopes on the major birch pollen allergen Bet v 1 in order to use this information for the production of hypoallergenic peptides for improved AIT.

Methods:
Blood from 30 birch pollen allergic patients (and 5 non-allergic control patients) was collected at the Allergy Unit of the University Hospital Zurich. Ten of the allergic patients had received subcutaneous and 10 patients had received sublingual AIT. Serological analysis of allergen-specific IgE and IgG4 was done with ImmunoCAP. Analysis of IgG-secreting B cells was done with ELISpot and by DropMap microfluidics. Linear and conformational IgG epitopes were analysed using CLIPS™ technology (Biosynth).

Results:
All allergic patients had Bet v 1 specific IgE, while control patients were negative. Both IgE and IgG4 rose upon SCIT and SLIT. ELISpot and DropMap microfluidics confirmed Bet v 1-specific IgG and IgG4, respectively. In a pilot study, specific IgG-binding Bet v 1 epitopes were identified with sera from AIT patients but not from healthy controls. Further epitope mapping with sera from the other patients is underway.

Conclusion:
CLIPS™ technology enables linear and conformational mapping of Bet v 1-specific IgG binding sites. It remains to be tested if the epitopes identified stimulate allergen-neutralising antibodies when used in AIT.

483

N. Schmid[1], L. Weidmann[1], S. von Moos[1], B. Helmchen[2], A. Gaspert[2], T. Müller[1], T. Schachtner[1]

Isolated glomerulitis is strongly associated with the absence of antibody-mediated rejection by molecular diagnostics

University Hospital Zurich, Division of Nephrology[1], University Hosptial Zurich, Institute of Pathology[2]

Introduction:
According to the 2018 Banff classification, the Molecular Microscope Diagnostic System (MMDx) is indicated in cases when histology is insufficient to diagnose antibody-mediated rejection (ABMR) due to an absence of diagnostic criteria groups 2 and/or 3. The impact of isolated glomerulitis (g>0, ptc0) on the likelihood of ABMR diagnosis by the MMDx appears critical to the implementation of this new biomarker.

Methods:
We analyzed 251 kidney allograft biopsies by histology and molecular diagnostics at the University Hospital Zurich from October 2018 to November 2022. Histologic findings were classified concerning the absence of (1) diagnostic criteria groups 2 and 3 (n=18), (2) diagnostic criteria group 2 only (n=18), and (3) diagnostic criteria group 3 only (n=28). In addition, cases with histologically proven ABMR were used for comparison (n=65). High-resolution re-typing was performed from the kidney allograft biopsies if necessary.

Results:
The MMDx diagnosed ABMR in 1 of 18 cases (6%) with absent diagnostic criteria groups 2 and 3, 4 of 18 cases (22%) with absent diagnostic criteria groups 2, and 19 of 28 cases (68%) with absent diagnostic criteria groups 3. On the contrary, MMDx confirmed the diagnosis of ABMR in 42 of 65 cases (65%) with histologically proven ABMR but did not in 23 of 65 cases (35%). Among 28 cases with absent diagnostic criteria group 3, only 2 of 19 cases (11%) with ABMR by MMDx but 6 of 9 cases (67%) with no ABMR by MMDx showed isolated glomerulitis (p=0.0048). Among 65 cases with histologically proven ABMR, only 7 of 42 cases (17%) with ABMR by MMDx but 14 of 23 cases (61%) with no ABMR by MMDx showed isolated glomerulitis (p<0.001). Overall, 14 of 65 cases (21%) with isolated glomerulitis showed ABMR diagnosis by MMDx.

Conclusion:
Isolated glomerulitis is strongly associated with the absence of ABMR by MMDx not only when diagnostic criteria group 2 is missing but also when diagnostic criteria 3 is missing or ABMR is proven by histology. Our results may help to guide the indication for MMDx in clinical practice. However, the clinical significance of these results needs further investigation.

484

N. Schmid[1], L. Weidmann[1], s. von Moos[1], B. Helmchen[2], a. Gaspert[2], t. Müller[1], T. Schachtner[1]

Prospective assessment of the need for and added value of molecular diagnostics of kidney allograft biopsies – An evaluation in clinical practice

University Hospital Zurich, Division of Nephrology[1], University Hosptial Zurich, Institute of Pathology[2]

Introduction:
The Molecular Microscope Diagnostic System (MMDx) may resolve inconclusive histology findings, as preserved biopsy material can be examined after histology findings have been obtained. The extent to which this proposed approach can be implemented in clinical practice remains an open question.

Methods:
We prospectively analyzed 104 consecutive indication kidney allograft biopsies by histology and molecular diagnostics at the University Hospital Zurich from April 2022 to December 2022. Pathologists and clinicians with experience in molecular diagnostics assessed the need for MMDx by questionnaire when the histology report was available. Clinicians then assessed the added value of the molecular diagnostics by questionnaire when the MMDx report was available.

Results:
29 of 104 cases (28%) showed rejection by histology, 42 of 104 cases (40%) showed no rejection by histology, and 33 of 104 cases (32%) showed histologic findings insufficient to diagnose ABMR due to an absence of diagnostic criteria groups 2 and/or 3. Pathologists considered molecular diagnostics indicated in 42 of 104 cases (40%), 9 cases to give extra confidence, and 33 cases for diagnostic clarification concerning rejection. Clinicians considered molecular diagnostics indicated in 54 of 104 (52%) cases, 5 cases to give extra confidence, and 49 for diagnostic clarification concerning rejection. In 33 cases with histologic findings insufficient to diagnose ABMR, molecular diagnostics were considered indicated by pathologists and clinicians. Molecular diagnostics allowed the diagnosis of ABMR in 8 of 33 cases (24%). In addition, 11 of 104 cases (11%) showed a discrepancy between the histologic findings and the molecular diagnosis. Clinicians considered adjustment of treatment based on the MMDx report in 3 of 11 discrepant cases. Pathologists and clinicians considered molecular diagnostics indicated in 2 of 11 and 3 of 11 discrepant cases, respectively.

Conclusion:
The need for molecular diagnostics goes beyond the recommendation of the 2018 Banff classification for histologic findings insufficient to diagnose ABMR. However, the added value of molecular diagnostics appears to be largely limited to these cases.

485

S. Sridhar[1, 2], A. Ibrahim[3], I. Tassi[3], A. Keller[1, 2]

Agonistic Anti-TREM2 administration as a potential therapy for Primary Familial Brain Calcification

Department of Neurosurgery, Clinical Neurocentre, Zurich University Hospital, Zurich University, Zürich, Switzerland[1], Neuroscience Center Zurich, University of Zurich and ETH Zurich, Zurich, Switzerland[2], Research and Development, Alector, South San Francisco, California, USA[3]

Introduction:
Primary Familial Brain Calcification (PFBC) is a rare neurodegenerative disease associated with cognitive, motor and psychiatric symptoms and characterized by bilateral brain vascular calcification in the basal ganglia. Currently there are no disease modifying therapeutics for PFBC. Microglia, the brain resident macrophages, are required to curtail the growth of small vessel associated calcifications in the Pdgfbret/ret mouse model of PFBC. They require functional Triggering Receptor Expressed in Myeloid cells 2 (TREM2) for this role. Here we investigated whether sustained TREM2 signaling would lead to reduction of brain vascular calcification on a mouse model of PFBC.

Methods:
Two-month-old mice received weekly injections of agonistic anti-TREM2 (AL002a; Alector) or isotype control IgG1 antibody for 8 weeks. Brains from these mice were harvested one week after the last dose. Regions with least variability in calcification load were immunostained and imaged for quantification. The amount of antibody received at the mouse brain, and the extent of activation by the agonist was determined. The microglial response to calcifications was also characterized using immunohistochemistry against microglial reactivity markers CLEC7A and CD68.

Results:
Although microglia surrounding calcifications showed increased TREM2 signaling, the administration of AL002a did not alter calcification load as measured by either number or size of the calcification nodules. Microglia surrounding calcifications did not change their phenotype upon AL002a treatment as assessed by IBA1, CD68 and CLEC7A expression. The brains of Pdgfbret/ret mice had 60-100 times more AL002a antibody than control mice. Thus, the absence of an effect on measured parameters was not due to the limited bioavailability of the antibody. However, anti-TREM2 treatment altered the deposition of cathepsin K (collagen I degrading enzyme secreted by microglia on to calcifications) as compared to control.

Conclusion:
Our results show that sustained stimulation of TREM2 in microglia did not potentiate microglial ability to control the extent of vascular calcification in a mouse model of PFBC. This data is in line with observations obtained from Alzheimer's mouse models where agonistic anti-TREM2 treatment did not increase microglial clearance of plaques. Thus, in a setting where microglia TREM2 function is unimpaired, agonistic TREM2 stimulation has no effect on controlling vascular calcification by microglia.

487

D. Fehr[1, 3, 6], L. Maintz[3, 4], N. Herrmann[3, 4], S. Müller[3, 4], R. Havenith[3, 4], C. Lang[1, 3], E. Bersuch[3], Y. Mitamura[3, 8], A. Dreher[3], G. Hammel[3, 5, 7], M. Reiger[3, 5, 7], D. Luschkova[3, 5, 7], E. Renner[9], C. Akdis[3, 8], R. Lauener[2, 3], C. Rhyner[3, 8], P. Schmid-Grendelmeier[1, 3], C. Traidl-Hoffmann[3, 5], T. Bieber[3, 4], M. Brüggen[1, 3, 6]

Association between atopic dermatitis and cardiovascular diseases: A large multicenter observational study (ProRaD)

Allergy Unit, Department of Dermatology, University Hospital Zurich, Zurich, Switzerland[1], Children's Hospital of Eastern Switzerland, St. Gallen, Switzerland[2], Christine Kühne-Center for Allergy Research and Education, Davos, Switzerland[3], Department of Dermatology and Allergy, University of Bonn, Bonn, Germany[4], Department of Environmental Medicine, Faculty of Medicine, University of Augsburg, Augsburg, Germany[5], Faculty of Medicine, University of Zurich, Zurich, Switzerland[6], Institute of Environmental Medicine, Helmholtz Zentrum München, Augsburg, Germany[7], Swiss Institute of Allergy and Asthma Research (SIAF), University of Zurich, Davos, Switzerland[8], Translational Immunology in Environmental Medicine, Technical University of Munich, Munich, Germany[9]

Introduction:
There is contradictory evidence on the association between atopic dermatitis (AD) and cardiovascular diseases (CVD). The aim of this study was thus to further explore this connection and how it relates to the presence of atopic comorbidities.

Methods:
This observational multicenter study included cross-sectional data of 705 adult patients suffering from AD and 80 control participants (without history of AD, allergic rhinitis, food allergy, asthma, or psoriasis) of the ProRaD cohort (Zürich, Davos, Bonn, Augsburg). EASI, body surface area (BSA), SCORAD and objective SCORAD were used to grade AD severity. The presence of atopic, cardiovascular, and metabolic conditions was assessed by a dermatologist. Cardiovascular risk factors (age, sex, smoking habits, physical activity, body mass index) as well as other clinical and epidemiological data were asked in a standardized questionnaire. The main outcome variable for statistical analysis was the presence of CVD, the main dependent variables being the presence of AD and the severity of AD respectively. In the minimally adjusted model, we controlled for age and sex, in the fully adjusted model for all the above-mentioned cardiovascular risk factors.

Results:
Our analysis did not show an overall association between AD and cardiovascular outcomes. However, patients with severe AD were significantly more often suffering from CVD than control participants (24.4% [29/119] vs. 10.0% [8/80]). Furthermore, AD patients without atopic comorbidities (pure AD) had a significantly higher prevalence of CVD compared to AD patients with atopic comorbidities (29.7% [41/138] vs. 14.3% [81/567]). Yet, both associations could not be confirmed in the adjusted models. In patients with pure AD, there was a statistically significant relation between the severity of AD (EASI and BSA) and the presence of cardiovascular comorbidities, which could be confirmed in multivariate analyses.

Conclusion:
Our study does not suggest an overall association between AD and cardiovascular comorbidities but suggests a more complex relation between the two conditions: A higher BSA involvement may be indicative of a stronger pro-inflammatory type 1 reaction in pure AD and represent a risk factor for CVD. Conversely, a more prominent type 2 response (clinically evidenced by atopic comorbidities) might counterbalance this tendency.

488

V. Schmidt[1, 6], S. Lalevée[5], S. Traidl[3, 7, 9], M. Ameri[1, 7, 9], R. Ziadlou[1, 7, 9], S. Ingen-Housz-Oro[5, 12, 14, 15], C. Barau[11], N. de Prost[10], M. Nägeli[7, 9], Y. Mitamura[13], B. Meier-Schiesser[7, 9], A. Navarini[2, 6], L. French[4, 8, 14], E. Contassot[2, 6], M. Brüggen[1, 7, 9, 14]

Intravenous immunoglobulins, cyclosporine and best supportive care in Epidermal Necrolysis: Diverse effects on systemic inflammation

Christine Kühne-Center for Allergy Research and Education, Davos, Switzerland[1], Department of Biomedicine, University Hospital and University of Basel, Basel, Switzerland[2], Department of Dermatology and Allergy, Hannover Medical School, Hannover, Germany[3], Department of Dermatology and Allergy, University Hospital, LMU Munich, Munich, Germany[4], Department of Dermatology, AP-HP, Henri Mondor Hospital, Créteil, Paris, France[5], Department of Dermatology, University Hospital Basel, Basel, Switzerland[6], Department of Dermatology, University Hospital Zurich, Zurich, Switzerland[7], Dr. Philip Frost Department of Dermatology and Cutaneous Surgery, University of Miami, Miller School of Medicine, Miami, United States of America[8], Faculty of Medicine, University Zurich, Zurich, Switzerland[9], Intensive Care Unit, AP-HP, Henri Mondor Hospital, Créteil, Paris, France[10], Platform of Biological Resources, BB-0033-00021, Henri Mondor Hospital, Créteil, Paris, France[11], Reference center for toxic bullous dermatoses and severe drug reactions TOXIBUL, Créteil, Paris, France[12], Swiss Institute of Allergy and Asthma Research (SIAF)[13], ToxiTEN group, ERN-skin[14], Université Paris Est, EpiDermE, Créteil, Paris, France[15]

Introduction:
Stevens-Johnson Syndrome (SJS) and toxic epidermal necrolysis (TEN) are rare but potentially life-threatening cutaneous adverse reactions. There is still no consensus on adjuvant treatments, and little is known about their effects on systemic inflammation in SJS/TEN. Our aim was to characterize the systemic and cutaneous immune profiles of SJS/TEN patients and to investigate whether/how intravenous immunoglobulins (IVIG), cyclosporine A (CSA) and best supportive care only (BSCO) affected the systemic immune signature and clinical outcome (6 week-mortality, complications, hospitalization stay).

Methods:
We included 16 patients with SJS/TEN, treated with high-dose IVIG (n=8), CSA (n=4) or BSCO (n=4). Serial serum samples were obtained prior-, 5-7 days and 21 days after treatment onset. Serum levels of inflammation-/immune response-associated proteins were measured by high-throughput proteomics assay (OLINK) and cytotoxic molecules by ELISA. RNA extracted from skin biopsies collected prior treatment was analyzed by Nanostring.

Results:
Serum inflammatory profiles in SJS/TEN patients were notably characterized by massive upregulation of type 1 immune response– and proinflammatory markers. Surprisingly, there was limited overlap between cutaneous and serum immune profiles. Serial serological measurements of immune response markers showed very diverse dynamics between the different treatment groups. IVIG-treated patients showed completely different dynamics and most significant proteomic changes in an early phase (day 5-7). In all treatment groups, type 1-/inflammatory response markers were dampened at day 21. Clinically, there were no outcome differences.

Conclusion:
Our study demonstrates that BSCO, CSA and IVIG have very diverse biological effects on the systemic inflammatory response in SJS/TEN, which may not correlate with clinical outcome differences.

489

MB. Kirschner[2], V. Orlowski[2], F. Schläpfer[2], I. Opitz[2], G. Reid[1]

Association of novel microRNAs with diagnosis and histology of malignant pleural mesothelioma

Department of Pathology, University of Otago, Dunedin, New Zealand[1], Department of Thoracic Surgery, University Hospital Zurich, Switzerland[2]

Introduction:
Achieving an accurate diagnosis of malignant pleural mesothelioma (MPM) can be quite difficult and time consuming, with the differentiation of MPM from pleural metastases of other cancers being particularly challenging. The availability of tissue-specific biomarkers could prove very helpful in this context. Through a recent analysis of the TCGA-MESO small RNA sequencing data previously undetected microRNAs have been identified, which showed significantly higher expression than in sequencing data from primary lung cancers. A signature of 10 of these microRNAs was able to distinguish MPM from lung cancer with high accuracy (Martinez VD et al, AJRCM 2019: 61(2)). In the present study, we evaluate the expression of these microRNAs in MPM tissue as well as pleural biopsies from benign inflammatory reactions and metastases of other cancers using an alternative detection approach (two-tailed RT-qPCR).

Methods:
We used diagnostic chemo-naïve biopsies from 32 MPM patients and 14 non-MPM cases who were treated at the University Hospital Zurich between 1999 and 2021. For 23 of our MPM cases microRNA expression was also assessed in the matching post-chemotherapy specimen. The non-MPM cases consisted of 8 patients with benign inflammatory reaction or plaques, 3 patients with metastasis due to lung adenocarcinoma and 3 patients with pleural metastases of other primaries. RNA was extracted from FFPE specimens and the 10 novel candidates as well as RNU48 as endogenous reference gene were detected by RT-qPCR. Independent or paired samples t-test was used to evaluate statistical significance of observed expression differences.

Results:
In this extended patient series, we could confirm our initial findings reported at WCLC 2021 regarding significantly higher expression of four of the novel mpm-microRNAs in chemo-naïve MPM tumours as compared to non-MPM controls. Specifically, we found significantly higher levels for mpm-miR-136 (6.1-fold, $p<0.001$), mpm-miR-72 (4-fold, $p=0.011$), mpm-miR-18 (4.3-fold, $p>0.001$), and mpm-miR-58 (5.6-fold, $p>0.001$). Furthermore, in the diagnostic, chemo-naïve specimens we could observe a trend towards higher expression in biphasic tumors (N=6) as compared to epithelioid tumours (N=26), which reached statistical significance for mpm-miR-136 (relative expression: 30.72 vs 10.28, $p=0.043$). In post-chemotherapy samples, this expression difference between epithelioid and non-epithelioid tumours could not be observed. When comparing chemo-naïve and chemo-treated tumour specimens small expression differences with slightly higher levels before chemotherapy were not statistically significant. Of the three non-MPM cases that showed levels of all four microRNAs comparable to those in MPM tumours, two were pleural metastases of lung adenocarcinomas.

Conclusion:
Findings from this extended patient series confirm the potential diagnostic value of novel mesothelioma-specific microRNAs in MPM. While chemotherapy does not appear to alter levels of these microRNAs, higher expression levels in biphasic tumours suggest an association between expression and histological subtype. The finding of higher expression in pleural metastases of lung cancer cases requires further investigations. Based on our present data, analyses in additional samples, including primary lung cancer cases is warranted and currently underway.

490

D. Schibler[4], A. Landsmann[3], P. Wolint[4], F. Starsich[1], I. Hermann[2], M. Calcagni[4], J. Buschmann[4], A. Boss[3]

Biodistribution of iron carbide nanoparticles in the living developing chicken embryo using magnetic resonance imaging

ETH Zurich, Nanoparticle Systems Engineering Laboratory, Department of Mechanical and Process Engineering[1], Laboratory for Particles Biology Interactions, Swiss Federal Laboratories for Materials Science and Technology (EMPA)[2], University Hospital Zurich, Institute of Diagnostic and Interventional Radiology[3], University Hospital Zurich, Plastic Surgery and Hand Surgery[4]

Introduction:
Magnetic nanoparticles (MNPs) serve in a wide array of biomedical applications, such as drug delivery, blood purification and hyperthermia cancer treatment, as well as magnetic resonance imaging (MRI). Especially iron-based nanoparticles may be used as contrast agents in magnetic-resonance imaging, among which iron carbide compounds seem to have especially favorable characteristics. However, these small particles easily penetrate the placenta, posing as a potential threat to embryological development. The aim of this study is to investigate a possible biodistribution of intravenously injected iron carbide nanoparticles (ICNPs) in chicken embryos, using MRI with T2-weighted sequences, histological analysis, and electron microscopy. This shall lead to a better understanding of the potential risks of ICNPs on embryogenesis.

Methods:
600 µg (high dose) or 300 µg (low dose) of ICNPs produced by flame spray pyrolysis were applied through the blood vessels visible on the chorioallantoic membrane (CAM) of 5-7 days old chicken embryos (18 subjects, Hamburger-Hamilton (H&H) stages 22-26) using self-made glass needles, pulled from capillaries. Subsequent fixation with formalin was done 24 h later, with some of the embryos having died sometime before. All fixated embryos later underwent high-resolution T2-weighted imaging in a 4.7 T small animal MRI using a 1 H mouse transmit-receive coil.

For both doses of ICNPs, three chicken embryos for each H&H stage 24, 25 and 26 were chosen for further analysis in this study. A more precise qualitative assessment of the MRI signal was then done, and they were histologically checked for ICNP deposits with Hematoxylin&Eosin and Masson Goldner Trichrome staining. Furthermore, single particle sensitivity electron microscopy was performed to visualize possible intracellular ICNP uptake.

Results:
In 7 (4 high dose, 3 low dose) of the embryos looked at in the T2-weighted sequences, strong signal void artifacts were visible, likely caused by the ICNP deposits. In 5 (1 high dose, 4 low dose) embryos, signal void artifacts were also visible, although less strong. In 6 (1 high dose, 5 low dose) embryos little to no void artifacts could be detected in the MRI. In the embryos with strong void artifacts, no clear demarcation of the regions with the ICNP deposits could be determined, as the void signals overlap. However, all the following organs appear to have deposits: The brain, retina, neural tube, heart, liver, mesonephros and the midgut. In the group with the less strong void artefacts, all embryos showed deposits in the brain, retina, and neural tube. Three of them additionally showed deposits in the heart and liver, and one each in additionally only the liver and only the heart. Intercellular ICNP deposits in the mentioned locations could also be confirmed in most histological slices and intracellular deposits were also hinted at in bright field microscopy. The Electron microscopy could confirm some of the intracellular deposits assumed during the histological assessment.

Conclusion:
The ICNPs, which enter the embryo via the vitelline vein, are distributed in the embryonic body through the vascular system and can be histologically found inside and close to blood vessels and the intercellular space of the retina, brain, neural tube, heart, liver, and mesonephros. As can be seen with electron microscopy, various cells are able to take up the ICNPs into the intracellular space, where they can potentially hamper with the embryonic development. The chicken embryo might be a suitable model to investigate toxic embryonic effects of theragnostic agents. In this case, the ICNPs may be declared unsafe to administer in pregnancy. Further studies need to be done, to determine the effect of ICNPs on mesenchymal cells found in embryological development.

491

J. Rieber[5], M. Gabriella[5], I. Miescher[5], F. Weber[3], P. Wolint[5], M. Zenobi-Wong[2], Y. Yang[1], E. Ongini[4], J. Snedeker[4], M. Calcagni[5], J. Buschmann[5]

Bioactive electrospun polymer tubes releasing IGF-1 for tendon repair

ETH Zurich, Department of Health Sciences & Technology & Department of Materials[1], ETH Zurich, Tissue Engineering and Biofabrication Group, Department of Health Science and Technology[2], Oral Biotechnology & Bioengineering, Center for Dental Medicine, Cranio-Maxillofacial and Oral Surgery, University of Zurich[3], University Clinic Balgrist, Orthopaedic Biomechanics[4], University Hospital Zurich, Plastic Surgery and Hand Surgery[5]

Introduction:
The majority of musculoskeletal injuries are tendon ruptures. The incidence of Achilles tendon rupture lies around 18 patients per 100,000 patients annually [1]. The healing process of tendons has some major drawbacks, like adhesion formation to surrounding tissue and rerupture [2]. Overall, the tendons do mostly not recover to initial functionality even with the newest approaches. GFs like IGF-1 and PDGF-BB play an important role during the process of tendon healing, which can take up to several months [3].

[1] Shamrock, A.G. and M. Varacallo, Achilles Tendon Rupture, in StatPearls. 2022: Treasure Island (FL).

[2] Ayhan, E., Z. Tuna, and C. Oksuz, Getting Better Results in Flexor Tendon Surgery and Therapy. Plast Reconstr Surg Glob Open, 2021. 9(2).

[3] Chartier, C., et al., Tendon: Principles of Healing and Repair. Semin Plast Surg, 2021. 35(3): p. 211-215.

Voleti, P.B., M.R. Buckley, and L.J. Soslowsky, Tendon Healing: Repair and Regeneration. Annual Review of Biomedical Engineering, Vol 14, 2012. 14: p. 47-71.

Methods:
A polymer tube made of Degrapol® (DP) was produced by electrospinning to be applied over a ruptured and sutured tendon to decrease adhesion formation and also increase tendon strength by incorporating IGF-1 into the scaffold. The tubes were characterized by scanning electron microscopy, Fourier transform infrared spectrometry and Differential scanning calorimetry. The water contact angle and mechanical properties of the scaffolds were assessed. With ELISA, the release of IGF-1 and was measured over time. The bioactivity of native IGF-1 and released IGF-1 was assessed by alamar blue, and the gene expression of Col1, ki-67 and tenomodulin by real time PCR was measured on day 1 and day 3.

Results:
The growth factor release kinetic shows a burst release of IGF-1 over the initial 4 h followed by a slow and steady release for up to 42 days. The incorporation of IGF-1 into the tube did not impair mechanical properties, but rather improved its mechanics. The other characterization methods could not detect a significant difference between pure DP and emulsion DP tube. Supplementation with 1 ng/ml of native IGF-1 resulted in an increased relative gene expression of Col1 at day 3 in rabbit Achilles tenocytes. Moreover, tenomodulin and ki-67 expression were also increased on day 3 compared to higher concentrations of IGF-1, such as 10 and 100 ng/ml, respectively.

Conclusion:
The emulsion electrospun DP tubes with IGF-1 were produced and characterized. They can now be used for in vivo experiments. We showed that the addition of GF had a positive effect on mechanical properties. IGF-1 did not show any negative effect on cell metabolism and increased the gene expression of Col1, ki-67 and tenomodulin when applied to rabbit tenocytes. Based on these results, the bioactive tubes can be produced reproducibly and tested in in vivo models for tendon ruptures.

492

S. Shim[1, 2], B. Karol[1], A. Ciritsis[1, 2], C. Rossi[1, 2], C. Ruppert[1, 2], A. Boss[2]

Radiation dose prediction for spiral breast CT using Monte Carlo simulation and machine learning model

b-rayz[1], University Hospital Zurich[2]

Introduction:
Spiral breast CT was applied for a clinical trial for the first time in 2018 at University Hospital Zurich. Now, it is adopted by several institutes around the world and widely used for opportunistic and diagnostic breast examinations. Yet, the standard radiation dose of the imager is not specified, and the dose given to patients during the scan cannot be evaluated on site. Especially, because the dose exposure of breast CT is not automatically controlled, such evaluation is important for dose optimization. This study aimed to evaluate the standard dose level for spiral breast CT and to estimate the radiation dose for individual patients.

Methods:
1For the retrospective dose analysis, 1,037 spiral breast CT images were used. The study was approved by the local ethics committee. The breast images were segmented by an in-house developed automatic segmentation method using adapted computer vision methods. [1] Monte Carlo (MC) radiation dose simulations were performed on the resulting segmented dataset. The dose simulation was validated based on the comparison of weighted CT dose index (CTDI) values to CTDI phantom measurements. [2] Five morphological features of breasts – breast volume, diameter, length, density, and skin volume – were measured on the segmented images. Five dose values – mean absorbed dose in the breast, mean glandular dose, mean skin dose, max 5% glandular dose, and max 5% skin dose – were calculated based on the simulated dose distribution using segmentation masks. The correlation of the dose values to the features were evaluated by Spearman's rank correlation coefficients. Different machine learning prediction models were applied to the datasets with the corresponding finely tuned hyper parameters by brute force search. The accuracy of the predictions was compared based on R2 scores in 10-fold cross validation.

[1] S. Shim, D. Cester, L. Ruby et al., "Fully Automated Breast Segmentation on Spiral Breast Computed Tomography Images," Journal of Applied Clinical Medical Physics, vol. e13726, 2022.

[2] S. Shim, N. Saltybaeva, N. Berger et al., "Lesion Detectability and Radiation Dose in Spiral Breast CT With Photon-Counting Detector Technology: A Phantom Study," Investigative Radiology, vol. 55, no. 8, pp. 515-523, 2020.

Results:
According to the correlation coefficients, Breast volume, diameter, length, and skin volume were relevant to dose value prediction according to the correlation coefficients. When all four features were applied, all of which can be acquired from segmented images, support vector regressor model with radial basis function kernel resulted in the most accurate prediction results. R2 of the test sets scored on average 0.98, 0.88, 0.79, 0.82, and 0.93 for mean absorbed dose, mean glandular dose, mean skin dose, max glandular dose, and max skin dose, respectively. When only a single feature was applied for the prediction, which can be easily measured on site, such as breast length, (bi-)exponential models could predict the five dose values with R2 scores ranging 0.57-0.87. [3]

[3] Shim, S, Kolditz, D, Steiding, C, et al. Radiation dose estimates based on Monte Carlo simulation for spiral breast computed tomography imaging in a large cohort of patients. Med Phys. 2023; 1- 12.

Conclusion:
We established radiation dose prediction models for spiral breast CT. Using the models, the radiation dose values delivered to individual patients can be accurately evaluated on site without a time-consuming dose simulation. The key dose values can be estimated even prior to a scan.

493

H. Seth-Smith[7], E. Badell[6], A. Berger[2], M. Blaschitz[1], J. D'Aeth[9], A. Dangel[2], K. Fabiánová[8], N. Fry[9], F. Imkamp[7], V. Hinic[7], A. Indra[1], G. Jost[4], N. Liassine[4], K. Lippert[1], D. Litt[9], G. Martinetti[5], T. Roloff[7], S. Schindler[1], S. Seiffert[3], A. Sprenger[2], J. Zavadilová[8], O. Nolte[3], S. Brisse[6], S. Pleininger[1], A. Sing[2], A. Egli[7]

Ongoing European outbreak of Corynebacterium diphtheriae among asylum seekers: situational report illuminated through whole genome sequencing

AGES, Vienna[1], Bavarian Health and Food Safety Authority[2], Center for Laboratory Medicine, St. Gallen[3], Dianalabs, Geneva[4], EOC, Bellinzona[5], Institut Pasteur[6], Institute of Medical Microbiology, University of Zurich[7], National Institute of Public Health, Prague[8], Respiratory and Vaccine Preventable Bacteria Reference Unit, UK Health Security Agency[9]

Introduction:
Increased numbers of cases of *Corynebacterium diphtheriae* have been observed in Europe since summer, predominantly among asylum seekers from Afghanistan. The ECDC have issued warnings since August 2022. Most cases are of cutaneous diphtheria, with some respiratory cases also reported. We aimed to investigate the relatedness of the strains responsible for this outbreak at the genomic level.

Methods:
Wound and nasopharyngeal swabs samples were taken from patients and contacts, predominantly asylum seekers in centers across Europe. Sporadic unrelated isolates were added for context. Isolates underwent WGS, using Illumina platforms. Data assembled using unicycler v0.4.8 was analysed within Ridom Seqsphere v8.4.1 using a cgMLST scheme (1,553 core genes). Database genomes (n=1029), included all from 2022 (NCBI) and all from key sequence types (STs; https://bigsdb.pasteur.fr/diphtheria). SNP analysis on cgMLST clusters used CLC Genomics Workbench v 22.0.2. Abricate (VFDB/NCBIAMRFinderPlus) identified genes encoding diphtheria toxin *tox*, adherence factor *spaABC* and *blaOXY-2*.

Results:
We analysed newly available data from 2022 from Switzerland, Germany, and Austria (n=68, 50, 40, respectively) in a global context. 87% (138/158) encoded *tox*, 97% (153/158) *spaABC*, and 8% (12/158) *blaOXY-2*. cgMLST analysis identified four clusters containing >10 genomes: ST377 (n=47, *tox*+, *spaABC*+, *blaOXY-2*-), ST574 (n=46, *tox*+, *spaABC*+, *blaOXY-2*-), ST384 (n=46, *tox*+/-, *spaABC*+, *blaOXY-2*-) and ST377 (n=12, *tox*+, *spaABC*+, *blaOXY-2*+) (Figure). Isolates from all three countries were found in all these clusters. No relevant connections to genomes from databases were found. Detailed SNP analysis within the four largest clusters showed pairwise SNP distances of 0-13 SNPs.

Conclusion:
Increasing *C. diphtheriae* case numbers among asylum seekers over the past few months is a cause for concern, particularly considering the presence of the identified virulence factors. The existence of several diverse clusters with different STs suggests several independent introductions and transmission chains. This abstract represents an outlook and will be updated including data from the UK, France and Czech Republic for final presentation. Additionally, the close relatedness within clusters suggests recent transmissions, possibly occurring during travel and within asylum seeker facilities. To reduce transmission, we recommend improving awareness among migrants and physicians, thorough vaccination protocols, and diagnosing symptomatic persons.

494

L. Heeb[1], L. Russo[1], E. Breuer[1], PA. Clavien[1], A. Gupta[1]

Perioperative immunotherapy controls tumor growth in the regenerating liver

Department of Visceral Surgery and Transplantation[1]

Introduction:
Due to the livers remarkable capacity to regenerate, the gold standard to treat liver cancer is the surgical resection of tumors (hepatectomy). However, if the future liver remnant is too small, regeneration is impaired and consequently leads to liver failure, thus limiting intervention at advanced cancer stages. Furthermore, during regeneration, unresectable occult micrometastases can start to regrow leading to cancer relapse, probably due to the growth-inducing microenvironment of the regenerating liver. Therefore, tumor-targeting treatments that do not impair liver regeneration are needed. Here we use tumor-specific immunotherapies during the perioperative window after cancer resection in a murine liver regeneration and tumor model. Overall, this project aims to prevent cancer relapse during liver regeneration.

Methods:
To study tumor growth during liver regeneration, we developed a two-step surgical mouse model that combines the selective syngeneic tumor cell injection into the portal vein with partial hepatectomy. In the first step, the selective clamping of the left and median lobes during tumor cell injection enables the restriction of tumor growth to the right and caudate lobe. After a 4 day healing period in which micrometastases can manifest, subsequent resection of the left and median lobe (68% hepatectomy) elicits liver regeneration.This model is suitable to study the dynamics of cancer relapse due to regenerative processes in the liver and allows us to administer novel therapeutic interventions to treat liver tumors during liver regeneration after resection in the preclinical mouse model.

Results:
Liver metastases grow faster after partial hepatectomy and blocking of PD-1, PD-L1 and LAG-3 does not impair liver regeneration. Furthermore, administration of anti-PD-1 and anti-LAG-3 antibodies during liver regeneration in micrometastases-carrying mice reduces tumor growth.

Conclusion:
Our data suggests that the immunomodulatory molecules PD-1, PD-L1 and LAG-3 can be safely targeted during liver regeneration, which decreases tumor size in the murine model and a change of the immune compartment in the tumor microenvironment.

495

jJ. Hench[1], D. Mihic-Probst[2], A. Agaimy[3], M. Massi[4], M. Mandala[5]

Comprehensive molecular profiling of dedifferentiated cutaneous melanomas reveals extensive epigenetic reprogramming

1. Institute of Medical Genetics and Pathology, Division of Neuropathology, University Hospital Basel, Basel, Switzerland[1], 2. Institute of Pathology and Molecular Pathology, University Hospital Zurich, University of Zurich, Zurich, Switzerland[2], 3. Institute of Pathology, Friedrich-Alexander-University Erlangen-Nürnberg, University Hospital, Erlangen, Germany[3], 4. Section of Pathology, Department of Health Sciences, University of Florence, Florence, Italy[4], University of Perugia, Unit of Medical Oncology, Santa Maria della Misericordia Hospital, Perugia, Italy[5]

Introduction:
Dedifferentiated melanoma (DedM) poses significant diagnostic challenges. Apart from the primary driver mutations, no specific genetic alterations are found in DedM. We aimed to investigate the methylation signature (MS) and the copy number profile (CNP) of clinically annotated primary and metastatic specimens from patients with DedM.

Methods:
A retrospective series of 78 formalin-fixed, paraffin-embedded samples of 61 DedM from patients retrieved from EORTC Melanoma Group centers were reviewed by three experienced dermatopathologists. Clinical and histopathological features were retrieved and analysed. In a subgroup of patients, genotyping through Infinium Methylation EPIC microarray (Illumina), and CNP analysis was carried out.

Results:
MS could be obtained for 18/61 (30%) patients. Of these, 11/18 patients (61%) had at least one tumor specimen that lost the cutaneous melanoma DNA MS while a retained MS was present in at least one specimen of 7/18 patients (39%). CNP could be obtained in parallel from 18 patients and exhibited changes typical of cutaneous melanoma in 12/18(67%) patients, and in the remaining cases, melanoma MS, clinical features, or sequence alterations were suggestive of melanoma. Of note, one melanoma lymph node metastasis examined demonstrated simultaneously melanoma MS in the lymph node parenchyma and conventional osteosarcoma in its extranodal involvement whereas under treatment the signature kept aligning with osteosarcomas. An independent patient exhibited a Malignant Peripheral Nerve Sheath Tumor MS in neoplastic subpopulations while a metastasis occurring three years later after immunotherapy solely exhibited a melanoma methylation profile.

Conclusion:
MS and genomic CNP can help pathologists to diagnose DedM in a large proportion of patients. We provide proof of concept that epigenetic modifications may be associated with dedifferentiation in melanoma.

497

R. Staeger[2], A. Tastanova[2], A. Ghosh[1], E. Ramelyte[2], N. Winkelbeiner[2], V. Haunerdinger[2], P. Shukla[2], P. Cheng[2], P. Turko[2], I. Kolm-Djamei[2], MP. Levesque[2], R. Dummer[2], B. Meier-Schiesser[2]

Tebentafusp induces activation and proliferation of cytotoxic T cells and downregulation of melanin synthesis in the skin of uveal melanoma patients

Functional Genomics Center Zurich, University of Zurich and ETH Zurich, Switzerland[1], University Hospital Zurich, Department of Dermatology, Switzerland[2]

Introduction:
Tebentafusp is a novel bispecific molecule redirecting T cells against gp100 (a melanocytic antigen) expressing cells, approved for metastatic uveal melanoma. Skin adverse events (incl. maculopapular rash, depigmentation) are frequent and were shown to be an off-tumor/on-target effect against gp100+ epidermal melanocytes. Thus, analysis of tebentafusp-induced cellular and molecular processes in patient skin samples may improve mechanistic understanding.

Methods:
Skin biopsies from patients treated with tebentafusp were collected at baseline and development of skin rash (n=11), as well as from depigmented areas (n=5). Spatial analysis was performed by histology and multiplex immunohistochemistry (7-plex, Akoya Opal). On paired baseline and rash samples skin samples from three patients, single cell RNA sequencing was conducted. Furthermore, proliferation of T cell subsets (naïve and memory of each CD4+ and CD8+) treated with tebentafusp or anti-CD3 antibody was assessed in vitro (3 healthy donors).

Results:
Rash showed increased numbers of CD4+ and CD8+ T cells and upregulated markers of activation/proliferation (*IFNG, GZMB, IL2RA, MKI67*) in the T cells. Tebentafusp's capacity to induce T cell proliferation was validated in vitro, predominantly in the CD8 memory subset, in contrast to the unselective effect observed by a high affinity anti-CD3 antibody. Recruitment of monocyte-derived M1-like macrophages and plasmacytoid dendritic cells (DC) was found. Interestingly, increased activity in regulatory T cells and immunoregulatory DC suggested early homeostatic regulation. Melanocytes were significantly reduced in rash and they upregulated interferon type I/II responses and antigen presentation, while melanin pigment synthesis was downregulated, resulting in an increased fraction of gp100-negative melanocytes.

Conclusion:
Longitudinal skin biopsies are a promising and minimally-invasive tool to study the pharmacodynamics of anti-melanocytic bispecifics. The skin microenvironment on tebentafusp treatment is characterized by T cell proliferation and cytotoxic activity, recruitment of myeloid cells as well as downregulation of the target gp100 in melanocytes and their partial loss in affected skin areas.

498

SN. Hobbie[3], S. Radmer Almind[1], JU. Hansen[2], M. Plattner[3], K. Haldimann[3], C. Vingsbo Lundberg[2], N. Frimodt-Møller[1]

Susceptibility of blood-culture isolates to apramycin and in-vivo efficacy against nine Escherichia coli and Klebsiella pneumoniae isolates in a mouse peritonitis model

Rigshospitalet Copenhagen[1], Statens Serum Institute[2], University of Zurich[3]

Introduction:
Bloodstream infections (BSIs) are a leading cause of sepsis, which is a life-threatening condition that significantly contributes to the mortality of bacterial infections. Aminoglycoside antibiotics such as gentamicin or amikacin are essential medicines in the treatment of BSIs, but their clinical efficacy is increasingly being compromised by antimicrobial resistance. The aminoglycoside apramycin has demonstrated preclinical efficacy against aminoglycoside-resistant and multidrug-resistant (MDR) Gram-negative bacilli (GNB) and is currently in clinical development for the treatment of critical systemic infections.

Methods:
We analyzed the genomes of 26 493 blood culture isolates in the NCBI National Database of Resistance Organisms (NDARO) for genotypic resistance to carbapenems, aminoglycosides, and colistin. The in-vivo efficacy of apramycin was studied in a mouse peritonitis model with wild-type and carbapenemase-expressing *E. coli* and *K. pneumoniae* clinical isolates.

Results:
Resistance gene annotations suggested genotypic aminoglycoside resistance in 85% of all 2761 carbapenem-resistant Enterobacterales blood-culture isolates, in comparison to 59% of colistin and only 4% of apramycin resistance. A single dose of 5 to 13 mg/kg, corresponding to an AUC of roughly 20 h*µg/mL in mice, resulted in a 1-log CFU reduction in the blood and peritoneum. Two doses of 80 mg/kg, resulting in an exposure that resembles the AUC observed for a single 30 mg/kg dose in humans, resulted in complete eradication of an MDR bacteremia at > 10^6 CFU/mL. In contrast, the bacterial burden in mice receiving the same dosing regimen of amikacin was not significantly different from that in the vehicle control group.

Conclusion:
Encouraging coverage of carbapenem-resistant GNB and potent in-vivo efficacy against a selection of highly drug-resistant Enterobacterales isolates in the mouse peritonitis model warrants further consideration of apramycin as a drug candidate for the treatment and prophylaxis of BSI.

499

E. Parietti[1], A. Gomez Mejia[1], C. Chun-Chi[1], S. Mairpady Shambat[1], A. Zinkernagel[1]

Investigating the effect of rifampicin on macrophage response during Staphylococcus aureus infection

Department of Infectious Diseases and Hospital Epidemiology, University Hospital Zurich, University of Zurich, Zurich, Switzerland[1]

Introduction:
Staphylococcus aureus is one of the major causes of both community and hospital associated infections, ranging from superficial skin lesions to life-threatening infections such as bacteremia and pneumonia to chronic/recurrent infections, including endocarditis and osteomyelitis. Infections with *S. aureus* are very difficult to treat, not only due to the development of antibiotic resistance, but also because of the formation of so-called persister cells. Persisters are a subpopulation of bacteria in a dormant phase that can survive high concentrations of antibiotics. It has been observed that the intracellular milieu of the host cells can trigger the formation of *S. aureus* non-stable small colonies (nsSCs) which have been associated to an increase in persistence. In this context, macrophages represent a privileged niche for *S. aureus* persistence. Therefore, the failure to completely eradicate persisters can result in relapse of infections when persisters resume growth upon removal of antibiotic treatment. Rifampicin in an antibiotic that can penetrate the host cells and target intracellular bacteria. It is also known to have immunomodulatory properties, and interact with host immune cells altering mitochondrial function, bioenergetics and immune cell function. In this project, we study the effect of rifampicin during *S. aureus* infection of macrophages, investigating the effect of the drug on macrophage activation and effector response and the effectiveness of rifampicin in eradicating intracellular *S. aureus* persisters.

Methods:
Human monocyte-derived macrophages (hMDMs) were infected with *S. aureus* and different combinations of antibiotics (flucloxacillin and rifampicin, alone or in combination) were used to treat macrophages after the infection along with rifampicin pre-treatment. First, we determined *S. aureus* uptake by macrophages and the kinetic of intracellular survival, making a comparison among different antibiotic treatments. In addition, we assessed *S. aureus* persister formation inside macrophages by measuring colony size heterogeneity using automated plates imaging and the ColTapp software. In a second step, we performed a multi-parametric flow cytometry analysis to measure the intracellular reactive oxygen spices (ROS) and reactive nitrogen spices (RNS), antimicrobial molecules used by macrophages, which were recently found to play a role in the generation of intracellular persisters.

Results:
We found that pre-treatment of macrophages with rifampicin increased the phagocytosis of *S. aureus* by macrophages and reduced the intracellular killing capacity against *S. aureus*. At the same time, the pre-treatment of macrophages with rifampicin reduced intracellular *S. aureus* nsSCs, which were associated with an increase in persistence. Our flow cytometry data showed that pre-treatment of macrophages with rifampicin dampened intracellular RNS production upon infection, while we did not find any significant difference in ROS production.

Conclusion:
Our data show that rifampicin exposure of macrophages before *S. aureus* infection altered the capacity of the cells to respond to bacteria. Specifically, exposure of macrophages with rifampicin had an effect on the phagocytosis of *S. aureus*, intracellular killing capacity and nsSC formation. The decrease in intracellular killing and nsSC formation could be a consequence of the inhibition of RNS production in macrophages following rifampicin treatment. Indeed, RNS are known to have an antimicrobial function and, more recently, they were found to be involved in *S. aureus* persistence inside macrophages. Nevertheless, further investigations are needed to verify these results. Considering the prominent role of *S. aureus* persistence in antibiotic treatment failure, this translational project has the potential to advance the current understanding as well as develop new strategies aimed to curb recurrent *S. aureus* infections.

500

J. Müller[2], L. Mayer[2], S. Schneider[2], A. Titz[2], E. Schwarz[2], S. Saxer[2], M. Furian[2], E. Grünig[1], S. Ulrich[2], M. Lichtblau[2]

Pulmonary arterial wedge pressure increase during exercise in patients with pulmonary vascular disease

Thoraxklinik Heidelberg gGmbH[1], University Hospital Zurich, Department of Pulmonology[2]

Introduction:
We investigated the course of pulmonary arterial wedge pressure (PAWP) during exercise in patients with pulmonary vascular disease (PVD) defined as pulmonary arterial or chronic thromboembolic pulmonary hypertension (PAH/CTEPH).

Methods:
Right heart catheter (RHC) data including PAWP, recorded during semi-supine, stepwise cycle exercise in patients with PVD were analysed retrospectively. We investigated PAWP-changes during exercise until end-exercise.

Results:
In 121 patients (49 female, 66 CTEPH, 55 PAH, 61.5 ± 16.5 years) resting PAWP was 10.2 ± 4.1 mmHg. Corresponding peak changes in PAWP during exercise were +2.9 mmHg (95% CI: 2.1 to 3.7 mmHg, $p<0.001$). Patients ≥50 years had a significantly higher increase in PAWP during exercise compared with <50 years ($p<0.001$). The PAWP/CO-slopes were 3.9 WU for all patients, and 1.6 WU for patients <50 years and 4.5 WU ≥ 50years.

Conclusion:
In patients with PVD, PAWP increased slightly but significantly with the onset of exercise compared to resting values. The increase in PAWP during exercise was age-dependent, with patients ≥50 years showing a rapid PAWP increase even with minimal exercise. PAWP/CO slopes >2 WU are common in patients with PVD ≥50 years without exceeding the PAWP of 25 mmHg during exercise.

501

M. Houtman[2], R. Micheroli[2], K. Bürki[2], S. Edalat[2], M. Frank Bertoncelj[2], C. Pauli[1], O. Distler[2], C. Ospelt[2], M. Elhai[2]

Deciphering the synovial tissue and fibroblast subsets in systemic sclerosis

Department of Pathology, University Hospital Zurich, Switzerland[1], Department of Rheumatology, University Hospital Zurich, University of Zurich, Switzerland[2]

Introduction:
Articular involvement is underestimated in systemic sclerosis (SSc), but represents a major cause of disability and is a marker of disease severity. There is no approved effective therapy for arthritis in SSc and immunosuppressive treatments are given to SSc patients by analogy with rheumatoid arthritis (RA), but with limited effect. The last few years have revolutionized the understanding of the pathogenesis of RA by deciphering the heterogeneity of synovium at both the tissue and molecular levels. Nevertheless, the pathogenesis of joint involvement in SSc remains largely unknown. We aimed to characterize the synovium in SSc at tissue and cellular levels and to compare it with RA synovium.

Methods:
Twelve consecutive SSc patients from the Zurich cohort having joint synovitis were included in this exploratory study. Patients with overlap with other autoimmune rheumatic diseases were excluded. Synovial tissues (11 wrists/finger, 1 knee) were obtained by ultrasound-guided biopsy and were compared to those obtained from six RF and CCP positive RA patients (4 wrists, 3 knees). Tolerance of the procedure was assessed after 3-5 days. Histological analysis of the synovium determined the Krenn synovitis score (0-9) and stratified the synovial tissue according to previously published histological features. One biopsy, without synovial tissue, was not processed further. ScRNA-seq libraries of 6 SSc and 6 RA synovium were prepared with 10X Genomics technology and sequenced on NovaSeq 6000. Integrated bioinformatics analysis used Cell Ranger and Seurat software. Overexpressed genes were selected using log2 ratio (>1 and <-1) and p value < 0.05 after adjustment by false discovery rate.

Results:
Of the twelve SSc-patients, 8 were women, median age was 65 [IQR: 60-71] years, median disease duration was 2.2 [0.4-6.5] years and 2 had diffuse cutaneous subtype. In the RA cohort, 5/6 were women, median age was 57 [54-63] years and median disease duration 7 [5.4-15.4] years. Synovial biopsy was well-tolerated by all the patients. Krenn synovitis score was lower in SSc as compared to RA across the three components of the synovitis score (lining layer, stroma and inflammatory infiltrate). In SSc, 10/11 (91%) biopsies were characterized by a pauci-immune pathotype, whereas in RA 3/7 (43%) were pauci-immune. Due to the low inflammatory pauci-immune pathotype in all but one SSc patients, we focused the scRNA sequencing analysis on synovial fibroblasts (SF) (number of SF studied: 4761 in SSc and 6059 in RA). We identified five clusters of SF with respective marker genes: SF CXCL12+, SF PRG4+, SF POSTN+, SF MFAP5+ and SF CHI3L2^{+}. Comparison between SSc and RA SF subtypes showed differences in the proportion of the clusters between both diseases. 1193 (p adj <0.05) genes were differentially expressed between SSc and RA SF. Pathway enrichment analysis of these 1193 genes identified interferon α and γ signaling pathways as the most enriched in SSc SF.

Conclusion:
Synovitis in SSc differs from RA synovitis both at histological and molecular levels. By highlighting the low inflammatory nature of the synovium and the enrichment in interferon signaling pathways in SSc SF, our study questions the use of the same immunosuppressive therapies in RA and SSc. These results are the basis for the development of specific targeted therapies for arthritis in SSc.

502

D. Voci[4], A. Götschi[5], U. Held[5], R. Bingisser[11], G. Colucci[15], D. Duerschmied[6], R.M. Fumagalli[4], B. Gerber[3], B. Hasse[8], D.I. Keller[12], S.V. Konstantinides[2], F. Mach[1], S.K. Rampini[10], M. Righini[9], H. Robert-Ebadi[9], T. Rosemann[14], S. Roth-Zetzsche[4], T. Sebastian[4], N.R. Simon[11], D. Spirk[13], S. Stortecky[7], L. Vaisnora[7], N. Kucher[4], S. Barco[2, 4]

Enoxaparin for outpatients with COVID-19: 90-day results from the randomised, open-label, parallel-group, multinational, phase III OVID trial

Cardiology Division, Geneva University Hospital, Geneva, Switzerland[1], Center for Thrombosis and Hemostasis, University Medical Center of the Johannes Gutenberg University Mainz, Mainz, Germany[2], Clinic of Hematology, Oncology Institute of Southern Switzerland, Ente Ospedaliero Cantonale, Bellinzona, Switzerland[3], Department of Angiology, University Hospital Zurich, Zurich, Switzerland[4], Department of Biostatistics at Epidemiology, Biostatistics and Prevention Institute, University of Zurich, Zurich, Switzerland[5], Department of Cardiology, Angiology, Haemostaseology and Medical Intensive Care, University Medical Centre Mannheim, Medical Faculty Mannheim, Heidelberg University, Germany[6], Department of Cardiology, Inselspital Bern, University of Bern, Bern, Switzerland[7], Department of Infectious Diseases and Hospital Epidemiology, University Hospital Zurich, Switzerland[8], Division of Angiology and Hemostasis, Department of Medicine, Geneva University Hospitals and Faculty of Medicine, Geneva, Switzerland[9], Division of Internal Medicine, University Hospital Zurich, Zurich, Switzerland[10], Emergency Department, University Hospital Basel, Basel, Switzerland[11], Emergency Department, University Hospital Zurich, Zurich, Switzerland[12], Institute of Pharmacology, University of Bern, Bern, Switzerland[13], Institute of Primary Care, University of Zurich, Zurich, Switzerland[14], Service of Hematology, Clinica Luganese Moncucco, Lugano, Switzerland[15]

Introduction:
The benefits of early thromboprophylaxis in symptomatic COVID-19 outpatients remain unclear. We present the 90-day results from the randomised, open-label, parallel-group, investigator-initiated, multinational OVID phase III trial.

Methods:
Outpatients aged 50 years or older with acute symptomatic COVID-19 were randomised to receive enoxaparin 40 mg for 14 days once daily vs. standard of care (no thromboprophylaxis). The primary outcome was the composite of untoward hospitalisation and all-cause death. Secondary outcomes included arterial and venous major cardiovascular events. The study was prematurely terminated based on statistical criteria after the analysis of 30-day data, which has been previously published. In the present analysis, we present the final, 90-day data from OVID and we additionally investigate the impact of thromboprophylaxis on symptoms resolution.

Results:
Of the 472 patients included in the intention-to-treat population, 234 were randomised to receive enoxaparin and 238 no thromboprophylaxis. Median age was 57 (Q1-Q3: 53-62) years and 217 (46%) were women. The 90-day primary outcome occurred in 11 (4.7%) patients of the enoxaparin arm and in 11 (4.6%) controls (adjusted relative risk 1.00; 95%CI: 0.44-2.25): 3 events per group occurred after day 30. The 90-day incidence of cardiovascular events was 0.9% in the enoxaparin arm vs. 1.7% in controls (relative risk 0.51; 95%CI: 0.09-2.75). Individual symptoms improved progressively within 90 days with no difference between groups. At 90 days, 42 (17.9%) patients in the enoxaparin arm and 40 (16.8%) controls had persistent respiratory symptoms.

Conclusion:
In adult community patients with COVID-19, early thromboprophylaxis with enoxaparin did not improve the course of COVID-19 neither in terms of hospitalisation and death nor considering COVID-19-related symptoms.

503

A. Balic[4], D. Perver[2], P. Pagella[4], H. Rehrauer[3], B. Stadlinger[1], V. Vogel[2], TA. Mitsiadis[4]

Extracellular matrix remodelling in dental pulp upon carious lesion through the prism of single-cell analysis

Clinic of Cranio-Maxillofacial and Oral Surgery, University of Zurich, University Hospital Zurich[1], Department of Health Sciences and Technology, Institute of Translational Medicine, ETH Zurich[2], Functional Genomics Center Zurich, ETH Zurich and University of Zurich[3], Orofacial Development and Regeneration, Institute of Oral Biology, Center of Dental Medicine, University of Zurich[4]

Introduction:
Carious lesion is a bacteria caused destruction of tooth mineralized matrices that, if untreated, leads to pulp necrosis. The course of carious lesion is marked by molecular and cellular changes in the underlying pulp tissue, which include reparative and immune responses that determine the outcome of carious lesion. While major molecular players in the carious lesion have been uncovered, a detailed map of the molecular and cellular landscape of carious lesion is missing.

Methods:
In this study we used single cell RNA sequencing (scRNAseq) and immunostaining analyses to generate a high-resolution map of the dental pulp tissue microenvironment in carious lesion.

Results:
Our data demonstrate a higher proportion of immune cells expressing IL-1B, IL-7, IL-16 and IL-18 in carious lesion. This was accompanied by the increased proportion of cells expressing Tenascin C (TNC) and the activation of myofibroblast-like identity in the entire stromal compartment of carious pulps. Two myofibroblast-like cell populations identified by CDH11 and CTHRC1, and ACTA2 expression are exclusively distributed between the fibroblast and mesenchymal stem cell (MSC) subclusters, respectively. In addition, the stromal cluster was marked by increased expression of major ECM constituents, such as COL1A1, COL3A1, FN1, DCN, LAMININ, FBLN1, FNB1, etc, suggesting an extensive restructuring of the cellular microenvironment in the dental pulp resembling the fibrosis-related changes. Evaluation of the mechanical strain of the fibronectin fibres, assessed by immunostaining with the Fibronectin tension nanoprobe (FnBPA5), showed a significant reduction in the tension of ECM fibres in the carious pulps, that likely impacts cell motility and differentiation capacity.

Conclusion:
This study demonstrates changes in the molecular, cellular and biomechanical properties of the carious dental pulp that indicate alterations of the dental pulp tissue microenvironment reminiscent of the fibrotic changes observed in other organs, which impact the reparative potential of the dental pulp and the outcome of carious lesion.

504

J. Pfister[1], T. Stein[1], S. Shllaku[1], N. Gölz[1], M. Schmugge[1], F. Franzoso[1]

Molecular Insights Into the Apoptosis and Autophagy Pathway Mechanisms Underlying the Pathogenesis of Pediatric Immune Thrombocytopenia

University Children's Hospital Zürich[1]

Introduction:
Immune thrombocytopenia (ITP) is an autoimmune bleeding disorder characterized by low platelets counts and a mostly mild- and in rare occasion life threatening bleeding symptoms. Previous studies, also from our group, have demonstrated a role of platelet apoptosis in the pathogenesis of childhood ITP. A mechanistic understanding of the ITP pathogenesis is still lacking, and most treatments increase the platelet counts and prevent the severe clinical manifestations in a limited number of the patients only.

Methods:
We isolated platelets in vitro as described before also by our group. We used the human megakaryoblastic cell line MEG-01, treated for 1 hour with plasma from newly diagnosed and chronic ITP patients and healthy controls. We determined the mRNA levels of apoptosis and autophagy pathway regulatory genes (p53, Bad, ATG5, ATG7, LAMP-1, LC3, Bcl-2, Apaf-1, cytochrome-c, caspase -8, -9 and GRP78) by qRT-PCR.

Results:
We could demonstrate increased expression levels of some apoptotic and autophagy genes such as GRP78, caspase-8 and LAMP-1 in ITP platelets and MEG-01 treated cells that could be silenced by using siRNA caspase-8.

Conclusion:
Our results indicate that differently regulated apoptosis- and autophagy pathways could play a role in platelet pathophysiology and platelet production by Megakaryocytes of patients with ITP.

505

V. Dimakopoulos[1], G. Selmin[1], L. Regli[1, 2], J. Sarnthein[1, 2]

Varying the stimulus repetition rate affects amplitude and noise of the somatosensory evoked potential.

Klinik für Neurochirurgie, Universitätsspital Zürich, Universität Zürich, Switzerland[1], Klinisches Neurozentrum, Universitätsspital Zürich, Switzerland[2]

Introduction:
The intraoperative averaging of the somatosensory evoked potential (SEP) requires reliable recordings within the shortest possible duration. We here systematically optimized the repetition rate of stimulus presentation.

Methods:
We recorded medianus and tibial nerve SEP during 22 surgeries and varied the rate of stimulus presentation between 2.7 Hz and 28.7 Hz. We randomly sampled a number of sweeps corresponding to recording durations up to 20 s and calculated the signal-to-noise ratio (SNR).

Results:
For the medianus nerve at 5 s recording duration, SEP stimulation rate at 12.7 Hz obtained the highest median SNR = 22.9 for the N20, which was higher than for rate 4.7 Hz ($p = 1.5e-4$). When increasing the stimulation rate, latency increased and amplitude decayed for cortical but not for peripheral recording sites. For the tibial nerve, the rate 4.7 Hz achieved the highest SNR for all durations.

Conclusion:
We determined the time-dependence of SNR for N20 and elucidated the underlying physiology. For short recordings, rapid reduction of noise through averaging at high stimulation rate outweighs the disadvantage of smaller amplitude. For a short duration of medianus nerve SEP recording only, it may be advantageous to stimulate with a repetition rate of 12.7 Hz.

506

E. Samara[3], L. Sazgary[1], A. Stüssi[3], M. Guckenberger[2], A. Saguner[1]

Preliminary study on the impact of clinical audits in patient radiation exposure

Department of Cardiology, University Hospital Zurich, University of Zurich, Zurich, Switzerland[1],
Department of Radiation Oncology, University Hospital Zurich, University of Zurich, Zurich, Switzerland[2],
Radiation Protection Unit, University Hospital Zurich, University of Zurich, Zurich, Switzerland[3]

Introduction:
The aim of clinical radiation audits is to ensure an ideal use of ionizing radiation in medicine. Their realization may enable to review the justification of the procedures and optimize the processes and resources of the providers. The first radiation audit in the cardiology department of USZ took place in September 2019 and the main recommendation regarding patient exposure was to establish local diagnostic reference levels (LDRLs). The objective of this study was to establish LDRLs before and after the audit and examine if patient exposure was affected by the audit.

Methods:
Data from 500 electrophysiology procedures performed 6 months before and after the audit were retrospectively collected. The procedures included in this evaluation were electrophysiologic study (EPS), catheter ablation (subdivided into right-sided and left-sided procedures with and without electroanatomical mapping (EAM), atrial fibrillation ablation with and without EAM, pacemaker/ICD implantation (single-chamber/dual-chamber) and CRT implantation. Patient exposure was evaluated in terms of dose-area product (DAP), fluoroscopy time (T) and cumulative dose at the reference point. The data were collected from a dose management system, cross-checked for accuracy with the patient information system and analyzed with a statistics software

Results:
LDRLs were established for all procedures and compared with national ones, where applicable. Results revealed that LDRLs were lower as compared to the national DRLS (Table 1). DAP and T remained similar prior to and after the audit for EPS, CRT implantation, catheter ablation with EAM, and significantly decreased for right-sided catheter ablation. T significantly decreased for atrial fibrillation ablation with and without EAM (p-value<0.0001), whereas DAP remained similar. For pacemaker/ICD implantation, the DAP was significantly decreased (p-value=0.01), while T remained the same.

Table 1: Local diagnostic reference levels after the audit

	DAP (Gy.cm²)	Cumulative Dose (mGy)	Fluoroscopy time (min)
CRT implantation	7.5	100	14
EPS	0.3	2	2
EPS - Swiss DRL	*20*	*300*	*10*
Catheter ablation, left-sided with EAM	5.3	45	13
Catheter ablation, left-sided without EAM	0.4	2	1
Catheter ablation, right-sided with EAM	0.6	3	2
Catheter ablation, right-sided without EAM	0.2	2	1
Catheter ablation without EAM - Swiss DRL	*150*	*2250*	*25*
Catheter ablation with EAM - Swiss DRL	*30*	*623*	*9*
Atrial fibrillation ablation with EAM	5.1	40	3
Atrial fibrillation ablation without EAM	20.0	150	15
Pacemaker/ICD implantation	3.5	2.4	4.1
Pacemaker/ICD implantation - Swiss DRL	*30*	*450*	*7*

Conclusion:
The purpose of clinical audits is to optimize radiation exposure without sacrificing patient safety. Our clinical audit significantly reduced radiation exposure of patients in pacemaker/ICD implantations and ablation procedures without EAM, whereas no differences were observed in other types of procedures. Regarding DRLs, local values were below national ones, which may indicate that national DRLs should be updated regularly.

507

L.P. Leuenberger[1], L. Isenegger[1], E. Zaninotto[1], C. Pauli[2], P.K. Bode[2, 3], U. Camenisch[2], C. Matter[1], H. Moch[2], C. Britschgi[1]

Targeting PI3K signaling is a potential therapeutic strategy in Clear Cell Sarcoma

Department of Medical Oncology and Hematology, University Hospital Zürich, Zürich, Switzerland[1], Institute of Pathology and Molecular Pathology, University Hospital Zürich, Zürich, Switzerland[2], Institute of Pathology, Cantonal Hospital Winterthur, Winterthur, Switzerland[3]

Introduction:
Clear cell sarcoma (CCSA) is a rare and highly malignant soft tissue sarcoma, characterized by expression of either of two oncogenic fusion proteins, EWSR1-ATF1 or EWSR1-CREB1, respectively. CCSA is notoriously resistant to systemic therapy. We therefore aimed at identifying novel therapeutic approaches by performing an unbiased, high-throughput compound (cpd) screen.

Methods:
We used a library of 960 candidate kinase modulators to screen two CCSA cell lines for reduction of viability, compared to a human fibroblast control cell line. Cell survival after drug exposure for 72 hrs was assessed using a resazurin read-out. The most promising cpds were validated extensively in vitro, by long-term proliferation assays, IC50 determination, apoptosis and autophagy assays. Additionally, in order to discover the potential target pathways of the two most promising cpds, we used ProteomeProfiler™ Human Phospho-Kinase Array membranes. To permit future in vivo validation, we have established xenograft models of CCSA in BALB/c nude mice.

Results:
The screen identified 14 cpds with the desired effect pattern, of which we have validated the 10 with the strongest effect using long-term proliferation assays. A more extensive in vitro validation was then performed on 4 cpds on multiple CCSA cell lines and other malignancies as controls, using IC50 determination, apoptosis and autophagy experiments. Those experiments robustly validated the results from the screen, but showed that neither apoptosis nor autophagy are responsible for the observed reduction in CCSA cell survival. The phospho-kinase array showed multiple up- and down regulated kinases pointing at multiple involved signaling pathways. One intriguing finding was a change in PI3K-signaling, which we studied further. Indeed, several inhibitors of the PI3K/AKT/mTOR pathway significantly impacted on CCSA cell survival.

Conclusion:
We have successfully performed and extensively validated an unbiased high-throughput cpd screen, which has identified several potential drug candidates. Investigation into the mode of action has pointed at a potential involvement of PI3K-signaling and CCSA cell lines are sensitive to pharmacologic inhibition of PI3K/AKT/mTOR signaling. Those observations will next be validated in in vivo experiments in our established CCSA xenograft models.

508

K. Huebel[4], F. Fehr[2], T. Müller[4], U. Schanz[3], P. Cippa[1]

Donor-specific tolerance induction by combined kidney and hematopoetic stem cell transplantation

Ente Ospedaliero Cantonale Lugano, Nephrology[1], Kantonsspital Graubünden[2], University Hospital Zuerich, Haematology[3], University Hospital Zuerich, Nephrology[4]

Introduction:
Long-term survival of kidney allografs is limited by either inadequately controlled rejection and/or by side effects of long-term immunosuppression (drug toxicity, infections and neoplasia). Induction of donor-specific tolerance would resolve most, if not all of these limitations. Here we report on 6 patients included in the first European trial of combined kidney and hematopoetic stem cell transplantation (HCST; swisstolerance.CH).

Methods:
Six patients (3 female / 3 male) underwent combined kidney and hematopoietic stem cell transplantation from their HLA-identical living siblings between 2016 and 2022. Conditioning therapy for HSCT and immunosuppression was performed according to the Stanford protocol including total lymphoid irradiation, anti-thymocyte globulin followed by corticosteroids (3 days), mycophenolate (1 months) and cyclosporine for 6-24 months. After 9-24 months all immunosuppression was withdrawn.

Results:
Five out of six patients were completely withdrawn from all immunosuppression (follow-up between 6 years and 4 months). No rejection or graft-versus-host disease episodes and no relevant infections occurred. Initial donor chimerism was seen in all patients. However, in 4/5 patients the chimerism level was declining, whereas one patient remained a stable mixed chimera. Specificity of tolerance was tested by molecular microscope analysis (absence of rejection signature) and by successful SARS CoV2 vaccination in some of the patients. One patient experienced a relapse of her primary glomerulonephritis in the allograft. She developed proteinuria, renal function slightly declined 3 years after recurrence.

Conclusion:
Combined HSCT and kidney transplantation from the same living donor provides tolerance to a kidney allograft. This tolerance is donor-specific, as shown by protective immune responses against a SARS-CoV2-specific vaccine and absence of "molecular rejection".

509

Y. Gütlin[3], D. Albertos Torres[3], A. Gensch[2], AK. Schlotterbeck[2], L. Stöger[2], S. Heller[2], L. Infanti[4], K. Leuzinger[1], HH. Hirsch[1], A. Buser[4], A. Egli[3]

Total anti-SARS-CoV-2 Immunoglobulin and neutralising antibody responses in healthy blood donors over the course of the pandemic - a single city experience

Clinical Virology, University Hospital Basel, Basel, Switzerland[1], Department of Biomedicine, University of Basel, Basel, Switzerland[2], Institute of Medical Microbiology, University of Zurich, Zurich, Switzerland[3], Swiss Red Cross Blood Donation Center, Basel, Switzerland[4]

Introduction:
Monitoring anti-SARS-CoV-2 and neutralizing antibodies (nAb) helps to understand protection at individual and population levels. Classical virus neutralization tests (VNT) are costly and time intensive, but ELISA-based surrogate VNTs (sVNT) or high throughput assays to detect anti-SARS-CoV-2 spike protein receptor binding domain immunoglobulins (anti-S-RBD Ig) may be alternatives. We aimed to explore (i) the correlation between anti-S-RBD Ig and sVNT measurements and (ii) describe humoral immunity against SARS-CoV-2 after vaccination, natural infection, and breakthrough infection.

Methods:
We measured total anti-SARS-CoV-2 Ig of 2748 healthy individuals (5714 samples) visiting the Swiss Red Cross blood donation centre from 03/2020-04/2022. We used the Elecsys® Anti-SARS-CoV-2 (Roche) against N and S proteins. Anti-S-RBD Ig were measured from 01/2021 onwards, when vaccines became available. In a subset of 548 samples of 123 donors, we conducted sVNTs against the wildtype SARS-CoV-2 (SARS-CoV-2 Neutralizing Antibodies Detection Kit, Adipogen™). Surveys were sent to the donors to collect data on their infection and vaccination status. Using this data, donors were categorised into: “vaccination only (V)”, “infection before vaccination (IV)”, “breakthrough infection (BT)”, and “natural infection only (NI)”.

Results:
Our large cohort of blood donors consists of 50.7% males with a median age of 31 years (IQR 26-44). Positivity rates per months are shown in Fig. 1 and indicate almost 60% infection until 04/2022. Furthermore, no differences in seropositivity were found within sexes, age groups, blood types (AB0, Rhesus), and CMV seropositivity. We observed a high correlation between anti-S-RBD Ig and inhibition percentage (inh%) (Spearman’s $\rho = 0.92$, $p < 0.0001$), compared sensitivity and specificity values to thresholds set by the Roche assay, and computed the “best” cut-off based on our data (Fig. 2). We successfully categorised 1127/1223 (92.2%) donors, who answered the questionnaire into: V (47.1%), IV (6.9%), BT (41.6%), and NI (4.4%). [YG1] [AE2] Overall, 292/548 samples (53.3%) were tested positive for nAb (median inh% = 29.4%). We observed lower inh% in the NI group, compared to all other groups with vaccination. Also, we observed, that the IV group shows higher anti-S-RBD Ig titres after the 1st vaccine dose as compared to the other groups with vaccination (Fig. 3).

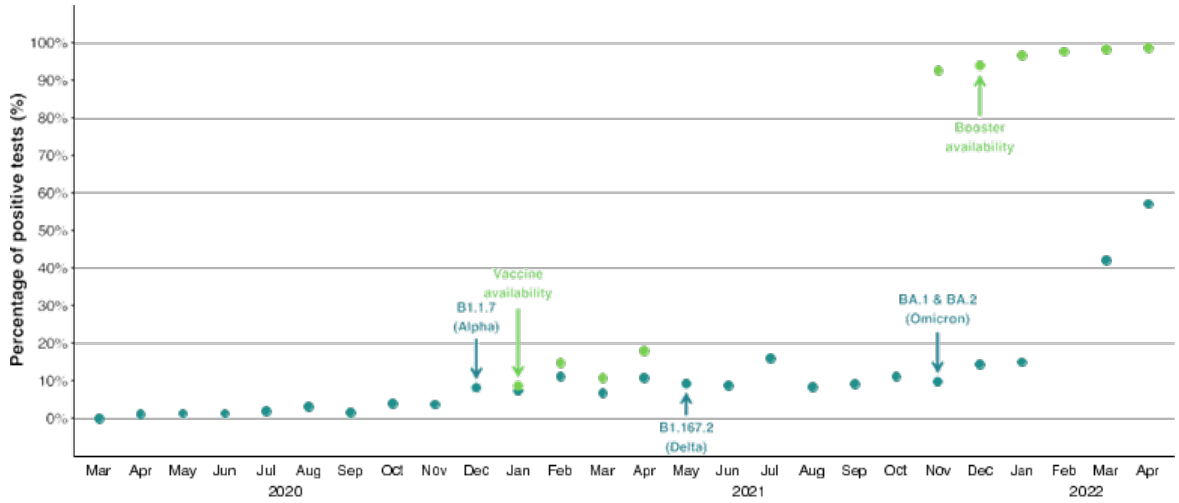

Fig. 1: Positivity rate for anti-N and anti-S protein antibodies calculated per month of sample collection

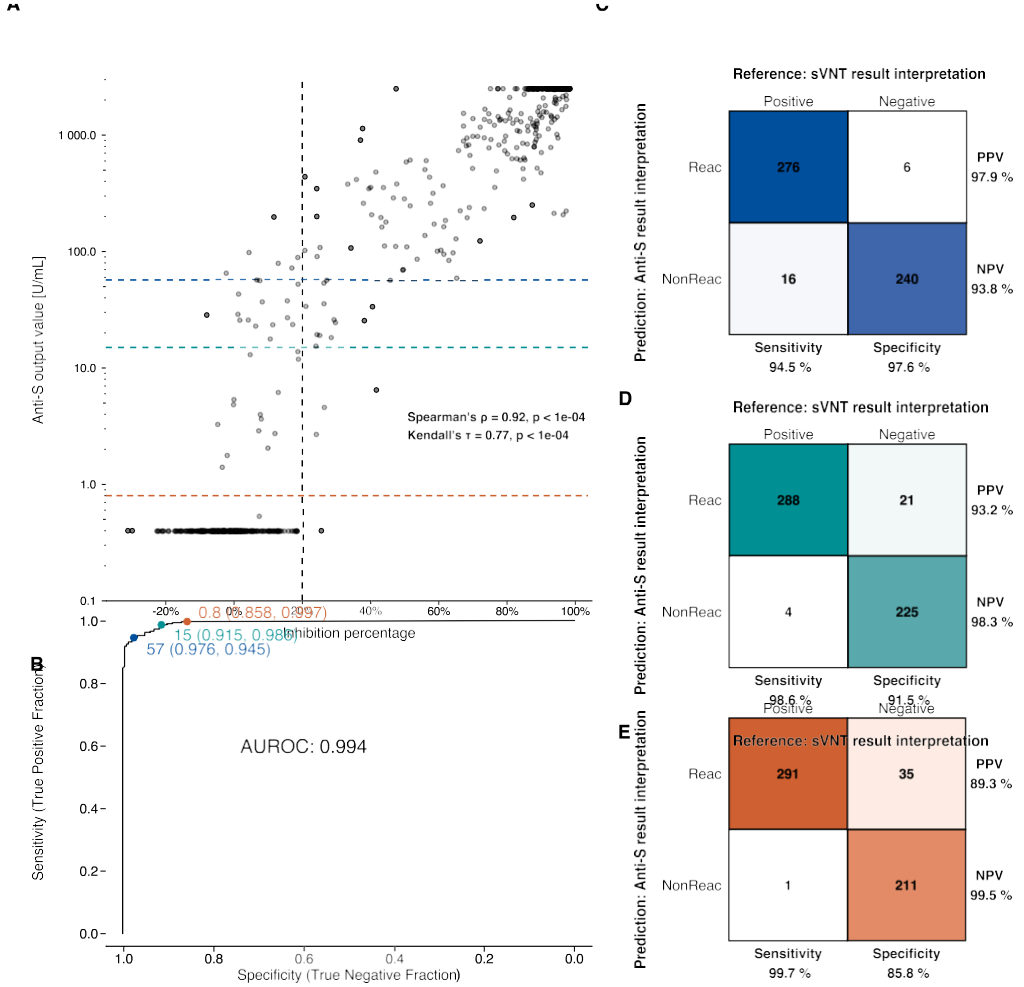

Fig. 2: Correlation analysis anti-S vs nAb. In A, anti-S output values were plotted against the results of the sVNT (inhibition percentage). A receiver operating curve analysis is shown in B. The “best” cutoff (blue) was determined as the anti-S output value at the Youden index. In teal and orange, the cutoff values as specified in the Elecsys® Anti-SARS-CoV-2 S package insert are shown respectively for nAb and anti-S-RBD Ig. In C, D, E, a confusion matrix for each cutoff and calculated sensitivities, specificities, and positive and negative predictive values (PPV, NPV) are shown.

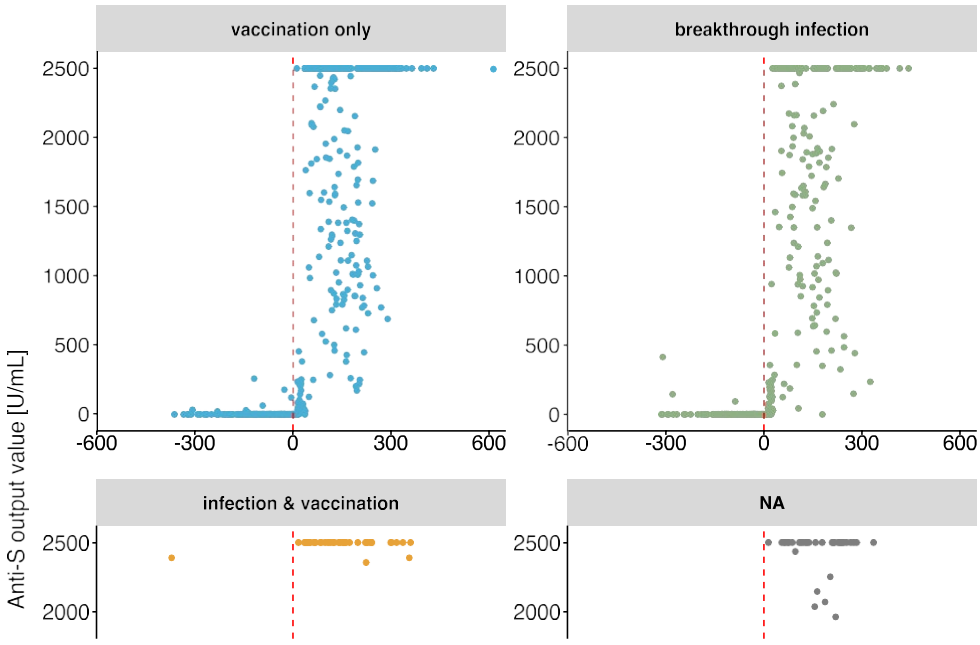

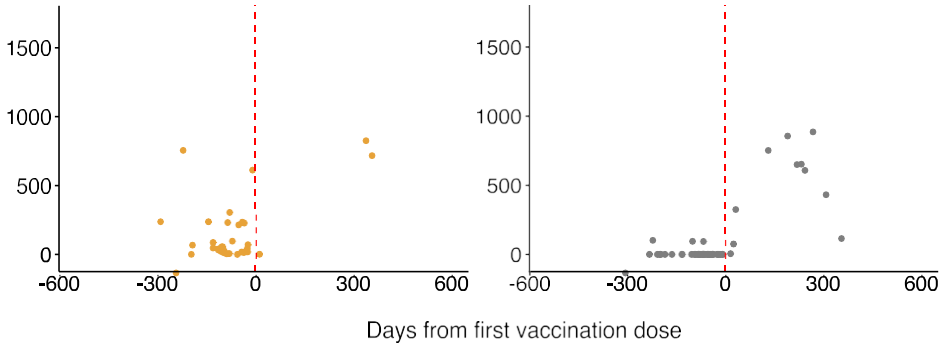

Fig. 3: Anti-S titres before and after the 1st vaccination dose grouped by vaccination and infection status. For each donor the samples closest to the date of the 1st vaccination dose were selected and the difference in days between sample collection dates and 1st vaccine dose dates were calculated.

Conclusion:
We observed that almost 60% of the population were infected with SARS-CoV-2, but natural infection without evidence for vaccination seems to result in substantial lower nAb levels. In order to assess the risk of re-infection, an estimate of neutralization may be helpful. Total anti-S-RBD Ig correlates with sVNT results; therefore, we suggest that total anti-S-RBD Ig may estimate the level of nAb. However, the threshold for protection from an unfavourable clinical outcome needs to be evaluated in prospective clinical cohorts.

511

F. Wegner[1], B. Cabrera Gil[2], A. Neves[2], A. Egli[1]

How much should we sequence? An analysis of the Swiss SARS-CoV-2 genomic surveillance effort

Institute of Medical Microbiology, University of Zurich, Zurich, Switzerland[1], SIB Swiss Institute of Bioinformatics, Geneva, Switzerland[2]

Introduction:
During the SARS-CoV-2 pandemic, many countries directed substantial resources towards genomic surveillance systems to track and detect both established and emerging viral variants. There is a debate over how much sequencing effort is useful in national surveillance programs for SARS-CoV-2 and future pandemic threats. We aimed to investigate how important surveillance outcomes would have been affected by a reduced sequencing effort in a large genomic dataset from Switzerland.

Methods:
We analysed all genomic data available on the Swiss Pathogen Surveillance Platform (SPSP) from February 2020 until August 2022. We employed a downsampling strategy to investigate the effects of fewer available sequences on the surveillance outcomes: (i) first detection of variants of concern (VOCs), (ii) speed of introduction of VOCs, (iii) first cluster detection of VOCs, (iv) density of active clusters, and (v) geographic spread of clusters.

Results:
A total of 143,260 SARS-CoV-2 sequences were available for a population of 8,7 million inhabitants. On average, 9.7% of all PCR-positive cases (n=3.95 million) were sequenced throughout the pandemic. We find that the impact of downsampling on the detection of VOCs is dependent on individual lineage dynamics, but that most dynamics including introduction and cluster detection could be recapitulated even with a reduced sequencing effort. For example, with 50,000 sequences (one third of the overall available sequences) there was no substantial increased delay in the detection of the VOCs. However, the effect on the observed speed of introduction is particularly sensitive to reduced sequencing effort. A stronger effort in sequencing was most accurate in capturing the respective growth of the emerging VOCs.

Conclusion:
A genomic surveillance program needs to strike a balance between societal benefits and program costs. While the overall national dynamics of the pandemic (distribution of lineages, detection of VOCs, cluster detection) could be recapitulated by a reduced sequencing effort, the effect is strongly lineage dependent – something that is unknown at the time of sequencing – and comes at the cost of accuracy, in particular for tracking the emergence of potential VOCs.

512

N. Winkler[1], S. Anwer[1], P. Rumpf[1], G. Tsiourantani[1], T. Donati[1], J. Michel[1], A. Kasel[1], F. Tanner[1]

Left atrial pump strain predicts long-term mortality in patients undergoing transcatheter aortic valve implantation

Department of Cardiology, University Heart Center, University Hospital Zurich and University of Zurich, Zurich, Switzerland[1]

Introduction:
Speckle-tracking echocardiography is an increasingly important tool for assessing aortic stenosis (AS). Left atrial reservoir (LARS) and pump strain (LAPS) were studied for their association with long-term mortality in AS patients undergoing transcatheter aortic valve implantation (TAVI).

Methods:
From our prospective AS cohort study, 198 patients with severe AS were identified who underwent TAVI and had a comprehensive preinterventional echocardiographic examination allowing full target analysis. Five-year all-cause mortality was defined as the endpoint.

Results:
Left atrial volume index (LAVI) was increased (mean (SD): 46.9 ml/m2 (±16.5)) and left atrial deformation impaired (LARS (21.7% (±6.9); LAPS (-9.5% (±4.5)), while left ventricular ejection fraction (LVEF) (56.7% (±11.5)) was preserved in the study population. Over a follow-up time of five years, 49 patients (24.7%) died. LARS and LAPS were more impaired in non-survivors (20.0% (±6.5) and -8.1% (±4.0), respectively; Figure) than in survivors (22.3% (±6.9); P=0.042 and -9.9% (±4.5), respectively; P=0.014; Figure), while LAVI did not differ (P=0.248). Univariable Cox regression models demonstrated that LAPS was associated with mortality (P=0.014), while LARS was not (P=0.066) (Table A). In bivariable and multivariable models, the association of LAPS with mortality was independent of LVEF and LAVI, and inclusion of LAPS improved the fitness (χ2) of these models (Table B). Furthermore, the improvement in χ2 was significant for all models (ANOVA P=0.012, P=0.013, and P=0.015, respectively).

Figure

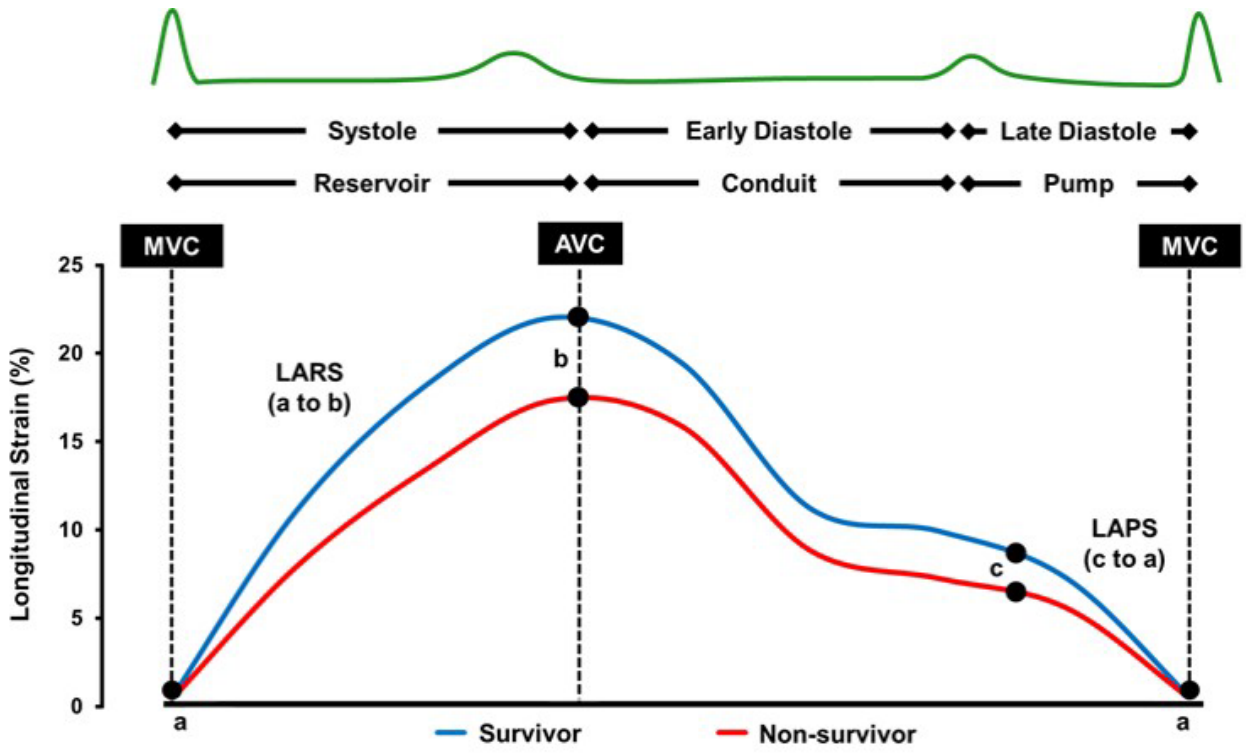

Table

A

Variables	Cox Regression			Model Fitness	
	HR	95% CI	P	χ2	χ2 P
LVEF	1.00	0.97 – 1.02	0.830	0.05	0.829
LAVI	1.01	0.99 – 1.02	0.450	0.55	0.458
LARS	0.96	0.92 – 1.00	0.066	3.57	0.059
LAPS	1.09	1.02 – 1.17	0.014*	6.47	0.011*

B

Variables	Cox Regression			Model Fitness	
	HR	95% CI	P	χ2	χ2 P
LVEF	1.00	0.98 – 1.02	0.920	0.62	0.733
LAVI	1.01	0.99 – 1.02	0.440		
LVEF	1.00	0.98 – 1.02	0.960	6.29	0.043*
LAPS	1.09	1.02 – 1.17	0.016*		
LAVI	1.00	0.99 – 1.02	0.650	6.67	0.036*
LAPS	1.09	1.02 – 1.17	0.017*		
LVEF	1.00	0.98 – 1.02	1.000	6.51	0.089
LAVI	1.00	0.99 – 1.02	0.630		
LAPS	1.09	1.01 – 1.17	0.019*		

Conclusion:
LAPS was associated with long-term mortality after TAVI, while LARS and LAVI were not. The association of LAPS was independent of LVEF and LAVI and showed potential incremental value for assessment of outcome association. Hence, LAPS may be useful for predicting long-term outcome after TAVI.

513

A. Roggo[1], A. Tastanova[2], E. Ramelyte[1], M. Levesque[2], R. Dummer[1]

Exploring 'Immunologic Itch' in Sézary Syndrome and Atopic Dermatitis using targeted spatial Transcriptomics

University Hospital Zürich, Department of Dermatology[1], University of Zürich[2]

Introduction:
Sézary Syndrome (SS) is an aggressive variant of cutaneous T-cell lymphoma (CTCL), where clones of malignant lymphocytes accumulate in the skin. >94% of patients report intractable pruritus (itch) with a persistent desire to scratch leading to a significantly reduced quality of life. Common antipruritic treatments are not effective in CTCL, partly due to the lack of understanding of the basic disease mechanisms.
In 'immunologic itch', the immune system plays a central role triggering itch by complex interactions via soluble molecules or direct cell-cell contact. Similar to SS, atopic dermatitis (AD), a benign inflammatory skin disease, presents with pruritus and characteristic cutaneous infiltration of predominant T-helper 2 (Th2) polarized immune cells. Novel antipruritic medication for AD targeting the immune system can potentially be repurposed for SS.
In this first project, we aimed to characterize pruritus in SS by differentiating disease-promoting and pruritus-inducing factors in the skin on the transcriptional level. We investigated the major contributing compartments within the tumor microenvironment (TME) to improve our understanding of the spatial interaction. Last, we focused on previously reported itch-mechanisms.

Methods:
In a spatial transcriptomics analysis, we compared archived skin samples of patients with SS (with and without pruritus, n=6), AD (n=3) and healthy donors (HD, n=3). Immunofluorescent staining on formalin fixed paraffin embedded (FFPE) cutaneous tissue was used to select relevant cell types. Paired regions of interest (ROIs) were chosen on epidermal and dermal levels. Subsequently, in a total of 96 ROIs, GeoMx Human Whole Transcriptome Atlas with 18'000 genes was quantified in cell-specific illumination areas.

Results:
Segmentation for key cell types was established for epidermal keratinocytes (E-cadherin) as well as immune cells (CD45) and fibroblasts (Vimentin) in the adjacent subepidermal layer. Significant upregulation of cell-specific pathways confirmed successful segmentation and targeting. We were able to identify pathways that distinguish malignant immune cells (SS), inflammation (AD) and intact immune system by comparing networks of hierarchical gene ontology (GO) pathways between the disease states. Clustered analysis of differential gene expression comparing equivalent areas of SS patients with and without itch identified a pruritus-specific gene signature. Single-cell deconvolution on all segments inferred cell-type composition and a contribution of the neuronal system to itch sensation. Linking the differentially expressed genes with the Kyoto Encyclopedia of Genes and Genomes (KEGG) database added a second biological reference highlighting the differences between pruritic and non-pruritic skin.

Conclusion:
We were able to apply high dimensional spatial profiling on clinically relevant samples to unveil differences in the TME of itchy and non-itchy skin. Successful segmentation for essential cell-types in small regions of interest was further analyzed to find key cell types orchestrating tumor progression and biomarkers on transcriptional level. In 'immunologic itch', the immune system can trigger itch by a neuroimmune interaction that can be considered as a therapeutic target in pruritic lymphoproliferative disorders.

514

E. Köksal[1], L. Madrigal[1], A. Levin[2], S. Cai[2], I. Condado-Morales[1], A. Aguzzi[1], T. Knowles[2], S. Hornemann[1]

Digital microfluidics for absolute quantification of α-synuclein propagons for Parkinson disease diagnosis

University Hospital Zürich[1], University of Cambridge[2]

Introduction:
Parkinson's disease (PD) is associated with the misfolding of the α-synuclein (αSyn) protein resulting in accumulation of pathological protein aggregates. The diagnosis of PD is based on clinical assessment, because reliable biochemical tests, in particular for the early diagnosis, are still missing. Recent progress has been made by the development of seed amplification assays (SAA). These assays are based on the amplification of signals derived from aggregates, also termed propagons, that seed monomeric αSyn in bulk solutions. Although SAAs allow the detection of αSyn aggregates in body fluids at minute concentrations, an absolute and precise quantitation is limited due to a restriction in the number of replicas. We therefore aim to use digital microfluidics to develop a diagnostic assay for the absolute and accurate quantification of single αSyn propagons in clinical samples of PD patients.

Methods:
We have set-up a microfluidics platform to generate thousands of picoliter sized water-in-oil microdroplets that act as microreacters and contain recombinant αSyn monomers mixed with a sample to be analysed. To identify specific and sensitive amplification conditions, several parameters were optimized in terms of monomer concentration, temperature and buffer composition using synthetic αSyn preformed fibrils (PFFs). Growth and proliferation of propagons inside up to 5,000 droplets were monitored simultaneously through Thioflavin T, a fluorescent probe that specifically detects amyloid aggregates. Obtained confocal microscopy images were analyzed by counting fluorescent positive, propagon containing, and negative microdroplets. Poisson statistics was applied for absolute quantification.

Results:
Growth and proliferation of αSyn aggregates were optimized in microdroplets. With optimized microdroplet composition, detection of aggregates in femtomolar range was achieved in less than 24 hours using confocal microscopy. The results obtained with synthetic PFFs were validated with CSF samples from PD patients and healthy controls. In the future, CSF samples from individual PD patients and healthy controls will be tested blindly for validation of the assay performance.

Conclusion:
Our digital microfluidic assay might allow for sensitive and rapid detection of αSyn aggregates in CSF samples of PD patients. Quantification at single aggregate level might enable monitoring disease progression and success of therapeutic strategies on preventing aggregation in PD patients.

515

N. Jarzebska[1, 2], J. Frei[1], M. Mellett[1], S. Pascolo[1], M. Tusup[1]

RNA with chemotherapeutic base analogues as a superlative dual-functional anti-cancer drug

University Hospital Zurich, Department of Dermatology[1], University of Zurich, Department of Science[2]

Introduction:
RNA-based therapies hold great promise for cancer treatment as they can be used to block oncogenes (using siRNA), or express proteins of interest (by mRNA) or activate the innate immune system (isRNA). Formulating immunostimulating (is)RNA with the pharmaceutical compound Protamine, a natural cationic histone, enables the generation of nanoparticles that induce IFNα releaseand limit tumour growth in mice.
To augment therapeutic, anti-tumour effects of Protamine-RNA nanoparticles, we incorporated the chemotherapeutic pyrimidine 5-fluorouracil (5FU) into RNA in place of uracil. We found that the modified 5FU-RNA is as potently chemotherapeutic as free 5FU. In addition, we could show that this substitution does not interfere with the capacity of the RNA to trigger TLR7 and induce production of type I interferons. Thereby 5FU-RNA exhibits dual-functionality and is immuno-chemotherapeutic (icRNA).

Methods:
Cytotoxicity of icRNA was evaluated in vitro on CT26 murine colon carcinoma cells. The cells were incubated with increasing concentrations of Protamine-RNA/5FU nanoparticles (PR 5FU) or Protamine-mRNA (PR Luc) or free 5FU and proliferation was measured. Therapeutic capacities of icRNA was assessed in mice implanted with CT26 colon carcinoma or B16F10 melanoma murine cell lines. On Day 4 and 11-post tumour cell implantation, mice were administered with two intravenous injections (10 µg of RNA each) of PR 5FU (i.e. immunochemotherapeutic) or PR Luc (i.e. immunostimulating only) particles.

Results:
Proliferation of CT26 cells in vitro was reduced in the presence of increasing concentrations of PR 5FU even more than in cells treated with standard free 5FU. This corresponds to a higher chemotherapeutic activity of the modified ribonucleoside versus the free base. PR 5FU particles retained their immunostimulatory effects on human PBMCs and induced IFNα secretion. Mice receiving PR 5FU showed a greater control of subcutaneous tumour volume compared to mice receiving PR Luc. This difference was dependent on the cytotoxic effect of 5FU, as both PR 5FU and PR Luc nanoparticles induced similar levels of IFNα 4 h after I.V. injection. However, despite inducing a control of the growth of CT26 subcutaneous tumours, icRNA nanoparticles failed to control tumours in a sub-cutaneous B16 melanoma model .

Conclusion:
We observed that substituting uracil with the chemotherapeutic pyrimidine 5FU bestowed the RNA oligo with a dual mechanism of action; they retained their ability to stimulate the innate immune response but now also exerted potent cytotoxic effects against rapidly dividing cells. These immunochemotherapeutic RNA (icRNA) nanoparticles demonstrate more effective killing of tumour cells in vitro and in vivo.
Therefore, we demonstrated that icRNAs are promising cancer therapies, which warrants their further validation for use in the clinic.

516

J. Baum[1], C. Boggon[2], N. Ranzoni[1], L. Isa[2], S. Brugger[1]

Microbiota engineering for the erradication of Staphylococcus aureus

Department of infectious diseases and hospital hygene, University Hospital Zurich[1], Department of Materials, ETH Zurich[2]

Introduction:
Staphylococcus aureus is a pathobiont that in addition to colonizing the upper respiratory tract (URT) of people also causes severe infections. Colonization is a major risk factor for infection and transmission; thus, measures are taken to decolonize at risk patients and reduce the risk of infection. However, all of them are tedious and resistance to common decolonization agents has been described highlighting the need for better and sustained decolonization strategies. One novel approach to decolonization is to reengineer the microbiome to exclude S. aureus colonization. Metagenomic analysis of the URT microbiome has revealed a negative correlation between commensal bacteria such as Dolosigranulum pigrum and Corynebacterium pseudodiphtheriticum. In vitro agar based studies of the interaction between these commensals with S. aureus have revealed a direct inhibition of S. aureus by D. pigrum. The nature of this inhibition as well as the single cell interactions between different members of the URT microbiome is yet unknown. In this project we aim to elucidate the interactions between different bacterial species on a single cell level. To this end we use a novel technique called sequential capillarity assisted particle assembly (sCAPA) to pattern bacteria on a polydimethylsiloxane (PDMS) template with high precision. Thus, leading to the establishment of minimal in vitro URT microbioms that can be used to investigate optimal microbe composition to confer colonization resistance to S. aureus.

Methods:
The bacteria to be deposited are solved in liquid medium. After deposition on a PDMS template we place a nutrient containing agar pad on top of the deposited bacteria. The bacteria are then placed under a microscope where we can take time lapse images of the growing bacteria. From the time-lapse images parameters such as deposition yield, lag time as well as growth rate of single bacteria can be extracted and compared. By placing an agar pad that has been pre-conditioned with commensal bacteria on top of deposited S. aureus we can recreate the previously established in vitro co-culture assay on a single cell level. This allows us to better understand the effect the inhibition has on the lag time as well as the growth rate of single S. aureus cells in a distance dependent manner. Additionally, by pre-conditioning the agar pad with deposited D. pigrum cells, we can track commensal growth and relate this to the inhibition we observe in S. aureus.

Results:
Here we show that single cells of both the commensals as well as S. aureus can successfully be deposited. By adding nutrient containing agar patterned bacteria can be regrown and growth kinetics of cells after deposition can be measured. All species tested survive the deposition well and without marked growth defect. Additionally, several assays to further investigate the observed inhibition of S. aureus by D. pigrum on a single cell level were established. Using agar pads pre-conditioned with D. pigrum revealed an inhibition gradient dependent on the distance from the D. pigrum colony. When pre-conditioning the agar pad with deposited D. pigrum cells we still observed inhibition even with little commensal growth.

Conclusion:
Here we present a proof of concept where we can deposit and grow multiple key species of the URT microbiome using CAPA. Furthermore, we show the inhibition of S. aureus by D. pigrum on a single cell level. This opens the door to explore the observed inhibition in more detail, answering questions such as what ratio of D. pigrum cells is required to achieve reliable inhibition. By patterning multiple species on the same template this technique will allow us to model minimal microbiota and identify communities that are predictive for stable decolonization and communities that are resilient to pathobiont decolonization. Ultimately, patient derived strains can be used to model individual patient microbiota thus tailoring the microbial compositions to the needs of the patient.

517

JM. Boss[2], J. Willms[1], E. Keller[2]

Bringing an AI Solution for Delayed Cerebral Ischemia Prediction Closer to Clinics through Intermediate Silent Validation

Institute of Intensive Care Medicine, University Hospital Zurich, Switzerland[1], Neurocritical Care Unit, Department of Neurosurgery and Institute of Intensive Care Medicine, Clinical Neuroscience Center, University Hospital Zurich and University of Zurich, Switzerland[2]

Introduction:
Clinical information systems (CIS) are gradually becoming indispensable to capture and integrate medical data from patient history, laboratory values, monitoring parameters, as well as medications. At the same time, there is exponential growth in published medical AI solutions for automated clinical decision support across all medical disciplines. In the Neurocritical Care Unit, for example, these medical AI solutions promise to support physicians in timely decision making by constantly integrate a vast set of input parameters. However, commercially available CIS do not meet the requirements to easily integrate such systems into near real-time data streams. This barrier has resulted in a phenomenon known as the “AI Chasm” in medicine describing the fact that only a small portion of AI solutions make it into clinics. To bridge this chasm, vertically integrated data platforms are needed for AI development and integration, and proper online silent validation phases to back its clamed benefits in clinical practice as well as to comply with regulatory frameworks.

Methods:
To tackle the technical aspects and starting in 2016, the ICU Cockpit IT data platform has been built with the paradigm of vertical integration in mind covering the entire data life cycle including the collection and processing of high-resolution data streams as well as enabling the seamless integration of stream processing algorithms and AI solutions. Since then, the ICU Cockpit has become an ideal platform for clinical validation as well as a valuable test bench to perform implementation research on. What is more, based on data collected via the ICU Cockpit, we developed and offline validated (10-fold nested cross-validation) a risk prediction software evaluating Logistic Regression and Decision Tree Ensemble models in the process. Subsequently, this software has been deployed in the live environment of ICU Cockpit. A browsable dashboard provides the necessary means for displaying risk scores and SHAP values. In the ongoing silent validation phase, the said dashboard is accessible only in the physicians' office while not on clinical duty.

Results:
The ICU Cockpit is built on modern and widely used Big Data software stacks using an Apache Kafka message broker at its heart. Moreover, live patient data is efficiently stored in a PostgreSQL database for easy access. Live data streams, camera feeds, and AI results can be visualized in a custom-built user interface, the ICU Cockpit Dashboard. The development dataset for the DCI prediction model included 222 patients of which 89 patients developed DCI (40%). In the ROC analysis, the best model achieves an AUC of 0.74 ± 0.06.

Conclusion:
The ICU Cockpit data platform allows to cover the entire AI life cycle from development, and integration, to clinical validation. Moreover, it can serve as a blueprint and inspiration for other research groups working on the implementation of AI solutions. We also invite researchers to take advantage of the ICU Cockpit to advance their medical AI solutions and bring them to clinics faster.

518

L. Dietsche[3, 4], K. Stirm[1, 2, 4], C. Schneidawind[3], A. Müller[1, 4], A. Theocharides[3]

SMAD1 is a silenced tumor suppressor in AML with MLL rearrangement

Institute of Molecular Cancer Research, University of Zurich, Zurich, Switzerland[1], Institute of Molecular Health Science, ETH Zurich, Zurich, Switzerland[2], University Hospital Zurich, Clinic for Medical Oncology and Hematology, Zurich, Switzerland[3], University of Zurich, Zurich, Switzerland[4]

Introduction:
Chromosomal translocations, so-called rearrangements, of the Mixed Lineage Leukemia 1 (MLL1) gene in hematopoietic stem and progenitor cells cause leukemias of myeloid and lymphoid origin. MLL1 is a histone lysine-methyltransferase, which methylates H3K4, acts as an epigenetic gene expression regulator and plays an important role in embryonic development and hematopoiesis. Due to aberrant function and protein complex formations of MLL1 fusion proteins (MLL-FPs) the expression of many target genes is dysregulated. Upregulation of genes such as the leukemogenic HOX family members and MEIS1 is a hallmark of MLL rearranged (MLLr) leukemias and reportedly critical for leukemia initiation and sustainment. Mothers Against Decapentaplegic Homolog 1 (SMAD1), a transcription factor which is part of the TGF-β and BMP signaling axes, was previously described as a tumor suppressor in Diffuse Large B-cell Lymphoma (DLBCL). Here we describe a similar tumor suppressive function of SMAD1 in MLLr Acute Myeloid Leukemia (AML) and provide evidence that SMAD1 expression is lost due to MLL rearrangement.

Methods:
We generated MLL-FP knockdown in MLLr MV4-11 cells using the CRISPR/Cas9 technology. We stably overexpressed SMAD1 in MV4-11 cells, which are originally SMAD1 negative, by lentiviral introduction of an overexpression cassette. We received cord blood derived cells containing MLL fusion genes, which were introduced by CRISPR/Cas9 mediated site-directed mutagenesis, from the collaborating Schneidawind Lab. We used an orthotopic xenograft NSG mouse model to study the engraftment of SMAD1 overexpressing MV4-11 cells compared to control cells. To study the H3K4 methylation at the SMAD1 promotor in cells with and without MLL rearrangement, we used Chromatin Immunoprecipitation (ChIP) coupled with RT-qPCR.

Results:
We observed that expression of SMAD1 is dramatically lower in bone marrow and peripheral blood cells of MLLr AML patients compared to other subtypes of AML. Knockdown of the MLL-FP in SMAD1 negative MV4-11 cells lead to an increase of SMAD1 mRNA and protein levels. Vice versa, SMAD1 expression was nearly abolished in cord blood derived MLL-FP cells compared to normal cord blood. ChIP coupled with RT-qPCR revealed that H3K4me3 levels at the SMAD1 promotor in MV4-11 cells (0.26 % Input) were much lower than in MLL1 WT HL-60 cells (9.8 % Input). Overexpression of SMAD1 in MV4-11 cells caused a TGF-β dependent growth disadvantage and G1 cell cycle arrest in vitro. Notably, the overexpression of SMAD1 decreased HOXA9 and MEIS1 mRNA levels, which was enhanced by TGF-β treatment. When transplanted orthotopically into NSG mice, SMAD1 overexpressing MV4-11 cells displayed reduced engraftment potential in bone marrow and spleen compared to the control cells.

Conclusion:
Together this data suggests that MLL rearrangement causes loss of SMAD1 expression due to reduced H3K4 methylation at the SMAD1 promotor and subsequently reduced transcription. Moreover, we conclude that SMAD1 has a tumor suppressive function and its loss contributes indirectly to the leukemogenesis of MLLr AML by impacting the cell cycle and the regulation of leukemic factors HOXA9 and MEIS1. There could be a therapeutic effect of SMAD1 re-expression in MLLr AML, as demonstrated for SMAD1 overexpression. We are currently investigating candidate compounds, which reportedly induced upregulation of SMAD1 in large drug screens.

519

A. Hukara[1], T. Tabib[2], M. Rudnik[1], O. Distler[1], P. Blyszczuk[1], R. Lafyatis[2], G. Kania[1]

FOSL-2 transcription factor as a driver of pro-phagocytic macrophages in patients with systemic sclerosis

Center of Experimental Rheumatology, Department of Rheumatology, University Hospital Zurich, University of Zurich, Zurich, Switzerland[1], Division of Rheumatology and Clinical Immunology, Department of Medicine, University of Pittsburgh, Pittsburgh, USA[2]

Introduction:
Phagocytosis is a crucial cellular process, which under certain immuno-pathological conditions can be activated in macrophages in an uncontrolled manner. Biomarker studies have implicated macrophages in the development and progression of systemic sclerosis (SSc). Fos-like 2 (FOSL-2) transcription factor has been associated with an alternatively-activated macrophage phenotype in SSc. We postulate that macrophage phagocytosis is a critical process in SSc progression. The aim of this study was to investigate the role of FOSL-2 in macrophage phagocytosis in patients with SSc.

Methods:
Single cell RNA sequencing (scRNAseq) of human explanted lung tissue from 4 SSc-ILD patients and 4 healthy controls (HC) was conducted using the 10X Genomics Chromium instrument. Transcriptomic analyses for this study were performed using the R package Seurat V2.3.4. Human monocyte-derived macrophages (hMDM) were differentiated from $CD14^+$ blood-derived monocytes from HC and SSc patients. hMDM were polarized with LPS (10 ng/ml) or remained unstimulated. Protein expression was detected by Western Blot. pHrodo Red *E.coli* particles were used to measure phagocytic activity, which was assessed by flow cytometry. hMDM were transfected with *FOSL2* or negative control siRNA.

Results:
scRNAseq analyses of lung macrophage populations focusing only on cells that expressed *FOSL2* (*FOSL2*^{hi}), identified upregulated phagocytosis-associated (*ARPC1B/ARPC2/ARPC5*) genes in *SPP1*^{hi}, *FCN1*^{hi} and *FABP4*^{hi} macrophage clusters in SSc-ILD patients compared to HC (p.adj.≤0.05; log2 FC≥0.5). Within a pool of genes enriched in *SPP1*^{hi}, *FABP4*^{hi} and *FCN1*^{hi} macrophages in SSc-ILD patients, we observed a significant increase of upregulated pathways, including FcγR-mediated phagocytosis, lysosome and regulation of actin cytoskeleton. In a next step, to assess a potential role of *FOSL2*, we split the cells from SSc-ILD patients into *FOSL2*^{hi} and *FOSL2*^{null} expressing cells and we found upregulated macrophage polarization (*MRC1*) and phagocytosis-associated genes (*MARCO/C1QA/C1QB/C1QC*) in *SPP1*^{hi} *FOSL2*^{hi} compared to *SPP1*^{hi} *FOSL2*^{null} lung macrophages. Gene ontology analysis further showed enriched phagocytosis-related processes in *SPP1*^{hi} *FOSL2*^{hi} macrophages, such as complement activation and defense responses to other organisms.

In the *in vitro* differentiated hMDM, we found enhanced phagocytic activity in untreated ($p<0.01$) and LPS ($p<0.05$) stimulated SSc (n=29-34) compared to HC hMDM (n=12-16). Moreover, when we split the patients by disease subtypes, we did not observe a difference in phagocytic activity between the different SSc subtypes. Therefore, these results support an increased phagocytic activity already in the early stage of the disease. Further, to study if FOSL-2 might play a role in macrophage phagocytosis, we first measured FOSL-2 protein levels in hMDM from SSc patients and HC. We observed enhanced FOSL-2 protein expression in untreated ($p<0.01$) and pro-inflammatory LPS ($p<0.01$) stimulated SSc hMDM (n=18-25) compared to HC hMDM (n=11-18). Subsequently, we aimed to assess phagocytic activity after siRNA transfection. We observed a reduction in phagocytic activity in untreated hMDM (n=8) transfected with *FOSL2* compared to negative control siRNA ($p<0.001$).

Conclusion:
For the first time, we show that FOSL-2 is a driver of newly identified pro-phagocytic macrophages and a crucial contributor of enhanced macrophage phagocytosis in patients with SSc.

520

A. Ritter[3], A. Wiegand[3], N. Graf[4], S. Dahdal[1], D. Sidler[1], S. Arampatzis[1], K. Hadaya[2], T. Müller[3], C. Wagner[5], R. Wüthrich[3], N. Mohebbi[3]

Effect of alkali therapy on kidney function in kidney transplant recipients with metabolic acidosis (Preserve-Transplant Study)

Division of Nephrology, Inselspital, Berne, Switzerland[1], Division of Nephrology, University Hospital, Geneva, Switzerland[2], Division of Nephrology, University Hospital, Zurich, Switzerland[3], Graf Biostatistics, Winterthur, Switzerland[4], Institute of Physiology, University of Zurich, Zurich, Switzerland[5]

Introduction:
Kidney transplantation is the preferred treatment for patients with end-stage renal disease. It is associated with reduced morbidity, mortality and cost in most affected patients compared to dialysis. As organs are short and long-term graft survival is still limited, a better understanding of the underlying causes and an improvement of treatment is needed. In the last years, several retrospective observational studies have shown that metabolic acidosis is highly prevalent and associated with graft loss in kidney transplant recipients. While randomized controlled trials have shown a beneficial effect of alkali treatment on CKD progression in the non-transplant chronic kidney disease (CKD) population an interventional trial in kidney transplant patients is lacking.

Methods:
We conducted a multi-centric, randomized, patient-blinded, placebo-controlled phase III trial over 2 years to test the effect of alkali therapy on allograft function. Patients were randomly assigned in a 1:1 ratio to receive either oral sodium bicarbonate (1.5 to 4.5 g per day) or matching placebo. The main eligibility criteria comprised renal transplantation of at least 12 months, baseline eGFR between 15 and 89 ml/min/1.73m2, serum bicarbonate levels ≤22 mmol/l. The primary outcome was the yearly slope of the estimated glomerular filtration rate (eGFR). eGFR was calculated with the creatinine-based CKD-EPI equation. Subgroup analyses were performed for different CKD stages, baseline serum bicarbonate levels, type of immunosuppression, immunization, transplantation vintage, and type of allograft. The trial is registered with ClinicalTrials.gov (NCT03102996).

Results:
Between June 2017 and July 2021, 240 patients were included into the intention to treat population. Their mean age was 55.5 ±13.5 years at baseline. The majority of the study population (92.5%) received a calcineurin inhibitor-based immunosuppressive treatment. Living donations accounted for 39.6% of patients. Baseline eGFR (47.7±15.8 ml/min/1.73m2 in the placebo group versus 48.2±16.3 ml/min/1.73m2 in the verum group) and serum bicarbonate levels at baseline (20.7±1.9 mmol/l versus 21.3±2.6 mmol/l) did not differ significantly between groups. We did not find a significant difference in yearly eGFR slopes over the 2-year study period, that amounted -0.722 (5.521) in the placebo versus -1.413 (5.642) in the bicarbonate group (median; IQR). This result was confirmed in the per protocol population and throughout the prespecified subgroup analyses. Safety was similar between the two treatment groups.

Conclusion:
Treatment of metabolic acidosis in adult kidney transplant patients with sodium bicarbonate over 2 years had no beneficial effect on eGFR slopes and should therefore not be recommended as treatment to preserve allograft function.

521

T. Roloff Handschin[1], H. Seth-Smith[1], F. Imkamp[1], A. Egli[1]

Optimizing the whole genome sequencing workflow in a diagnostic microbiology lab to improve the utility for clinical customers

Institute for Medical Microbiology[1]

Introduction:
Whole genome sequencing (WGS) of pathogens is an important tool for diagnostic and epidemiologic analyses in clinical microbiology. Typical requests are for (i) identification, (ii) resistance gene detection, and/or (iii) typing. However, workflows are laborious and expensive, and utility of WGS data is reduced by the long turn-around time (TAT). Furthermore, the upcoming regulation (IVDR) introduces many uncertainties. Practical guidelines on how to assess the performance in different applications are lacking in the literature. We aimed to validate and improve our current workflows and highlight the critical steps.

Methods:
We compared different protocols for WGS library preparation (Table 1), as well as different combinations of Illumina sequencers and sequencing kits (Table 1). Reference strains with a range of genome sizes and %G+C (Table 2), as well as strains from local and published outbreaks, were used in the evaluation and the time-to-results from sample to sequencing data for subsequent analysis was measured. Sequencing data was processed with a custom pipeline (Figure). SeqSphere+ (Ridom) and CLC Genomics Workbench (Qiagen) were used for core genome MLST (cgMLST) and cluster analysis. Antimicrobial resistance (AMR) genes (Figure) were detected using NCBI AMRFinderPlus implemented in Seqsphere+ and ABRicate.

Results:
Critical sequencing data quality control criteria include: minimum mean read depth, species identification (rMLST, MetaPhlAn3)[HSS1] , species-appropriate assembly length and contig count, and number of mixed base-calls. Pre-sequencing steps including isolate purity and library size [HSS2] and concentration were found to have the largest influence on these parameters. Comparison of library preparation and sequencing kit combinations on the sequencing platforms shows a high concordance in identification, AMR gene detection, and cgMLST typing results, as well as SNP-based outbreak analysis. TAT was reduced by switching to a PCR free library preparation protocol, especially combined with the MiniSeq Rapid kit.

Conclusion:
We performed a critical re-evaluation of our workflows, fulfilling the ISO17025 norm. Documentation of QC at several stages helped us to set check-points within the sequencing workflows. We propose a rapid workflow for urgent WGS from bacterial cultures that can improve decision-making of our customers in infectious disease or hospital epidemiology departments.

522

J. Hoffmann[1], R. Grossmann[1], A. Widmann[1]

Academic clinical trials: Publication of study results on an international registry – we can do better!

Clinical Trials Center, University of Zurich and University Hospital Zurich, Zurich Switzerland[1]

Introduction:
Clinical research is vital for evaluation and development of new therapeutic medical approaches. After completion of any clinical study it is essential to share the main results with the scientific community and with general public as well. Results and conclusions from academic clinical trials (Investigator Initiated Trials, IITs) support the treating physicians to determine evidence-based therapeutic approaches or to avoid unnecessary and expensive therapies. Therefore, omitting unexpected or negative outcomes introduces not only a huge publication bias but research community misses a big chance for closing gaps in real-world evidence. As one of the largest Clinical Trial Units (CTUs) in Switzerland the Clinical Trials Center Zurich supports IITs in all relevant research aspects including registration on an international clinical trials registry. We noticed that many IIT sponsors did not register their studies properly even though this is essential within the scientific community for transparency reasons.

Methods:
To gain a clearer view regarding the registration status of interventional clinical trials we conducted a detailed analysis by extracting data published on ClinicalTrials.gov and investigated clinical trials worldwide started between January 01, 2015 and December 31, 2021. ClinicalTrials.gov also allowed us a comparison between IITs and industry-sponsored studies by selecting the type of funding. We analyzed the completion status (not completed/ongoing vs. completed with final results not available vs. completed with final results available) of IITs and industry-sponsored studies for direct comparison.

Results:
With a share of more than 70%, Phase I trials (first-in-human) were mostly industry-sponsored projects. Exploratory Phase II trials were equally distributed between sponsors from academia and industry (50% each) and responsibility for confirmatory Phase III trials almost reached parity as well (IIT: 47%, industry: 53%). Most of postmarket Phase IV trials were sponsored by academia with 75%. More than 45% of the registered clinical trials were ongoing at the time of analysis across all phases. The percentage of ongoing IITs was always higher vs. the share of ongoing industry-sponsored studies. The overall percentage of completed clinical studies with final results available (out of all registered completed trials) was low in both groups, i.e., 18% for IITs and 34% for industry-sponsored studies. Results were published for 12% of IITs in Phase I, 20% in Phase II, 13% in Phase III and 21% in Phase IV. In contrast, industry-sponsors made the results of their studies available for 15% in Phase I, 46% in Phase II, 56% in Phase III and 46% in Phase IV. Academic sponsors reported their clinical trial results significantly less often than industrial sponsors for all four clinical trial phases as shown by the odds ratio (OR) – Phase I: 0.72 (95% CI 0.61–0.84); Phase II: 0.30 (95% CI 0.27–0.33); Phase III: 0.12 (95% CI 0.10–0.14); Phase IV: 0.30 (95% CI 0.26–0.34). Researchers in the United States of America registered their results for completed IITs most frequently with 54%, followed by research fellows in the United Kingdom (12%), Germany (8%), Japan (7%) and China (4%).

Conclusion:
Currently, researchers in general and academic sponsors in particular do not focus sufficiently on the obligations for results‘ publication. Reasons for non-publication could be restricted financial and personal capacities, concerns of intellectual property rights, detrimental outcomes or premature study discontinuation. Thus, measures for improvement of regulatory compliance and quality are needed to increase researchers’ awareness and also to enhance the trust of the public and individual study participants in clinical research activities.

523

J. Hoffmann[1], A. Blümle[3], R. Grossmann[1], H. Yau[2], B. Lang[3], C. Bradbury[3]

The Importance of international Harmonization for Clinical Research – a global survey on quality standards and services of academic Clinical Trial Units

Clinical Trials Center, University of Zurich and University Hospital Zurich, Zurich Switzerland[1], Clinical Trials Centre, The University of Hong Kong, Pokfulam, Hong Kong[2], Clinical Trials Unit, Faculty of Medicine and Medical Center - University of Freiburg, Freiburg, Germany[3]

Introduction:
Clinicians around the globe perform clinical research in addition to their high workload in everyday medical life. In order to meet the demands of high quality Investigator Initiated Trials (IITs), Clinical Trial Units (CTUs) as part of Academic Research Institutions are implemented worldwide and are considered a core element to enable and coordinate excellence in academic clinical research. In this project, we aimed to identify essential services for CTUs, ensuring a smooth processing of a clinical trial.

Methods:
According to the AMEE guide, we developed a questionnaire, addressing the perceived importance of different CTU-services. Survey participants were senior representatives of CTUs being part of the International Clinical Trials Center Network (ICN) with long-lasting experience in their field and institution.

Results:
The CTUs were founded between 1952 and 2013 with a median founding year of 2006. The median number of employees was 42 with a maximum of 260 and a minimum of eight. The estimated percentage of the coordinated IITs out of all studies (i.e. IITs plus industry-sponsored studies) from January to December 2020 reached a median of 90%. Each CTU ranked the 23 service categories selected by us through our national document review process. Services concerning quality and coordination of a research project were considered most essential, i.e. *Quality management*, *Monitoring* and *Project management*, followed by *Regulatory & legal affairs*, *Education and training* and *Data management*. Operative services for conducting a research project, i.e. *Study Nurse with patient contact* and *Study Nurse without patient contact*, were considered as least important. We analyzed the coverage of the services *Study Nurse with patient contact* and *Study Nurse without patient contact* depending on the number of employees of the CTUs. We performed a Chi-Square Test of Independence: with a p-value of 0.39 and 0.71 for the services *Study Nurse with patient contact* and *Study Nurse without patient contact*, respectively, we could assume that the two variables “coverage” and “number of employees” were independent. The number of employees had no effect on whether the services were covered or not.

Conclusion:
Emerging CTUs should primarily focus on (quality) management services and regulatory & legal affairs. Additionally, especially for IITs, well-trained clinicians with good knowledge on current GCP practice are essential. Therefore, education and training should not be neglected. Each CTU should evaluate whether the expertise and the resources are available to offer operative services. Independent of the services provided by the CTU, a good collaboration between CTUs and sponsors, investigators and clinicians is most important, leading to GCP compliant conduct of studies, keeping the study costs reasonable and profiting both researchers and the public. There should be international efforts to set standards and to create concepts for harmonization of trial processes and trial-related services. Our work constitutes a focused resource that can scientifically inform such (future) efforts.

524

J. Epprecht[4], B. Ledergerber[4], M. Frank[3], M. Greutmann[3], M. Van Hemelrijck[2], L. Ilcheva[2], M. Padrutt[4], B. Stadlinger[1], M. Özcan[5], T. Carrel[2], B. Hasse[4]

Increase of infective endocarditis due to viridans Streptococci among patients at moderate risk after change of guidance on antibiotic prophylaxis to prevent infective endocarditis: Results from a tertiary care referral centre in Switzerland

Clinic of Cranio-Maxillofacial and Oral Surgery, University of Zurich[1], Department of Cardiac Surgery, University Hospital Zurich[2], Department of Cardiology, University Hospital Zurich[3], Department of Infectious Disease and Hospital Epidemiology, University Hospital Zurich[4], Division of Dental Biomaterials, Centre of Dental Medicine, Clinic of Reconstructive Dentistry, University of Zurich[5]

Introduction:
The link of oral bacteria with infective endocarditis (IE) has been known for many decades. It is an ongoing conundrum whether to prescribe antibiotic prophylaxis (AP) to prevent IE prior to invasive dental procedures or not. In 2007/2008, Swiss and international guidelines restricted AP to patients at high risk of IE. We aimed to evaluate factors associated with IE due to viridans Streptococci (VGS) among the different IE risk groups using data of the University hospital of Zurich (Switzerland).

Methods:
We assessed patients with any type of IE aged 18 or older from January 1, 2000 through September 30, 2022 and categorized patients as “high-risk” in case of a previous history of IE, a prosthetic or repaired heart valve, an unrepaired cyanotic congenital heart disease, or certain repaired congenital heart defects. Patients with a history of rheumatic fever or non-rheumatic valve disease (e.g. mitral valve prolapse or bicuspid aortic valve) and hypertrophic cardiomyopathy were classified as “moderate risk” individuals. Patients with an implanted pacemaker/cardioverter, left ventricular assist devices, and cardiac transplant recipients with cardiac valvulopathy were categorized in the “low/ unknown risk” group. In order to study the possible impact of the 2008 AP recommendations, we divided the observation period in two periods (period one: January 1, 2000 to December 31, 2008; and period two: January 1, 2009 to September 30, 2022). We analysed prevalence differences of VGS IE among participants of different IE risk groups and fit univariable and multivariable logistic regression models for the odds (OR) of IE due to VGS. Final models were adjusted for age per 10 years older, sex, Charlson Comorbidity Index (CCI), intravenous drug abuse (IVDU), poor oral hygiene, high-risk dental procedures, IE risk category and time period.

Results:
Overall, 752 cases of IE were identified, whereby 163 cases were detected in period one and 589 in period two. Compared to other pathogens, the overall proportion of IE due VGS was 21%, Proportions for period one vs. two were 24% vs. 16%, 24% vs. 37%, 33% vs. 7% and 18% vs.13% for the high-risk, moderate-risk, unknown/low risk or no risk group, respectively. Participants in the moderate risk group and an IE episode in period two had a 21% [95% Confidence interval (C.I.) 4.5-38] higher chance of an IE due to VGS. Univariable associations with IE due to VGS were: Age (per 10 year older OR 0.80 [0.72-0.88]), CCI >5 (OR 0.47 [0.27-0.81]), IVDU (OR 0.47 [0.25-0.89]) and dental procedure (OR 2.28 [1.40-3.69]). After multivariable adjustment, the moderate risk group had a twofold risk of developing an endocarditis due to VGS (OR 2.38 [1.07-5.29]) in period two compared to period one. The other associations such as age (OR 0.79 [0.70-0.89]), dental procedures (OR 2.50 [1.34-4.65]), and IVDU (OR 0.35 [0.17-0.71]) remained unchanged.

Conclusion:
Prevalence rates of IE and IE due to VGS in particular increased over time. An association was found between IE due to VGS with the IE moderate risk group and the period after the AP guideline change. While the guidelines currently do not recommend AP, we recommend regular annual dental review and comprehensive knowledge transfer about IE risk for patients at moderate risk.

525

A. Tarnutzer[1], V. Haunreiter Dengler[1], M. von Matt[1], J. Bär[1], S. Hertegonne[1], F. Andreoni[1], C. Vulin[1], L. Künzi[1], C. Menzi[1], P. Kiefer[2], J.A. Vorholt[2], A.S. Zinkernagel[1]

C-di-AMP levels influence Staphylococcus aureus cell wall thickness and virulence

Department of Infectious Diseases and Hospital Epidemiology, University Hospital Zurich, University of Zurich, Zurich, Switzerland[1], Institute of Microbiology, Department of Biology, ETH Zurich, Zurich, Switzerland[2]

Introduction:
The second messenger molecule cyclic di-3′, 5′-adenosine monophosphate (c-di-AMP) plays a crucial role in many bacterial species as it affects various cellular processes, including virulence, salt and cell wall homeostasis and resistance to beta-lactams. Beta-lactams are widely used to treat infections caused by the important human pathogen *Staphylococcus aureus*. However, methicillin-resistant *Staphylococcus aureus* (MRSA) are common in hospital-acquired infections. In general, resistance to beta-lactam antibiotics in *S. aureus* is mediated by the additional penicillin-binding protein 2a (PBP2a) encoded on the *mec* genes or by upregulation of PBP4 in *mec*-negative strains. Recently, c-di-AMP was shown to be an additional resistance mechanism with a clinical importance. Beta-lactam-resistant clinical isolates without *mec* determinants and normal PBP4 levels harboured mutations in the *gdpP* gene. GdpP is one out of two phosphodiesterases that degrade c-di-AMP in *S. aureus*. In the absence of GdpP or Pde2, the second phosphodiesterase, c-di-AMP levels are elevated while a reduction in the c-di-AMP synthesizing enzyme DacA leads to decreased c-di-AMP levels.
In this work, we assessed the impact of c-di-AMP levels on various virulence determinants such as growth, oxidative stress survival and resistance to cell wall active antibiotics in a set of strains with either increased or decreased c-di-AMP levels.

Methods:
Colony growth rates of the S. aureus Lac* WT strain and its isogenic mutants characterized by either high (Δ*gdpP*, Δ*pde2*) or low (*dacA*$_{G206S}$) c-di-AMP levels were assessed based on OD and colony forming units (CFUs). Cell size and division time were quantified using single cell microscopy of bacteria growing in a mother-machine microfluidic device and cell wall thickness was evaluated using transmission electron microscopy. Resistance to various cell-wall active antibiotics, survival upon H_2O_2 stress as well as staphyloxanthin concentrations were assessed.

Results:
We found that a previously described growth defect in bacteria with high c-di-AMP levels is mainly attributable to a smaller cell size. Strains with high c-di-AMP levels showed decreased survival after oxidative stress, had reduced staphyloxanthin concentrations, increased resistance to oxacillin and fosfomycin, and increased cell wall thickness. The increase in antibiotic resistance and cell wall thickness diminished in the ΔgdpP mutant by deletion of *vraR*, the regulator of the three-component regulating system VraTSR, which activates a set of genes leading to an increase in cell wall synthesis upon cell wall stress.

Conclusion:
High c-di-AMP levels lead to increases oxacillin and fosfomycin resistance and a thicker cell wall. Mutations in the c-di-AMP-degrading enzyme GdpP are a clinically relevant mechanism for beta-lactam resistance in *mec*-negative strains. It is hence important to gain more knowledge about the impact of altered c-di-AMP levels in *S. aureus*.

526

L. Luise[1], V. Matus[1], R. Sánchez Álvarez[1], A. Montalban-Arques[1], M. Scharl[1], M. Spalinger[1]

The role of PTPN23 in intestinal epithelial cells and macrophages in acute colitis

Klinik für Gastroenterologie and Hepatologie[1]

Introduction:
Protein tyrosine phosphatase (PTP) non-receptor type 23 (PTPN23) is a member of the PTP family. By removing phosphate groups from tyrosine residues PTPs are involved in cell differentiation, proliferation, apoptosis, adhesion, motility, invasion and migration. In addition to its PTP function, PTPN23 is also involved in endosomal sorting and responsible for epidermal growth factor receptor (EGFR) internalization from the cell surface and thereby negatively controls EGFR signaling. PTPN23 is highly expressed in intestinal epithelial cells and intestinal macrophages, but its role in these cell types remains elusive.

Methods:
Floxed PTPN23 mice were crossed with mice expressing Cre-recombinase (Cre) under different tissue specific promotors. Cre expression under Villin promotor was used to delete PTPN23 in intestinal epithelial cells (PTPN23fl/flVilCre+/-) mice expressing a tamoxifen inducible Cre- under the villin promotor (PTPN23fl/flVilCreERT+/-) for an inducible knockout in intestinal epithelial cells and mice expressing Cre under Lyz2 promoter to delete PTPN23 in myeloid cells (PTPN23fl/flLysMCre+/-).
Expression of Cre-recombinase in PTPN23fl/flVilCreERT+/- mice was induced by daily i.p. injection of 1mg tamoxifen for five days. EGFR inhibition was realized by treatment with 0.2mg Gefitinib. Microbiota was depleted by daily gavage with 200 µl antibiotics solution (5 mg/ml Metronidazole, 2.5 mg/ml Ampicillin, 5 mg/ml Neomycin and 5 mg/ml Vancomycin). Acute colitis was induced in PTPN23fl/flLysMCre+/- mice by the administration of 2% DSS in drinking water for 7 days. All animal experiments were performed according to local animal welfare legislation and were approved by the Veterinary Office of the Canton Zurich. Molecular biology methods (RNA isolation, qPCR, Western blots) were performed following standard protocols.

Results:
Deletion of PTPN23 in intestinal epithelial cells (IEC) resulted in spontaneous intestinal inflammation in mice (PTPN23fl/flVilCre+/-) as observed by lower body weight, higher spleen weight in relation to body weight and higher proliferation presenting itself in longer colon and small intestine. EGFR inhibition could not compensate this inflammatory phenotype. Antibiotic treatment prevented the phenotype and resulted in normal weight development and reduced disease activity, normal colon and small intestine length and spleen weight.
In contrast, PTPN23fl/flLysMCre+/- mice showed no spontaneous phenotype, but they were protected against DSS induced acute colitis when compared to their PTPN23fl/flLysMCre-/- (WT) littermates. This was apparent by a lack of DSS-induced weight reduction. Reduced colon length, elevated endoscopic colitis scores and higher spleen weights seen in WT mice were not present in PTPN23fl/flLysMCre+/- mice. On RNA level a lower expression of proinflammatory cytokines interleukin 6 (IL6) and tumor necrosis factor α (TNFα) in PTPN23fl/flLysMCre+/- mice compared to WT mice was detected.

Conclusion:
PTPN23 deletion in IECs causes intestinal inflammation and elevated proliferation of IECs. Antibiotic treatment rescues this phenotype and suggests the involvement of microbiota in PTPN23 KO-mediated inflammation in intestinal epithelia, while EGFR signaling seems not to be responsible for the phenotype. This implies the involvement of other cell proliferation and inflammation pathways. The protective effect of PTPN23 KO in myeloid cells against DSS induced acute colitis indicates a different role of the protein in IECs compared to myeloid cells.

527

A. Kraft[1, 2, 4], M. Meerang[2], MB. Kirschner[2], V. Boeva[1, 3, 4], I. Opitz[2]

Transcriptomic Characterization of Extracellular Vesicles Secreted In Pleural Mesothelioma

Department of Computer Science, Institute for Machine Learning, ETH Zurich, Zurich, Switzerland[1], Department of Thoracic Surgery, University Hospital Zurich, Zurich, Switzerland[2], INSERM, U1016, Cochin Institute, CNRS UMR8104, Paris Descartes University, Paris, France[3], Swiss Institute of Bioinformatics (SIB), Zurich, Switzerland[4]

Introduction:
Given the mediating role of extracellular vesicles (EVs) in cell-cell communication, our goal is to study the transcriptomic profile of EVs secreted by pleural mesothelioma (PM) cell lines. We believe that understanding the composition of the vesicles will help to identify potential markers for early diagnosis and new targets of this devastating disease.

Methods:
We established primary cell cultures from pleural effusion of 4 PM patients. We cultured cells in serum free medium for 24 hours and isolated EVs from cell culture supernatants using Qiagen Exoeasy kit. RNA was extracted using the mirVana PARIS kit followed by transcriptome sequencing. Data was mapped on the GRCh38 genome, gene expression was calculated using Kallisto. Publicly available data from healthy plasma samples (GSE100206) was analysed analogously. Differentially expressed genes were analysed using edgeR. Enriched pathways were called with fgsea and MSigDB hallmarks of cancer.

Results:
We identified 15,822 expressed genes in the mesothelioma EV samples: mainly protein coding genes (12,644), but we also identified a significant number of long non-coding RNAs (2,052). By comparing gene expression of healthy and mesothelioma EVs, we identified genes upregulated in mesothelioma (logFC>5, FDR<0.05), including long non-coding RNAs already shown to be associated with cancer: SNHG15 (linked with worse overall survival in mesothelioma) and SNHG17 (associated with cell cycle progression and proliferation in a pan-cancer study). Epithelial-to-Mesenchymal Transition, Glycolysis and Hypoxia were the most enriched processes in mesothelioma-derived EVs (FDR<10^-7).

Conclusion:
We characterised transcriptomic profiles of EVs obtained from mesothelioma primary cell lines and compared them with transcriptomic profiles of vesicles from healthy samples. We identified genes upregulated in mesothelioma secretome and their key molecular processes. In next steps, we will study the main drivers of the key processes and their association with patients' clinical features. More primary cells will be screened in the next months.

528

J. Mengers[2], M. Haberecker[1], M. Kirschner[2], N. Bosbach[2], O. Lauk[2], I. Opitz[2], M. Meerang[2]

Low Ki-67 Positive Index is Prognostic Factor for Better Survival Outcomes of Patients Treated with Intracavitary Cisplatin-Fibrin

Department of Pathology and Molecular Pathology, University Hospital Zurich, Zurich, Switzerland[1], Department of Thoracic Surgery, University Hospital Zurich, Zurich, Switzerland[2]

Introduction:
Novel therapeutic approach is needed for patients with pleural mesothelioma (PM), an aggressive cancer driven by asbestos exposure. Our phase II clinical trial for localized chemotherapy with cisplatin-fibrin after surgery (INFLuenCe – Meso) investigated safety and efficacy of this novel approach. Here, we aimed to identify biomarkers associated with outcomes for future application in patient selection.

Methods:
We collected tumor tissues at surgery, before start of localized treatment, from all patients enrolled (n=23). FFPE tissues were immunohistochemically stained for p21 (cisplatin resistance) and Ki-67 (proliferation). Using Qupath software, we classified tumor cells from stroma. Number of positive cells (%) were automatically counted from 1,050 - 208,751 tumor cells/slide. For P21, we also differentiated weak (1), moderate (2) and strong (3) staining. Thus, we also acquired H-score (sum of intensity x % positive cells). The association between marker expressions with clinical parameters and disease outcomes including progression free survival (PFS) and overall survival (OS) was analysed by SPSS software.

Results:
Ki-67 staining index (%) ranged from 1.2 - 44 (median 12.4). P21 staining index and H–score (range (median)) are 0 - 96 (21) and 0 - 225 (32), respectively. High Ki-67 labelling index was significantly associated with shorter PFS (p=0.001, median (95% CI): 26.6 (11.7 - 41.6) vs 8.6 (6.8 -10.4) months) and OS (p<0.001, 39 (27.2 – 50.9) vs 16 (12.3 – 19.6) months). There was no association between clinical parameters with Ki-67 or p21 staining. p21 staining index and H-score showed no association with disease outcomes.

Conclusion:
Although a small patient cohort, Ki-67 showed significant association with disease outcomes for patients receiving localized cisplatin-fibrin. We are currently assessing Ki-67 in tissues collected at diagnosis to confirm the association with survival prior to therapy. Ki-67 may be useful for the selection of patients for this treatment regimen.

529

B.M. Carrara[1], Q. Vallmajo-Martin[1], M. Ehrbar[1]

Mesenchymal Stromal Cells Characterized Through In Vivo Bone Marrow Organoids

Laboratoty of Fetal Healing and Tissue Engineering, Department of Obstetrics, University Hospital Zürich, Schmelzbergstr. 12, 8091, Zürich, Switzerland[1]

Introduction:
The bone marrow (BM) is a dynamic organ whose main function is to support haematopoietic cells, which assure life-long production of blood. The haematopoietic compartment is supported by the stromal fraction of the BM that comprises mesenchymal stromal cells (MSCs), a heterogeneous cell population undergoing osteogenic, chondrogenic, adipogenic differentiation. Following a tissue engineering approach, we combine the knowledge on BM-MSCs with biomaterials to dissect such cells heterogeneity and model BM biology. Our technology consists in encapsulating BM-MSCs in synthetic, biocompatible polyethylene glycole (PEG) hydrogels and following cells developmental potential in vitro and in vivo. We are currently focusing on the in vivo characterization of several BM-MSCs populations, both of human and murine origin, such as Skeletal Stem Cells (SSCs) and Bone Cartilage Stromal Progenitors (BCSPs), aiming at generating new knowledge for bone and bone marrow biology and regenerative strategies.

Methods:
Human BM-MSCs were isolated from bone marrow aspirates of healthy donors during orthopedic surgical procedures after informed consent and in accordance with the local ethical committee (University Hospital Basel; Prof. Kummer; approval date 26/03/2007 Ref. Number 78/07). Murine BM-MSCs subsets, SSCs and BCSPs, were mechanically and enzymatically extracted from limbs and sternum of post-natal day3 GFP+-C57/BL6 mice and separated by FACS using the marker panels CD45-Ter119-Tie2-AlphaV+Thy-6C3-CD105-CD200+ and CD45-Ter119-Tie2-AlphaV+Thy-6C3-CD105+, respectively.
Due to the high amount of cells needed for in vivo trials, the cells were expanded under standard culture conditions for 7 days. Subsequently, the cells were encapsulated at different cell densities in PEG hydrogels with or without minimal amounts of BMP-2. Such scaffolds were subcutaneously implanted at the back of NMRI-Foxn1nu immunocompromised mice and harvested after 8 weeks. Upon explantation, samples were macroscopically inspected, imaged and fixed. Bone formation was quantified through micro-CT analysis, followed by decalcification and histological characterization.

Results:
At explantation, all the scaffolds were found back with their initial size (0.5 cm), confirming biomaterial stability. A first macroscopic evaluation showed murine SSCs and human BM-MSCs being more performant than murine BCSPs as they induced the formation of stiffer ossicles with high degree of vascularization both with and without BMP-2, at different cell densities. BCSPs generated ossicles only when in combination with BMP-2. These observation were confirmed via microCT. Histological analysis showed higher morphological complexity in ossicles derived from murine SSCs and human BM-MSCs. In particular, cortical and trabecular bone together with marrow cavities carrying a marrow inside with hematopoietic cells and adipocytes were observed in sections from these samples. A lower morphological complexity level was detected in sections from murine BCSPs-derived ossicles.

Conclusion:
The results suggest that our technology can generate 3D in vivo BM organoids recapitulating the structural compartments of native bone and marrow. Moreover, it proved to be a good instrument for investigating the biological function of BM-MSCs subsets, since different outcomes from SSCs or BCSPs-loaded scaffolds were observed.

530

F. Xiu[1], M. Visentin[1]

The Effect of 7-ketocholesterol on the Function of Organic Cation Transporter 2 (OCT2)

University Hospital Zurich[1]

Introduction:
The organic cation transporter 2 (OCT2) is a membrane transporter mediating the renal elimination of several endobiotics, xenobiotics and drugs. OCT2 function is highly dependent on the membrane cholesterol content, which can be altered in physio-pathological conditions such as aging and acute kidney injury. The balance between cholesterol and ROS-induced oxidized cholesterol, which displays one oxygen-containing group in position C7, can also change in kidney disease.
Aim: To characterize the effect of 7-ketocholesterol substitution on protein stability, substrate binding and cycling of OCT2 in vitro.

Methods:
Experiments were performed in wild type and OCT2 stably transfected HEK293 cells. Cholesterol depletion and exchange was achieved by 30-min exposure to empty methyl-β-cyclodextrin (mβcd) or to sterol-saturated mβcd, respectively. Sterols quantification has been performed by high performance thin layer chromatography. Uptake of the radiolabeled model substrate 1-methyl-4-phenylpyridinium (MPP+) was measured using a protocol for rapid uptake determination in adherent cells. Surface labeling coupled to western blotting was used for assessing OCT2 localization on the plasma membrane. Stepwise solubilization was used to assess the localization of OCT2 in lipid rafts and the effect of cholesterol manipulation on lipid raft integrity.

Results:
A 30 min-exposure to 5 mM mβcd reduced the total cholesterol content by 50%. Exposure to 5 mM 7-ketocholesterol-mβcd did not alter the total content of sterol, however 50% of endogenous cholesterol was replaced by exogenous 7-ketocholesterol. MPP+ OCT2-mediated maximal transport capacity (Vmax) in cells exposed to mβcd or 7-ketocholesterol-mβcd was significantly lower than that in cells exposed to cholesterol-mβcd. However, OCT2 expression level on the plasma level was comparable between treatments. OCT2 was not localized in lipid rafts. Moreover, 7-ketocholesterol did not alter lipid raft integrity.

Conclusion:
Substitution of cholesterol with 7-ketocholesterol increased the binding affinity of OCT2 for MPP+ but reduced the Vmax. 7-ketocholesterol might constrain the transporter to a higher affinity state at the expense of insufficient free energy to overcome this constraint to achieve mobility and transport.

531

C. Perez-Shibayama[3], C. Gil-Cruz[3, 5], N. Cadosch[3], M. Lütge[3], H. Cheng[3], K. Frischmann[3, 5], A. Joachimbauer[3, 5], L. Onder[3], I. Papadopoulou[3], C. Papadopoulou[3], S. Ring[3], P. Krebs[4], V. Vu[4], M. Nägele[5], V. Rossi[5], D. Parianos[5], V. Zsilavecz[2], L. Cooper[1], A. Flammer[5], F. Ruschitzka[5], P. Rainer[2], D. Schmidt[5], B. Ludewig[3, 5]

Bone morphogenic protein-4 availability in the cardiac microenvironment controls myocardial inflammation and fibrosis

Department of Cardiovascular Medicine, Mayo Clinic, Jacksonville, Florida, USA[1], Division of Cardiology, Medical University of Graz, Graz, Austria[2], Institute of Immunobiology, Kantonsspital St.Gallen, St. Gallen, Switzerland[3], Institute of Pathology, University of Berne, Berne, Switzerland;[4], University Heart Center, University Hospital Zurich and University of Zurich, Zurich, Switzerland[5]

Introduction:
Myocarditis is a prototypic inflammatory heart disease and one of the most common causes of myocardial damage in patients with suspected myocardial infarction but non-obstructive coronary arteries. Acute myocardial inflammation develops into chronic, potentially lethal inflammatory cardiomyopathy in 20-30% of patients. Currently, treatments for acute and chronic myocardial inflammation have limited effectiveness, despite the identification of a plethora of pathways leading to myocardial inflammation, the elucidation of effective therapeutic intervention remains incomplete because the overarching molecular mechanisms that govern the balance between myocardial homeostasis and inflammation are incompletely understood.
Recent single cell transcriptomics-based analyses of healthy and diseased human cardiac tissues have revealed that inflammation is a common denominator associated with a wide range of cardiomyopathies and heart failure. The interaction of immune cells with non-hematopoietic cells in the cardiac microenvironment is regulated by surface molecules and soluble factors that act at short range. For example, tissue cytokines belonging to the transforming growth factor-b superfamily including bone morphogenetic proteins (BMPs) are of particular importance for the homeostasis and functional preservation of the cardiac tissue. Although BMP signaling appears to be involved in the remodeling process of the injured heart, surprisingly little is known about the role of this pathway in cardiac inflammation and fibrosis.

Methods:
We used single cell transcriptomics of inflamed human and murine heart tissue to assess whether and to what extent dysregulation of BMPs is associated with myocardial inflammation and cardiac tissue integrity. To further study the role of BMPs in myocarditis we developed monoclonal antibodies that block the BMP inhibitors Gremlin-1 and Gremlin-2.

Results:
Our results revealed that the BMP4-Gremlin (GREM)1/2 axis is a key pathway involved in the maintenance of homeostatic heart function. Antibody-mediated neutralization of both GREM1 and GREM2 reinvigorated BMP signaling in the inflamed myocardium and thereby attenuated immune cell activity, reduced fibrotic remodeling and preserved cardiomyocyte integrity in a mouse model of myocarditis.
To validate translational relevance for the observed dysregulated cardiac BMP activity during myocardial inflammation, we used snRNA-seq analysis to characterize the cellular and molecular landscape of inflamed human cardiac tissue. We analyzed endomyocardial biopsies from patients with suspected cardiac inflammation (acute myocarditis), inflammatory cardiomyopathy, dilated cardiomyopathy, as well as from patients undergoing routine EMB sampling after heart transplantation. These data indicate that the global level of immune cell concentration and activation in the inflamed human myocardium is linked to dysregulated BMP signaling. Moreover, we found significantly reduced BMP4 serum concentration in myocarditis patients in comparison to age-matched healthy volunteers.

Conclusion:
Selective restoration of BMP signaling in the inflamed heart facilitates treatment of myocardial inflammation and thereby efficiently diminishes cardiac fibrosis and prevents heart failure in a mouse model of myocarditis. Moreover, reduced BMP4 production is a major trait of perturbed myocardial homeostasis and a potential biomarker for the diagnosis in human myocarditis.

532

P. Wallimann[2], B. Pouymayou[1, 2], M. Mayinger[2], S. Nowakowska[3], A. Boss[3], M. Guckenberger[2], S. Tanadini-Lang[2], N. Andratschke[2]

Phantom measurements of apparent diffusion coefficient on a 0.35T MR-Linac

Department of Neuroradiology, University Hospital Zürich, Zürich, Switzerland[1], Department of Radiation Oncology, University Hospital Zürich, Zürich, Switzerland[2], Department of Radiology, University Hospital Zürich, Zürich, Switzerland[3]

Introduction:
Using diffusion-weighted MR imaging (DWI) on an MR-Linac could enable new ways of early response monitoring or adapting treatment during radiotherapy. We investigated the feasibility of DWI on the MRIdian 0.35T MR-Linac (ViewRay) by analyzing the impact of different receiver coils and imaging settings on apparent diffusion coefficient (ADC) values in a phantom.

Methods:
We used a spin echo, single shot echo planar imaging DWI sequence with the settings: TR=3200, TE=120, flip angle=90, receiver bandwidth=1352, voxel size 3x3x6, 20 slices without gap, linac gantry angle 330, three orthogonal diffusion directions and five b values (0, 200, 300, 500, 800).
Furthermore, we varied the number of signal averages (NSA) (6 or 24 per b image), the coil used (head & neck coil (HNC) or prototype head coil (PHC)) and the application of prescan normalization (PN).
For each coil, a noise shot (RF transmit turned off) was acquired with NSA 6 and with PN.
We calculated the ADC values with an in-house python script using a voxel-wise mono-exponential fit. The different diffusion directions were combined using the geometric average of the intensities.
We analyzed three different variations of noise correction: No correction for noise, a correction for uniform Rician background noise (Dietrich et al, 2001) and a correction of the same form but using the non-uniform noise shot.
We investigated a custom-built phantom (HQ imaging) containing four vials with calibrated ADC values (400, 1000, 1600 and 2020), in each of which a homogeneous region of interest (ROI) was manually selected. The determined ADC values were corrected per phantom manual from the measured temperature of 20.5°C to the calibration temperature of 20°C.

Results:
The images with NSA 6, with the HNC and using PN showed a strong inhomogeneity of noise across the image, which remained roughly constant for different b values. The same pattern could also be observed on the noise shot, but to a lesser degree on images with the PHC and not at all without PN (Figure 1).

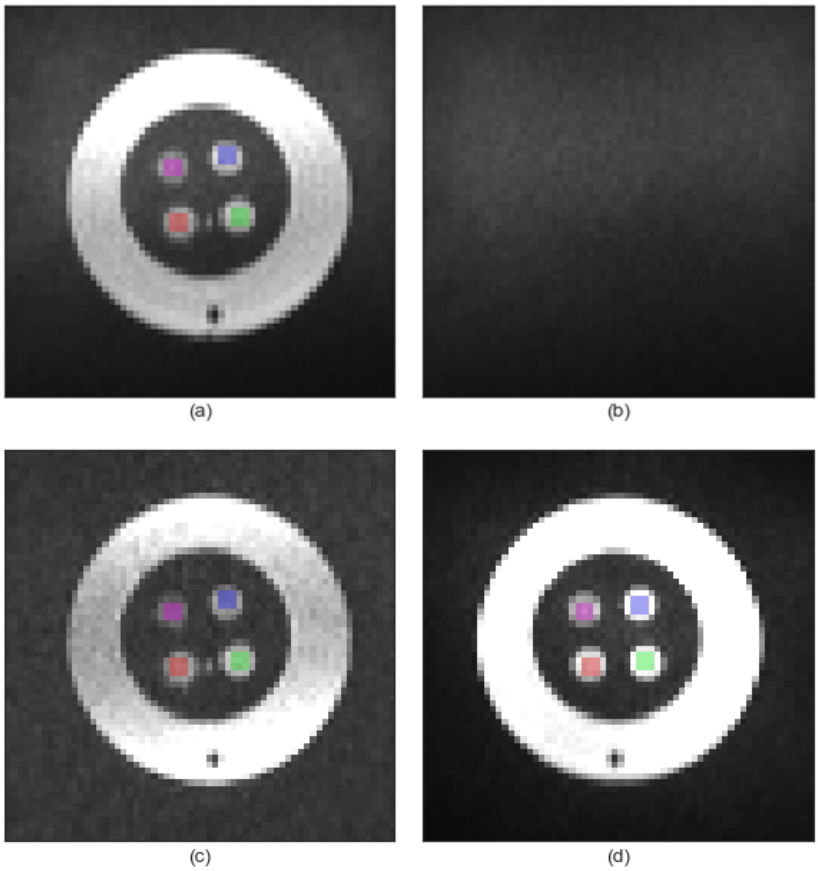

Figure 1. A single slice through four diffusion images at $b = 800 \frac{s}{mm^2}$. The selected regions of interest are highlighted in color. All images are windowed to the same intensity values to facilitate comparison. (a) head & neck coil, 6 signal averages, PN (b) head & neck coil, 6 signal averages, PN, noise shot (c) head & neck coil, 6 signal averages, no PN (d) prototype head coil, 6 signal averages, PN

Figure 2 shows the determined ADC values in each ROI. Increasing the NSA leads to smaller interquartile ranges, but almost unchanged median. Correcting for noise brings the median ADC closer to the true value in most cases. The best accuracy of the median was seen with the PHC without PN and with the uniform noise correction, where relative difference of the median to the true value ranged from -2.3% to 0.3% for the different vials.

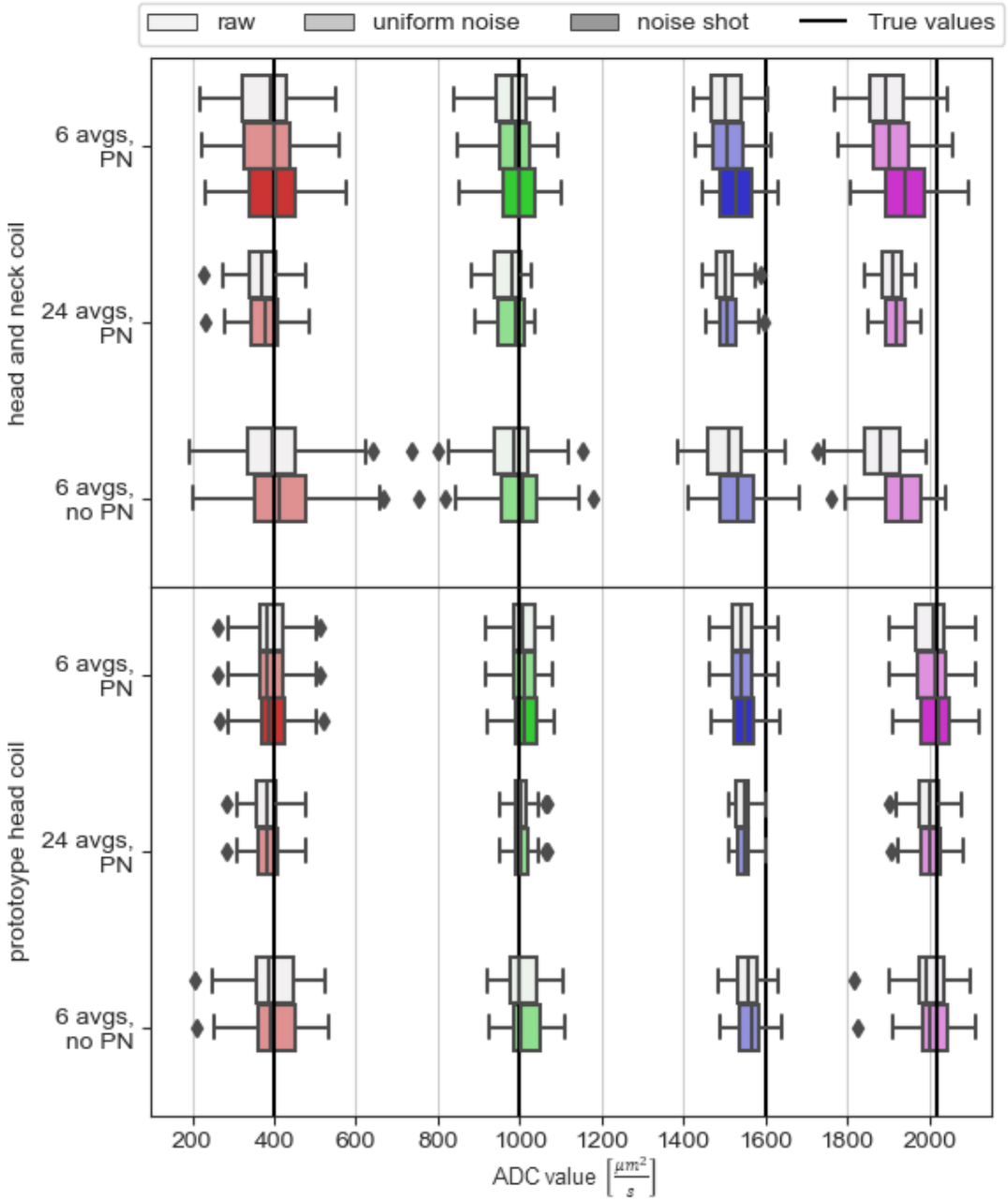

Figure 2. Boxplot of ADC values determined in each of the four vials for each setting. The different colors denote the different vials while the different shades denote different noise correction methods.

Conclusion:
The accuracy of the ADC estimates is satisfactory (error <3%) but requires special attention to noise contamination. The latter depends on the setting used, including the choice of the coil, the elements combination and the noise correction strategy. A higher NSA can increase the precision but has little benefit on accuracy of ADC values. Potential errors in the calibration of the phantom or the temperature correction were not considered for this analysis.

533

A. Zbinden[4], H. Seth-Smith[4], v. beltrami[4], S. Mancini[4], A. Egli[4], S. Droz[3], U. Bürgi[1], J. Barben[5], N. Müller[2], F. Imkamp[4]

Characterization of Burkholderia cenocepacia ST-250 isolates in patients with cystic fibrosis (CF) in Switzerland

Department of internal Medicine, Service of Pulmonology, Lucerne Cantonal Hospital, Lucerne,[1], Division of Infectious Diseases and Hospital Epidemiology, University Hospital Zurich, Zurich[2], Institute of Infectious Diseases, University of Bern, Bern[3], institute of medical microbiology, university of zurich[4], Paediatric Pulmonology and CF Centre, Children's Hospital of Eastern Switzerland, St. Gallen[5]

Introduction:
The *Burkholderia cepacia* complex (Bcc) comprises a group of genetically distinct bacteria. Colonization of the respiratory tract in CF-patients is associated with poor clinical outcome. We aimed to investigate Bcc strains from CF-patients and non-CF patients obtained in our center over a period of 20 years on a genomovar, genetic, and epidemiological level.

Methods:
We analyzed a total of 100 Bcc strains collected from 2001-2021 in our routine diagnostics using whole-genome sequencing (Illumina MiSeq, paired-end 150nt). We determined the multi-locus sequence types (MLST) from PubMLST. We performed single nucleotide polymorphism (SNP)-analysis in CLC Genomics Workbench v22.0.2. We measured antibiotic susceptibility with disk diffusion using clinical breakpoints from the Clinical and Laboratory Standards Institute (M100 32th edition).

Results:
The genomovars identified were *Burkholderia cenocepacia* n=44, *B. multivorans* n=32, *B. contaminans* n=15; *B. cepacia* n=3; *B. anthina* n=2; *B. stabilis* n=2; *B. gladioli* n=1; and *B. vietnamensis* n=1. MLST revealed B. cenocepacia ST-250 in 18 clinical samples obtained from eight CF-patients, with multiple isolates collected over up to nine years from five patients. SNP-analysis of these ST-250 strains showed clustering of isolates from patients. A within-patient genomic variation of up to 114 SNPs and a between patient variation of 68-252 SNPs were observed, respectively, suggesting that this cluster has a recent common ancestor.

B. cenocepacia ST-250 isolates exhibited high resistance towards meropenem (14/18, 77.8%), minocycline (13/18, 72.2%), and trimethoprim-sulfamethoxazole (17/18, 94.4%). Only 12/18 (66.7%) were resistant towards ceftazidime. Isolates derived over time from the same patients displayed a progressive increase in resistance towards different antibiotics.

Conclusion:
We present whole-genome data from *B. cenocepacia* ST-250. *B. cenocepacia* ST-250 isolates from five CF-patients showed within-host diversity over several years of colonization and evolution of antimicrobial resistance. Further analyses are underway to infer the timing of a common ancestor and possible transmission of B. cenocepacia ST-250 isolates.

534

N. Hermann[4, 5], L. Maul[3], M. Ameri[2, 4, 5], S. Traidl[1, 2, 4], R. Ziadlou[2, 4, 5], K. Papageorgiou[4], I. Kolm[4, 5], M. Levesque[4, 5], J. Maul[4, 5], M. Brüggen[2, 4, 5]

Vitiligo-like-depigmentation in patients with melanoma under immunotherapy: Clinical presentation and prognostic features - A monocentric prospective observational study

Hannover Medical School, Departement of Dermatology and Allergology[1], Medical Campus Davos[2], University Hospital of Basel, Departement of Dermatology[3], University Hospital of Zurich, Departement of Dermatology[4], University of Zurich[5]

Introduction:
A frequent immune-related adverse event of checkpoint-inhibitor (CPI) treatment, which manifests as depigmented spots on the skin is known as Vitiligo-like depigmentation (VLD). It has been associated with a favourable prognosis in metastatic melanoma. The aim of this study was to further characterize clinical, biological and prognostic features of melanoma patients with VLD under CPI-treatment and to explore whether they exhibit a characteristic immune response profile in peripheral blood.

Methods:
Melanoma patients developing VLD under CPI were prospectively included. We collected and analysed clinical parameters, serum samples and skin biopsies from 28 VLD patients.

Results:
They received pembrolizumab (36%), nivolumab (11%), ipilimumab/nivolumab (32%) or immunotherapy-based clinical trial medications (21%). Our clinical assessments showed that VLD lesions had a predominantly symmetrical distribution pattern, with mostly smaller “freckle-like” macules and a preferential distribution in UV-exposed areas. Patients with previous targeted therapy showed a significantly longer time lapse between CPI initiation and VLD onset compared to non-pre-treated patients. A high-throughput proteomics assay (OLINK) was performed, in which we identified a distinct proteomic signature in VLD patients in comparison to non-VLD CPI patients. A principle component analysis showed a separation and a more diverse picture in the VLD cohort. Of note, several proinflammatory chemokines such as CXCL5 and CXCL6 were reduced in VLD patients, whereas ITGA11 was increased. Therapy responders exhibited a distinct proteomic profile when compared with non-responders in VLD, e.g. with downregulation of LAG3. A survival-analysis revealed ITGA11 to be the most closely associated protein with an improved overall survival.

Conclusion:
On a proteomic level, our findings demonstrate that VLD is characterized by a distinct immune signature and that therapy responsiveness is reflected by a characteristic immune profile. Further studies are needed to explore the pathomechanisms underlying these findings.

535

L. Moser[1, 3], K. Gegenschatz-Schmid[1], N. Ochsenbein-Kölble[1, 2], M. Ehrbar[1, 3]

A 3D printed device for the in vitro investigation of novel healing strategies for fetoscopic interventions sites in fetal membrane

Department of Obstetrics, University and University Hospital of Zurich, Switzerland,[1], The Zurich Center for Fetal Diagnosis and Therapy, Switzerland[2], University of Zurich, Switzerland,[3]

Introduction:
The interest in fetal surgeries has greatly increased over the last 20 year. This is underlined by the number of clinical studies, which rose from around 20 clinical studies in 2005 to over 140 in 2019. Correspondingly, the desire for minimally-invasive prenatal interventions received more attention as well. However, a central obstacle is iatrogenic preterm premature rupture of the membrane (iPPROM) after these interventions. Despite affecting up to 30% of the operations, very little is known about the direct cause of iPPROM. However, it is known that the punctured site in the fetal membrane (FM) is often unable to heal and increases in size during the remaining pregnancy. This is in contrast to the fact, that amnion cells, which are part of the fetal membrane, can induce wound healing in various tissues such as chronic skin wounds. Despite multiple effort in the last years, there is currently no treatment to heal the fetal membrane and for the prevention of iPPROM. Therefore, novel in vitro model could help to develop new therapies.

Methods:
Punch biopsies of fetal membranes at term were embedded into enzymatically cross-linked poly(ethylene glycol) (TG-PEG) as previous described in Famos et al 2022. In contrast to the previous study, amnion and chorion were both embedded. Further FMs were placed into 3D printed devices and a punched hole was filled with TG-PEG. The response of the fetal membrane was investigated over time with viability markers and antibody staining for actin, nuclei and collagen.

Results:
Some of the fetal membrane punches embedded in TG-PEG showed proliferation or migration after embedding, even if amnion and chorion were embedded together. Others did not show any activity. FMs in the 3D devices indicated viable cells even after two weeks. A living cell ring could be seen around the punctured side and the TG-PEG gel stayed during the whole two weeks on the excavation. Without a hole the devices remained sealed and it is possible to have two separate solution on both side of the membrane. However, even with the TG-PEG in place, the solution was leaking through the punctured FMs. No spontaneous ingrowth into the TG-PEG could be observed without growth factors.

Conclusion:
The 3D devices is an interesting platform to bridge the gap between in vitro 3D cultures and in vivo studies of fetal membranes. After a first screening with embedded FM punches in hydrogels for promising factors such as growth factor or gel properties, the 3D printed devices could be the next step to investigate promising candidates. The device additionally enables the possibility to investigate the influences of “one sided” amniotic fluid on the healing process. In conclusion this device could be an additionally in vitro platform to investigate promising approaches and reduces the candidates needed to be tested in animal trials.

536

R. Fumagalli[2], A. Fürbringer-Schwarz[2], F. Catalani[2], N. Kucher[2], S. Konstantinides[1, 3], S. Barco[1, 2]

CAtheter-directed Thrombolysis for Acute PULmonary Thromboembolism (CATAPULT) study: interim analysis of individual patient-level data

Center for Thrombosis and Hemostasis (CTH), University Medical Center Mainz, Mainz, Germany[1], Department of Angiology, University Hospital Zurich, Zurich, Switzerland[2], Department of Cardiology, Democritus University of Thrace, Alexandroupolis, Greece[3]

Introduction:
Catheter-directed thrombolysis (CDT) can rapidly reverse right ventricular dysfunction due to acute pulmonary embolism (PE). Its effectiveness in patients at a higher risk of complications as well as patients with remarkably high baseline pulmonary artery pressure (PAP) is unknown.

Methods:
After a systematic review of the literature to identify randomized trials and cohort studies of CDT-based therapies for intermediate- and high-risk acute PE, we obtained and pooled the datasets of those fulfilling the eligibility criteria to conduct an individual patient-level analysis. The effectiveness outcome was the improvement in mean pulmonary arterial pressure (mPAP) after CDT, while the safety outcomes included (i) in-hospital death, (ii) in-hospital hemodynamic decompensation, and (iii) in-hospital major bleeding and intracranial bleeding (ICH). Safety outcomes were also studied for three subgroups of patients at increased bleeding risk (age > 75, active cancer, surgery in the 4 weeks preceding the PE diagnosis).

Results:
Until now, data collection and analysis were completed for 11 studies for a total of 772 patients. Median age was 63 (Q1-Q3 51-72) years with 54.3% men. Median mPAP decreased overall from 34.7 (Q1-Q3: 29.0-41.0) to 24.8 (Q1-Q3: 20.3-29.4) mmHg after treatment, corresponding to a 28.9% relative reduction. Patients with higher baseline mPAP values appeared to have a higher degree of absolute and relative mPAP reduction: -8.5 mmHg (relative reduction 27.7%) for baseline mPAP 20-39 mmHg; -14.0 mmHg (relative reduction 31.3%) for mPAP 40-54 mmHg; and -21.8 mmHg (relative reduction 36.5%) for mPAP >55 mmHg. There were 142 (18.4%) patients of 75 years of age and older, 63/556 (11.3%) had active cancer and 29/258 (11.2%) underwent surgery in the month prior to PE. Compared to younger patients, those of 75 years and older had a higher rate of hemodynamic decompensation (7.8% vs 2.2%; p=0.015), major bleeding (13.2% vs 5.8%; p=0.01), and death (9.3% vs 2.6%; p<0.001). After adjustment for a key prognostic factor (PE associated with hemodynamic decompensation), age was not found to be independently associated with death, but remained strongly associated with major bleeding. The rates of clinical outcomes were similar in patients with (vs. without) cancer or recent surgery.

Conclusion:
CDT appears to be effective and safe in improving the hemodynamic parameters of patients presenting with acute PE, also in those with higher mPAP at presentation, but age may represent a key risk factor to consider in relation to the higher bleeding risk. To our knowledge this is the largest individual patient-level study on CDT ever performed.

538

N. Schmid[1], T. Schachtner[1]

Isolated glomerulitis is strongly associated with the absence of antibody-mediated rejection by molecular diagnostics

Klinik für Nephrologie, Universitätsspital Zürich[1]

Introduction:
According to the 2018 Banff classification, the Molecular Microscope® Diagnostic System (MMDx) is indicated in cases when histology is insufficient to diagnose chronic-active antibody-mediated rejection (caABMR) due to an absence of diagnostic criteria groups 2 and/or 3. The impact of isolated glomerulitis (g>0, ptc0) on the likelihood of ABMR diagnosis by the MMDx appears critical to the implementation of this new biomarker.

Methods:
We analyzed 251 kidney allograft biopsies by histology and molecular diagnostics at the University Hospital Zurich from October 2018 to November 2022. Histologic findings were classified concerning the absence of (1) diagnostic criteria groups 2 and 3 (n=18), (2) diagnostic criteria group 2 only (n=18), and (3) diagnostic criteria group 3 only (n=28). In addition, cases with histologically proven caABMR were used for comparison (n=65). High-resolution re-typing was performed from the kidney allograft biopsies if necessary.

Results:
The MMDx diagnosed ABMR in 1 of 18 cases (6%) with absent diagnostic criteria groups 2 and 3, 4 of 18 cases (22%) with absent diagnostic criteria groups 2, and 19 of 28 cases (68%) with absent diagnostic criteria groups 3. On the contrary, MMDx did not confirm the diagnosis of ABMR in 23 of 65 cases (35%) with histologically proven caABMR. Among 28 cases with absent diagnostic criteria group 3, only 2 of 19 cases (11%) with ABMR by MMDx but 6 of 9 cases (67%) with no ABMR by MMDx showed isolated glomerulitis ($p=0.0048$). Among 65 cases with histologically proven caABMR, only 7 of 42 cases (17%) with ABMR by MMDx but 14 of 23 cases (61%) with no ABMR by MMDx showed isolated glomerulitis ($p<0.001$). Overall, 14 of 65 cases (21%) with isolated glomerulitis showed ABMR diagnosis by MMDx.

Conclusion:
Isolated glomerulitis is strongly associated with the absence of ABMR by MMDx not only when diagnostic criteria group 2 is missing but also when diagnostic criteria 3 is missing, or caABMR is proven by histology. Our results may help to guide the indication for MMDx in clinical practice. However, the clinical significance of these results needs further investigation.

539

M. Lone[3, 4], M. Aaltonen[6], A. Zidell[1], P. Helio[2], S. Saute[5], S. Mathew[4], P. Mohassel[7], C. Bonnemann[7], T. Hornemann[4]

SPTLC1 variants associated with ALS produce distinct sphingolipid signatures through impaired interaction with ORMDL proteins

Center for Genetic and Genomic Medicine, Hackensack University Medical Center, Hackensack, NJ, USA[1], Center for Genetic and Genomic Medicine, Hackensack University Medical Center, Hackensack, NJ, USA[2], Institute for Clinical Chemistry, University Hospital of Zurich[3], Institute of Clinical Chemistry, University Hospital Zurich, University of Zurich, Zurich, Switzerland[4], Medical Genetics division and Neurology division, Hospital de Clínicas de Porto Alegre, Porto Alegre, Brazil; Graduate Program in Medicine: Medical Sciences, and Internal Medicine Department; Faculdade de Medicina, Universidade Federal do Rio Grande do Sul, Porto Alegre, Brazil[5], Montreal Neurological Institute, McGill University, Montreal, Canada[6], Neuromuscular and Neurogenetic Disorders of Childhood Section, National Institute of Neurological Disorders and Stroke, NIH, Bethesda, MD, USA[7]

Introduction:
Amyotrophic lateral sclerosis (ALS) is a devastating neurological disorder. Etiologies for ALS are heterogeneous but rarely genetic. Clinically, it is characterized by severe muscle wasting, finally leading to paralysis and death. Recently, we identified a set of missense and deletion mutations in the SPTLC1 subunit of the enzyme Serine-palmitoyltransferase (SPT) that were associated with juvenile ALS. SPT catalyzes the first and the rate-limiting step in the de novo synthesis of sphingolipids (SL). SPT conjugates palmitoyl-CoA with L-serine to form long chain bases (LCB), that are structural moieties of all 'canonical' SL. The conjugation of fatty acids to LCB forms dihydroceramides (dhCer), which are desaturated in the LCB to form ceramides (Cer). Complex sphingolipids, such as glycosphingolipids (GlycoSL) and sphingomyelins (SM) are derived from Cer. Permutations and combinations of various fatty acids, presence of double bonds, and head groups produces immense species diversity at each SL class.
SPT is composed of two SPTLC1-SPTLC2 dimers that interact with functionally redundant, ORMDL-1, -2 and -3 proteins that negatively regulate SPT activity. The N-terminal transmembrane domain (TMD) of SPTLC1 tethers the SPT complex to the ER and interacts with ORMDLs to inhibit its activity in response to Cer levels. Previously, mutations in the cytoplasmic domain of SPTLC1 were associated with the Hereditary Sensory and Autonomic Neuropathy type 1 (HSAN1). The HSAN1 mutations shift the substrate specificity of the SPT enzyme from L-serine to L-alanine which leads to the formation of an atypical and neurotoxic class of 1-deoxysphingolipids (1-deoxySL). In contrast, the SPTLC1-ALS mutations lead to unregulated canonical SL synthesis.

Methods:
Confocal imunofluorescence microscopy was used to determine cellular lolcalization of SPTLC1-ALS mutants and compared them to HSAN1 variants. Immuno-prepcipitations and biochemcial analysis (blue-native PAGE) were used to determine effects of SPTLC1 variants on SPT structure in CRISPR derived SPTLC1 deficient cell models. High-resolution mass spectrometry, was used for quantification of sphingolipids in patient serum and dermal fibroblasts of affected individuals. Allele specific siRNAs were desinged and validated in patient derived primary fibroblasts.

Results:
Through deep phenotyping and extensive genetic testing, we identified seven unrelated families with a severe childhood form of ALS associated with six novel variants in SPTLC1. ALS causing mutations reside in exon 2 of the SPTLC1 gene encoding the only TMD of the protein. One ALS variant, (c.58G>T), causes an in-frame splice skip of exon 2 that results in the deletion of the TMD. ALS mutations alter protein-protein interaction and alter complex assembly. Using high-resolution mass spectrometry, SL and 1-deoxySL were quantified in patient serum and dermal fibroblasts of affected individuals. We modeled the variants in human HEK293 cells, and showed that ALS mutations impair feedback inhibition of the enzyme along the ceramide-ORMDL3 axis. We deduced lipid signatures specific to SPT-ALS and HSAN1 mutations in HEK293 cells as well as patient plasma and patient derived primary fibroblasts. Limiting L-serine availability in SPTLC1-ALS expressing cells increased 1-deoxySL and shifted the SL profile from an ALS to an HSAN1-like signature. This effect was corroborated in an SPTLC1-ALS pedigree in which the index patient uniquely presented with an HSAN1 phenotype, increased 1-deoxySL levels, and an L-serine deficiency. Finally, we also designed and validated allele specific siRNAs that selectively target two of the pathogenic deletion SPTLC1 variants, and examined their effect on the biochemical abnormalities in patient-derived fibroblasts.

Conclusion:
Loss of homeostatic inhibition of SPT due to SPTLC1-ALS variants causes motor neuron degeneration and childhood ALS, associated with specific lipid signatures that could serve as markers for this form of ALS.

540

H. Bolck[3], A. Kriston[1], E. Migh[1], D. Rutishauser[3], S. Kreutzer[2], P. Leary[2], P. Schraml[3], N. Rupp[3], P. Horvath[1], h. Moch[3]

Addressing the challenges of intra-tumor heterogeneity in clear cell renal cell carcinoma (ccRCC)

Biological Research Centre of the Hungarian Academy of Sciences, Szeged, Hungary[1], Functional Genomics Center Zurich, ETH Zurich/University of Zurich, Switzerland[2], University Hospital Zürich, Switzerland[3]

Introduction:
Most tumors are composed of subpopulations of cells that can display a remarkable molecular and phenotypic variability, including clinically important features such as ability to seed metastases and to survive therapy. Clear cell renal cell carcinoma (ccRCC) is a prototype heterogeneous tumor displaying both extensive morpho-histological as well as genetic intra-tumor heterogeneity (ITH). It has been suggested that ITH can foster tumor evolution and adaptation thereby contributing to treatment failure and drug resistance. However, little is known about the molecular aberrations that are responsible for the extensive phenotypic ITH in ccRCC and their biological consequences. Therefore, we believe that a better understanding of ITH will promote the development of more effective diagnostic and therapeutic strategies for profoundly heterogeneous tumors such as ccRCC.

Methods:
To uncover the molecular aberrations underlying the extensive phenotypic ITH of ccRCC lesions, we combined state-of-the-art image analysis algorithms with microscopy-assisted single cell isolation and molecular analysis to unambiguously quantify morphological and molecular differences between individual ccRCC cells. Our deep digital pathology workflow classified neighboring low-grade, high-grade and aggressive rhabdoid ccRCC cells as well as normal renal tubule cells in a histological patient sample. Subsequently, we micro-dissected 1000 individual cells for each morphological class from five patient cases. We subjected these groups of cells to RNA sequencing (RNAseq) and proteomics and performed sophisticated data analysis and integration.

Results:
Our transcriptomic analyses revealed that normal and low-grade cells as well as aggressive high-grade and rhabdoid cells cluster together across five individual patients. All tumor groups over-expressed canonical ccRCC markers such as Carboanhydrase 9 (CAIX), Vimentin (VIM) or Glucose transporter 1 (SLC2A1). Samples collected from different grade group morphologies exhibited distinct up- and downregulated genes. These specific gene expression patterns were overrepresented in pathways like the immune response, angiogenesis and fatty acid metabolism, which are critical for cancer progression in ccRCC. We are currently analyzing the significances of these ITH-specific differentially expressed genes.
In addition, we used ultra-high-sensitivity mass spectrometry analysis from individually isolated representative cells for each of the ccRCC grade morphologies from the same five patients to corroborate these findings and uncover the contribution of protein expression for morpho-histological ITH. To this end, we have developed a data-independent acquisition method (diaPASEF) for the analysis of less than 1000 cells and will apply this technology to address if morphological differences are also reflected in their proteomes.

Conclusion:
ITH is prevalent in ccRCC histology but a deep understanding of the molecular aberrations that underlie this morphological diversity is still elusive to date. By converging state-of-the-art digital pathology with RNA and protein expression analysis for the joint investigation of morphological and molecular data from histological tissue sections we will provide novel insights into the molecular complexity that determines ITH. We believe that such analysis will help us to recognize molecular characteristics of aggressive components of ccRCC and their potential functional or pathogenic consequences.

541

L. Russo[1], L. Heeb[1], S. Ulugöl[1], L. Roth[1], L. Scherer[1], A. Gupta[1], K. Lehmann[1]

Improving treatment of peritoneal metastasis originating from metastatic colorectal cancer

University Hospital Zurich, Department of Surgery and Transplantation[1]

Introduction:
Peritoneal metastasis (PM), a terminal disease, often arises from gastric or colorectal cancer. PM Patients are treated either with systemic chemotherapies or with the combination of cytoreductive surgery (CRS) and local hyperthermic intraperitoneal chemotherapy (HIPEC). Studies suggest that compared to systemic chemotherapy CRS/HIPEC enhances survival of the patients; but frequent recurrence of the disease limits overall 5-years survival. Therefore, new effective treatments are needed to improve survival of PM patients. Since chemotherapeutics used for local treatments of PM have been shown to affect cancer-specific immunity in other cancers, we want to assess the immune-related protective mechanisms of locally applied chemotherapeutics and further combine them with other drugs for improved protective immunity.

Methods:
Different drug combinations were tested in-vitro on human colorectal cancer cell lines (HT-29, HCT-8). Cell viability was measured using the cell titer-glo assay and immunogenic changes using flow cytometry. In-vivo C57BL/6 mice were injected i.p with murine colorectal cancer cell lines MC-38 and treated with Oxaliplatin and ATRi. Tumorload was assessed by PCI-scoring and tumor microenvironment was analysed using flow cytometry.

Results:
To identify novel drug combinations we treated human colorectal cancer cells with either oxaliplatin alone or in combination with DNA damage inhibitors, cell proliferation inhibitors or multi-kinase inhibitors. We noticed enhanced cytotoxicity when cells were treated with oxaliplatin + ATRi (ataxia telangiectasia and Rad3-related). Using our PM mouse model, we showed that the combination of oxaliplatin + ATRi significantly reduced growth of PM lesions, which was due to accumulation of functional CD8+T cells within the lesions. Furthermore, depletion of CD8+ T cells abrogated the protective effects of the combination therapy suggesting that CD8+ T cells are crucial to control tumor growth.

Conclusion:
Overall, these results suggest that optimal priming of the immune system with novel drug combinations may provide long-term control of PM lesions.

542

A. Hülsmeier[3], S. Toelle[2], C. Wentzel[1], T. Hornemann[3]

The sphingolipid C18SOΔ14Z is a potential biomarker for DEGS1 related hypomyelinating leukodystrophy

Department of Women's and Children's Health, Pediatric oncological and neurological research, Uppsala University, Uppsala, Sweden[1], University Children's Hospital, Department of Neurology, Zurich, Switzerland[2], University Hospital Zurich, Institute of Clinical Chemistry, Zurich, Switzerland[3]

Introduction:
Variants in DEGS1, causing a newly described sphingolipidosis, have been first reported in 2019. The entity was named DEGS1 related hypomyelinating leukodystrophy, HLD18 respectively. All affected individuals have a severe regressive phenotype with tetraspasticty, variable degree of intellectual disability, no verbal communication and epilepsy in the majority. DEGS1 encodes C4-dihydroceramide desaturase, an enzyme of the ceramide synthesis pathway. In recent studies, the activity of the DEGS1 enzyme was shown to be decreased in cultured fibroblasts of affected individuals.

Methods:
We use clinical examination, magnetic resonance imaging and sphingolipid profiling in plasma, utilizing liquid chromatography coupled multi-reaction monitoring mass spectrometry.

Results:
We measured the sphingolipid profiles in plasma of two individuals with new, different homozygous DEGS1-variants. Increased dihydrosphingolipids, elevated levels of the novel metabolite C18SOΔ14Z and decreased overall sphingolipids were detected in patient 1 only. This individual shows the typical clinical phenotype and brain magnetic resonance imaging findings of HLD18, whereas patient 2 has a phenotype not compatible with the individuals published to date.

Conclusion:
We hypothesize that C18SOΔ14Z might be a sensitive biomarker to discriminate individuals with disease-causing DEGS1 from benign variants.

543

N. Desboeufs[2, 3, 4], G. Semere[2, 3], C. Pauli[2], P. Leary[3], J. Jetzer[2], LK. Chan[2, 3], AE. Kremer[1], L. Planas-Paz[2], LA. Clerbaux[2, 3], M. Lopes[3], A. Weber[2, 3]

DNA replication stress as molecular driver and potential therapeutic target in hepatocellular carcinoma

Department of Gastroenterology and Hepatology, University Hospital Zurich[1], Department of Pathology and Molecular Pathology, University Hospital Zurich[2], Institute of Molecular Cancer Research, University of Zurich[3], Life Science Zurich Graduate School, Cancer Biology Program[4]

Introduction:
For hepatocellular carcinoma (HCC), precision medicine is still in its infancy. In particular there is a lack of biomarkers that predict novel efficient therapeutic strategies. Genomic instability is a hallmark of HCC independent of the etiology. In this light, DNA replication stress, a major cause of genomic instability, constitutes a potential biomarker and a promising starting point for efficient systemic treatment options. Our research aims to shed light on the mechanism of perturbed DNA replication during hepatocyte hyperproliferation under physiological (developmental growth) and pathophysiological conditions (acute and chronic regeneration, hepatocarcinogenesis) and to develop novel biomarker-stratified therapies for HCC patients.

Methods:
By implementing specialized single-cell and single-molecule in vitro assays to study DNA replication stress and DNA damage (e.g. comet assay, DNA fiber spreading assay, electron microscopy), we will investigate DNA replication stress and DNA damage in HCC patient-derived organoids (HCC-org) and in mouse hyperproliferative hepatocytes (juvenile, partial-hepatectomy and hepatocarginogenesis mouse models). Furthermore, taking advantage of multi-omics data, we will define a LIVer Replication Stress Signature (LIVRESS) and then challenge it in a drug screen on HCC-org to evaluate its predictive power with respect to the response to compounds targeting DNA damage and replication stress.

Results:
We have successfully established specialized single-cell and single molecule assays in HCC patient-derived organoids and mouse models, and we are now able to characterize DNA replication defects under pathophysiological and treated conditions.

Conclusion:
By combining these approaches, the better understanding of DNA replication stress-based mechanisms of hepatocytes hyperproliferation and hepatocarcinogenesis and the definition of LIVRESS might be the basis for novel biomarker-stratified therapies for HCC patients.

544

J. Fullin[1], E. Topcu[1], N. Klemm[1], R. Schimmer[1], C. Koch[1], S. Boettcher[1]

The divergent roles of mono- and biallelic TP53 mutations in leukemogenesis

Department of Medical Oncology and Hematology, University Hospital Zurich[1]

Introduction:
Mutations in the tumor suppressor gene TP53 affect approximately 10% of myeloid neoplasms and are associated with chromosomal aberrations and an inferior patient survival. However, recent analyses of patient data indicated, that these well-established associations are often confined only to patients with biallelic inactivation of TP53. These observations implicate divergent roles of mono- and biallelic loss of functional TP53 regarding both, their functional effects and their clinical consequences. We therefore sought to further study this putative functional divergence and unravel the underlying molecular mechanisms.

Methods:
We have generated a versatile model system allowing us to study the functional and molecular consequences of mono- and biallelic TP53 mutations in hematopoietic progenitor cells both in vitro and in vivo. To that end, we made use of a knock-in mouse model with inducible expression of Trp53.R245W - the murine equivalent of one of the most common TP53 missense mutations in cancer - linked to a GFP marker. We isolated bone marrow cells from mice encompassing all possible Trp53 allelic states and reversibly immortalized them by forced expression of estrogen receptor-coupled Hoxb8, allowing us to keep them in culture under addition of β-estradiol, while maintaining their genomic integrity. Introduction of a doxycycline inducible Cre recombinase allowed us to precisely control the timing of induction of Trp53 mutations, as well as the proportion of Trp53 mutated cells in the population, which can be traced by analyzing GFP expression. This allowed us to characterize the unconfounded effects of the Trp53 allelic state on clonal expansion, maintenance of genomic stability and potential for malignant transformation of hematopoietic progenitor cells. In parallel, we verified our findings using the corresponding in vivo model of Trp53.R245W-GFP x SCL-CreERT2 mice, allowing us to obtain a titratable and temporally controllable induction of Trp53 mutant cells specifically in the hematopoietic system.

Results:
Competitive cell growth assays in vitro and in vivo revealed a competitive advantage of cells with both mono- and biallelic Trp53 mutations over their wild-type counterparts upon treatment with chemotherapeutic agents or γ-irradiation. In contrast, after recovery from DNA damage, only cells with biallelic mutations exhibited an increased persistence of γH2AX signal, as well as a higher amount of DNA fragmentation. Mechanistic studies suggested that this increased genomic instability in the biallelic state might be mediated by an elevated resistance to apoptosis, which potentially prevents the elimination of cells subjected to excessive DNA damage. Finally, while wild-type and monoallelic mutated cells underwent terminal differentiation and cell death upon termination of Hoxb8 overexpression, biallelic mutated cells, pre-treated with DNA damaging agents, formed rare colonies of surviving cells with blocked differentiation and extensive chromosomal aberrations – two clinical hallmarks of TP53-mutated myeloid neoplasms.

Conclusion:
Our data confirm the clinical observations suggesting divergent roles of mono- and biallelic Trp53 mutations in leukemogenesis. While monoallelic mutations seem to be sufficient to induce clonal expansion, as it is observed in clonal hematopoiesis of indeterminate potential, inactivation of the second functional allele is necessary to promote genomic instability and provide the potential for transformation into highly aggressive myeloid neoplasms, which are characterized by complex karyotypes and a dismal prognosis.

546

R. Fumagalli[2], F. Catalani[2], A. Fürbringer-Schwarz[2], I. Farmakis[1], L. Valerio[1], K. Christodoulou[1], K. Keller[1], L. Hobohm[1], N. Kucher[2], S. Konstantinides[1], S. Barco[1, 2]

Effectiveness and safety of catheter-directed thrombolysis for acute pulmonary embolism: A systematic review and meta-analysis

Center for Thrombosis and Hemostasis (CTH), University Medical Center Mainz, Mainz, Germany[1], Department of Angiology, University Hospital Zurich, Zurich, Switzerland[2]

Introduction:
Catheter-directed thrombolysis (CDT) can relief an overloaded right ventricle in patients with acute pulmonary embolism (PE). One of the main concerns is about the safety of this approach. We conducted a systematic review and meta-analysis to assess effectiveness and safety of CDT for intermediate- and high-risk acute PE.

Methods:
We systematically searched PubMed, Web of Science and CENTRAL (inception-December 2022) and selected randomized controlled trials (RCTs), observational studies, and epidemiological analysis focusing on standard CDT (sCDT) vs. ultrasound-assisted catheter-directed thrombolysis (USAT) for intermediate- and high-risk acute PE. We obtained pooled estimate rates for bleeding (intracranial haemorrhage [ICH] and major bleedings), in-hospital/30-day fatality rate, and hemodynamic parameters (i.e. right/left ventricle [RV/LV] ratio, pulmonary artery pressure [PAP]).

Results:
We identified 3 RCTs, 44 single-arm cohort studies, and 11 epidemiological studies. The mean age of patients (N total: 37,496) was 60 years. In observational studies, 8.4% patients had high-risk PE; only intermediate-risk PE patients were enrolled in RCTs. The pooled ICH rate was 0.16% (95%CI:0-0.6%) in cohort studies and trials, and 0.87% (95%CI:0.44-1.42%) in epidemiological studies. The highest ICH rate events were observed in studies using longer CDT schemes (>14 hours) and higher t-PA dose (>24 mg), namely 1.26% (95%CI:0.02-3.60%). Higher rates of major bleeding events were observed with longer (3.7%; 95%CI:1.7; 6.1%) vs. shorter CDT duration (0.7%; 95%CI:0.0-2.2%), irrespective of the dose. The early fatality rate was 1.7%: longer CDT duration was associated with higher fatality (2.8%; 95%CI:1.5-4.2%) vs. shorter one (0.1%; 95%CI:0.0-1.1%). No differences in hemodynamic outcome improvement were observed across dose and duration groups. sCDT and USAT led to similar degree of RV/LV (-0.41; 95%CI -0.27 to -0.55 vs. -0.35; 95%CI -0.30 to -0.41, respectively) and sPAP reduction (-13.12 mmHg; 95%CI -9.58 to -16.66 vs. -17.03 mmHg; 95%CI -13.93 to -20.14, respectively). If one considers RCTs alone, no ICH and one major bleeding were observed in the interventional arm, and no deaths were reported in CDT-treated patients.

Conclusion:
Outcome-driven RCTs with CDT are currently lacking. The available evidence supports the notion that CDT strategies may represent a safe option for reversing right ventricular dysfunction in patients with acute PE. Overall, the reported rate of ICH was below 1%. Longer CDT duration was associated with more major bleeding events and higher fatality.

547

C. Moreira[1], A. Müllner[1], P. Hofmann[1], M. Gönel[1], C. Baumann[1], D. Noain[1]

Reduced axonal injury, demyelination and cognitive decline upon enhancement of slow waves by closed-loop auditory stimulation in traumatic brain injury rats

University Hospital Zurich[1]

Introduction:
High slow-wave activity (SWA), a feature of deep sleep, is believed to be essential for repair mechanisms to take place in the rodent brain. Our past work showed that both sleep induction via sodium oxybate administration and partial sleep restriction followed by sleep rebound in TBI rats promoted enhanced SWA associated with preserved posttraumatic cognition in the novel object recognition test (NORT) and ~90% reduction in amyloid precursor protein (APP), a marker of diffuse axonal injury (DAI). Although these strategies provided encouraging results, they lacked the specificity needed to point out SWA as unequivocal mechanistic player behind ameliorated recovery. Moreover, establishing sleep pharmacotherapy as potential TBI treatment in clinical environments is challenging due to tolerance, dependency, and specificity concerns. Therefore, we recently developed a preclinical closed-loop auditory stimulation (CLAS) method to enhance SWA by precisely targeting the up-phase of ongoing slow waves in the rodent brain.

Methods:
We implanted EEG/EMG electrodes in a rat model of TBI allowing for real-time staging of vigilance states and closed-loop delivery of auditory stimulation in a phase-targeted manner. We tested the effect of mock (flagging of targets with no sound delivery, n=5-8) vs. up-phase targeted CLAS (n=5-8) applied for 5 days acutely after trauma onto SWA (% of delta power change from baseline), DAI (number of APP+ axonal varicosities), demyelination (via optical density quantification of myelin basic protein –MBP– staining), and cognition (NORT performance). Two-way ANOVA, one-way ANOVA and multiple comparisons' corrections were applied as appropriate.

Results:
Up-phase targeted CLAS enhanced 24 h SWA up to 18%, in association with reduced number of APP+ axonal bulbs (~58% mean decrease compared to TBI + mock) and increased intensity of MBP staining (~37% mean increase compared to TBI + mock) in the corpus callosum of TBI rats. These findings were accompanied by preserved cognitive ability in TBI animals (~75% recognition index in NORT).

Conclusion:
Improving SWA in a highly specific manner by delivering up-phase CLAS acutely after brain trauma might constitute a novel non-pharmacological neuroprotective approach for preventing TBI sequelae. Moreover, our TBI + CLAS model will shed light onto the pathways linking deep sleep and disease recovery mechanisms, helping pave the way to upcoming less invasive, non-pharmacological sleep modulation therapies for TBI patients.

548

S. Salemi[3], L. Schori[4], T. Gerwinn[1], M. Horst[1], D. Eberli[2]

Inhibition of myostatin/Smad pathway signalling in smooth muscle cells

Department of Urology, University Children's Hospital Zurich, Switzerland[1], Department of Urology, University Hospital Zurich, Switzerland[2], Department of Urology, University Hospital Zurich, Switzerland.[3], Department of Urology, University Hospital Zurich, Switzerland.[4]

Introduction:
Tissue engineering and cell based therapies using smooth muscle cells may offer alternative treatments for diseases such as end stage lower urinary tract dysfunction (ESLUTD), urinary incontinence and bladder dysfunction. Myostatin (growth differentiation factor 8) is a negative regulator of muscle growth and development, its inhibitors are used in clinical trials as a therapy for skeletal muscle diseases such as muscular dystrophies and cachexia. The role of myostatin has not yet been reported within bladder smooth muscle cells (SMCs). Therefore, the ultimate goal of our research is to improve the SMCs quality and quantity by direct inhibition of myostatin with Domagrozumab.

Methods:
Human bladder derived SMCs were isolated and characterized by flow cytometry. SMCs were cultured in the presence and absence of Domagrozumab (1pg- 100 ng/ml). Proliferation was evaluated by WST-1 assay. The impact of Domagrozumab on SMCs protein expression was analyzed by FACS, immunoblotting and immunofluorescent staining.

Results:
Decreased cell proliferation was observed in ESLUTD compared to control bladder SMCs. Key contractile genes and proteins, such as α-SMA, calponin, smoothelin and MyH11, as well as a lower degree of contraction was observed in ESLUTD-derived compared to control SMCs. Increased expression of myostatin was detected in ESLUTD compared to control SMCs. These data were further analysed by WES, showing a significantly increased expression of p-Smad 2, Smad 7 and decrease in Smad 2 and follistatin proteins in ESLUTD hSMCs. Treatment with Domagrozumab (1 pg/ml) increased the cell proliferation in both groups. Down regulation of myostatin protein expression was observed upon treatment with Domagrozumab. Decrease in myostatin led to increase in α-SMA and MyH11 proteins in ESLUTD SMCs and higher degree of contraction.

Conclusion:
Our study demonstrates for the first time that myostatin is expressed in bladder SMCs. In addition, Domagrozumab improve bladder SMCs proliferation and increase in the expression of late contractile proteins. This study indicates that myostatin inhibitor may have a tissue engineering therapeutic potential for patients with incontinence and other smooth muscle disorders.

549

ME. Healy[1, 3], P. Leary[1, 3], LK. Chan[1, 3], S. Gabriel[1, 3], R. Parrotta[1, 3], R. Jackson[2], A. Weber[1, 3]

Identification of protein-encoding lncRNA as potential new targets for HCC

Department of Pathology and Molecular Pathology, University Hospital Zurich, Switzerland[1], Harvard Medical School, Boston, USA[2], Institute of Molecular Cancer Research, University of Zurich, Switzerland[3]

Introduction:
Hepatocellular carcinoma (HCC) represents one of the most prevalent and deadly cancers worldwide. However, current treatment options available remain insufficient. While the need for targeted molecular therapies against HCC is clear, attempts to identify specific molecular targets have had limited success. Recent challenges to traditional criteria governing protein annotation have identified thousands of novel non-canonical open reading frames (ncORFs) which are essential for critical cellular processes including cell survival. To date however, no studies investigating the role of ncORF-encoded proteins in HCC survival have been performed. Our research aims to identify protein-coding ncORFs within lncRNA which are differentially regulated in HCC and may represent novel therapeutic targets.

Methods:
Ribosome profiling was established and performed on a non-neoplastic liver cell line (HepaRG cells) and two different HCC-derived cell lines (Huh-7 and JHH-5). Next generation sequencing was performed and ncORFs were identified using two distinct bioinformatical tools (RiboCode and Ribo-TISH). We then developed a novel bioinformatical pipeline to strictly identify ncORFs within lncRNAs (lncRNA-ORFs), which were differentially expressed in Huh-7 or JHH-5 cells when compared to HepaRG cells. Differentially expressed lncRNA-ORFs were then filtered to only include genes which showed characteristics consistent with canonical protein coding genes.

Results:
We have successfully identified 3,487 ncORFs with high protein coding potential across the 3 different cell lines using RiboCode. Of these transcripts, 2,616 ncORFs were located within lncRNAs. We performed differential expression analysis to determine which of these lncRNA-ORFs were significantly dysregulated (p-value < 0.05 and fold change > 2) in our HCC-derived lines compared to HepaRG cells. In order to increase confidence in our results, only differentially expressed lncRNA-ORFs which were detected by both RiboCode and Ribo-TISH (59 lncRNA-ORFs) were analysed further. To demonstrate that these predicted lncRNA-ORFs were capable of forming stable protein products, we designed and developed novel polyclonal antibodies against the amino acid sequences of the top 10 candidate lncRNA-ORFs.

Conclusion:
The emerging field of novel ncORF-encoded proteins has the potential to herald a new chapter in cancer research and may potentially uncover missing pieces to currently unanswerable molecular questions in cancer biology. Not only does our study have implications for basic cancer biology but the protein-encoding lncRNA-ORFs identified in this project may represent potential new therapeutic targets for HCC therapeutics. In addition, the experimental design of this project is directly transferable to other tumor entities and may be paradigmatic for a new era in the identification of cancer therapeutics.

550

V. Baumgartner[1], S. Salemi[1], d. Eberli[1]

Targeting metabolic vulnerabilities in androgen-mediated reprogramming of prostate cancer

Urology[1]

Introduction:
In castration resistance, prostate cancer (PCa) cells rewire their metabolism as a pro-survival mechanism to cope with external insults and to sustain their anabolic growth. In particular, PCa cells rely heavily on oxidative phosphorylation (OXPHOS) for energy production. Mitophagy, a self-eating recycling process that degrades mitochondria, is known to be dysfunctional in cancer and has been linked to drug resistance. Therefore, we investigate whether metabolic reprogramming of PCa is modulated by mitophagy and how metabolic adaptations can be therapeutically targeted.

Methods:
Human PCa cells (PNT1A, LNCaP, C4-2, PC-3) were treated for 3 days with 25 µM anti-androgen apalutamide, 10 nM complex-I inhibitor IACS-010759 and combination (apalutamide+IACS). Cell proliferation was assessed by CellTiter-Glo. Seahorse and colorimetric Mitoplate assays were used to evaluate mitochondrial respiration and substrate utilisation. Mitochondrial network was visualised by TOM20 staining. Fission (p-DRP1) and fusion (OPA1) proteins were quantified by western blot. Mitochondrial reactive oxygen species (ROS) and apoptosis were monitored by MitoSOX staining and Annexin V.

Results:
Cell proliferation was significantly decreased in LNCaP after 3 days of treatment with apalutamide and/or IACS. Treated LNCaP cells exhibited long tubular mitochondrial networks along with a decrease in fission protein DRP1. Untreated LNCaP cells showed high dependency on OXPHOS indicated by high oxygen consumption rate (OCR) and preferred utilization of tricarboxylic acid (TCA) cycle intermediates such as succinate, fumarate and malate. Treatment with apalutamide and/or IACS decreased OCR. Apalutamide treated LNCaP cells downregulated their mitochondrial substrate metabolism. Moreover, upon drug treatment, mitochondrial ROS and apoptosis increased in androgen-sensitive LNCaP and C4-2 cells, whereas no changes were observed in PNT1A and PC-3 cell lines.

Conclusion:
Our data demonstrates that during androgen-mediated reprogramming, prostate cancer cells switch towards OXPHOS to meet new anabolic needs. This metabolic change can be exploited by blocking mitophagy, which reduces OXPHOS and has a strong antitumor effect. Finally, targeting the energy metabolism might open a new therapeutic window to tackle drug-resistance mechanisms in advanced prostate cancer.

551

I. Dias[2, 3, 4], M. Lopez[3], S. Kollarik[3], C. G. Moreira[3], C. R. Baumann[1, 3, 4], D. Noain[1, 3, 4]

Establishing up-phase closed-loop auditory stimulation of slow-waves in mouse models of neurodegeneration

Center of Competence Sleep and Health, University of Zurich (UZH), Switzerland[1], Department of Health Sciences and Technology (D-HEST), ETH Zurich, Switzerland[2], Department of Neurology, University Hospital Zurich (USZ), Switzerland[3], Neuroscience Center Zurich (ZNZ), Switzerland[4]

Introduction:
Recent evidence from murine models of neurodegeneration suggests that long-term slow-wave activity (SWA) enhancement may be neuroprotective. Boosting SWA via manipulation of slow waves through techniques such as closed-loop auditory stimulation (CLAS), may provide a powerful non-pharmacological tool to investigate the link between sleep and neurodegeneration. Nevertheless, the precise effects of CLAS and its parameters' optimization still need to be tackled before implementing this technique in the clinic, advocating for CLAS assessment in preclinical models. Even though the implementation of CLAS has been proved successful in rat models, no evidence is yet available on its effects and feasibility in mice, the most used species in preclinical neurodegeneration.

Methods:
Therefore, aiming to determine the feasibility of CLAS in mouse models of neurodegeneration, we explored the efficacy of SWA modulation in mouse model lines of Alzheimer's disease (AD, Tg2576), Parkinson's disease (PD, A53T) and their wild-type littermates (WT). We aimed at enhancing delta power during non-rapid eye movement sleep (NREM) by targeting the up-phase of slow waves through CLAS. For this effect, we isolated either the 1, 1.5, 2 or 2.5 Hz components of ongoing EEG signal in the AD line and its WT littermates. We then tested different up-phase (30º, 40º or 60º) targeted auditory stimuli delivery in AD, PD and WT mice, to determine which target reflects the highest significant delta power increase within each mouse strain and genotype. We assessed online precision (correctly real-time identified NREM events compared to an offline tool), phase targeting and EEG delta power as percentage of change from baseline, across conditions in all groups.

Results:
We found that tracking the 2 Hz frequency component led to the highest precision of online NREM detection in WT mice (60%) versus 38%, 46% and 45% in 1, 1.5 and 2.5 Hz, respectively. For AD mice, we also obtained highest precision with 2 Hz (61%), versus 43%, 56% and 60% in 1, 1.5 and 2.5 Hz, respectively. Following this result, we isolated the 2 Hz component and tested three up-phase targets of stimuli delivery. We observed maximum precision (70%) with a target at the 30º phase in AD, which translated into a significantly higher delta power increase when compared to the mock group (*$p<0.05$, unpaired one-tailed t-test, $n_{mock}= 8$, $n_{AD} = 7\text{-}10$). The same increase was observed in their WT littermates (*$p<0.05$, $n_{mock}= 7$, $n_{WT} = 7\text{-}10$). In PD animals, 40º CLAS targeting translated into a significant delta power increase in comparison with the mock group (*$p<0.03$, one-way ANOVA, $n_{mock}= 8$, $n_{PD} = 5\text{-}7$) and their WT littermates (*$p<0.03$, $n_{mock}= 7$, $n_{WT} = 5\text{-}6$). When comparing the delta changes in each genotype (WT versus AD, and WT versus PD) the distributions within the same transgenic strain overlap, even though the distributions between the strains with distinct genetic backgrounds (B6;SJL for AD versus B6C3H Mixed Background for PD) differ.

Conclusion:
Our data suggest that a 2 Hz component coupled with tailored phase-targeting is essential to successfully increase delta power during mouse NREM sleep using CLAS. Strains with distinct genetic backgrounds require a different set of stimulation parameters, whereas different genotypes within the same strain appear to react similarly to up-phase CLAS. These findings may strikingly benefit future preclinical/clinical studies applying CLAS in healthy and diseased populations, which may particularly shape the therapy of neurodegenerative diseases and set CLAS as a candidate preventive/therapeutic technique.

552

S. Pravato[2], L A. Krattiger[2], D V. Deshmukh[1], M. Ehrbar[2], M. Tibbitt[1]

Tunable patterning of vascular networks for tissue engineering

ETH[1], UZH[2]

Introduction:
When a cellularized vascular scaffold is implanted in vivo, it is necessary that it integrates as fast as possible inside the host vascular system in order for cells to survive. This integration can be enhanced if the implant is already prevascularized. Before an in vivo application, in vitro models need to be established.

Methods:
In this project, the main aim was the development and the validation of an in vitro model for vasculo-/angiogenesis using an acoustofluidic system. Cells, in particular Human Umbilical Vein Endothelial Cells (HUVECs) and Bone Marrow derived Mesenchymal Stem Cells (BM-MSCs), were patterned into lines inside a photopolymerizable Gelatin-Methacryloyl (GelMA) solution and extruded. In order to do that, a piezoelectric transducer was employed to convert a signal into physical waves inside a squared glass capillary, where the suspension of hydrogel and cells was present. The travelling wave and its reflected wave met in a nodal point, exerting a force on the cells that maintains them in place forming lines. The transition of GelMA from liquid-like to solid-like state due to blue light (405 nm) crosslinking maintain the cells in the fixed position after they do not have the influence of the acoustic field anymore.

Results:
This method results in a high local cell density and improve the cell-cell interaction, which is important for tissue formation. Cells have been pre-patterned to form a line, facilitating the development of long, continuous and parallel vessels. First, a comparison between patterned and not-patterned samples was performed. The capillaries obtained in the first case showed a structure that is closer to that present in vivo: the vascular network was formed by a main vessel, from which numerous sprouts grown. For every extrusion, a total of four lines were formed, two on the front and two on the back, using a frequency of 1.682 MHz. The supporting role of MSCs has been researched with the use of two different assays: an extruded sample and a spheroid model as control. It appeared that in the absence of this type of cell, Endothelial Cells (ECs) are not be able to form any vascular structure, thus confirming the need for a co-culture for the development of this model. Once the vasculo-/angiogenesis model is established, the next goal was to interface it with a model of tumor to study its influence. In order to do this, cancer spheroids containing HUVECs, BM-MSCs and M.D. Anderson - Metastatic Breast 231 (MDA MB 231) cells were brought into contact with the GelMA fiber using polyethylene glycol (PEG). The influence of the cancerous cells on the preformed vessels was studied in terms of length of vascular network.

Conclusion:
The analysis showed that the length of the network is reduced in the presence of the tumor. This was not the expected result. In fact, due to the fact that in vivo tumors begin to develop the need for angiogenesis and try to attract new blood vessels to grow larger, longer spouts connecting the two systems were expected.

554

L. Chan[1, 2], M. Healy[1, 2], G. Semere[1, 2], N. Desboeufs[1, 2], J. Jetzer[1, 2], R. Parrotta[1, 2], A. Leblond[1, 2], A. Weber[1, 2]

STING-independent function of cGAS reduces liver apoptosis and tumorigenesis in Mcl-1Dhep mice

Department of Pathology and Molecular Pathology, University Hospital of Zurich, Switzerland[1], Institute of Molecular Cancer Research, University of Zürich, Zürich, Switzerland[2]

Introduction:
Liver cancer is the fourth most common cause of cancer-related death. Hepatocellular carcinoma (HCC) accounts for over 80% of all primary liver cancers. HCC mostly develops on the background of a chronic liver disease (CLD). Our group previously developed a mouse model of CLD based on an ablation of the anti-apoptotic protein myeloid-cell leukemia 1 (MCL-1) specifically in the liver parenchymal cells (Mcl-1^{Dhep} mice). Deficient of MCL-1 in hepatocytes promotes apoptosis, which is followed by increased compensatory proliferation and DNA damage. This phenomenon is also observed in CLD patients. The cGAS-STING pathway was identified recently to participate in the sensing of cytosolic DNA which connects DNA damage response to the activation of the innate immune response. Although both cGAS and STING are essential in the activation of the downstream IRF3 and NF-kB, studies have reported specific functions which are independent of each other. We aim to study the consequence of inhibiting this pathway in the Mcl-1^{Dhep} mice by targeting cGAS and STING separately.

Methods:
We analyzed the activation status of the cGAS-STING pathway in Mcl-1^{Dhep} mice. We then generated Mcl-1^{Dhep}/STING-/- and Mcl-1^{Dhep}/cGAS-/- double knockout mice to study the effects of cGAS and STING in liver homeostasis and the tumorigenesis process. RNAseq was performed on all animal groups from the 2-month cohort to allow comparisons of their transcriptomic profiles.

Results:
Mcl-1^{Dhep} mice at 2 months had increased micronuclei frequency in hepatocytes and enriched cytosolic DNA sensing and interferon alpha signatures. In parallel, there was an increase in immune cell infiltrations, particularly macrophages, neutrophils and B cells. Deletion of STING in Mcl-1^{Dhep} mice reduced immune cell chemotaxis, without affecting the level of apoptosis. In contrary, deletion of cGAS resulted higher apoptosis and proliferation. These results suggested that deletion of STING or cGAS had very different effects on the phenotype observed in the Mcl-1^{Dhep} mice. While Mcl-1^{Dhep}/STING-/- mice showed a reduced tumor incidence (33%) at 12 months compared to the Mcl-1^{Dhep} counterparts (46%), MCL-1^{Dhep}/cGAS-/- mice showed the opposite (75%). Staining of cGAS and STING indicated that both hepatocytes and non-parenchymal cells expressed cGAS, whereas STING expression was restricted to non-parenchymal cells. The number of hepatocytes with nuclear cGAS was significantly higher in Mcl-1^{Dhep} mice compared to wild-type mice. The protective function of cGAS in hepatocytes in reducing apoptosis and tumorigenesis may be associated with its non-canonical function in the nucleus.

Conclusion:
Our findings indicate that cGAS and STING play different functions in liver carcinogenesis. Deletion of STING exerted an impact on the immune cell infiltration and thus reduced tumor incidence. However, deletion of cGAS might disrupt its non-canonical function in the nucleus which resulted an increase in cell death and tumor incidence.

555

S. Hertegonne[1], T. Schweizer[1], S. Mairpady Shambat[1], A. Zinkernagel[1]

Neutrophil and Staphyloccus aureus infection dynamics and interactions

Departement of Infectious Diseases and Hospital Epidemiology, University Hospital Zurich, University of Zurich, Zurich, Switzerland[1]

Introduction:
Staphylococcus aureus is a pathobiont causing invasive infections in humans, which are often difficult-to-treat as a result of emerging antibiotic resistance and antibiotic tolerance. Antibiotic tolerance is a transient phenomenon where a bacterial population can withstand high antibiotic concentrations which are otherwise lethal. Under certain conditions during infection a subpopulation of bacterial cells enter the dormant phase that can survive and tolerate high concentrations of antibiotics due to the formation of so-called persister cells. While these cells are naturally present in a bacterial population, several environmental stressors, e.g. acidic pH, antibiotic stress and immune cell mediated stress can induce their formation. The inability to clear persistent bacteria can lead to chronic and relapsing infections, characterized by recurring abscess formation. In order to treat a deep-seated abscess, surgical debridement is needed, which can be a challenging procedure for the patient, in addition adds to the overall health care associated costs. Previously we have shown that acidic pH and neutrophil mediated stress, 2 characteristics from abscess environment, can induce formation of non-stable small colonies (nsSCs), a proxy for persister cells. However, it remains unclear whether persister cells modulate the neutrophil functional responses allowing the bacteria to better withstand neutrophil mediated killing.

Methods:
In this study, the role of differential functional responses of neutrophils during persistent vs. acute *S. aureus* infections was investigated using flow cytometry and colorimetric analyses. For this, *S. aureus* persister formation was induced utilizing a well-established in vitro low pH media to mimic abscess environment. Intracellular survival and persister formation of *S. aureus* upon subsequent neutrophil exposure was quantified using the automated plate imaging and the in-house developed ColTapp software.

Results:
Acidic stress altered both extracellular and intracellular survival of *S. aureus* upon subsequent neutrophil challenge leading to increased bacterial survival after 4 hours of infection. This higher percentage of intracellular survival was accompanied by an increased formation of nsSCs and reduced uptake of *S. aureus* by neutrophils. We observed an induction of regulated cell death and stronger degranulation of primary granules in neutrophils when infected with pH stressed *S. aureus*. When stimulating neutrophils with supernatant that contained released virulence factors, this previous observation could not be replicated.

Conclusion:
We have seen that acidic stress changed the behaviour of *S. aureus* during subsequent infection of neutrophils. More specifically, pH stressed bacteria evaded neutrophil mediated killing by modulating regulated cell death mechanisms and inducing degranulation of primary granules. The components of the primary granules play a central role in the antimicrobial response of the host innate immune system. Further experiments should elucidate whether these antimicrobial peptides show an impaired functionality. Additionally, the subpopulation of pre-stressed bacteria surviving neutrophil mediated killing, showed an increased nsSC formation, indicating the presence of persister cells. Overall, neutrophils pose as a host mediated stress, which induced persister formation in *S. aureus* thereby allowing the bacteria to evade neutrophil mediated clearance during infection. Nevertheless, additional investigations into the dynamics between *S. aureus* and neutrophils are needed. Taking into account, the high infiltration of neutrophils inside an abscess in combination with the link of bacterial persistence to treatment failure, this project has great potential of furthering our understanding of host-pathogen interactions as well as develop new treatment strategies in the context of recurring abscess formation.

557

K. Sun[2], D. Bochicchio[2], F. Seehusen[1], E. Breuer[2], S. Da Silva Guerra[2], P. Dutkowski[2], B. Humar[2], P. Clavien[2]

Novel animal model for donation after circulatory death in rat uterine transplantation - a new tool for assessing ischaemia and reperfusion (I/R) injury?

Institute of Veterinary Pathology, University Zurich[1], Surgery and Transplantation, Universtity hospital Zurich[2]

Introduction:
Uterine transplantation (UTx) is an emerging therapy for absolute uterine infertility and the need for organ donors is increasing. Despite the associated warm ischemia, organs from donors after circulatory death (DCD) could meet this need. However, no DCD transplantation has been used for UTx in humans. Hence, this model could be used to assess the impact of warm ischemia on graft integrity.

Methods:
Adult virgin female Lewis rats served as donors and recipients of uterine grafts. Uteri were subjected to warm ischaemia in situ for 60 minutes followed by 4 h of cold storage, mimicking DCD organ retrieval and conventional organ transportation (n=5). Outcomes were assessed 12 hours after uterine transplantation.

Results:
We successfully established a rat model for DCD uterus transplantation. Our results on early graft viability suggest that the rat uterus can survive 60 min of warm ischaemia in situ and 4 h of cold storage without detrimental effects on graft integrity and recipient survival.

Conclusion:
Our study demonstrates that a DCD model for uterine transplantation is feasible in rats. The rat uterus displays remarkable resistance to warm ischaemia up to 60 minutes.

558

Z K. Kotkowska[1, 3], Y. Waeckerle Men[3], I. Kolm[2], A. Duda[2], F. Sella[2], H. Fischer[2], L. Hausamann[2], J. Rust[2], A. Høgset[4], T M. Kündig[2, 3], C. Halin Winter[1], P. Johansen[2, 3]

Photochemical internalization (PCI): when photodynamic therapy (PDT) becomes an integral of potential cancer vaccines

Department of Chemistry and Applied Biosciences, ETH Zurich, Zurich, Switzerland[1], Department of Dermatology, University Hospital Zurich, Zurich, Switzerland[2], Department of Dermatology, University of Zurich, Zurich, Switzerland[3], PCI Biotech, Oslo, Norway[4]

Introduction:
Background: Cancer vaccination approaches aim at enhancing the patient's immune response against the tumor. Cytotoxic T lymphocytes (CTLs) are the most potent anti-tumor immune cells, capable of recognizing tumor antigen presented by antigen presenting cells (APC) in complex with major histocompatibility complex class I molecule (MHC I). The main problem of cancer vaccines is the inefficacious delivery of antigens to the cytosol of APC, which results in not efficient stimulation of CTLs. Photodynamic therapy (PDT) might provide the required help, by facilitating cytosolic release of antigens co-administered with a photosensitizer. Upon endocytosis by APC, the photosensitizer localizes in the endosomal membranes. Subsequent light treatment activates the photosensitizer, causes membrane disruption and cytosolic release of endosomal content. This process is called photochemical internalization (PCI).
Objectives: The main aim of the project is to optimize PCI-based vaccination for cytosolic delivery of antigens in APC and for the stimulation of CTLs. The current subproject studies local immune reactions in the treated skin.

Methods:
Mice were intradermally injected with a photosensitizer or a photosensitizer and an antigen. After subsequent illumination, the skin harvested at distinct time points was characterized for local inflammatory and immune responses. Skin specimens were investigated by histology and fluorescence microscopy. CTL responses were measured by FACS and ELISA.

Results:
Light- and photosensitizer-dependent innate inflammatory responses in the skin. The reactions were transient and ceased after approximately four weeks. In the draining lymph nodes and spleen, stimulation of CD8 T-cells was observed with a photosensitizer dose-dependent proliferation and cytokine production.

Conclusion:
The results suggest that early innate immune responses may be an important part of the mechanism of action of PCI-based vaccines, and further studies will focus on how these innate immune responses translate into effective anti-tumor CTL responses.

560

IS. Martinez Lopez[2], T. Papasotiropoulos[2], F. Schläpfer[2], S. Ulrich[1], I. Opitz[2], MB. Kirschner[2]

MicroRNA expression correlates with clinical presentation of Chronic Thromboembolic Pulmonary Hypertension

Department of Pulmonology, USZ[1], Department of Thoracic Surgery, USZ[2]

Introduction:
Chronic Thromboembolic Pulmonary Hypertension (CTEPH) is a rare, debilitating disease characterized by pathological changes that obstruct both sides of the pulmonary arteries (PA). Aiming to understand a possible contribution of microRNA expression to the thus far poorly understand CTEPH pathophysiology, we here analysed the expression of four candidate microRNAs in pulmonary endarterectomy (PEA) specimens.

Methods:
MicroRNA specific RT-qPCR for miR-939, miR-942, let-7b and let-7d was done on RNA from PEA specimens of 50 CTEPH patients and from PAs resected from explant lungs of 48 transplant recipients (25 due to COPD, and including n = 22 with PH). Associations between microRNA expression and clinical presentation (not all factors available for every patient) were assessed by Spearman correlation. MicroRNA expression between CTEPH and reference PAs was compared by Mann Whitney test.

Results:
Expression levels in left-side PEA-derived tissues correlated negatively with: CRP for let-7d (n = 49, R = -0.29, p=0.039), oxygen saturation (SpO2) at peak 6-minute walk distance for miR-939 (n = 44, R = -0.39, p=0.007), and Right Jamieson classification for miR-942 (n = 40, R = -0.34, p=0.03). Right-side samples let-7d levels correlated negatively with mPAP (n = 42, R = -0.33, p=0.031). Contrastingly, mean expression levels of miR-942 showed positive correlation with mPAP (n = 49, R = 0.28, p=0.049) and Borg Scale showed a similar tendency with miR-939 (n = 50, R = 0.31, p=0.027). Compared to reference PAs, right-side expression of miR-942 reached significance (n = 47 CTEPH vs n = 46 Reference, p<0.0001).

Conclusion:
Correlations with clinical parameters suggest that miRNAs may be associated with clinical presentation of CTEPH. Furthermore, the significant elevation compared to reference PA tissue suggest that microRNA dysregulation might be involved in CTEPH pathophysiological mechanisms, encouraging us to investigate further.

561

M. Ahmadsei[2], J. von Spiczak[3], B. Kovacs[1], R. Manka[1, 3], A. SAGUNER[1], M. Guckenberger[2], N. Andratschke[2], M. Mayinger[2]

Structural cardiac changes detected by MRI after stereotactic body radiotherapy for targets in close proximity to the heart

Department of Cardiology, University Heart Center, University Hospital Zurich, University of Zurich[1], Department of Radiation Oncology, University Hospital Zurich, University of Zurich[2], Diagnostic and Interventional Radiology, University Hospital Zurich, University of Zurich[3]

Introduction:
Stereotactic body radiation therapy (SBRT) has become a standard of care for inoperable early stage non-small cell lung cancer and in case of pulmonary oligometastases. Recent studies indicate that incidental irradiation of the heart may be associated with an increased risk of non-cancer related deaths. This study aims to assess and examine structural cardiac changes following peri- and myocardial SBRT using a systematic cardiac follow-up protocol including cardiac magnetic resonance (CMR) imaging.

Methods:
For 1485 patients treated with local-ablative SBRT from January 2014 to February 2022 at our institution, the distance between the planning target volume (PTV) and the heart was measured. Forty-eight out of 134 patients treated in close proximity (<2cm) to the heart were alive at follow-up. Of those, 20 were randomly invited to undergo a structured cardiac follow-up protocol including CMR, transthoracic echocardiography (TTE), ECG, blood sampling, and two questionnaires, evaluating the quality of life and cardiac symptoms after SBRT, respectively. Ten patients consented to participate and underwent a structural follow-up protocol. Registration of CMR image data and the SBRT treatment plan was performed to examine a possible correlation between the dose delivered to the myocardium and structural cardiac changes assessed by CMR. Automated segmentation of 17 heart sub-structures (great vessels, atria, ventricles, coronary arteries, valves, sinoatrial and atrioventricular nodes) was performed for detailed anatomical analysis.

Results:
Among the 10 participating patients, the most common primary tumors were non-small cell lung cancer (n=3) and small-cell lung cancer (n=2) (Table 1). Five patients presented with pre-SBRT cardiovascular comorbidities including coronary artery disease and atrial fibrillation. Seven patients received SBRT for pulmonary or vertebral metastases and three patients for primary lung cancer with a median dose of 42.5 Gy (30.0-48.0 Gy) in 3-10 fractions. The mean heart dose (Dmean) and maximum heart dose (Dmax) were 4.9 Gy (0.7-8.4 Gy) and 36.2 Gy (8.3 – 64.1 Gy), respectively. On CMR, five patients showed myocardial alterations, such as late gadolinium enhancement and edema after a median follow-up time of 5.6 years (0.1-6.3 years). All detected lesions were overlapping or in close proximity to the PTV within the myocardium (Figure 1). In patients with structural changes of the myocardium the median distance between treated lesion and myocardium with 0.0 (0.0-1.08) cm vs. 1.4 (0.41-2.0) cm was significantly lower (p=0.015). Additionally, patients with structural changes on CMR showed significantly higher Dmax (135.4 Gy vs. 25.4 Gy, p=0.009), Dmean (4.4 Gy vs. 3.4 Gy, p=0.05), D0.1cc (106.3 Gy vs. 21.5 Gy, p=0.006) and D0.03 (117.2 Gy vs. 22.9 Gy, p=0.007). Structural changes on CMR showed a Dmean of 25.9 Gy (21.7-38.3 Gy; EQD2 α/β=3 Gy: 49.4 Gy, 24.8-64.9 Gy) and a Dmax of 40.5 Gy (29.1-61.8 Gy; EQD2 α/β=3 Gy: 110.65 Gy, 38.6-146.2 Gy).

Table 1: *Patient characteristics*

Parameter	Data (n=10 patients)
Age at primary diagnosis in years, median (range)	63 (35–85)
Female gender, n (%)	4 (40.0)
Single dose in Gray, (range)	6 (4.3-15.0)
Fractionation, median (range)	7 (3-10)
Total dose in Gray, (range)	42.5 (30-48)
EQD2 dose, median (Gray)	62.0 (50.0-94.0)
Isodose, mode (%, range)	65 (65-80)
Maximal heart dose in Gray, median (range)	36.2 (8.3-64.1)
Median heart dose in Gray, median (range)	4.9 (0.7-8.4)
ECOG, median (range)	1 (0-2)
KPS, median (range, %)	80 (10-90)
Primary tumor histology, n (%)	
➢ Non-small cell lung cancer	3 (30.0)
➢ Small-cell lung cancer	2 (20.0)
➢ Other[1]	5 (50.0)
Tumor stage	
○ III	2 (20.0)
○ IV	8 (80.0)
Alive at time of analysis, n (%)	10 (100)
Disease status at last visits	
➢ Stable disease, n (%)	8 (80.0)
➢ Progression, n (%)	2 (20.0)
Prior thoracic surgery, n (%)	1 (10.0)
Prior thoracic radiotherapy, n (%)	3 (30.0)
Systemic therapy before index RT	
➢ None, n (%)	2 (20.0)
➢ Chemotherapy and/or Immunotherapy, n (%)	8 (50.0)
Systemic therapy after index RT	
➢ None, n (%)	2 (20.0)
➢ Chemotherapy, n (%)	3 (30.0)
➢ Immunotherapy, n (%)	7 (70.0)
➢ Chemotherapy and Immunotherapy, n (%)	2 (20.0)
Systemic therapy 30 days before last visit	
➢ None, n (%)	5 (50.0)
➢ Chemotherapy, n (%)	3 (30.0)
➢ Immunotherapy, n (%)	2 (20.0)
➢ Chemotherapy and Immunotherapy, n (%)	0 (0.0)
Outcome, n (%)	
➢ New onset CAD	2 (20.0)
➢ Structural pathologies on cardiac MRI	5 (50.0)

[1] Includes urothelial carcinoma, malignant melanoma, leiomyosarcoma, CUP and ductal breast cancer

Figure 1a-d: *Stereotactic body radiation therapy plan (SBRT) with dose distribution and cardiac structural changes as assessed by cardiac magnetic resonance (CMR) imaging*

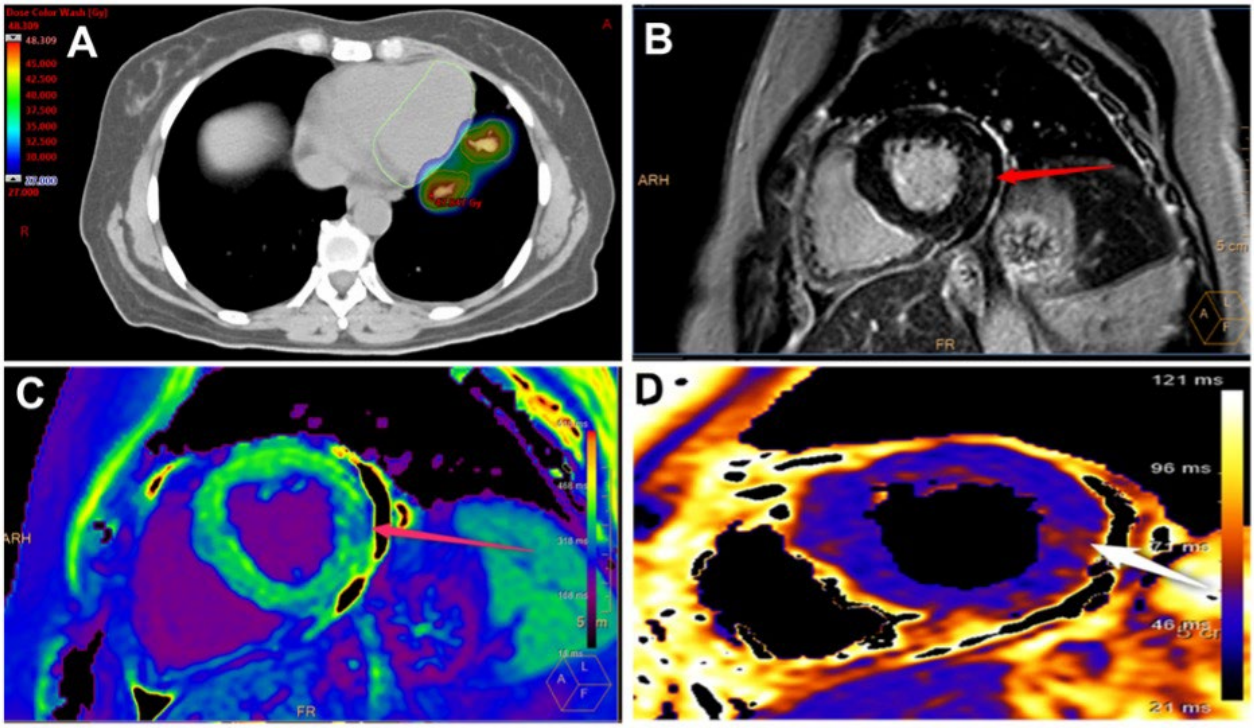

Figure 1a: Axial computed tomography image with overlayed SBRT plan with planning target volume overlapping the basal and midventricular lateral myocardium.
Figure 1b: Basal CMR image in short axis geometry demonstrating inferolateral late gadolinium enhancement (representing myocardial fibrosis).
Figure 1c: Basal CMR image in the same short axis geometry demonstrating post-contrast T1 relaxation time shortening (correlating to myocardial alterations).
Figure 1d: Basal CMR image in the same short axis geometry demonstrating inferolateral prolongation of T2 relaxation times (correlating to myocardial alterations, e. g. edema).

Conclusion:

In this pilot-study, patients treated with SBRT for pulmonary targets with PTV overlapping the heart showed structural changes of the myocardium in CMR. The presence of structural changes correlates with higher heart doses.

562

J. Tschumi[1, 2], L. Jörimann[1, 2], K. Neumann[1, 2], M. Zeeb[1, 2], D. Braun[1], R. Kouyos[1, 2], K. Metzner[1, 2], H. Günthard[1, 2], S. Swiss HIV Cohort Study[1]

Investigating the origins of intermittent viremia in individuals who initiate therapy during primary HIV-1 infection

Division of Infectious Diseases and Hospital Epidemiology, University Hospital Zurich, Zurich, Switzerland[1], Institute of Medical Virology, University of Zurich, Zurich, Switzerland[2]

Introduction:
In most HIV-1 infected individuals, antiretroviral therapy (ART) reduces viral loads to undetectable levels. However, in some individuals, viremia remains detectable despite very early initiation of ART during primary infection, adherence to drug regimens and the absence of drug resistance mutations. The causes of such residual viremia remain unclear. This project aims to characterize the HIV-1 latent reservoir in early treated individuals with persistent low-level viremia and to investigate the presence of HIV-1 evolution compared to fully suppressed individuals.

Methods:
We identified seven individuals from the Zurich Primary HIV Infection Study (ZPHI) that presented low-level viremia over a time course of at least two years. Three longitudinal PBMC samples were collected from each individual, including the baseline sample prior to ART initiation, and a sample two years and four years after ART initiation. HIV-1 reservoir size was measured using digital PCR. Near full-length HIV-1 proviral DNA was amplified and sequenced in bulk and on the single genome level to infer genome intactness and viral diversity. Integration sites of single proviruses will be identified using ligation mediated PCR, and together with single proviral sequences, they will be used to identify clones. The same analysis will be performed on a control group not showing low-level viremia.

Results:
So far, we don't find evidence for evolution of the proviral reservoir in individuals showing low-level viremia. Genetic distances of consensus sequences do not increase over time, and the total number of archived drug resistance mutations in proviruses remains stable. Ongoing quantification of HIV-1 DNA and RNA forms, as well as results from single proviral sequencing, will help to better characterise the proviral landscape in these individuals.

Conclusion:
Overall, differences in HIV-1 proviral landscapes compared to fully suppressed individuals could provide insights into the origins and mechanisms of intermittent viremia.

563

M. Ahmadsei[1], V. Jegarajah[1], R. Dal Bello[1], L. Stark[1], P. Balermpas[1], N. Andratschke[1], S. Tanadini-Lang[1], M. Guckenberger[1]

Dosimetric analysis of proximal bronchial tree sub-segments to assess the risk of severe toxicity after stereotactic body radiation therapy of ultra-central lung tumors

Department of Radiation Oncology, University Hospital Zurich, University of Zurich[1]

Introduction:
Stereotactic body radiotherapy (SBRT) is a guideline-recommended treatment option for patients with medically inoperable early stage lung cancer and pulmonary oligometastases. In case of ultra-central tumor location - defined as tumor contact (PTV) with proximal bronchial tree (PBT), trachea or esophagus - SBRT is associated with an increased risk of severe toxicity. Therefore, the role of SBRT for ultra-central lung tumors remains controversial. The aim of this study was to perform a detailed dosimetric analysis of PBT subsegments to evaluate safety of SBRT in ultra-central lung tumors.

Methods:
Fifty-seven ultra-central lung tumor patients treated with SBRT at our institution from 2014 to 2021 were included. Ultra-central lung tumors were defined as tumor (PTV) abutting or involving trachea, PBT or esophagus. Descriptive analysis, Cox regression, Kaplan-Meier method and log-rank test were employed to analyze overall survival (OS), local control (LC) and progression-free survival (PFS). Bayesian inference was employed to build a dose-response model for toxicity. While the prior was based on meta-analysis of previous literature, the likelihood was computed based on a binomial distribution taking into account the number of observed patients without toxicity.

Results:
Twenty-seven (47.4%) of the irradiated lesions were primary lung tumors and 30 (52.6%) metastases.The most common primary tumor was non-small cell lung cancer (NSCLC) with 37 (64.9%) cases, of which 12 patients had primary non-metastatic NSCLC, and 25 patients had locally recurrent or oligometastatic NSCLC. Colorectal cancer, small-cell lung cancer, head-and-neck cancer, metastatic melanoma and sarcoma combined accounted for twenty oligometastatic patients (35.1%). Patients were treated with risk-adapted SBRT of median 45.0 Gy (30.0-60.0 Gy) respectively 55.2 Gy (33-88 Gy, EQD2, α/β = 10 Gy) in 8 or 10 fractions. The most commonly prescribed dose was 48 Gy in 8 fractions (n=30, 53.0%). The median prescription isodose to the PTV was 65.0% (65.0-85.0%). The median planning target volume was 30.0 cm3 (6.0-199.0 cm3). After a median follow-up of 2.2 years (0.6-9.3 y), the one-year and two-year LC rates were 85.2% and 77.1%, respectively. The median OS was 3.4 years (0.6-9.3 y), OS at 2 years was 71.3%. The median PFS was 1.0 year (0.2-5.7y). Grade ≥3 radiation pneumonitis was observed in two patients (3.5%), while no bronchial stenosis, hemorrhage or fistula was observed. The median D0.02cc to PBT was 84.4 Gy (EQD2, α/β = 3 Gy: 43.9-159.3 Gy). The dose-response model predicted a toxicity limited to 4.9% (0 - 11.4%) when delivering 100 Gy (EQD2, α/β = 3 Gy) to any location of the PBT (D0.2cc) (Figure 1b).

Table 1: General patient-and tumor characteristics

Parameter	Results (%)
Total number of patients	**n=57 patients**
Age at diagnosis in years, median (range)	67.7 (33.0–83.0)
Age over 70 years	29 (50.9)
Male gender, n (%)	42 (73.7)
Female gender, n (%)	15 (26.3)
Median follow-up time in years (range)	2.2 (0.63-9.30)
Primary tumor histology	
• All NSCLC	37 (64.9)
○ Primary, non-metastatic NSCLC	12 (32.5)[1]
▪ *Adenocarcinoma*	5 (41.7)[2]
▪ *Squamous-cell carcinoma*	7 (58.3)[2]
• Recurrent NSCLC	15 (40.5)[1]
▪ *Adenocarcinoma*	10 (66.7)[2]
▪ *Squamous-cell carcinoma*	4 (26.7)[2]
▪ *Large-cell carcinoma*	1 (6.6)[2]
Oligometastatic disease	30 (53.6)
• NSCLC	10 (27.0)[1]
○ *Adenocarcinoma*	9 (90.0)[2]
○ *Large-cell carcinoma*	1 (10.0)[2]
• SCLC	1 (1.8)
• Colorectal adenocarcinoma	4 (7.0)
• Head-and-Neck cancer	4 (7.0)
• Melanoma	3 (5.3)
• Sarcoma	3 (5.3)
• Other[3]	5 (8.8)
Patients alive at time of data analysis	27 (47.4)
ECOG-PS before index RT, median (range)	1 (0–2)
Smoking status	
• Current	10 (17.5)
• Former	35 (61.4)
• Never	12 (21.1)
Symptoms at time of radiotherapy	
• None	30 (52.6)
• Cough	20 (35.0)
• Dyspnea	6 (10.5)
• Hemoptysis	2 (3.5)

Figure 1: A: Schematic overview of PBT and PBT sub-segments, B: Dose-response model for PBT

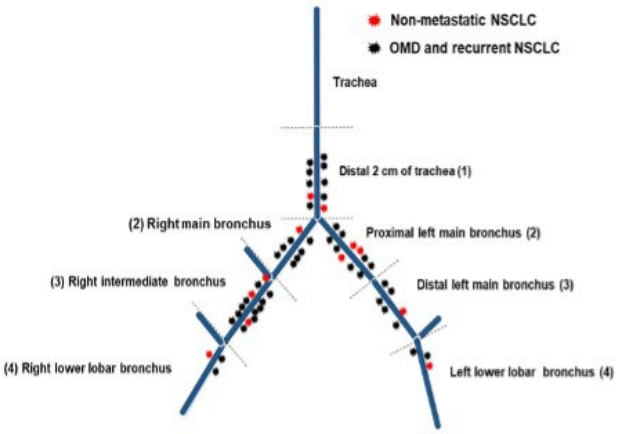

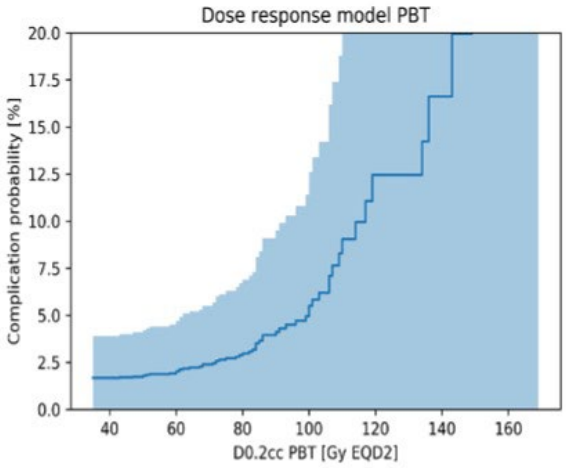

Conclusion:

This study reports a detailed dosimetric analysis of PBT subsegments after SBRT for ultra-central lung tumors. A dose threshold of 100Gy EQD2 to the PBT and its sub-segments is expected to result in low rates of severe bronchial toxicity, while maintaining high rates of local tumor control.

564

L. Jörimann[1, 2, 3], J. Tschumi[1, 2, 3], M. Zeeb[1, 2], C. Leemann[1, 2], C. Schenkel[1, 2], K. Neumann[1, 2], S. Chaudron[1, 2], M. Zaheri[2], P. Frischknecht[1], N. Neuner-Jehle[1, 2], H. Kuster[1, 2], D. Braun[1], C. Grube[1], R. Kouyos[1, 2], K. Metzner[1, 2], H. Günthard[1, 2], S. SHCS[1]

Absence of HIV-1 evolution in early treated individuals switching to Dolutegravir monotherapy for 48 weeks

Division of Infectious Diseases and Hospital Epidemiology, University Hospital Zurich[1], Institute of Medical Virology (IMV), University of Zurich (UZH)[2], Microbiology and Immunology (MIM) Program, Life Science Graduate School of Zurich[3]

Introduction:
HIV-1 infection is treated with antiretroviral therapy, usually consisting of three - and more recently also with two - different drugs. The “early simplified study”, a recent randomized, clinical trial (CID, 2019;69(9):1489–97) comparing dolutegravir-monotherapy with triple drug therapy in early treated and suppressed patients from the Zurich Primary HIV infection study (ZPHI) demonstrated sustained virological suppression over 48 weeks. Here, in a subset of patients we characterize the longitudinal landscape of the latent reservoir and potential differences between dolutegravir monotherapy and continued standard of care triple therapy with respect to HIV-1 evolution as an indirect measure of potential undetected, low-level HIV-1 replication.

Methods:
Patients in the early simplified study were assigned 2:1 to either dolutegravir-monotherapy or continued triple therapy (NCT02551523). Near full-length HIV-1 proviral PCR and next generation sequencing was established and applied to longitudinal patients’ PBMC one year after individual ART initiation, at week 0 and 48 after randomization. Genetic distance over the four timepoints was calculated and maximum-likelihood phylogenetic trees were constructed. Average pairwise diversity score of each sequences was calculated based on ambiguous nucleotides as a measure for diversity of the sequence. Additionally, drug resistance mutations, especially in integrase, were compared between the two treatment groups. Furthermore, single genome amplification was performed for a subset of patients and intactness and hypermutations was assessed.

Results:
All patients had undetectable viral load (<50 copies/ml) and in general low levels of HIV proviral DNA during the whole study period (CID,2019:69(9):1489-97). After stringent quality control near full-length sequencing was successful for 43 patients (25 monotherapy, 18 triple therapy) out of 101 patients. Mean pairwise genetic distance of patients’ proviral sequences measured from week 0 to week 48 was not significantly different with 0.0102 substitutions/nt in the monotherapy (n=25) and 0.0104 substitutions/nt in the triple therapy group (n=18) (p=0.56). At week 48 of “early simplified”, median average pairwise diversity within patients’ sequences for gag, pol and env individually, were not significantly different between the two study groups (p=0.57, p=0.87, p=0.26). Two drug resistance mutations conferring resistance to dolutegravir were found at week 48 each in the monotherapy and triple therapy group. Whereas in the triple therapy group they appeared individually in two patients at a frequency of 100%, in the monotherapy group they were found combined in one patient at frequencies of 25% and 28%. Single genome landscape analysis showed 4% intact sequences and more hypermutated sequences at week 48 in both the triple and the monotherapy group.

Conclusion:
Longitudinal sequence analysis of 25 patients from the dolutegravir-monotherapy groups showed no signs of HIV-1 evolution over 48 weeks. In addition, no difference between the monotherapy and the triple therapy group was found regarding genetic distance, viral diversity or development of minor frequency drug resistance mutations. In conclusion, no evidence for ongoing low-level replication during dolutegravir monotherapy was found in these early-treated patients.

565

E. Müller[1, 3], K. Gegenschatz-Schmid[1], L. Moser[1, 4], N. Ochsenbein-Kölble[1, 2], M. Ehrbar[1, 4]

The Effect of WNT Signalling and External Cues on Migration of Isolated Fetal Membrane Cells

Department of Obstetrics, University and University Hospital Zurich, Switzerland[1], The Zurich Center for Fetal Diagnosis and Therapy, Switzerland[2], University of Basel, Switzerland[3], University of Zurich, Switzerland[4]

Introduction:
In the last ten years the number of minimally invasive surgeries has increased to treat different fetal illnesses such as twin-to-twin transfusion syndrome (TTTS). However, in an average of 30% of the cases the iatrogenic intervention is responsible for preterm premature rupture of the fetal membranes (iPPROM) leading to premature labour. One of the potential reasons for iPPROM could be the insufficient healing potential of the fetal membranes (FM). FMs are composed of three layers, the epithelial layer facing the amniotic fluid, the amnion and the chorion. The inability of the FMs to heal themselves poses a big enigma. This is especially astonishing, considering the healing and regenerating potential of amniotic membranes, and their clinical use in the treatment of chronic skin wounds and ocular surface pathologies.
The aim of this project is to investigate potential factors influencing FM healing. Platelet-Derived Growth Factor (PDGF) has been previously reported to have a positive effect on amniotic cell migration. Furthermore, recent proteome analysis of the amnion reported the presence of several WNT members. Here, we analyzed the effect of WNT signalling and the presence of external factors on FM cell migration.

Methods:
Term FMs were collected and washed with PBS prior processing. Pieces of ~5 cm^2 were cut and the amnion was separated from the chorion. Human amniotic cells (hAMCs) were isolated as described previously [Kivelio et al., 2015], while the digestion step with collagenase A was replaced with the digestion mix provided by the Umbilical Cord Dissociation Kit (UCDK, Miltenyi Biontec). Chorionic cells were isolated according to UCDK instructions. Isolated cells were cultured in MEMα++ (supplemented with 10% FBS and 1% PenStrep) at 37°C in a humidified chamber with 5% CO^2.
Cell spheroids of 9000-10000 cells were formed by hanging drop in MEMα++ and 20% methylcellulose. To analyze cell migration, cells or cell spheroids were encapsulated in 1.7% TG-PEG hydrogels or on 3DProSeed plates (Ectica) and cultured up to 7 days. For the different conditions, MEMα++ was supplemented with WNT activator (BML284, 0-100nM), with WNT inhibitor (WNTC59, 0-100nM), PDGF-BB (0-100ng/ml) or 0.1% DMSO as negative control. Cell migration was quantified using ImageJ (Fiji).
For confocal imaging samples were fixed in 4% PFA and immunostained for actin, fibronectin and with DAPI for cell nuclei.

Results:
The presence of chorionic cells as well as the supplementation of BML284 inhibited PDGF-stimulated and unstimulated migration of hAMCs. The addition of WNTC59 supported hAMC migration only slightly. No significant difference was observed on chorionic cell migration upon WNT inhibitor or activator addition.

Conclusion:
Our results have shown a significant effect of the WNT activator BML284 on the migration of hAMCs. Considering the finding that chorionic cells inhibit hAMCs migration, and WNT proteins were identified in the amnion layer, it would be interesting to evaluate in a next step whether chorionic cells are the potential WNT source. Furthermore, we will analyze additional effectors on hAMCs migration such as amniotic fluid.

At this point, our results showed an unknown inhibiting effect of WNT signalling on hAMCs migration. This could bring us one step closer to the understanding why fetal membranes after a prenatal surgery heal insufficiently, and could help to design FM healing biomaterials.

566

G. Panteloglou[5], P. Zanoni[5], A. Othman[6], J. Haas[4], R. Meier[7], S. Radosavljevic[5], E. Schlumpf[5], M. Futema[1], S. Humphries[2], W. März[8], B. Staels[4], B. van de Sluis[3], J. Kuivenhoven[3], J. Robert[5], A. von Eckardstein[5]

Genome-wide siRNA screen unravels novel potential Familial Hypercholesterolemia (FH) causing genes

Cardiology Research Centre, Molecular and Clinical Sciences Research Institute, St George's, University of London, London, UK[1], Cardiovascular Genetics, Institute of Cardiovascular Science, University College London, London, United Kingdom[2], Department of Pediatrics, Section Molecular Genetics, University of Groningen, University Medical Center Groningen, Groningen, the Netherlands[3], INSERM, UMR1011, University of Lille, CHU Lille, Institute Pasteur de Lille, Lille, France[4], Institute of Clinical Chemistry, University & University Hospital of Zurich, Zurich, Switzerland[5], Institute of Molecular Systems Biology, ETH Zurich, Zurich, Switzerland[6], Scientific center for optical & electron microscopy (ScopeM), ETH Zurich, Zurich, Switzerland[7], Vth Department of Medicine (Nephrology, Hypertensiology, Endocrinology, Diabetology, Rheumatology), Medical Faculty of Mannheim, University of Heidelberg, Mannheim, Germany[8]

Introduction:
The hepatic Low Density Lipoprotein (LDL) receptor (LDLR) is the major determinant of LDL-cholesterol (LDL-C) in the plasma. For up to 40% of patients with FH, the genetic origin is unknown. We aimed at the discovery and validation of novel genes limiting the uptake of LDL into hepatocytes

Methods:
We performed a genome wide siRNA screening in Huh7 hepatocarcinoma cells. We used siRNAs from different vendors to knockdown candidate genes in Huh7 cells. We measured the uptake of LDL and the cell surface abundance of LDLR with FACS. We examined the splicing of LDLR mRNA through sequencing, microarrays and qRT-PCR and characterized the glycosylation of LDLR with WB. We explored data banks for the association of SNPs in candidate genes with LDL-C levels. Finally, we analyzed whole exome sequencing data for the existence of rare mutants in individuals suffering from FH and functionally characterized some rare variants in vitro.

Results:
Several members of the U2-spliceosome and the COP I coatomer were among the top hits limiting LDL uptake into Huh-7 cells. Silencing of different subunits from either complex resulted in marked reduction of LDL uptake and LDLR cell surface abundance. As the underlying pathomechanisms, we found aberrancies in splicing and glycosylation of LDLR, respectively. Analysis of microarray and RNA sequencing data from human liver and blood samples revealed a correlation of the aberrant LDLR transcript expression with the status of Non Alcoholic Fatty Liver Disease (NAFLD) and age, respectively. Analysis of data from the Global Lipids Genetic Consortium revealed significant associations of SNPs in genes encoding for the U2-spliceosome subunit RBM25 or the COP I subunit ARCN1 with LDL-C levels. Analysis of whole exome sequencing data from severely hypercholesterolemic individuals with no loss-of-function mutation in the canonical FH genes, revealed rare variants in the genes encoding RBM25, COPA, COPB2, or COPG1. Finally, in vitro characterization of three rare RBM25 variants confirmed their limiting role for LDL uptake

Conclusion:
Our findings provide evidence for the involvement of the U2-spliceosome and the COP I complex in the post-transcriptional and the post-translational regulation of LDLR, respectively. Genetic or acquired alterations in these genes or proteins may contribute to hypercholesterolemia.

567

S. Graf[1], G. Rathmes[1], R. Lehmann[1], C. Cavelti-Weder[1]

Real-World Evidence Supporting The Use Of Advanced Hybrid Closed Loop In Poorly Controlled Type 1 Diabetic Patients

University Hospital Zurich[1]

Introduction:
The advanced hybrid closed loop (a-HCL) algorithm of the MiniMed 780G includes automated basal and correction bolus insulin and offers the possibility to choose between three glucose targets. The aim was to evaluate the effectiveness of the a-HCL compared to its predecessors, the predictive low glucose suspension (PLGS, MiniMedTM 640G) and the standard hybrid closed loop (s-HCL, MiniMedTM 670G), and to assess which group of patients benefitted the most from the implementation of the a-HCL.

Methods:
Type 1 diabetes patients >18 years of age followed at the University Hospital Zurich (USZ), who initially used a PLGS or a s-HCL and were subsequently switched to the a-HCL until December 2021, were included in the study. Glucose metric data regarding HbA1c, time in range (TIR), time above range (TAR), time below range (TBR), average sensor glucose (SG), and variation coefficient (VC) was retrospectively analyzed before and after the conversion to the a-HCL.

Results:
88 patients were screened, and 71 patients were included in the analyzes. After the implementation of the a-HCL, there was a significant decrease in HbA1c (pre 7.3±0.7% to post a-HCL 6.8±0.5%, $p<0.001$), SG (8.8±1.2 mmol/L to 7.9±0.8 mmol/L, $p<0.001$) and a significant increase in TIR (73.5% to 81%, $p<0.001$). Additionally, a significant decrease in TAR (23% to 17%, $p<0.001$) was observed, while TBR (1.5% to 1%, $p=0.573$) and the VC did not significantly change (33±6.6% to 32.4±5.8%, $p=0.313$). The changes in glycemic control were most pronounced in patients with a higher baseline HbA1c, a higher baseline SG, a lower baseline TIR, and a higher VC, all measures of poor glycemic control. Furthermore, patients with a body-mass index (BMI) >30kg/m2 achieved the greatest changes in HbA1c and TIR.

Conclusion:
In conclusion, our data support the use of a-HCL in all patients, but especially in poorly controlled type 1 diabetic patients with a high BMI.

569

H. Lakshminarayanan[1], K. Yim[3], S. Pfammatter[2], A. Banaei-Esfahani[1], D. Rutishauser[1], P. Schraml[1], R. Chahwan[3], H. Bolck[1], H. Moch[1]

Exploring extracellular vesicles as liquid biopsy biomarkers for clear cell renal cell carcinoma

Department of Molecular Pathology and Pathology, University of Zurich and University Hospital Zurich, Zurich, Switzerland[1], Functional Genomics Center Zurich, ETH Zurich University of Zurich, Zurich, Switzerland[2], Institute of Experimental Immunology, University of Zurich, Zurich, Switzerland[3]

Introduction:
Clear cell renal cell carcinoma (ccRCC) is the most lethal urological malignancy, where 30% patients already present with metastasis upon diagnosis and another 30% further develop metastasis during their disease. Currently, disease prognosis is based on histopathological characterization. However, often this cannot correctly predict metastatic dissemination or patient survival. In this context, liquid biopsies, such as patient plasma, are a powerful tool to aid in correct prognostication and enable better clinical management of ccRCC patients. Secreted, nanoscale, membrane-bound extracellular vesicles (EVs) are promising biomarkers that can be found in circulation. During ccRCC tumorigenesis, they are implicated in cell communication and metastatic progression. Therefore, EVs are an attractive constituent of liquid biopsies with potential prognostic power. In this study, we aim to identify EV-derived protein biomarkers for the prognosis of ccRCC patients.

Methods:
Our workflow starts with a preliminary investigation in patient-derived cell culture (PDC) and commercial cell culture models to generate ccRCC-specific EV signatures. To this end, we used three ccRCC PDCs (G17.1150, G18.617, G14.276), 786-O cell line, and a non-ccRCC control cell (HeLa). We isolated ccRCC-specific EV populations from media supernatant using serial ultracentrifugation. We then characterized the EVs using transmission electron microscopy (TEM) and nano flow cytometry (nFCM) to observe their morphology, size distribution, and concentration. Following this, we analyzed the EV proteome in comparison to the cellular proteins (CP) from our models using liquid chromatography-tandem mass spectrometry (LC-MS/MS). This EV protein-based signature will later be applied to isolate EVs from patient plasma samples, which contain a complex mix of EVs, shed from all tissues in the body.

Results:
TEM imaging and nFCM analysis showed cup-shaped ccRCC-derived EVs that fall in the expected size range of 40-80 nm, indicative of exosomal EV populations. Through LC-MS/MS, we identified 4693 total proteins, of which 1342 were common between the EVs and CP, confirming the biogenesis of the isolated EVs. Interestingly, we were able to observe an intersection of 47 proteins common amongst all PDC-derived EVs, apart from unique proteins for each PDC. Functional annotation of these proteins highlighted the enrichment of several known vesicular and associated proteins. Since we observed a subset of proteins that were common in EVs from our PDCs, we will now perform replicate mass spectrometry analysis to corroborate our findings and generate robust ccRCC-specific EV protein signatures.

Conclusion:
We successfully isolated ccRCC-specific EVs from in vitro cell models and were able to identify exosomal populations. Our preliminary proteomic analysis revealed an enrichment of known vesicular proteins in the EVs. We will investigate ccRCC-specific protein signatures in cell culture models in more depth and then use this to explore EVs as liquid biopsy markers in ccRCC patient plasma. This will allow us to develop a tool for the active surveillance of ccRCC patients using specific molecular biomarkers, and thereby help improve prognostication and cancer management in ccRCC patients who currently remain at risk for developing aggressive disease.

570

A. Taner[2], J. Hanson[2], C. Weber[1], D. Bassler[1], D. McCulloch[3], C. Gerth-Kahlert[2]

Flicker electroretinogram in preterm infants

Department of Neonatology, University Hospital Zurich and University of Zurich, Zurich, Switzerland[1], Department of Ophthalmology, University Hospital Zurich and University of Zurich, Zurich, Switzerland[2], School of Optometry and Vision Science, University of Waterloo, Waterloo, Canada[3]

Introduction:
Infants born prematurely are at risk of developing retinopathy of prematurity which is associated with abnormalities in electroretinography. The aim of this study was to analyse non-invasive flicker electroretinograms (ERGs) of preterm infants.

Methods:
In this non-randomized, cross-sectional study, 40 moderate preterm (gestational age (GA) 34 0/7 to 36 6/7 weeks, group A) and 40 very or extremely preterm infants (GA ≤ 31 weeks, group B) were recruited for flicker ERG recording through closed eyelids using the portable RETeval® device and skin electrodes. Testing was performed within the first week of life in group A and between 34th and 37th week postmenstrual age (PMA) in group B. Flicker stimuli were presented at 28.3 Hz with stimulus levels of 3, 6, 12, 30, and 50 cd•s/m2 while infants were sleeping. Two measurements per stimulus level were recorded and averaged after verifying reproducibility. Primary endpoints were peak time (ms) and amplitude (µV) for each stimulus level.

Results:
With increasing stimulus levels flicker ERGs were reproducibly recorded in a greater number of infants, with the highest number of reproducible ERG responses at 30 cd•s/m2. Amplitudes increased with stronger flicker stimulation, while peak times did not differ significantly between stimulus levels. Amplitudes were significantly greater in Group B at the highest stimulus level (Mann-Whitney-U-Test = 198.00, Z = - 4.097, p = <0.001). No inter-group differences in peak times were detected. Eight infants later developed ROP: six infants with stage 1, zone II, one with stage 2, zone II, and one with stage 3, zone II.

Conclusion:
Feasibility of collecting flicker ERG data in most preterm infants was confirmed in this study. Although the groups were comparable in terms of PMA at the time of data collection, very and extremely preterm infants tended to have higher amplitudes than moderate preterm infants with significant higher amplitudes in one stimulus level. The difference detected could indicate acceleration of retinal development following birth, triggered by visual stimulation. Since only eight infants who developed ROP were tested, we were unable to draw firm conclusions regarding effects of ROP on the flicker ERG.

571

O. Hasan Ali[4, 13, 17], T. Sinnberg[3], C. Lichtensteiger[13], O. Pop[13], A. Jochum[13], L. Risch[1], SD. Brugger[5], A. Velic[21], D. Bomze[22], P. Kohler[8], P. Vernazza[8], WC. Albrich[8], C. Kahlert[8], M. Abdou[13], N. Wyss[13], K. Hofmeister[3], H. Niessner[3], C. Zinner[20], M. Gilardi[20], A. Tzankov[20], R. Martin[3], A. Dulovic[19], . Shambat[5], N. Ruetalo[11], P. Buehler[14], T. Scheier[5], W. Jochum[15], L. Kern[18], S. Henz[6], T. Schneider[9], G. Kuster[2], M. Lampart[2], M. Siegemund[16], R. Bingisser[10], M. Schindler[11], N. Schneiderhan-Marra[19], H. Kalbacher[12], C. McCoy[23], W. Spengler[7], M. Brutsche[14], B. Maček[21], R. Twerenbold[24], J. Penninger[17], M. Matter[20], L. Flatz[3]

Pulmonary surfactant proteins are inhibited by immunoglobulin A autoantibodies in severe COVID-19

Center of Laboratory Medicine, Vaduz, Liechtenstein[1], Department of Cardiology and Cardiovascular Research Institute Basel (CRIB), University Hospital Basel[2], Department of Dermatology, University Hospital Tübingen, Tübingen, Germany[3], Department of Dermatology, University Hospital Zurich[4], Department of Infectious Diseases and Hospital Hygiene, University Hospital Zurich[5], Department of Internal Medicine, Cantonal Hospital St. Gallen[6], Department of Medical Oncology and Pneumology, University Hospital Tübingen, Tübingen, Germany[7], Division of Infectious Diseases and Hospital Epidemiology, Cantonal Hospital St. Gallen[8], Division of Pneumology, Cantonal Hospital St. Gallen[9], Emergency Department, University Hospital Basel[10], Institute for Medical Virology and Epidemiology, University Hospital Tübingen, Tübingen, Germany[11], Institute of Clinical Anatomy and Cell Analysis, University of Tübingen, Tübingen, Germany[12], Institute of Immunobiology, Cantonal Hospital St. Gallen [13], Institute of Intensive Care Medicine, University Hospital Zurich[14], Institute of Pathology, Cantonal Hospital St. Gallen[15], Intensive Care Unit, Department of Acute Medicine, University Hospital Basel[16], Life Sciences Institute, University of British Columbia, Vancouver, Canada[17], Lung Center, Cantonal Hospital St. Gallen[18], NMI Natural and Medical Sciences Institute, University of Tübingen, Tübingen, Germany[19], Pathology, Institute of Medical Genetics and Pathology, University Hospital Basel[20], Proteome Center Tübingen, Interfaculty Institute for Cell Biology, University of Tübingen, Tübingen, Germany[21], Sackler Faculty of Medicine, Tel Aviv University, Tel Aviv, Israel[22], Snyder Institute for Chronic Disease, Cumming School of Medicine, University of Calgary, Calgary, Alberta, Canada[23], University Center of Cardiovascular Science and Department of Cardiology, University Heart and Vascular Center Hamburg, University Medical Center Hamburg-Eppendorf, Partner Site Hamburg-Kiel-Lübeck, Hamburg, Germany[24]

Introduction:
Coronavirus disease 2019 (COVID-19) can lead to acute respiratory distress syndrome with fatal outcomes. Evidence suggests that dysregulated immune responses, including autoimmunity, are key pathogenic factors. The objective of this study was to assess whether IgA autoantibodies target lung-specific proteins and contribute to disease severity.

Methods:
We collected 147 blood, 9 lung tissue, and 36 BAL fluid samples from three tertiary hospitals in Switzerland and one in Germany. Severe COVID-19 was defined by the need to administer oxygen. We investigated the presence of IgA autoantibodies and their effects on pulmonary surfactant in COVID-19 using the following methods: immunofluorescence on tissue samples, immunoprecipitations followed by mass spectrometry on BAL fluid samples, enzyme-linked immunosorbent assays on blood samples, and surface tension measurements with medical surfactant.

Results:
IgA autoantibodies targeting pulmonary surfactant proteins B and C were elevated in patients with severe COVID-19 but not in patients with influenza or bacterial pneumonia. Notably, pulmonary surfactant failed to reduce surface tension after incubation with either plasma or purified IgA from patients with severe COVID-19.

Conclusion:
Our data suggest that patients with severe COVID-19 harbor IgA autoantibodies against pulmonary surfactant proteins B and C and that these autoantibodies block the function of lung surfactant, potentially contributing to alveolar collapse and poor oxygenation.

572

M. Jacobs[1, 2], M. Ehrbar[1, 2]

Development of an in vitro ovary model for the sustained culture of primary follicles

University Hospital Zurich[1], University of Zurich[2]

Introduction:
Most chemo- and radiotherapeutic cancer treatments are toxic to the ovaries, which can result in impaired fertility and/or endocrine function in female patients. The state-of the art method to preserve fertility is the cryopreservation of the ovaries. As this method for some types of cancer poses the risk to reintroduce malignant cells, current approaches in research aim to develop an artificial ovary for the temporary and safe culture of the patients' follicles. This engineered scaffold would consist of different biomaterials and celltypes to ensure follicle survival and growth. In the present study we develop 3D scaffolds using combinations of natural and synthetic biomaterials to culture follicles and ovary cells for several days. We will evaluate cell viability, morphology, and functionality in response to the different biomaterial combinations.

Methods:
Hydrogels as 3D scaffolds were fabricated by combining the synthetic polymer polyethylene glycol (PEG) with different natural biomaterials, such as collagen type I and fibronectin (PEG-ECM). The ECM molecules were used to promote cell adhesion in the bioinert PEG matrix. First, a protocol was established for the sequential isolation of mouse follicles and ovary cells from the same sample. Next, ovary cells, follicles or both together were embedded in PEG-ECM hydrogels and observed for several days regarding cell viability and morphology.

Results:
By using established protocols to seed PEG hydrogels with cells, follicles and ovary cells were successfully incorporated into PEG-ECM scaffolds. Follicles remained viable in plain PEG hydrogels and some increased in size during a culture period of five days. Embedded ovary cells spreaded faster in PEG-Collagen hydrogels compared to the other PEG-ECM hydrogels.

Conclusion:
A protocol for the sequential isolation of mouse follicles and ovary cells from the same sample was established and both were successfully incorporated into different PEG-ECM scaffolds. Next experiments will explore different concentrations of cells and ECM molecules in PEG-ECM hydrogels to evaluate their effect on ovary cell viability and morphology over one week. Additionally, immunofluorescence staining will be applied to detect matrix deposition of cells and possible differences in cell morphology. Eventually, PEG-ECM hydrogels will be adapted for the encapsulation of bovine and human ovary cells, to investigate their effect on follicle growth and maturation.

573

D. Rodriguez Gutierrez[2], A. Astourian[2], M. Hartmann[2], I. Dedes[1], P. Imesch[1], J. Metzler[1], G. Schär[1], M. Shilaih[2, 3], V. Valentina[2, 3], B. Leeners[2]

Endometriosis and Fibrosis: Reduction of deep endometriosis lesions through a novel immunotherapy treatment.

Department of Gynecology, Universitätsspital Zurich, Zurich, Switzerland[1], Department of Reproductive Endocrinology, Universitätsspital Zurich[2], FimmCyte AG, Basel, Switzerland[3]

Introduction:
Endometriosis is a chronic disease that affects 6-10% of women of reproductive age globally and is associated with severe pelvic pain and infertility. Due to the unclear etiology and pathogenesis of endometriosis, there are limited pharmacological treatments besides hormones. Due to the observed fibrotic nature of the tissue, at a cellular level fibroblasts are considered to play a central role in endometriotic lesions. In this study, we report on the efficacy of a novel monoclonal antibody targeting an extracellular matrix protein central to endometriotic lesions invasion and proliferation. This immunotherapy has the potential of targeting endometriotic tissue and reducing fibrotic lesions in deep endometriosis (DE).

Methods:
We used 14 NOG-F mice (Taconic) to create an endometriosis human xenograft model (BASEC 2020-02117). One week before engraftment, all mice got 17b-estradiol pellets (60 days release, 1,5 mg pellet). Ten mice received five fragments of 1m 3 of eutopic tissue from patient PE587. In addition, six mice received five fragments of 1m 3 of ectopic deep endometriosis tissue from patient PE583. The body weight (BW) was measured twice a week. At study day 7, mice of group A (4x PE587, 3x PE583) were treated intravenously with 1x10 7 patient derived T-cells. Group B was treated with 1 mg/kg of FMC2D12 and 1x10 7 patient derived T-cells. T-cell injection +/-antibody was repeated at study day 13 and 20. On study days 9, 16, 23, 27 and 30 group B received further antibody treatments, whereas group A was treated with saline solution. Two weeks after the final T-cell injection, lesions were searched, counted, and weighed after excision. Samples of the lesions, organs and serum were harvested. The FFPE lesion samples were sectioned for Gomori's Trichrome, Hematoxylin-Eosin and anti-CD3. A pathologist performed evaluation of cell death and inflammation degree. Fibrosis intensity, coverage, and cell count were quantified with Qupath software.

Results:
All animals were healthy and there was no significant body weight change between them (20.78 ± 0.85 g eutopic vehicle, 20.85 ± 0.85 g eutopic treated, 20.77 ± 2.03 g ectopic vehicle, and 21.17 ± 1.20 g ectopic treated). Ectopic lesion mice treated with FMC2D12 had a lower number of recovered lesions than vehicle group (1 ± 0.00 ectopic treated vs 2.67 ± 1.16 ectopic vehicle) while no change was appreciated between eutopic endometrium groups (vs 2.5 ± 0.58 eutopic treated vs 2.5 ± 1.30 eutopic vehicle). When compared with the compact fibers' distribution in untreated lesions, we observed a decrease of fibrotic collagen fibers and expanded interstitial space in FMC2D12 treated tissues, reflecting the structure of observed in normal eutopic endometrium. Treated ectopic lesions also showed reduced fibrotic lesion coverage (42.3 ± 4.6% eutopic vehicle, 42.2 ± 18.3% eutopic treated, 79.7 ± 8.8% ectopic vehicle, 54.1 ± 12.1% ectopic treated) and intensity (0.21 ± 0.03 eutopic vehicle, 0.23 ± 0.11 eutopic treated, 0.63 ± 0.29 ectopic vehicle, 0.26 ± 0.05 ectopic treated), comparable to baseline eutopic endometrium levels.

Conclusion:
Treatment with FMC2D12 effectively targeted endometriotic lesions without negatively affecting the eutopic endometrium. This resulted in a reduction of dense fibrosis areas and a reversion to normal structure observed in eutopic tissue. These results confirm the potential of a new therapeutical target for endometriotic lesions and opens a door for the development of precision therapies that target lesions in DE patients.

574

A. Plüss[1, 2], A. Korczak[1, 2], M. Ehrbar[1, 2]

3D bioprinted, perfused and vascularized bone organoids to study extravasation and metastasis of cancer

University Hospital Zurich[1], University of Zurich[2]

Introduction:
Metastasis as a leading cause of cancer-related death drives patient morbidity. Bone is the most common site for metastasis. The understanding of the pathophysiological mechanism is incomplete and models to study invasion and colonization of cancer cells in the bone are of great need.
3D bioprinting, a process in which cells within a biomaterial are deposited layer-by-layer, enables the precise formation of biologically active 3D tissue constructs. The overall aim of this project is to establish an *ex vivo* model based on printed vascularized and perfused bone organoids that allows the investigation of the pathophysiology of cancer metastasis. Therefore, in a first step we aim to engineer printable poly (ethylene glycol) (PEG) formulations that support the formation of bone and blood vessels.

Methods:
Osteogenic differentiation and network formation of mesenchymal stromal cells (MSCs) and human umbilical vein endothelial cells (HUVEC) co-cultures at different cell ratios were analysed in previously established transglutaminase cross-linked PEG hydrogels. 3D cultures were maintained in osteogenic differentiation medium containing bone morphogenetic protein 2 (BMP-2), fibroblast growth factor 2 (FGF-2) or no growth factor.

Results:
Alkaline phosphatase staining revealed osteogenic differentiation of MSCs cultured in medium containing BMP-2 independent of cell ratio and presence of HUVECs. FGF-2 promoted the network formation of HUVECs. In the absence of FGF-2 HUVECs only minimally spread in the hydrogel.

Conclusion:
The preliminary data demonstrates that HUVECs and MSCs were successfully co-cultured in the bulk PEG hydrogel. To observe network formation of HUVECs in the absence of FGF-2, the stiffness of the hydrogel should be optimized in future experiments. Furthermore, optimizing the shear-thinning characteristics of the material will be of great importance to enable its printability.

575

U. Maheshwari[2], J. Melero[1], R. Ni[3], U. Weber[4], A. Keller[2]

Microangiopathy and arteriole-associated calcifications in the brain of Xpr1 heterozygous mice

Center for Microscopy and Image analysis, University of Zurich, Zurich, Switzerland[1], Department of Neurosurgery, Clinical Neuroscience Center, Zürich University Hospital, Zürich University, Zürich, Switzerland[2], Institute for Biomedical Engineering, ETH Zurich & University of Zurich, Zurich, Switzerland[3], Institute of Experimental Immunology, University of Zurich, Zürich, Switzerland[4]

Introduction:
Mutations in *XPR1*, Xenotropic and Polytropic Retrovirus Receptor 1, gene are known to cause primary familial brain calcification (PFBC) in humans. It is an inherited neurodegenerative disease characterized by the presence of abnormal vascular calcifications in the basal ganglia. Clinical phenotypes associated with PFBC are variable ranging from asymptomatic patients to highly affected patients presenting neuropsychiatric disorders. So far, four causative genes, namely *PDGFB*, *PDGFRB*, *XPR1*, and *SLC20A2* have been identified to cause autosomal dominant-PFBC (AD-PFBC) in humans. However, the pathomechanisms underlying formation of brain vascular calcification in PFBC patients remain poorly understood. This study aims to understand the role of *XPR1*, the only known inorganic phosphate exporter in metazoans, in development and progression of brain vessel associated calcifications in mice.

Methods:
We utilized a combination of histological stainings, immunohistochemistry, fluorescent confocal microscopy, light-sheet microscopy, electron microscopy (EM), magnetic-resonance imaging (MRI), and blood plasma electrolyte analyses to characterize brain vessel associated calcifications and their progression in *Xpr1* heterozygous mice. We also investigated the changes in cellular components of neurovascular unit surrounding vascular calcifications in these mice.

Results:
Here, we report that brain arteriolar calcification in *Xpr1* het mice are first observed in the thalamus of 7-month-old animals and the calcification phenotype worsens with age. We also observed a sexual dimorphism in calcification phenotype with larger nodules appearing in aged males. We identified wide-spread occurrence of reactive astrocytes and microglia in deepbrain region, along with microangiopathy, suggesting a change in brain homeostatic state. We also observed expression of osteogenic markers around calcified nodules.

Conclusion:
We have characterized a new mouse model for PFBC where arteriole-associated calcifications are observed in the thalamus of heterozygous animals. Our data provides a closer insight into pathophysiology of PFBC and role of phosphate balance in maintaining a homeostatic state in brain vasculature.

576

A. Majcher[1], H. Aleš[1], P. Bjorkund[2], T. Hornemann[1]

Type 2 diabetes causes an elevation of neurotoxic 1-deoxysphingolipids in skin and plasma: A cause for diabetic neuropathy?

Institute of Molecular Systems Biology, Department of Biology, ETH Zurich[1], Karolinska Universitetssjukhuset Huddinge[2]

Introduction:
Type 2 diabetes (T2D) and its comorbidities are among the most prevalent health related problems of humankind. T2D and other metabolic diseases are associated with dysregulation of SL metabolism.

Particularly 1-deoxySL, neurotoxic atypical SLs produced by misplacement of Alanine (Ala) instead of Serine (Ser) in the SL lipid backbone, are elevated in plasma of patients with T2D.
One of the major T2D complications is diabetic neuropathy. Many studies investigated potential new biomarkers for T2D. However, as for now there is no reliable causal mechanism for diabetic neuropathy.
Therefore, we investigated 1-deoxySL as potential causal biomarker for diabetic neuropathy on a cohort of 36 T2D and 39 control skin biopsies and plasma samples.

Methods:
Comprehensive Lipidomics and Proteomics analysis of T2D skin biopsies, Comprehensive lipidomics and amino acids analysis of T2D plasma Stable isotope metabolic labelling

Results:
Increase in Ala/Ser ratio in primary skin fibroblasts and human hepatocytes lead to a formation of neurotoxic 1-deoxySLs. Additionally, we found elevated Ala/Ser ratio in a cohort of T2D patients, This elevation was also observed in tissues of diabetic rats.
Lastly, we have shown elevated neurotoxic 1-deoxySLs in skin and plasma of T2D patients, as well as tissues of diabetic rats. Together with a proteomics analysis, we provide a solid base for a new mechanism of diabetic neuropathy.

Conclusion:
As for now, no causal mechanism for diabetic neuropathy has been shown. Here we propose a new mechanism of diabetic neuropathy mediated via elevation of Ala/Ser ratio that leads to formation of neurotoxic 1-doxSL. These data will serve as a baseline for development of new biomarkers and therapeutic opportunities of diabetic neuropathy.

577

A. Korczak[2], B. Carrara[2], Q. Vallmajó Martín[1, 2], K. Gegenschatz-Schmid[2], M. Ehrbar[2]

High efficiency functional elucidation of human bone marrow stromal cells in vivo

Gene Expression Laboratory, Salk Institute for Biological Studies, USA[1], Laboratory for Cell and Tissue Engineering, Department of Obstetrics, University and University Hospital Zurich, Switzerland[2]

Introduction:
The human bone marrow (BM) contains a whole plethora of cells of hematopoietic and non-hematopoietic origin. Among others, Hematopoietic Stem Cell (HSC) niches as well as skeletal stem cell populations can be found within the Bone Marrow Stromal Cell (hBMSC) compartment. Unlike the well-characterized HSCs, the identity and function of the hBMSC populations remain ambiguous and call for rigorous studies. A clearer overview of the BM and the present cells is necessary as alterations in the microenvironment may lead to severe disorders such as leukemia. Modern techniques including single cell analysis highlight the heterogeneity of hBMSCs and manifest that only a small portion of cells is capable of multilineage differentiation and long-term self-renewal.1 To reveal the true fate of hBMSCs we carry out cell implantations in vivo to reliably validate their role in the complex native environment.

Methods:
To reveal the function and hierarchical organization of distinct hBMSC subpopulations we propose to engineer a multiplexing screening device for efficient in vivo testing. Additionally, using transglutaminase crosslinked poly(ethylene glycol) (PEG) hydrogels we are establishing robust microenvironmental conditions for the osteo-, chondro- and adipogenic differentiation of hBMSCs. Then, we will encapsulate prospectively isolated hBMSC populations in defined microenvironments and place them in the implantable multiplexing device. Finally, multiplexing devices will be implanted in subcutaneous pouches of immune-deficient mice and used to assess the in vivo differentiation capacity of candidate subpopulations of hBMSCs.

Results:
First experiments dedicated to minimize the number of required hBMSCs and increasing the number of test conditions have revealed in vivo differentiation in an osteogenic microenvironment and formation of small bone ossicles containing a hematopoietic niche within the multiplexing device.

Conclusion:
In this project, we develop a multiplexing platform to screen hBMSC behavior in vivo in a higher throughput manner. We will optimize the designs for multiplexed testing of health and disease-related low-abundant hBMSC subpopulations, requiring minimal cell numbers and tiny hydrogel volumes. The results of this project will constitute an important foundation to study human BM stromal hierarchy and elucidate the functional role of individual hBMSC subpopulations.

578

M. Lapaeva[1, 2, 3], A. Agustina[2, 3], P. Wallimann[3], M. Günther[1], E. Konukoglu[2], N. Andratschke[3], M. Guckenberger[3], S. Tanadini-Lang[3], R. Dal Bello[3]

Synthetic computed tomographies for low-field magnetic resonance-guided radiotherapy in the abdomen

Artificial Intelligence and Machine Learning Group, Department of Informatics, University of Zurich, Zurich, Switzerland[1], Computer Vision Laboratory, ETH Zurich, Zurich, Switzerland[2], Department of Radiation Oncology, University Hospital Zurich and University of Zurich, Zurich, Switzerland[3]

Introduction:
Magnetic resonance guided radiation therapy (MRgRT) combines the superior soft tissue contrast imaging with a linear accelerator to allow radiotherapy (RT) treatment adaptions based on the patient's daily anatomy. The imaging without additional dose allows also to perform gating of the RT delivery based on intra-fractional motion. However, a computed tomography (CT) is required for radiotherapy planning. This may be bypassed by synthetic CT (sCT) generated from magnetic resonance (MR), which has recently led to the clinical introduction of MR-only radiotherapy for specific sites. Further developments are required for abdominal sCT, mostly due to the presence of mobile air pockets affecting the dose calculation. In this study we aimed to overcome this limitation for abdominal sCT at a low field (0.35T) hybrid MR-Linac.

Methods:
This study retrospectively analysed 215 MR-CT pairs from 168 patients treated at the University Hospital Zurich in the period August 2020 - May 2022 with MRgRT. After the exclusion criteria, 152 volumetric images were used to train the cycle-consistent generative adversarial network (cycleGAN) and 34 to test the sCT. Image similarity metrics and dose recalculation analysis were performed.

Results:
The generated sCT faithfully reproduced the original CT and the location of the air pockets agreed with the MR scan. The dose calculation did not require manual bulk density overrides and the mean deviations of the dose-volume histogram dosimetric points were within 1% of the CT, without any outlier above 2%. The mean gamma passing rates were above 99% for the 2%/2mm analysis and no cases below 95% were observed.

Conclusion:
This study presented the implementation of CycleGAN to perform sCT generation in the abdominal region for a low field hybrid MR-Linac. The sCT was shown to correctly allocate the electron density for the mobile air pockets and the dosimetric analysis demonstrated the potential for future implementation of MR-only radiotherapy in the abdomen. Further work will focus on the development of quality assurance procedures, towards the implementation of MR-only radiotherapy in the clinical workflows.

579

Y. Achermann[1, 3], T C. Scheier[1], C. Quiblier[2], N K. Kuleta[2], D. Albertos-Torres[2], T. Roloff-Handschin[2], M. Meola[2], F. Imkamp[2], R. Zbinden[2], S D. Brugger[1], A. Egli[2], I. Frey-Wagner[2]

C. difficile abundance and gut microbiota composition in the first three weeks after antimicrobial treatment for C. difficile infection

Infectious Diseases and Hospital Epidemiology, University Hospital Zurich, Zurich, Switzerland[1], Institute for Medical Microbiology, University of Zurich, Zurich, Switzerland[2], Spital Zollikerberg, Zurich, Switzerland[3]

Introduction:
Antimicrobial treatment is a major risk factor for development of *Clostridioides difficile* infection (CDI) and antimicrobial treatment for CDI further disturbs the endogenous gut microbiota, contributing to the risk of recurrent CDI (rCDI). Asymptomatic *C. difficile* colonization can be observed in 4-15% of healthy people. Yet, little is known about asymptomatic *C. difficile* colonization directly after treatment of a CDI episode. We aimed to study *C. difficile* abundance and gut microbiota composition in the first three weeks after antimicrobial treatment for CDI.

Methods:
15 CDI patients were enrolled for the study and fecal samples were collected on a weekly basis during the first three weeks after antimicrobial treatment for CDI (metronidazole or vancomycin). Frequency of bowel movement and stool consistency were retrieved during telephone-follow ups on the same days as fecal sample collection. Gut microbiota composition and relative *C. difficile* abundance were studied by amplicon-based 16S rRNA metagenomic sequencing. Library preparation was performed by multiplex PCR for amplification of variable regions 1-9 of the 16S rRNA gene (Swift Biosciences). Libraries were sequenced paired end (2x150nt) on an Illumina MiSeq instrument. Sequencing data was processed with the 16S SNAPP APP (Swift Biosciences) and analyzed with NAMCO and with an in house developed pipeline.

Results:
Of 15 participants one (7%) developed a rCDI during the study period. *C. difficile* was present with varying abundance in 53% of participants at any of the timepoints for fecal sample collection one to three weeks after antimicrobial treatment for CDI. The relative abundance was ranging from 0.001 % to 32 % in *C. difficile* positive samples. At the last time-point still 38% of samples remained positive for *C. difficile*. Mean gut microbiota alpha-diversity was lowest directly after antimicrobial treatment and increased over the three weeks study period, but not all participants showed a continuous increase.

Conclusion:
Our preliminary results show that *C. difficile* can be detected with varying abundance in 53% of patients in the first three weeks after CDI treatment. Our data provide the basis for further research into asymptomatic *C. difficile* colonization and the role of the endogenous gut microbiota for protection against rCDI.

580

G. Azzarito[2], L. Kurmann[2], B. Leeners[2], RK. Dubey[1, 2]

Micro-RNA193a-3p Inhibits Breast Cancer Cell Driven Growth of Vascular Endothelial Cells by Altering Secretome and Inhibiting Mitogenesis: Transcriptomic and Functional Evidence

Department of Pharmacology & Chemical Biology, University of Pittsburgh, Pittsburgh, PA 15219, USA[1], Department of Reproductive Endocrinology, University Hospital Zurich, 8952 Schlieren, Switzerland[2]

Introduction:
Breast cancer (BC) cell secretome in the tumor microenvironment (TME) facilitates neo-angiogenesis by promoting vascular endothelial cell (VEC) growth. Drugs that block BC cell growth or angiogenesis can restrict tumor growth and are of clinical relevance. Molecules that can target both BC cell and VEC growth as well as BC secretome may be more effective in treating BC. Since small non-coding microRNAs (miRs) regulate cell growth and miR193a-3p has onco-suppressor activity, we investigated whether miR193a-3p inhibits MCF-7-driven growth (proliferation, migration, capillary formation, signal transduction) of VECs.

Methods:
To test the growth effects of miR193a-3p and estradiol (E2) in BC cells and VECs in monolayers or 3D spheroids cells were transfected using Lipofectamine 2000 and counted using Coulter Counter or total spheroid area calculation. To assess cell–cell crosstalk and the impact of paracrine factors in modulating tumor growth we formed conditioned medium (CM) from MCF-7 and MDA-MB231 pre-transfected with miR193a-3p or miR control. To investigate the impact of miRNA-CM activity on VECs migration and invasion we performed the wound-healing and capillary formation assays, respectively. To explore the potential molecular mechanisms underlying the VEC growth inhibitory effects of miRNA-CM, we assessed its impact on key signal transduction enzymes ERK1/2 and PI3K-Akt by Western blot. In order to identify VEC genes regulated by miRNA-CM and the biological significance of DRGs, we performed microarray and pathway enrichment analysis. The Proteome Profiler Angiogenesis kit was used to determine changes in 55 angiogenesis-related factors in VECs in response to miR193a-CM. Moreover, Immunohistochemical staining was performed to assess cell proliferation in spheroids formed by MCF-7 cells and VECs transfected with miR193a-3p.

Results:
Pro-growth effects of MCF-7 and MDA-MB231 CM are lost in miR193a-CM. Moreover, miR193a-CM inhibited MAPK and Akt phosphorylation in VECs. In microarray gene expression studies, miR193a-CM upregulated 553 genes and downregulated 543 genes in VECs. Transcriptomic and pathway enrichment analysis of differentially regulated genes revealed downregulation of interferon-associated genes and pathways that induce angiogenesis and BC/tumor growth. An angiogenesis proteome array confirmed the downregulation of 20 pro-angiogenesis proteins by miR193a-CM in VECs. Additionally, in MCF-7 cells and VECs, estradiol (E2) downregulated miR193a-3p expression and induced growth. Ectopic expression of miR193a-3p abrogated the growth stimulatory effects of estradiol E2 and serum in MCF-7 cells and VECs, as well as in MCF-7 and MCF-7+ VEC 3D spheroids. Immunostaining of MCF-7+VEC spheroid sections with ki67 showed miR193a-3p inhibits cell proliferation. Taken together, our findings provide first evidence that miR193a-3p abrogates MCF-7-driven growth of VECs by altering MCF-7 secretome and downregulating pro-growth interferon signals and proangiogenic proteins. Additionally, miR193a-3p inhibits serum and E2-induced growth of MCF-7, VECs, and MCF-7+VEC spheroids.

Conclusion:
miRNA193a-3p can potentially target/inhibit BC tumor angiogenesis via a dual mechanism: (1) altering proangiogenic BC secretome/TME and (2) inhibiting VEC growth. It may represent a therapeutic molecule to target breast tumor growth.

581

N. Klemm[1], N. Konrad[1], J. Fullin[1], R. Schimmer[1], E. Topcu[1], S. Stolz[1], S. Böttcher[1]

Elucidating the molecular mechanism of the dominant-negative effect of the p53 missense variant R248Q

University Hospital Zurich, Depatment of medical Oncology and Hematology[1]

Introduction:
TP53 – encoding the transcription factor p53 – is the most frequently mutated gene in virtually all cancer types. Unlike other tumor suppressors, most *TP53* mutations are missense mutations clustering in the DNA-binding domain and leading to the expression of aberrant p53 variants. The driving force for the selection of *TP53* missense mutations during tumorigenesis – creating this unusual mutational spectrum – is the ability of missense p53 variants to exert a dominant-negative effect (DNE) over wild-type p53 in a heterozygous genotype. However, since the mechanism of the DNE has not been thoroughly studied so far, we aim to characterize the DNE and elucidate its molecular mechanism while focusing on $TP53^{R248Q}$ - one of the most common *TP53* missense mutations.

Methods:
To characterize the DNE, isogenic human acute myeloid leukemia (AML) cell lines MOLM13 harboring a full allelic series of *TP53* mutations ($TP53^{+/+}$, $TP53^{+/-}$, $TP53^{-/-}$, $TP53^{R248Q/+}$, $TP53^{R248Q/-}$) generated by CRISPR-mediated genome editing were used to perform competition assays upon treatment with p53-activating agents. Its dependency on p53-regulated pathways was validated by flow cytometry-based analysis of their apoptotic potential and cell cycle progression. Given that p53 is a tetrameric protein, the dependency of the DNE on heterotetramerization was determined by transient transfection of plasmids encoding oligomerization-deficient p53 variants into reporter cell lines expressing a p53-regulated p21-GFP fusion protein and subsequent flow cytometric analysis. Prior and post cycloheximide treatment, Western Blot (WB) analysis was performed to determine the abundance and stability of $p53^{R248Q}$ versus $p53^{WT}$. Whether mutant p53 accumulation provokes the DNE was determined by an inducible and quantifiable targeted $p53^{R248Q}$ degradation assay using an artificial degron protein tag.

Results:
We identified a competitive growth advantage of $TP53^{R248Q/+}$ over $TP53^{+/-}$ cells, but none between $TP53^{R248Q/+}$ and $TP53^{R248Q/-}$ cells. Upon DNA damage, the apoptotic potential, and the ability to undergo cell cycle arrest was equally lost in $TP53^{R248Q/+}$ and $TP53^{R248Q/-}$ cells as compared to $TP53^{+/-}$ cells thereby clearly indicating that $p53^{R248Q}$ exerts a DNE over $p53^{WT}$. Transient expression of tetramerization-deficient $p53^{R248Q}$ variants partially restored $p53^{WT}$ function, whereas it was fully recovered upon impairment of $p53^{R248Q}$ dimerization, suggesting that heterotetramerization is required to exert the DNE. Surprisingly, transfecting $p53^{WT}$ into otherwise $p53^{R248Q}$ expressing reporter cells rescued p53 function in a dose-dependent manner, suggesting that the DNE further depends on $p53^{R248Q}$ protein abundance. The observed accumulation of $p53^{R248Q}$ in the isogenic cell models was shown to be caused by an increased protein half-life. In addition, targeted $p53^{R248Q}$ degradation abrogated the DNE when $p53^{R248Q}$ levels equalized to $p53^{WT}$ levels confirming the necessity of $p53^{R248Q}$ accumulation to exert the DNE.

Conclusion:
We have established unique cellular model systems demonstrating that the $p53^{R248Q}$ missense variant exerts a DNE over $p53^{WT}$ and was shown to be dependent on: (1) heterotetramerization of both protein variants and (2) supraphysiological levels of missense mutant protein levels resulting from an increased protein half-life of $p53^{R248Q}$. Our ongoing studies will address the exact mechanism of $p53^{R248Q}$ protein accumulation, and how $p53^{R248Q}$ protein abundance could be pharmacologically targeted – potentially providing a therapeutic window of opportunity for cancer patients with heterozygous TP53 missense mutations.

582

G. Azzarito[3], M. Henry[1, 4], T. Rotshteyn[1, 4], B. Leeners[3], RK. Dubey[2, 3]

Transcriptomic and Functional Evidence That miRNA193a-3p Inhibits Lymphatic Endothelial Cell (LEC) and LEC + MCF-7 Spheroid Growth Directly and by Altering MCF-7 Secretome

Center for Physiology, Faculty of Medicine and University Hospital Cologne, University of Cologne, 50931 Cologne, Germany[1], Department of Pharmacology & Chemical Biology, University of Pittsburgh, Pittsburgh, PA 15219, USA[2], Department of Reproductive Endocrinology, University Hospital Zurich, 8952 Schlieren, Switzerland[3], Institute of Neurophysiology and Center for Molecular Medicine Cologne (CMMC), University of Cologne, 50931 Cologne, Germany[4]

Introduction:
MicroRNA 193a-3p (miR193a-3p) is a short non-coding RNA with tumor suppressor properties. Breast cancer (BC) progression is governed by active interaction between breast cancer cells, vascular (V) / lymphatic (L) endothelial cells (ECs), and BC secretome. We have recently shown that miR193a-3p, a tumor suppressor miRNA, inhibits MCF-7 BC cell-driven growth of VECs via direct antimitogenic actions and alters MCF-7 secretome. Since LEC-BC cross-talk plays a key role in BC progression, we investigated the effects of miR193a-3p on MCF-7 secretome and estradiol-mediated growth effects in LECs and LEC + MCF-7 spheroids, and delineated the underlying mechanisms.

Methods:
To simulate the tumor microenvironment, we collected the secretome/conditioned medium (CM) from MCF-7 cells pre-transfected with either miR193a-3p (CM miR193a) or with the mimic control (CM mimic CTR). To assess the growth effects of miR193a-3p, estradiol (E2) and CM, the LECs and MCF-7 cells were transfected using Lipofectamine2000 and counted using Coulter Counter (2D) or the spheroid area was analyzed using ImageJ software (3D). To elucidate the potential intracellular mechanisms in spheroids or LECs the activation of signal transduction proteins, PI3/Akt and ERK1/2 or MAPK, was evaluated by Western Blot. The expression of miR193a-3p in response to E2 was detected by RT-PCR and Western Blot. Microarray analysis was performed to investigate genes associated with the growth inhibitory actions and the biological functions of differentially regulated genes (DRGs) of miR193a-3p on LEC + MCF-7 spheroids. Proteome Profiler Apoptosis and XL Cytokine Array Kits were used to determine changes in apoptosis-associated genes in LECs transfected with miR193a-3 and growth-modulating cytokines in MCF secretome in response to miR193a-3p, respectively.

Results:
Transfection of LECs with miR193a-3p, as well as secretome from MCF-7 transfected cells, inhibited LEC growth, and these effects were mimicked in LEC + MCF-7 spheroids. Moreover, miR193a-3p inhibited ERK1/2 and Akt phosphorylation in LECs and LEC + MCF-7 spheroids, which are importantly involved in promoting cancer development and metastasis. Treatment of LECs and LEC + MCF-7 spheroids with estradiol (E2)-induced growth, as well as ERK1/2 and Akt phosphorylation, and was abrogated by miR193a-3p and secretome from MCF-7 transfected cells. Gene expression analysis (GEA) in LEC + MCF-7 spheroids transfected with miR193a-3p showed significant upregulation of 54 genes and downregulation of 73 genes. Pathway enrichment analysis of regulated genes showed significant modulation of several pathways, including interferon, interleukin/cytokine-mediated signaling, innate immune system, ERK1/2 cascade, apoptosis, and estrogen receptor signaling. Transcriptomic analysis showed downregulation in interferon and anti-apoptotic and pro-growth molecules, such as IFI6, IFIT1, OSA1/2, IFITM1, HLA-A/B, PSMB8/9, and PARP9, which are known to regulate BC progression. The cytokine proteome array of miR193a-3p transfected MCF secretome and confirmed the upregulation of several growth inhibitory cytokines, including IFNγ, Il-1a, IL-1ra, IL-32, IL-33, IL-24, IL-27, cystatin, C-reactive protein, Fas ligand, MIG, and sTIM3. Moreover, miR193a-3p alters factors in MCF-7 secretome, which represses ERK1/2 and Akt phosphorylation, induces pro-apoptotic protein and apoptosis in LECs, and downregulates interferon-associated proteins known to promote cancer growth and metastasis.

Conclusion:
These results suggest that miR193a-3p may abrogate BC growth by targeting a key component of BC TME, i.e., the growth of BC cells, LECs, VECs, and BC secretome. In conclusion, miR193a-3p can potentially modify the tumor microenvironment by altering pro-growth BC secretome and inhibiting LEC growth, and may represent a therapeutic molecule to target breast tumors/cancer.

583

S. Guerra[1], DL. Birrer[1], P. A. Clavien[1], B. Humar[1]

Macroscopic division of tasks: a basis for accelerated regeneration after ALPPS surgery

Laboratory of the Swiss Hepato-Pancreato-Biliary and Transplantation Center, Department of Surgery, University Hospital Zurich[1]

Introduction:
Liver regeneration after ALPPS (associating liver partition and portal vein ligation for staged hepatectomy) surgery is singularly accelerated compared to standard hepatectomy. We hypothesized that the future liver remnant (FLR) can mantain an accelerated proliferation because the ligated lobes (LLs), absent after standard resection, take over vital metabolic tasks.

Methods:
Mice were assigned for sham (control) or ALPPS surgery. We performed liver tissue untargeted metabolomic and lipidomic analysis combined with transcriptomics separately for sham surgery, the FLR, and the adjacent ligated right median lobe (RML). Functional surgery was applied to test the role of the LLs.

Results:
PCA analysis of untargeted metabolomics data showed that at 4h and 8h after surgery, the FLR and RML become metabolically different. In comparison, they are similar again after the major growth phase of the FLR (24h). Both have elevated energy demands with active lipid oxidation; however, the RML is also enriched with glycolytic activity, while the FLR has an increased ability for lipid storage. Notably, total metabolite levels were higher in the RML than in the FLR and displayed elevated activities in gluconeogenesis and glycogen synthesis. Moreover, RML showed increased bile acid synthesis/transport, bilirubin clearance, and xenobiotic detoxification. Surgical removal of the LLs revealed their requirement for the FLR to regenerate.

Conclusion:
Our findings suggest the LLs (incl. the RML) act as an auxiliary liver during ALPPS regeneration. This enables the FLR to fully engage in proliferation, causing acceleration of regeneration. Metabolic pressure acting on the remnant is therefore a key factor in defining the regenerative capacity of the liver.

584

J. Scherer[1, 2], M. Held[1], R. Dunn[1], F. Thienemann[1, 2]

Clinical, radiological and histological findings of spinal tuberculosis: Results of the Cape Town Spinal TB cohort study

University of Cape Town[1], University of Zurich[2]

Introduction:
South Africa has the world`s largest HIV and tuberculosis (TB) epidemic. The estimated overall HIV prevalence rate is approximately 14% among the South African population with a total number of people living with HIV (PLH) of 8.2 million in 2021. South Africa is also among the World Health Organization's list of the 30 high-burden TB countries and has one of the highest TB incidence rates. In 2019, an estimated 360,000 people developed active TB in South Africa. PLH have an increased risk of TB infection: 58% of reported TB cases were HIV-coinfected. TB/HIV-coinfected patients are more likely to develop extrapulmonary TB (EPTB) with approx. 20% accounting for skeletal TB with spinal involvement in approx. 60% of the cases. We report data of the Cape Town Spinal TB cohort study and compare clinical, radiological, and histological findings of HIV-uninfected patients presenting with STB (STB^{HIV-}) to STB in the context of HIV (STB^{HIV+}).

Methods:
We analysed data of the Cape Town Spinal TB cohort study included from January 2013 to December 2016 at Division of Orthopaedics Surgery, Groote Schuur Hospital and University of Cape Town, South Africa. A retrospective folder review was performed. STB was defined by at least one positive spinal specimen of 1) Xpert® MTB/RIF, 2) MGIT culture, or 3) histology with granuloma formation.

Results:
52 cases of STB were included in the analysis. Mean age was 38 years (SD 15.2 years) with a range of 17-80 years; 44.2% were male. Almost half of the cases were TB/HIV co-infected and comprise the STB^{HIV+} group (40.4%). 34 (65.4%) patients showed at least one neurological symptom with 10 (19.2%) presenting with neurogenic symptoms (urinary and/or bowel involvement). STB^{HIV+} were less likely to present with neurogenic symptoms when compared to STB^{HIV-} (p=0.029). The mean overall erythrocyte sedimentation rate (ESR) was 69.3 mm/1h (SD 35.9 mm/1h) with no significant difference between STB^{HIV-} and STB^{HIV+} (p=0.086). The mean number of granulomata per low-power field (LPF) in spinal tissue was 10 (SD 12.6) of the entire cohort with no difference between STB^{HIV-} and STB^{HIV+} (p=0.185). We detected a mean of 3.4 (SD 2.35) affected vertebrae amongst the entire cohort with no significant difference between STB^{HIV-} and STB^{HIV+} (p=0.214). Half of the assessed patients (50%) had radiologically (MRI) confirmed vertebral collapse with higher rates in STB^{HIV+} compared to STB^{HIV-} (67% vs. 39%, p=0.048) but no difference in (para-)vertebral abscess formations was detected (p=0.767). The mean CD4-count amongst the STB^{HIV+} group was 362.3 (SD 219.5). No correlation between CD4-count and the number of affected vertebras was detected (Pearson -1.58, p=0.507). A positive correlation between CD4-count and granuloma count in STB^{HIV+} was detected (Pearson 0.503, p=0.02) with a significantly higher formation of granulomata at CD4-counts >400 cells/µL (p=0.045).

Conclusion:
To our knowledge, this is the third largest STB cohort described to date. Most of the patients were of young age at STB diagnosis which is in keeping with the mean age of the HIV epidemic in South Africa. We were able to demonstrate a high prevalence of PLH in our cohort which highlights the increased risk of developing EPTB with spinal involvement in PLH. We detected vertebral collapses in half of the patients, with increased rates in the STB^{HIV+} group. These findings reflect the high clinical burden of the disease, especially in patients with TB/HIV-coinfection. We detected significantly fewer granulomata in patients with decreased CD4-counts and significantly more granuloma formations at a CD4-count of >400 cells/µL. These findings suggest that the CD4-count affects granuloma formation and course of disease and emphasizes the need for early ART in PLH with STB.

585

P. Bellstedt[1]

A prove-of-concept study to identify a first Aprataxin inhibitor for sensitizing cancer cells

USZ, Institute of Clinical Chemistry, Bellstedt Lab[1]

Introduction:
Cancer is the second leading cause of death worldwide. The treatment options and perspective of recovery depends on the location/subtype of the tumor and the state of progression. Besides surgery and immunotherapy, an important therapeutic concept is to kill (the fast dividing) tumor cells by inducing DNA damage either by chemical agents (chemotherapy) or by high energy radiation (radiotherapy). However, the cell-own DNA repair pathways counteract these therapies and often limit the therapeutic outcome. One unique enzyme involved in DNA repair is Aprataxin (Aptx), which resolves abortive ligation intermediates. Downregulation of Aptx have been shown to sensitize cervical cancer cells against DNA damage induced by radiotherapy and colorectal cancer patients with inherent low expression levels of Aptx have much better survival probability under (irinotecan-based) chemotherapy. Also, in gastric cancer the expression level of Aptx has been found to be a predictive biomarker for (irinotecan-based) chemotherapy sensitivity.

Up to date there is no Aptx inhibitor available that could be used as cotreatment to sensitize cancer cells for chemo- or radiotherapy. We therefor address the identification of a first generation Aptx inhibitor.

Methods:
Structure-based *in silico* methods (docking, molecular dynamics simulation) and subsequent biophysical characterization are employed to drive an iterative inhibitor optimization process. Available high-resolution structures of the drug target are used to validate data from an initial high throughput virtual screening. Obtained hits have been clustered based on their molecular fingerprint and representatives subjected to absolute free energy binding calculations and filtered by commercial availability/chemical accessibility. The binding of the top ranked ligands to recombinantly expressed Aptx are currently characterized with localized plasmon resonance (LSPR) spectroscopy and provide detailed kinetic parameters (Kd, Kon, Koff).

Results:
We will present the results of the *in silico* docking of Aptx against a (virtual) library of more than 2 million compounds as well (real) binding data of selected compounds to recombinantly expressed and purified enzyme as provided by localized plasmon resonance spectroscopy.

Conclusion:
In silico methods like docking and the prediction of binding energy are helpful tools of a drug discovery program to prioritize compounds/ligands for further characterization. By employing these methods, we could identify promising molecules that bind to the drug target Aptx. The generation of crystal structures of these top-ranked molecules bound to the protein will be the next step to guide the structure-based optimization process with the aim to further increase the binding affinity to the nM range. Treatments of (colorectal) cancer cell lines with the selected compounds under therapy mimicking conditions will show soon, if we were able to correctly identify a suitable drug-like compound to sensitize cancer cells. Of course, the development of inhibitor is a long-term project and include much more work to be done (SAR studies, ADME profiling, pharmacokinetic studies, off target characterization) before it can enter clinical trials, but we are optimistic that we are paving the road towards a first-in-class Aprataxin inhibitor.

586

D. Spiess[1, 3], V. Abegg[3], S. Kuoni[1], A. Chauveau[3], M. Reinehr[2], O. Potterat[3], M. Hamburger[3], AP. Simões-Wüst[1]

Transplacental passage of compounds from St. John's wort

Department of Obstetrics, University Hospital Zurich, University of Zurich, Zurich, Switzerland[1], Department of Pathology and Molecular Pathology, University Hospital Zurich, Zurich, Switzerland[2], Division of Pharmaceutical Biology, Department of Pharmaceutical Sciences, University of Basel, Basel, Switzerland[3]

Introduction:
Mild depressions are common during pregnancy and can lead to complications like preterm birth if left untreated. Most medications for depression may not only cause side effects in the mother, but also easily cross the placental barrier and reach the foetus. Concerns on tolerability, teratogenicity and impact on neonatal outcomes exist. Pregnant women in need of antidepressants therefore face a dilemma between using and refraining from using them. Safe medications for mild mental diseases in pregnancy are therefore needed. In the treatment of mild to moderate depression, the herb St. John's wort (*Hypericum perforatum* L.) has become an alternative to already established pharmacological antidepressants. However, the use of St. John's wort during pregnancy is not recommended due to insufficient toxicological data.

Methods:
To find out whether the main compounds St. John's wort can cross the placental barrier, the transplacental transport of hyperforin and hypericin was evaluated using the human *ex vivo* placental perfusion model. This model is considered to be the gold-standard among placental transfer models, and we have recently shown its usefulness for studying the transplacental transfer of phytochemicals in comparison with that of the connectivity marker, antipyrine. All samples were quantified by a newly developed and validated U(H)PLC-MS/MS bioanalytical method.

Results:
Perfusion data obtained with donated term placentae showed that only minor amounts of hyperforin passed into the foetal circuit, reaching maximal FM (foetal-maternal concentration) ratio of 0.18 after 180 minutes. Hypericin, on the contrary, did not cross the placental barrier, resulting in FM ratios of zero. None of the two compounds affected metabolic, functional, and histopathological parameters of the placenta.

Conclusion:
Since the *ex vivo* perfusion model mimics the placental barrier structure at term, where transplacental transfer is known to be maximal, the potential foetal exposure to hypericin and hyperforin is likely expected to be minimal throughout the pregnancy. Recent in vitro data on the effects of St. John's wort on placenta cells suggesting moreover low toxicity at concentrations to be expected in humans at the recommended doses support this conclusion.

587

LA. Krattiger[1, 2], R. Odabasi[1], B. Simona[3], MW. Tibbitt[2], M. Ehrbar[1]

An in vitro platform to study the recovery of therapeutically ablated vascular networks

1Department of Obstetrics, University and University Hospital of Zurich, Zurich Switzerland[1], 2Department of Mechanical and Process Engineering, ETH Zurich, Switzerland[2], ECTICA Technologies, Zurich, Switzerland[3]

Introduction:
Cycles of vascular growth and regression can be observed in both physiology and pathology. Angiogenic phases are intermitted by vessel regression in the menstrual or hair cycle, and tumor-supplying vasculature can regrow after therapeutic intervention through anti-angiogenic therapies (AATs). AATs based on limiting the availability of VEGF have been successfully used in the clinics, however, it has also long been established that their efficacy varies with tumor types and can lead to development of more aggressive and heavily vascularised phenotypes upon termination of the treatment. While to this day, a multitude of in vitro angiogenesis assays have been described, in vitro systems for modelling the recovery of a vascular network are lacking. In this study, we establish and describe a platform for the generation of controlled yet complex vascular networks which are sensitive to treatment with bevacizumab and which can be replenished through the addition of new endothelial cells.

Methods:
Three-dimensional cultures were grown by seeding cells onto a commercially available 96 well-plate featuring pre-cast poly(ethylene glycol)-based hydrogels (3DProSeed, Ectica Technologies). The sequential seeding of bone marrow-derived mesenchymal stem/stromal cells (BM-MSCs) and human umbilical vein endothelial cells (HUVECs, GFP expressing) allowed for their assembly into vascular-like networks over four days in presence of 50 ng/mL FGF-2. Networks were characterized by quantifying the total length of GFP-positive-structures and staining for extracellular matrix molecules fibronectin and laminin. Bevacizumab was supplied either from the start of endothelial culture to study its influence on network formation or after the four-day formation-period to study its effect on the maintenance or ablation of vascular networks. RFP-expressing HUVECs were added to pre-formed networks and their relative localization and potential role in a recovery of regressing GFP-HUVEC-structures was assessed.

Results:
After three days of BM-MSC pre-culture and four days of co-culture with GFP-HUVECs, intricately interconnected endothelial networks had formed. The two co-cultured cell types shared a layer of fibronectin and laminin resembling a basement membrane and could be maintained for several days of co-culture. The formation of vascular networks on this platform appears to be sensitive to bevacizumab, as a low concentration of this compound (10 µg/mL) prevented this morphogenic process. Interestingly, pre-formed networks were seen to deteriorate only in presence of higher bevacizumab concentrations (100 µg/mL), while no change could be observed in cultures grown in presence of low concentrations (10 µg/mL) compared to control conditions for at least four more days of culture. When RFP-HUVECs were added to pre-formed day four-GFP networks, they were seen to integrate into the established GFP-structures and helped to extend the overall longevity of the vascular networks.

Conclusion:
Our results suggest that the herein established and characterized platform can be employed to study processes involved in the formation as well as the maintenance of vascular structures. As this system allows the sequential seeding of cells, it will be used to study if and how endothelial cells can recover an AAT-compromised or regressed vascular network.

588

M. Sachs[3], S. Makieva[3], M. Xie[3], A. Velasco[3], F. Ille[2], M. Schmidhauser[1], M. Saenz-de-Juanco[1], S. Ulbrich[1], B. Leeners[3]

Biomarker for Embryo Selection: Transcriptomic signature of live birth revealed in luteinised cumulus cells of women undergoing an ICSI cycle for infertility treatment

ETH Zürich[1], Lucerne University of Applied Sciences and Arts[2], University Hospital Zuerich[3]

Introduction:
The selection of the best embryo for transfer is currently based on standard morphological assessment, which is intrinsically subjective, and time-lapse monitoring that fails to show benefit in predicting pregnancy potential. Alternative non-invasive methods have been in development including utilisation of cumulus cells (CCs) to predict competence of the transferred embryo. However the majority of the studies have been conducted using outdated methodologies for transcriptomic analysis such as PCR and microarrays. Moreover, the studies associating CCs transcriptome with ART outcomes lack consensus due to non-homogenous study cohorts and outcome measures, while the outcome of live birth has been inadequately explored.

Methods:
CC samples (n=17), collected between 2018 and 2021, were retrospectively selected for RNA sequencing analysis on the basis of their ART outcome. Thus, we analysed CCs associated with an oocyte that resulted in pregnancy (n=6), no pregnancy (n=7), live birth (n=5) and pregnancy only (n=5). Differential gene expression analysis identified the differentially expressed genes (DEGs) between the groups in relation to pregnancy or live birth. The samples were retrieved from subfertile couples undergoing controlled ovarian superstimulation and intracytoplasmic sperm injection with subsequent unbiopsied embryo transfer at the IVF centre of University Hospital Zurich. Maternal age was under 43 years. Libraries from CCs were prepared using the Smart-seq2 kit and the RNA sequencing was performed on the NovaSeq6000. The DESeq2 workflow was conducted and the threshold for the adjusted p-values (FDR) was set to 0.05.

Results:
RNAseq did not reveal DEGs when comparing the transcriptomic profiles of the groups “no pregnancy” with “ pregnancy”, whereas 139 DEGs were identified in the comparison of “pregnancy only” with “live birth” of which 28 belonged to clusters relevant to succesful ART outcomes. Functional enrichment analysis revealed that the transcriptome of CCs associated with live birth favors pathways of extracellular matrix, inflammatory cascades leading to ovulation, cell patterning, proliferation and differentiation and silencing pathways leading to apoptosis.

Conclusion:
We identified a CC transcriptomic profile associated with live birth following embryo transfer that may serve the prediction of successful ART outcomes upon further validation. Definition of relevant pathways of CCs related with oocyte competency contributes to a broader understanding of the cumulus oocyte complex.

589

L. Zurfluh[1, 2], S. Santos[1, 2], M. Mennet[3], O. Potterat[1], U. von Mandach[2], M. Hamburger[1], AP. Simões-Wüst[2]

Bryophyllum pinnatum Attenuates Oxytocin-Induced Pro-inflammatory Signalling Pathways in Human Myometrial Cells

Division of Pharmaceutical Biology, University Basel, Basel[1], University Hospital Zurich, Zurich[2], Weleda AG, Arlesheim[3]

Introduction:
Preterm birth is one of the leading causes of neonatal morbidity and mortality. Preterm myometrial contractions are a common cause of preterm labour and are treated with tocolytic agents. Over the past few years, the potential of anti-inflammatory substances in the treatment of preterm labour has become apparent. *Bryophyllum pinnatum* - a traditional medicinal plant with, among other, anti-inflammatory properties - has been used in the treatment of preterm labour, first in anthroposophic hospitals and, recently, in conventional settings where it is mainly used as add-on therapy. Secondary plant metabolites believed to be mainly relevant for biological effects are flavonoids and bufadienolides. The main advantage of *B. pinnatum* compared to synthetic tocolytic agents is the rare occurrence of side effects. Furthermore, *in vitro* work with human myometrial cells has shown that *B. pinnatum* leaf press juice (BPJ) inhibits intracellular calcium signalling induced by oxytocin, a hormone known to play a major role in labour. The aim of this work was therefore to characterise the effect of *B. pinnatum* on the pro-inflammatory MAPK cascade of the oxytocin-signalling pathway.

Methods:
Experiments were performed with an immortalised human myometrial cell line (hTERT-C3). Cells were pre-treated with either BPJ, a bufadienolide-enriched fraction, a flavonoid-enriched fraction, a mix of flavonoids aglycons (A-mix), and combinations of fractions (same concentrations as in the single treatments), or just medium for 30 min before stimulation with oxytocin for 5 min. As a positive control, the tocolytic agent atosiban was used. Activation of the MAPK proteins p38, SAPK/JNK and ERK1/2 by phosphorylation was analysed by immunoblotting.

Results:
Stimulation of hTERT-C3 cells with oxytocin led to an increase in phosphorylated MAPKs compared to unstimulated control. BPJ and the bufadienolide-enriched fraction inhibited this oxytocin-driven activation of the MAPKs SAPK/JNK and ERK1/2, but not of p38. The effect of BPJ on the MAPK signalling cascade was comparable to that of the oxytocin-receptor antagonist and tocolytic agent atosiban.

Conclusion:
BPJ inhibits activation of the MAPKs SAPK/JNK and ERK1/2, an effect also exerted by the bufadienolide-enriched fraction and to a similar extent by the oxytocin receptor antagonist and tocolytic agent atosiban. Since these MAPKs are involved in the MAPK cascade of the oxytocin-signalling pathway, it is likely that BPJ attenuates inflammatory processes triggered by this hormone. In a next step, the effect of *B. pinnatum* on downstream enzymes in the MAPK cascades (e.g. the enzyme COX-2, relevant for prostaglandin production) needs to be investigated. Our findings further substantiate the use of *B. pinnatum* as a well-tolerated treatment for preterm labour.

590

D. Heuberger[1], P. Wendel-Garcia[1], O. Sazpinar[1], M. Mueller[1], H. Klein[2], B. Kim[3], R. Andermatt[1], R. Erlebach[1], R. Schuepbach[1], P. Buehler[1], S. David[1], D. Hofmaenner[1]

Role of circulating Angiopoietin-2 in severely burned patients

Institute of Intensive Care Medicine, University Hospital Zurich, Zurich, Switzerland[1], Plastic and Hand Surgery, Cantonal Hospital Aarau, Aarau, Switzerland[2], Plastic and Hand Surgery, University Hospital Zurich, Zurich, Switzerland[3]

Introduction:
The Angiopoietin (Angpt)/Tie2 ligand-receptor system is a major player in the regulation of endothelial permeability, which is a tightly coordinated process controlling the local bidirectional passage of molecules and immune cells. However, when the vascular activation occurs on a systemic level, endothelial inflammation and hyperpermeability can lead to a global barrier breakdown, resulting in multiple organ failure and ultimately death. Although endothelial permeability and the Angpt/Tie2 system has extensively been studied in sepsis relatively little is known about severe burns despite massive vascular leakage is a classical hallmark of these patients. In this study, we aimed to assess whether serum Angpt-2 levels, as surrogate marker and potential mediator of hyperpermeability, are i) elevated over the first two days in critically ill burn patients and ii) associated with clinical parameters and survival.

Methods:
Serum samples of adult burn patients with a total burn surface area (TBSA) ≥ 20% treated in the Institute of Intensive Care Medicine of the University Hospital of Zurich were prospectively collected over the first two days after burn insult. Angpt-2 levels were measured by ELISA. Due to hemodilution in the initial resuscitation phase, Angpt-2 levels were normalized to serum albumin. The Angpt-2 levels were stratified according to survival status, TBSA and the abbreviated burn severity index (ABSI) and Angpt-2 was further correlated to surrogates of inflammation and infection i.e. C-reactive protein (CRP), procalcitonin (PCT), leucocyte count and the microcirculation i.e. lactate.

Results:
Fifty-six patients were included with a median age of 51.5 years. Overall mortality was 14.3% (8/56 patients). Albumin-corrected Angpt-2 levels continuously increased over the first 48 hours after the burn insult (d0: 455 [95% CI 366 - 565] pg*l/ml*g; d1: 642 [95% CI 536 - 770] pg*l/ml*g; d2: 907 [95% CI 733 - 1124] pg*l/ml*g; $p < 0.001$) and were significantly higher in eventual ICU non-survivors compared to survivors ($p=0.019$), in patients with a higher TBSA ($p=0.04$) and in patients with a higher ABSI ($p=0.008$). Eventual non-survivors were treated with higher amounts of infused crystalloids and required higher quantities of infused albumin over the first two days compared to survivors.

Conclusion:
In our study, we found that elevated Angpt-2 levels are associated with increased mortality and higher disease burden as TBSA and ABSI. Furthermore, Angpt-2 levels correlated with CRP, PCT and lactate levels. Based on previous research on sepsis demonstrating the involvement of Angpt-2 in the pathogenesis of hyperpermeability, it seems reasonable that comparable molecular mechanisms are involved in the pathogenesis of capillary leakage in critically ill burn patients.

591

S. Kakava[1], E. Schlumpf[1], A. von Eckardstein[1], J. Robert[1]

Apolipoprotein E defines the trafficking of High-density lipoprotein (HDL) particles in brain endothelial cells

Institute of Clinical Chemistry[1]

Introduction:
Alzheimer's disease (AD) is the leading cause of senile dementia with over 50 million affected individuals worldwide. Its well-known neuropathological hallmarks, beta-amyloid and tangles, are preceded by cerebrovascular damage. High-density lipoprotein (HDL) possesses several vasoprotective functions and epidemiological studies showed associations of very low and very high HDL-cholesterol levels with the risk of AD. Several lines of evidence suggest that HDL reduces AD risk by decreasing both beta-amyloid deposition within the vasculature and vascular inflammation. We previously found that HDL enriched in apolipoprotein (apo)E (HDLE+) are more effective in removing vascular beta-amyloid deposits than those lacking apoE (HDLE-). However, HDL circulating in the blood must first interact with brain endothelial cells (EC) to display its anti-AD properties, a process that is poorly understood.

Methods:
HDL was isolated from plasma of healthy donors by ultracentrifugation before being further fractionated into HDLE+ and HDLE- by the use of apoE immunoaffinity chromatography. Fluorescent or ^{125}I-radio labeled HDL were used to measure binding (4^{o}C), association, internalization or transport (37^{o}C) through a cell line of brain endothelial cells, hCMEC/D3.

Results:
We confirmed that total HDL, HDLE+ and HDL and HDLE- bind to, are internalized and transported through brain endothelial cells. HDLE+ particles showed more interaction with the endothelial cells while they only partially co-localized with HDLE- suggesting independent trafficking pathways. Moroever, using RNA interference we showed that HDL uptake is dependent of scavenger receptor BI (SR-BI). Interestingly, interference of the low-density lipoprotein receptor (LDLR) also reduced HDL internalization and transport but not binding to brain endothelial cells.

Conclusion:
Together our findings suggest distinct trafficking pathways for HDLE+ and HDLE- through brain endothelial cells that might imply different cerebrovascular functions relevant to AD.

592

F. Costa[1, 2], G. Indiveri[1], J. Sarnthein[2]

Real-time and low-power framework to detect epilepsy biomarkers in electrocorticography with a neuromorphic hardware.

Universität Zürich, Institut für Neuroinformatik, Zürich, Schweiz[1], Universitätsspital Zürich USZ, Klinik für Neurochirurgie, Zürich, Schweiz[2]

Introduction:
Interictal High Frequency oscillations (HFO) and interictal epileptogenic discharges (IED) are biomarkers for epileptogenic brain tissue. Their co-occurrence may be specific for the delineation of the epileptogenic zone. During epilepsy surgery, the automated real-time detection of these epilepsy biomarkers in intracranial EEG reduces human workload and bias. Fast and lightweight algorithms are needed to operate in real-time. We propose a real-time framework that comprises a low-power device to detect epilepsy biomarkers for intracranial EEG. We test whether this framework can detect HFO and IED in prerecorded intraoperative ECOG.

Methods:
We use the BCI2000 real time framework to analyze prerecorded intraoperative ECOG data. ECOG activity is replayed to simulate a real time scenario and is converted into discrete events through an Asynchronous Delta Modulator. For these types of signals, this circuit encodes the recorded data with asynchronous digital events in a way that is typically more power efficient than conventional clocked analog-to-digital converters. The discrete events are then processed with a hardware Spiking Neural Network (SNN). The SNN performs a highly selective compression of the signal. A final lightweight algorithm detects HFO and IED from the SNN compressed signal.

Results:
The real time framework has been tested on prerecorded ECOG and has been proven capable of detecting HFO and IED with clinical value.

Conclusion:
The real time processing pipeline is capable of detecting pathological interictal patterns in ECOG. The low power consumption makes the solution suitable for intraoperative monitoring applications.

593

O. Gallou[1, 2, 3], J. Sarnthein[4], G. Indiveri[2], D. Ledergerber[1], L. Imbach[1]

Detection of electrographic seizures with a low-power neuromorphic hardware in real-time

Schweizerisches Epilepsie Zentrum, Klinik Lengg, Zürich, Schweiz[1], Universität Zürich, Institut für Neuroinformatik, Zürich Schweiz[2], Universitätsspital Zürich USZ, Klinik für Neurochirurgie, Zürich, Schweiz[3], Universitätsspital Zürich USZ, Klinik für Neurochirurgie, Zürich, Schweiz[4]

Introduction:
Research Question: The onset of epileptic seizures in the intracranial EEG (iEEG) denotes the seizure onset zone (SOZ), which is a biomarker for epileptogenic brain tissue. In the presurgical diagnostic workup of iEEG, automated real-time seizure detection would reduce human workload and bias. In implantable and wearable devices, long-term monitoring of seizure occurrence and epilepsy biomarkers could aid in the prognostication of epilepsy severity and treatment response. We propose a spiking neural architecture compatible with low-power neuromorphic hardware able to process real-time analog signals and detect epilepsy biomarkers for iEEG. Signals measured by the sensor are encoded into spikes and transmitted using a low-power communication scheme, making the system suitable for long-term monitoring. We test whether this architecture can identify ictal events in the iEEG.

Methods:
Methods: iEEG data were converted into discrete events through an Asynchronous Delta Modulator (ADM). This converter captures the essential aspects of the recorded signals and transmits them using much lower power consumption than traditional analog-to-digital converters.

Results:
Results: The architecture has been tested on 10 recorded iEEG seizures of one patient with focal epilepsy that subsequently underwent epilepsy surgery. It detects seizure activity in agreement with epileptologists' markings.

Conclusion:
Conclusions: The neural processing pipeline can detect seizure activity in the iEEG. The low power consumption makes the pipeline suitable for long-term monitoring of seizure occurrence and treatment response applications in real time.

594

V. Dimakopoulos[6], J. Gotman[7], W. Stacey[3], N. von Ellenrieder[7], J. Jacobs[1], C. Papadelis[2], J. Cimbalnik[9], G. Worrell[5], M. Sperling[4], M. Zijlmans[10], L. Imbach[8], B. Frauscher[7], J. Sarnthein[6]

Multicenter comparison of interictal high frequency oscillations as a predictor of seizure freedom

Alberta Children's Hospital, University of Calgary, Calgary[1], Cook Children's Health Care System[2], Department of Neurology and Department of Biomedical Engineering, University of Michigan[3], Department of Neurology, Jefferson University Hospitals, Philadelphia[4], Department of Neurology, Mayo Clinic[5], Klinik für Neurochirurgie, University Hospital Zurich[6], Montreal Neurological Institute & Hospital, McGill University[7], Schweizerisches Epilepsie Zentrum[8], St. Anne's University Hospital, Brno,[9], University Medical Center, Utrecht, and Stichting Epilepsie Instellingen Nederland (SEIN), Utrecht[10]

Introduction:
In drug-resistant focal epilepsy, interictal high frequency oscillations (HFO) recorded from intracranial EEG (iEEG) may provide clinical information for delineating epileptogenic brain tissue. The iEEG electrode contacts that contain HFO are hypothesized to delineate the epileptogenic zone; their resection should then lead to postsurgical seizure freedom.
The main objective of the proposed study is to test whether our prospective definition of clinically relevant HFO is in agreement with postsurgical seizure outcome. The aim is to assess the reliability of the proposed detector and analysis approach.

Methods:
We use an automated data-independent prospective definition of clinically relevant HFO. The algorithm was first developed on iEEG data from Montreal. It was then validated prospectively on iEEG data of 20 patients from Zurich. Then it was validated in a blinded study on iEEG data of 16 patients from Geneva as an independent epilepsy center where we were blinded to the clinical outcome. This study setting was highlighted in an editorial of Brain Communications as an example for "ethos of rigour and reproducibility".

Results:
The algorithm uses 5-minute iEEG recording epochs during non-rapid eye movement sleep. We automatically detect HFO in the ripple (80-250 Hz) and in the fast ripple (250-500 Hz) band. The type of HFO that we consider clinically relevant is defined as the co-occurrence of a fast-ripple and a ripple. We determine whether all electrode contacts with high HFO rate are included in the resection volume and whether seizure freedom was achieved at ≥2 y follow-up. The validated HFO detection pipeline is fully automated and is equally applied to all data sets. The proposed study extends our previous small pilot studies but now with sufficient statistical power. We now combine retrospectively collected datasets from 9 independent epilepsy centers. The study protocol was preregistered both as a clinical trial (NCT05332990) and as a registered report. This enables rigorous communication and transparent clinical research even before the research is undertaken. To establish regulatory compliance and protocol adherence, the study is supervised by the Clinical Trials Center of University Hospital Zurich.

Conclusion:
Applying a previously validated algorithm to a large cohort from several independent epilepsy centers may advance the generalizability of HFO analysis to prove its clinical relevance. This is an essential next step for the use of HFO in clinical practice.

596

A. Joachimbauer[1, 2], N. Cadosch[2], C. Gil-Cruz[1, 2], C. Perez-Shibayama[2], K. Frischmann[1, 2], F. Tanner[1], D. Schmidt[1], B. Ludewig[1, 2]

Treatment of autoimmune myocarditis-associated heart failure through restoration of bone morphogenic protein signalling

Department of Cardiology, University Hospital Zurich, Switzerland[1], Institute of Immunology, Kantonsspital St. Gallen, Switzerland[2]

Introduction:
Myocarditis is an inflammatory heart disease that frequently leads to myocardial remodelling and progress in 20-30% of patients to inflammatory cardiomyopathy. However, the molecular mechanisms governing the balance between immune cell activation and maintenance of tissue integrity in the inflamed myocardium are still elusive. Here, we have assessed whether the restoration bone morphogenic protein-4 (BMP-4) concentration in the cardiac microenvironment exerts beneficial effects on cardiac function and myocardial structure in a pre-clinical model of autoimmune T cell-driven myocardial inflammation.

Methods:
We have employed the myosin heavy chain-6 (MYH6)-specific T cell receptor transgenic mouse model (TCR-M) that develop spontaneous autoimmune myocarditis followed by inflammatory cardiomyopathy and heart failure. To investigate the effect of anti-gremlin antibody treatment on the heart function during myocardial inflammation TCRM mice were treated with an anti-GREM1/2 antibody (14-D10-2) or IgG2b isotype control for four weeks during the onset of acute myocardial inflammation. Measurement of structural and functional changes in the heart was performed by high resolution ultrasound. The detailed mechanical analysis was performed by using speckle tracking-based global and regional strain to determine the extent of functional impairment in the left ventricle. In addition, histopathologic analysis and quantification of collagen deposition to assess the degree of myocardial inflammation and fibrotic remodelling were performed.

Results:
We found that TCRM mice treated with isotype control antibody showed rapid deterioration of cardiac function and myocardial dilation resulting in heart failure. Conversely, treatment with the GREM1/2-specific monoclonal antibody during the acute phase of myocardial inflammation prevented cardiac dysfunction and the development of left ventricular dilation.

Conclusion:
This study reveals that the BMP-4 Gremlin axis is a promising therapeutic approach for the treatment of myocardial inflammation limiting the deterioration of cardiac function, fibrotic remodelling and the progression to heart failure.

597

S. Anwer[1], G. Miriam[1], A. Marchetti[1], N. Winkler[1], V. Wilzeck[1], C. Gruner[1], F. Tanner[1]

Left ventricular early diastolic strain rate and cardiovascular outcome in patients with left ventricular non-compaction phenotype

University Heart Center, University Hospital Zurich and University of Zurich, Zurich, Switzerland[1]

Introduction:
Speckle-tracking echocardiography is an increasingly important tool for assessing left ventricular non-compaction phenotype (LVNC). This study aims to analyse left ventricular early diastolic strain rate (eSR) in LVNC and explore its association with mortality during long-term follow-up.

Methods:
Fifty-nine patients meeting prespecified criteria were included from our prospective LVNC cohort. eSR was determined using TomTec ImageArena (Figure A). A combined endpoint (cardiovascular events) was defined including atrial flutter/fibrillation, sustained ventricular arrhythmias, aborted cardiac arrest, and cardiovascular mortality.

Results:
Baseline characteristics were comparable between patients reaching the endpoint (16 [27%]) and those without (43 [73%]) except for a higher prevalence of ischemic heart disease in the former (event group: 13%; no-event group: 2%; P=0.019). In the event group, there was a non-significant tendency for a lower LVEF (38 [26–56]% vs 51 [43–56]%; P=0.091) and LVGLS (-12.3 [-16.3 to -9.7]% vs -15.2 [-17.7 to -12.8]%; P=0.111). In contrast, eSR was significantly lower in the event group (0.45 [0.30–0.65]s-1 vs 0.70 [0.39–0.93]s-1; P=0.018; Figure B). Patients with an eSR ≤ 0.70 s-1 (ROC AUC 70%; P=0.005) exhibited a lower event-free probability in Kaplan-Meier survival analysis (P=0.001; Figure C). Inclusion of eSR improved the fitness (χ2) of a multivariable logistic regression model for clinical characteristics (age, gender, and NC:C ratio; Figure D), while LVEF and LVGLS did not (Table). This improvement in χ2 by eSR was significant (ANOVA P=0.033), while that by LVEF or LVGLS was not (P=0.302 and 0.152, respectively).

Table

Variables	Logistic Regression			Model Fitness	
	OR	95% CI	P	χ^2	χ^2 P
Clinical model	**0.94**	**0.25 – 3.49**	**0.511**	**5.1**	**0.164**
+ LVEF	**0.97**	**0.92 – 1.02**	**0.088**	**5.7**	**0.221**
+ LVGLS	**1.14**	**1.06 – 1.35**	**0.049***	**7.5**	**0.113**
+ eSR	**0.73**	**0.53 – 0.90**	**0.036***	**9.9**	**0.042***

Figure

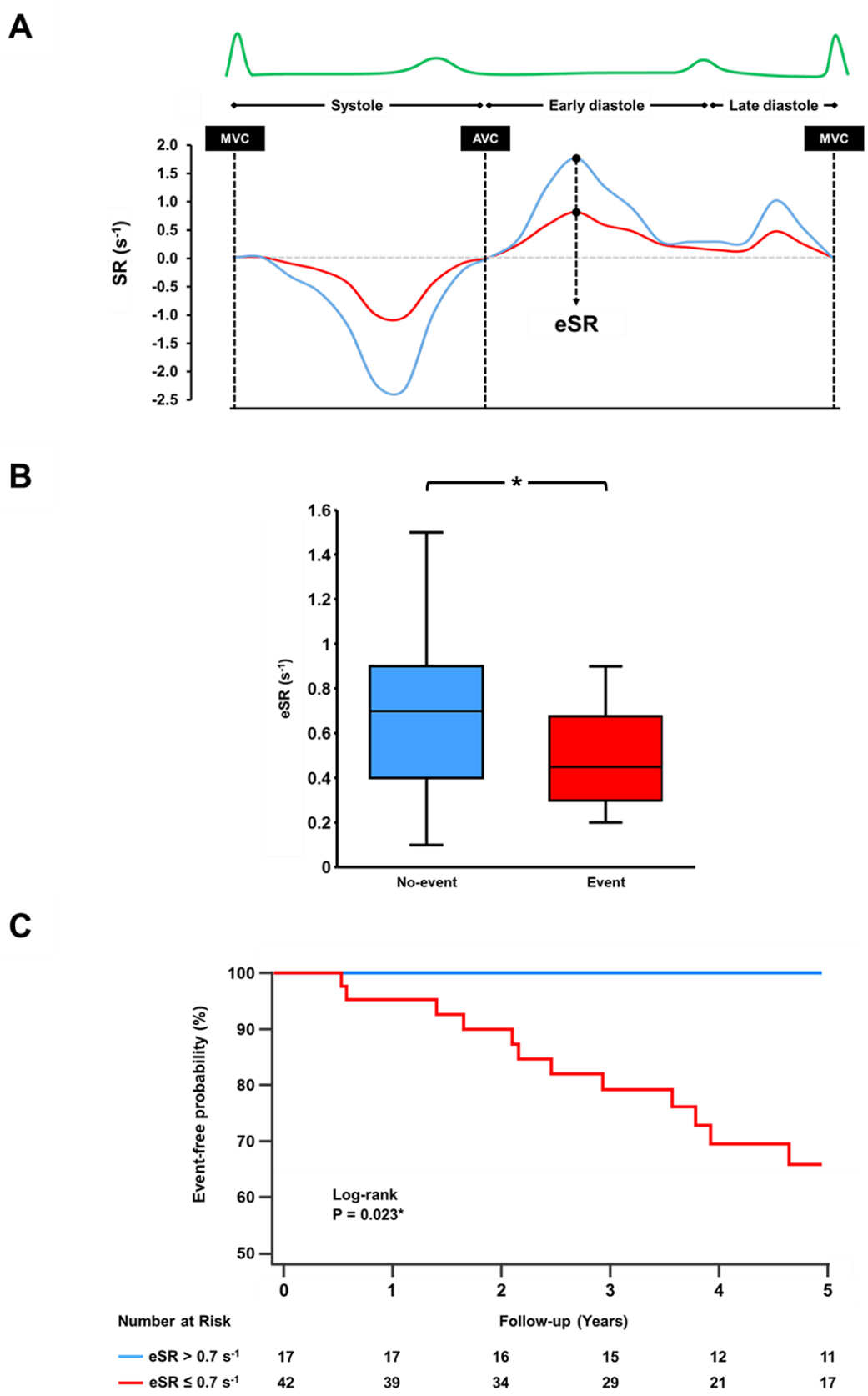

Conclusion:
eSR was lower in LVNC patients with events, differentiated those with events from those without, and was associated with a higher risk of events during long-term follow-up. Outcome association of eSR was independent of age, gender, and NC:C ratio and improved their event prediction. eSR has potential value for functional characterization and outcome prediction in LVNC

598

S. Anwer[1], D. Zuercher[1], D. Benz[1], N. Winkler[1], T. Donati[1], G. Tsiourantani[1], V. Wilzeck[1], J. Michel[1], A. Kasel[1], F. Tanner[1]

Left ventricular early diastolic strain rate predicts mortality after transcatheter aortic valve implantation

University Heart Center, University Hospital Zurich and University of Zurich, Zurich, Switzerland[1]

Introduction:
Speckle-tracking echocardiography is an increasingly important tool for assessing degenerative aortic valve stenosis (AS). This study aims to analyse left ventricular early diastolic strain rate (eSR) in patients with severe AS undergoing transcatheter aortic valve implantation (TAVI) and explore its association with mortality during long-term follow-up.

Methods:
From our prospective AS cohort study, 100 patients with severe AS and a comprehensive echocardiographic examination prior to TAVI were identified and eSR was determined using TomTec ImageArena v.4.6 (Figure A). All-cause five-year mortality was defined as the endpoint.

Results:
Baseline characteristics were comparablebetween non-survivors (14%) and survivors (86%) except for a higher STS-Score among the former (non-survivors: 3.6 [2.7–7.4]%; survivors: 2.6 [1.8–3.7]%; P=0.024). There was no significant difference between non-survivors and survivors with regard to LVEF (54 [50–58]% vs 58 [52–63]%; P=0.069) and LVGLS (-14.8 [-15.8 to -12.7]% vs -15.4 [-15.8 to -14.7]%; P=0.339). In contrast, eSR was significantly lower in non-survivors (0.72 [0.67–0.87]s-1) than survivors (0.88 [0.73–1.22]s-1); P=0.013; Figure B). Patients with an eSR ≤ 0.72 s-1 (ROC AUC 71%; P=0.008) exhibited a lower survival probability as revealed by Kaplan-Meier survival analysis (P=0.001; Figure C). Inclusion of eSR improved the fitness ($\chi 2$) of a multivariable logistic regression model for LV systolic function (LVEF and LVGLS; Figure D). A similar effect was observed when eSR was included in a model for LV diastolic function (E/A and E/e'; Figure D). These improvements in $\chi 2$ were significant for both models (ANOVA P=0.026, and P=0.037, respectively).

Figures

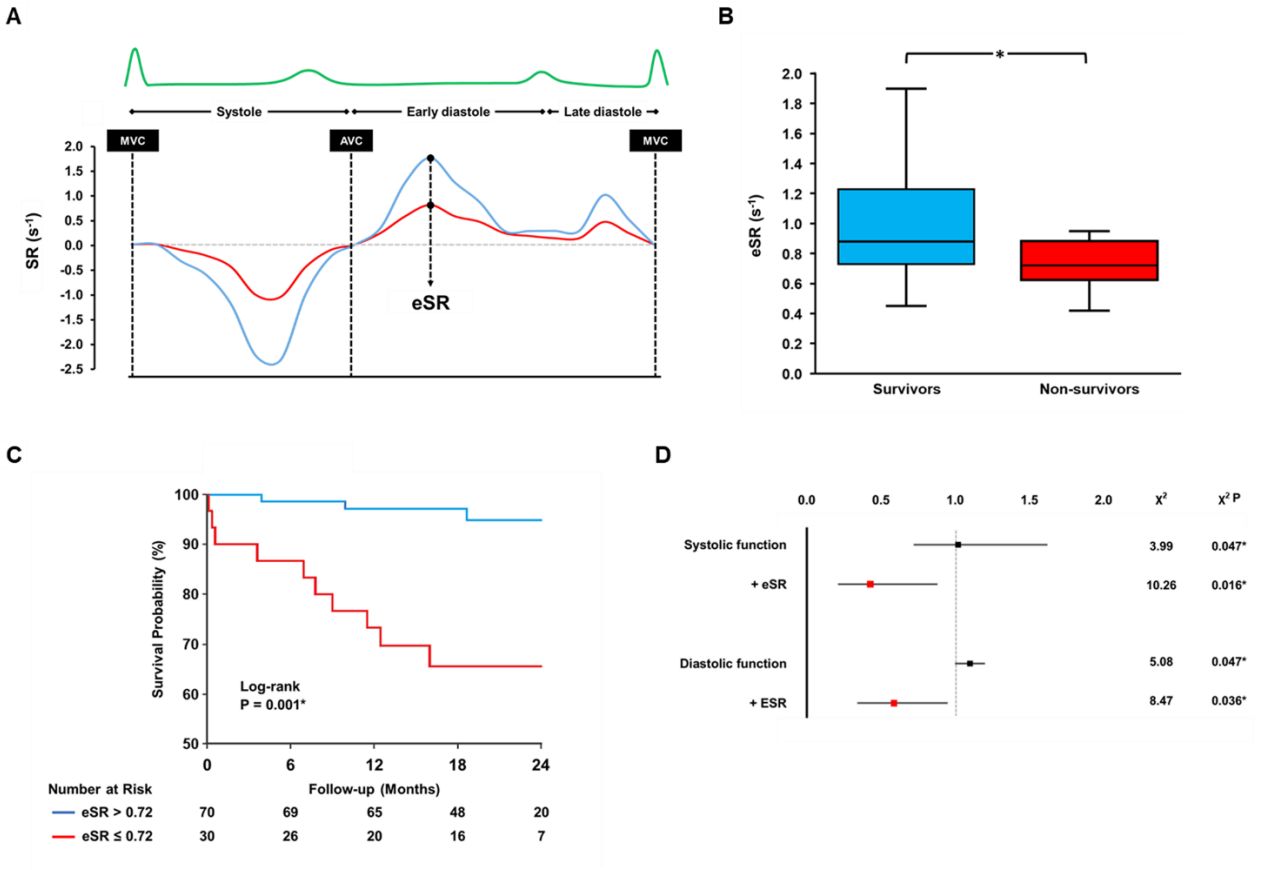

Conclusion:
eSR differentiated non-survivors from survivors and was associated with long-term mortality after TAVI. This association was independent of and improved outcome prediction by LV systolic or diastolic function parameters. These findings highlight the potential value of eSR for assessing long-term mortality after TAVI.

599

Z. Khodabakhshi[2], Y. Huang[1], F. Rainer[1], S. Tanadini-Lang[2], F. Putz[1], N. Andratschke[2]

Fully Automated Detection and Segmentation of Brain Metastasis Using a Deep Continual Learning Approach: A Multicentric Study

Department of Radiation Oncology, University Hospital Erlangen, Erlangen, Germany[1], Department of radiation oncology, University Hospital Zurich, Zurich, Switzerland[2]

Introduction:
Stereotactic radiosurgery (SRS) for brain metastases (BM) requires accurate identification and segmentation of BM, the latter still being a manual and time-consuming task. Deep learning (DL) has been successfully applied in computer vision for image segmentation, but is a challenging task in BM of varying size, location and appearance. The performance of deep learning models highly depends on the amount and quality of training data. To increase the amount of available data, collaboration between different centers is of crucial importance. However, data privacy restrictions impede sharing of data among different centers. One possible solution is peer to peer continual learning technique. In this study, we applied a continual learning approach for BMs segmentation on the MRI dataset of two different centers to investigate the potential of data preserving DL for autosegmentation of BM.

Methods:
In center 1 (University Hospital Erlangen), the dataset contained 700 T1-weighted MRI scans from 230 BMs patients with a total of 1540 BMs for the training and 103 MRI volumes with 278 metastases for the testing. In center 2 (University Hospital Zurich), we used 169 T1-weighted scans with 620 BMs for fine-tuning and 35 MRI scans with 195 BMs for the test set.Before feeding the data into the model, bias field correction, skull stripping, Z-score normalization, and resampling to an isotropic voxel size of 1mm were applied on all MRI scans.We used DeepMedic as the baseline model for brain metastases segmentation. Our model's loss function was a combination of binary cross entropy and volume level sensitivity specificity with a fixed alpha value (α=0.95). In a single visit continual learning approach, the same model was sequentially trained at each center only one time via weight transfer. The synaptic intelligence technique was used as a regularization method to preserve the important parameters for previously learned knowledge.

Results:
In center 1 the model achieved sensitivity, specificity, and average dice scores of 0.91,0.83, and 0.79, respectively, on the test set. In center 2, the pre-trained model achieved average sensitivity, specificity, and dice scores of 0.35, 1, and 0.41, respectively. After regular model fine-tuning on the training set in center 2, the average sensitivity specificity and dice score increased to 0.7, 1, and 0.55.

Conclusion:
Based on the preliminary results of this study, fine-tuning the pre-trained model significantly increased the model's performance on the test set in center 2. However, for better results on center 2, more data should be used, and iterative continual learning should be applied in our future plan.

601

S. Steiner[2], S. Hussung[1], A. Pliego[2], M. Haberecker[2], F. Arnold[2], D. Lenggenhager[2], R. Fritsch[1], C. Pauli[2]

Ex vivo patient-derived pancreatic cancer organoids to uncover individual therapeutic vulnerabilities and model acquired resistance

Department of Medical Oncology and Hematology, University Hospital Zürich, Switzerland[1], Department of Pathology and Molecular Pathology, University Hospital Zürich, Switzerland[2]

Introduction:
The acquisition of drug resistance mechanisms highly contributes to poor survival of pancreatic cancer patients. The use of tumor organoid models not only bridges the gap between research and clinics but also offers an ideal platform to study intrinsic drug sensitivities and the predisposition to drug resistances.

Methods:
After establishing patient derived tumor organoids from a rare BRAF mutated pancreatic cancer patient and their genetic evaluation, we performed an ex vivo functional drug testing in order to identify specific drug vulnerabilities. The continuous exposure with trametinib lead to the formation of drug resistant organoid clones used for the subsequent RNA sequencing and expression analysis.

Results:
In an ex vivo functional drug testing, the BRAF organoids revealed a genotype specific sensitivity towards the MEK inhibitor trametinib when compared to other drugs. The induction of a drug resistance by continuous trametinib selection pressure further lead to the formation of resistant clones indicating a change in Wnt signal regulation compared to their untreated counterparts. Sequencing analysis performed on the patient's primary tumor specimen and the metastatic lesion revealed the acquisition of a GATA6 amplification, indicative for the underlying resistance mechanism, which resulted in the progression of the disease.

Conclusion:
We conclude that the use of patient derived tumor organoids represents a patient centered approach to investigate drug sensitivities and explore predispositions for drug resistances. The results generated by this approach assist in guiding and customizing therapy decision with the fundamental goal to improve the survival of pancreatic cancer patients.

602

Y. Chen[1], A. Pliego-Mendieta[1], M. Herzog[1], L. Planas-Paz[1], c. Pauli[1]

Functional Screening to Unravel Novel Therapeutic Vulnerabilities in Soft Tissue Sarcoma

Institute of Pathology and Molecular Pathology[1]

Introduction:
Soft Tissue Sarcomas (STS) are a heterogeneous group of mesenchymal tumors with more than 70 histological subtypes. Standard treatments for the majority of STS have been limited to surgery, radiation and chemotherapy for decades without significant advances, causing poor patient prognosis. Despite recent advances in genomic landscape profiling, there is no existing targeted therapy for complex karyotype STS due to a lack of recurrent genomic aberration and high genomic instability. Notably, CRISPR/Cas9 knockout systems provided a technique to directly interrogate gene functions, linking genotype to phenotype. However, the lack of well characterized patient-derived cell models (sacrosphere models) has impeded the employment of CRISPR screening for target discovery in STS. Hence, this project aims to identify novel therapeutic targets for complex karyotype STS majorly by whole-genome CRISPR/Cas9 knockout screens, complemented by drug screens, with in-house established and well characterized ex vivo cell models.

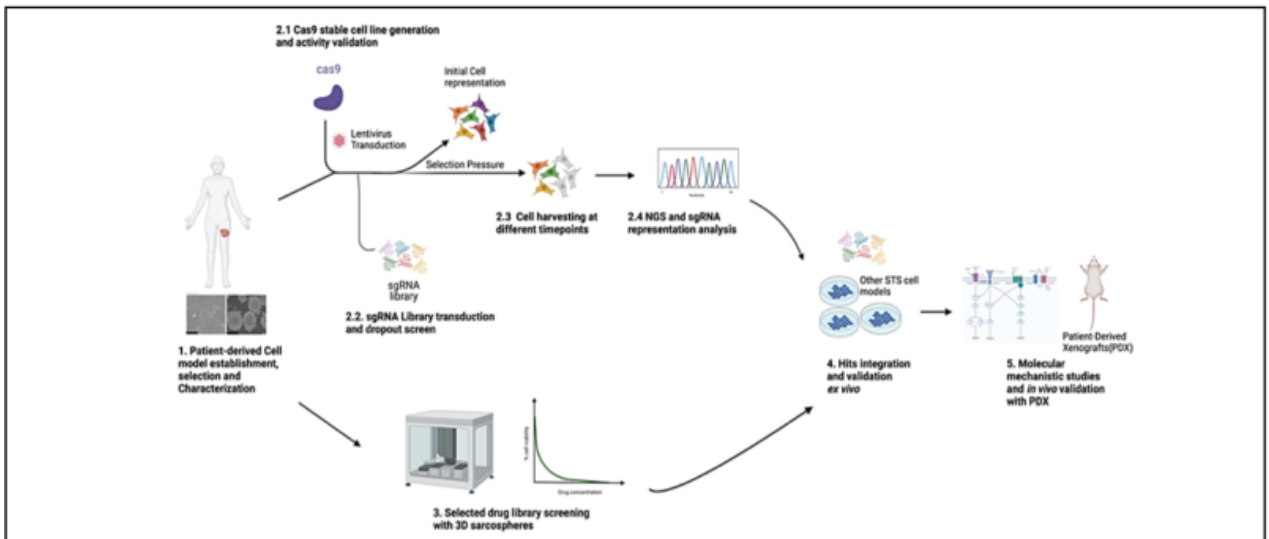

Figure 1. The overall flow of project. 1) Patient-derived STS cell model establishment and characterization by genomic profiling. 2.1) Lentiviral transduction of Cas9 and EGFP-based Cas9 functional assay for evaluating Cas9 editing efficiency. 2.2) Cell transduction with Brunello whole-genome CRISPR KO library. 2.3) Cell harvesting at different time points to represent full library coverage. 2.4) After DNA extraction and PCR amplification, next generation sequencing will allow mapping of sgRNA representation. 3) Mid-throughput drug screening of 3D sarcospheres. 4) Hit selection and validation with multiple STS cell models by individual or sublibrary CRISPR KO, activation and drug testing. 5) Mechanistic studies and PDX validation. Illustration created with BioRender.

Methods:
Establishment and characterization of appropriate patient-derived STS cell models. Ex vivo soft tissue sarcoma models were derived from surgical resection specimens. After cell dissociation and culturing, cell models and corresponding patient tissue were characterized by sequencing, immunofluorescence, proliferation assay and invasion assay to ensure fidelity. Whole genome CRISPR/Cas9 knockout screen Cas9-expressing ex vivo models were infected with Brunello whole-genome sgRNA library lentivirus at an MOI = 0.5 with 1,000 times coverage. Cells underwent selection pressure for 28 days, and were collected at 4 time points. Samples were submitted to the Functional Genomics Centre Zurich for NGS. Next, hits were identified by comparing day 21 with day 0 using the MAGeCK algorithm. We then performed gene set enrichment analysis (GSEA). Drug screening on established ex vivo 3D sarcospheres We performed a mid-throughput semi-automated drug screen using CyBio Felix liquid handler. Compound screening was performed with 6 dilutions of 77 selected clinically-available or preclinical drugs, concentrations ranging from 10 mM to 100 pM. After 8 days of treatment, cell viability was assessed using CellTiter-Glo® as a readout. Luminescence measurements were analyzed with BREEZE.

Results:
We established a range of patient-derived STS cell models with complex karyotype. The myxofibrosarcoma (MFS) cell model USZ-21_MFS2 showed high proliferative capacity and were selected for our initial CRISPR/Cas9 screen (Fig. 2) Our data analysis of the screen showed a shift in the distribution of sgRNA across time points, highlighting the validity of the screen (Fig. 3a). Next, hits were cross-referenced to common essential and non-essential gene datasets to further confirm the reliability of results (Fig. 3b). To select hits, we performed GSEA and identified pathways involved in cell survival(Fig. 4). DNA repair pathways, especially Homologous recombination-mediated DNA repair (HRR) were identified as enriched pathways. Interestingly, MFS are known to be genomically unstable. Further, proteasome-related pathways and unfolded protein response (UPR) were also among the top enriched pathway. Simultaneously, we also performed a mid-throughput semi-automated drug screen using CyBio Felix liquid handler. Among the top hits, we identified the proteasome inhibitors bortezomib and oprozomib, and the poly ADP-ribose polymerase (PARP) inhibitor olaparib (Fig. 5). Both pathways were also scoring in our functional genomic screen. The overlap of our drug and CRISPR screening results suggests further investigation into DNA repair and proteasome/UPR pathways.

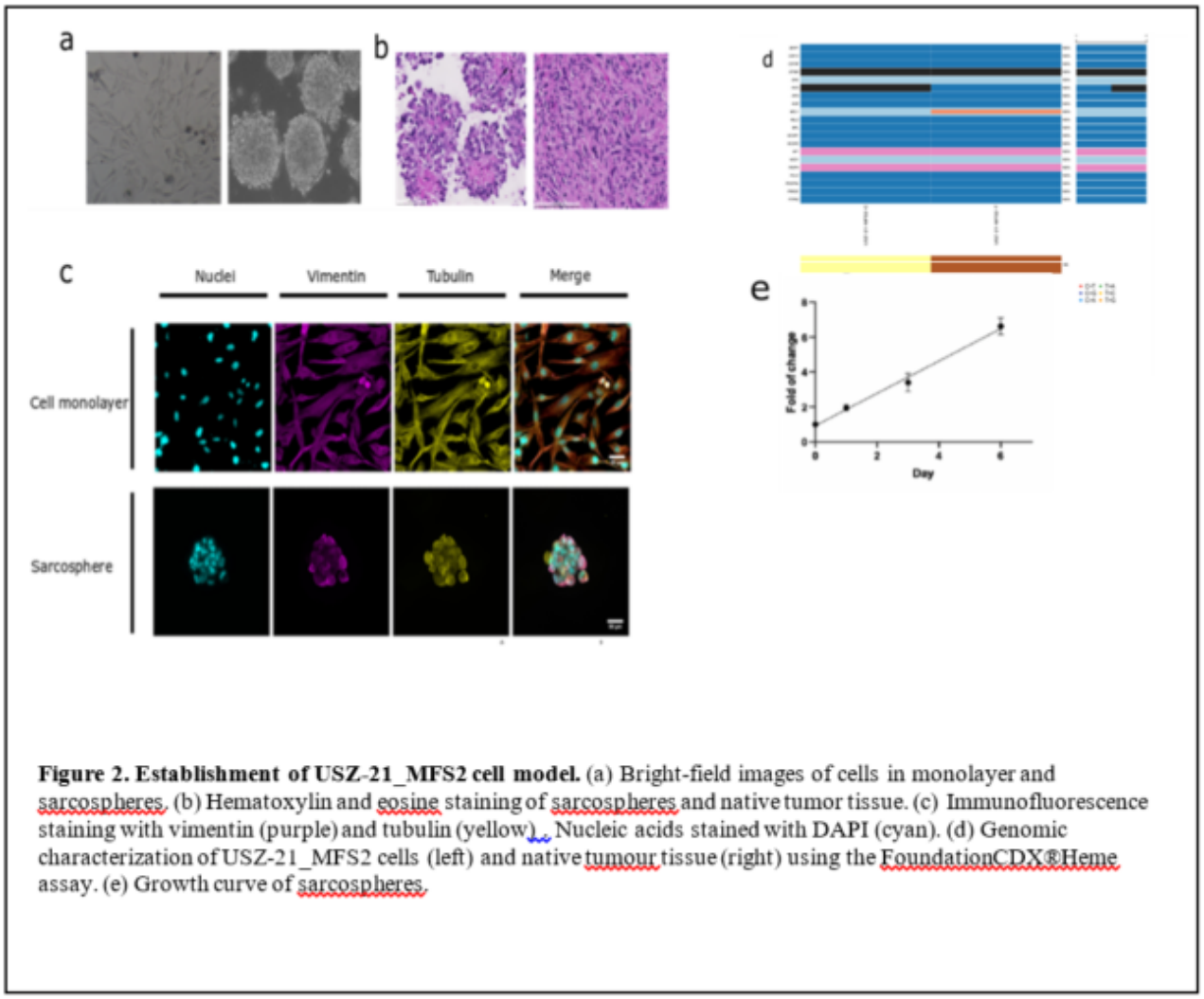

Figure 2. Establishment of USZ-21_MFS2 cell model. (a) Bright-field images of cells in monolayer and sarcospheres, (b) Hematoxylin and eosine staining of sarcospheres and native tumor tissue. (c) Immunofluorescence staining with vimentin (purple) and tubulin (yellow). Nucleic acids stained with DAPI (cyan). (d) Genomic characterization of USZ-21_MFS2 cells (left) and native tumour tissue (right) using the FoundationCDX®Heme assay. (e) Growth curve of sarcospheres.

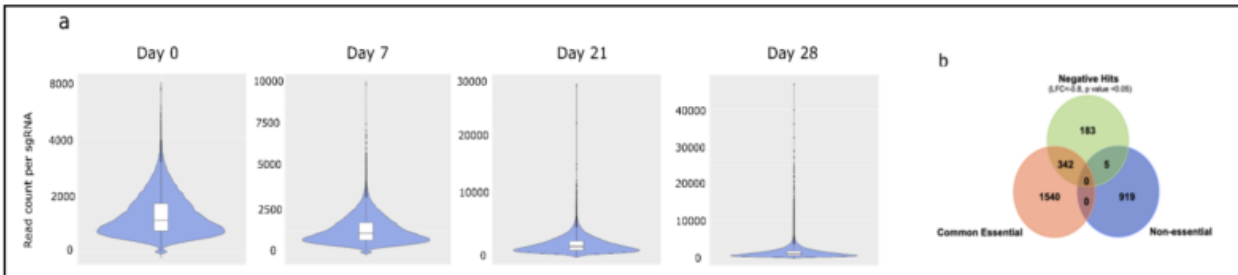

Figure 3. CRISPR screen quality control. (a) Distribution of read count per sgRNA across four timepoints. The pattern of read count per sgRNA shifted, illustrating the enrichment and depletion of cells. (b) The overlap of screen hits and curated common essential/non-essential gene list. The screen has 530 negative hits, among which 342 overlapped with common essential gene list, while only 5 overlapped with the non-essentials gene list. This supports the reliability of our results. Common essential/non-essential lists were extracted from Depmap.

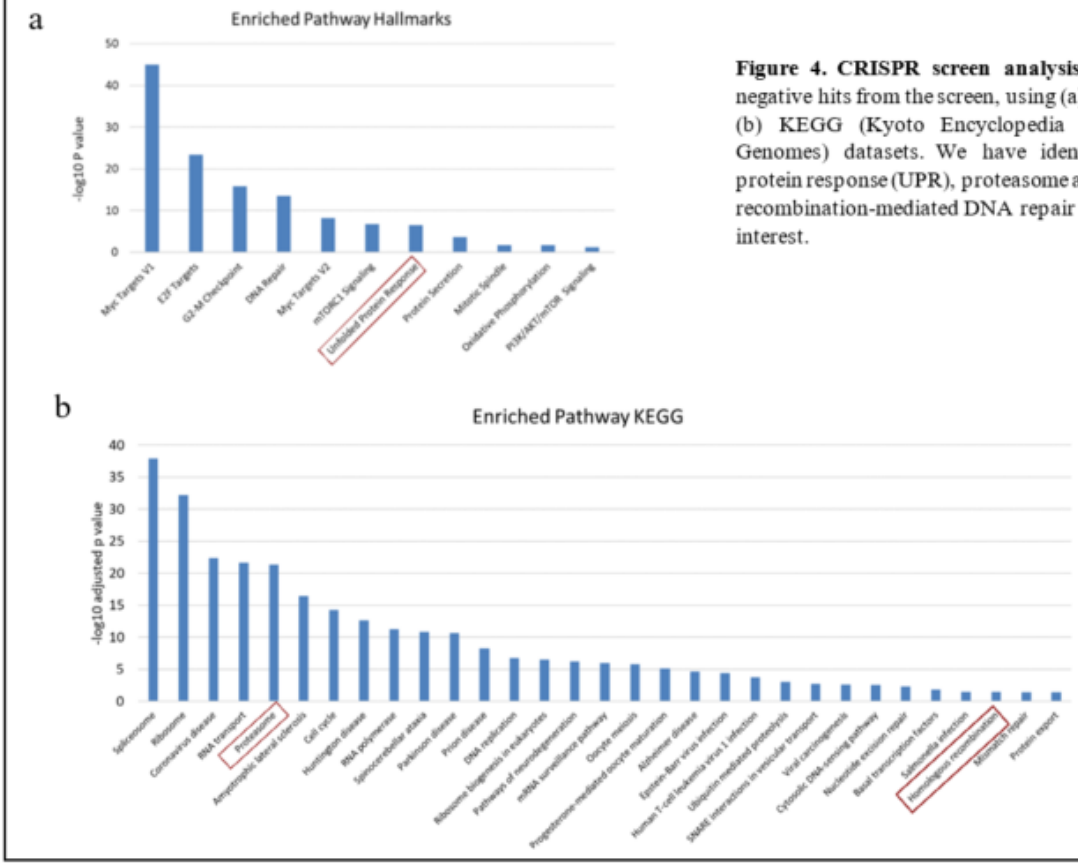

Figure 4. CRISPR screen analysis. GSEA of the negative hits from the screen, using (a) Hallmarks and (b) KEGG (Kyoto Encyclopedia of Genes and Genomes) datasets. We have identified unfolded protein response (UPR), proteasome and homologous recombination-mediated DNA repair (HRR) to be of interest.

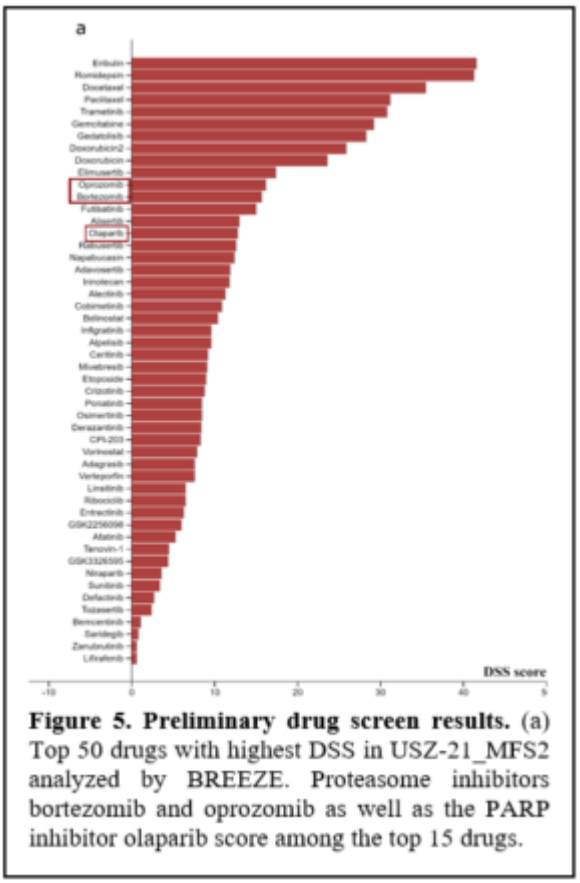

Figure 5. Preliminary drug screen results. (a) Top 50 drugs with highest DSS in USZ-21_MFS2 analyzed by BREEZE. Proteasome inhibitors bortezomib and oprozomib as well as the PARP inhibitor olaparib score among the top 15 drugs.

Conclusion:
By CRISPR and drug screening, we have identified several pathways exhibiting therapeutic potential in STS. In particular, proteasome/UPR and HRR pathways scored high in both screens and will be further investigated to assist future clinical decision-making.

603

A. Mengozzi[1, 2, 3], S. Costantino[1], S. Mohammed[1], E. Gorica[1], A. Mongelli[1], E. Duranti[2], S. Taddei[2], S. Masi[2], A. Virdis[2], F. Paneni[1]

BRD4 inhibition attenuates obesity related microvascular dysfunction: role of endothelium and perivascular adipose tissue

Center for Translational and Experimental Cardiology (CTEC), Department of Cardiology, University Hospital Zurich, University of Zurich, Switzerland[1], Department of Clinical and Experimental Medicine, University of Pisa, Italy[2], Scuola Superiore Sant'Anna, Pisa, Italy[3]

Introduction:
Bromodomain and extraterminal (BET) proteins, particularly BRD4, are epigenetic readers modulating transcriptional programs implicated in inflammation, cancer and renal disease. Though several findings suggest that BET proteins' inhibition might be particularly relevant in the cardiometabolic field, an apparent evidence gap hinders its therapeutic potential. We aimed to define the impact of BRD4-related inflammatory response in the early stages of obesity to exploit the therapeutic potential of its inhibition.

Methods:
Healthy controls (n=13) and patients with obesity without other comorbidities (n=13) were included in a case-control study. Small arteries from visceral fat depots were mounted on a pressurised myograph to assess vasorelaxation to acetylcholine and inhibition to L-NAME at baseline and after incubation with RVX-208 (an FDA-approved BRD4 inhibitor), canakinumab (targeting IL-1β), tocilizumab (targeting IL-6 receptor) and infliximab (targeting TNF-α). The experiments were conducted, in parallel, on two vessels, one mounted with perivascular adipose tissue (PVAT) and the other without PVAT. Vascular- and PVAT-specific levels of NAPDH-derived ROS, mtROS and nitric oxide availability were assessed by confocal microscopy. Gene expression was evaluated by qPCR.

Results:
In patients with obesity, microvascular function and nitric oxide availability were reduced, where NADPH- and mtROS were increased. BRD4, TNF-α, IL-1β and IL-6 expression levels were higher in the vessel wall and in the PVAT of patients with obesity. In these patients, RVX-208 substantially attenuated microvascular dysfunction. The effect was more significant in vessels with intact PVAT, implying a restoration of the PVAT anti-contractile phenotype (**Figure**). The exploration of the distinct inflammatory pathways showed that the amelioration observed with BRD-4 inhibition was higher than with canakinumab, tocilizumab or infliximab. Peculiarly, anti-IL-1β restoration of microvascular function was not affected by the presence of the PVAT, while the ones observed with the targeting of IL-6 receptor and TNF-α were.

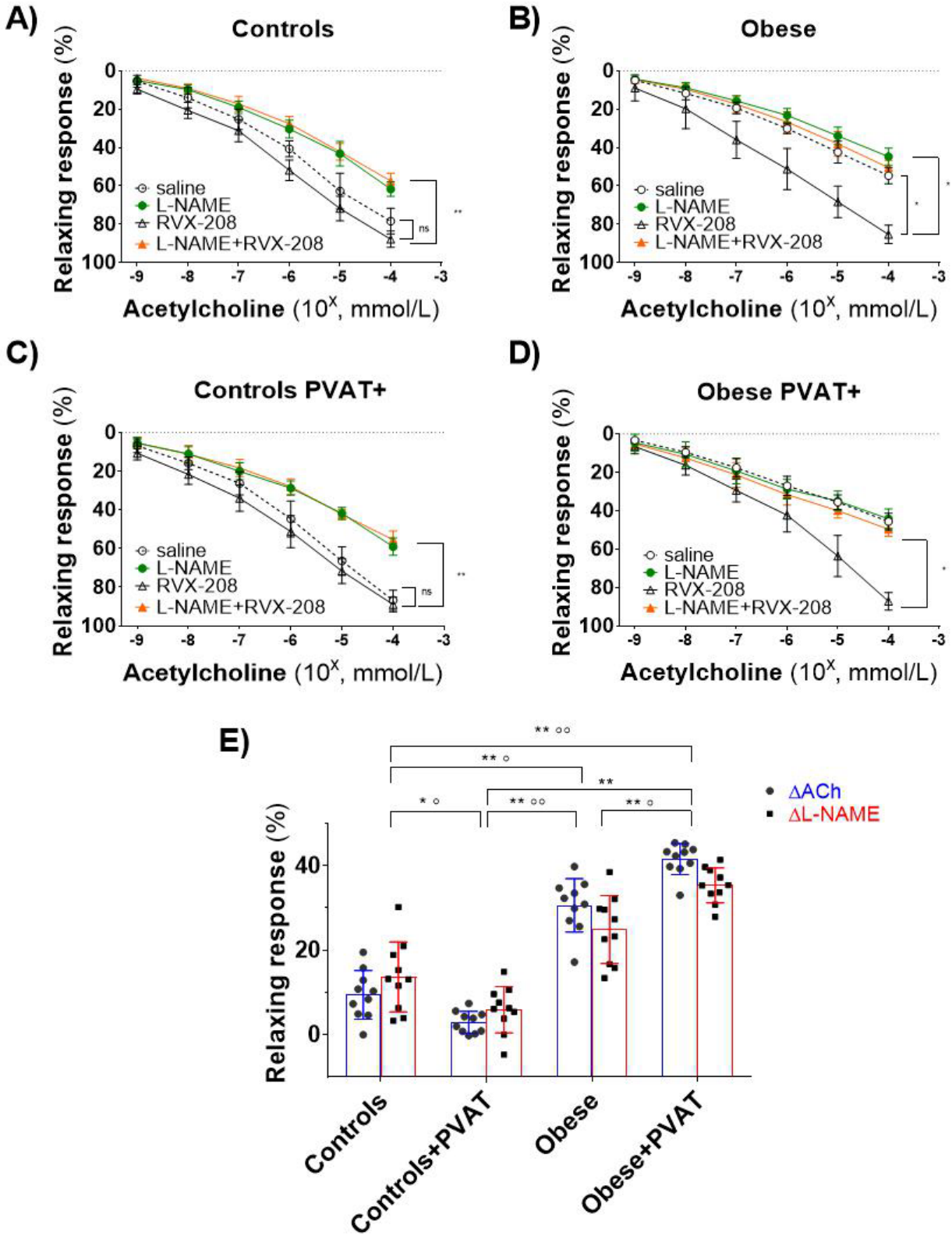

Conclusion:
The inhibition of BRD4 restores microvascular homeostasis in patients with obesity by modulating pan-inflammatory response with the distinct contribution of IL-1β, IL-6 and TNF-α pathways, rescuing endothelial function and restoring PVAT anti-contractile properties. Epigenetic drugs already FDA-approved as BET proteins inhibitors might represent a promising therapeutic strategy to rescue microvascular dysfunction, a hallmark of early cardiometabolic disease.

604

SA. Mohammed[1], E. Gorica[1], G. Karsay[3], M. Albiero[2], GP. Fadini[2], S. Costantino[1], F. Ruschitzka[4], F. Paneni[1]

A Chromatin Signature by the Methyltransferase SETD7 Orchestrates Angiogenic Response in Diabetic Limb Ischemia

Centre for Translational and Experimental Cardiology, University Hosptial Zurich, Switzerland[1], Department of Medicine, University of Padova, Padua, Italy[2], Institute for Clinical Chemistry, University Hospital Zurich, Switzerland[3], University Heart Center, Cardiology, University Hospital Zurich, Zürich, Switzerland[4]

Introduction:
Peripheral artery disease (PAD) is highly prevalent in patients with diabetes (DM) and associates with a high rate of limb amputation and poor prognosis. Surgical and catheter-based revascularization have failed to improve outcome in DM patients with PAD. Hence, a need exists to develop new treatment strategies able to promote blood vessel growth in this setting. Mono-methylation of histone 3 at lysine 4 (H3K4me1) - a specific epigenetic signature induced by the histone methyltransferase SETD7 - favours an open chromatin thus enabling gene transcription

Methods:
Primary human aortic endothelial cells (HAECs) were exposed to normal glucose (NG, 5 mM) or high glucose (HG, 25 mM) concentrations for 48 hours. Unbiased gene expression profiling was performed by RNA sequencing (RNA-seq) followed by Ingenuity Pathway Analysis (IPA). In vitro assays, namely cell migration and tube formation were employed to study angiogenic properties in HAECs. SETD7 and H3K4me1 levels were investigated by Western blot and Chromatin immunoprecipitation (ChIP). Pharmacological blockade of SETD7 was achieved by using the highly selective inhibitor (R)-PFI-2. Mice with streptozotocin-induced diabetes were orally treated with (R)-PFI-2 or vehicle and underwent hindlimb ischemia by femoral artery ligation for 14 days. Blood flow recovery was analysed at 30 minutes, 7 and 14 days by laser Doppler imaging. Our experimental findings were also translated in gastrocnemius muscle samples from patients with and without diabetes.

Results:
RNA-seq in HG-treated HAECs revealed a profound upregulation of the methyltransferase SETD7, an enzyme involved in mono-methylation of lysine 4 at histone 3 (H3K4me1). SETD7 upregulation in HG-treated HAECs was associated with increased H3K4me1 levels as well as with impaired endothelial cell migration and tube formation. Both SETD7 gene silencing and pharmacological inhibition by (R)PFI-2 rescued hyperglycemia-induced impairment of HAECs migration and tube formation, while SETD7 overexpression blunted the angiogenic response. RNA-seq and ChIP assays showed that SETD7-dependent H3K4me1 regulates the transcription of the angiogenesis inhibitor semaphorin-3G (SEMA-3G). Moreover, SEMA-3G overexpression blunted migration and tube formation in SETD7-depleted HAECs. In diabetic mice with hindlimb ischemia, treatment with (R)-PFI-2 improved limb vascularization and perfusion as compared to vehicle. Finally, SETD7/SEMA3G axis was upregulated in muscle specimens from T2D patients as compared to controls.

Conclusion:
Targeting SETD7 represents a novel epigenetic-based therapy to boost neovascularization in diabetic patients with PAD.

607

E. Gorica[1], S. Mohammed[1], S. Ambrosini[1], A. Mengozzi[1], A. Mongelli[1], F. Wenzl[2], F. Ruschitzka[1, 3], N. Hamdani[4], S. Costantino[1, 3], F. Paneni[1, 3]

Pro-inflammatory Macrophage Role in the Heart Failure with Preserved Ejection Fraction

1. Center for Translational and Experimental Cardiology (CTEC), University of Zurich and Zurich University Hospital, Schlieren, CH[1], 2. Center for Molecular Cardiology, University of Zurich, Schlieren[2], 3. University Heart Center, University Hospital Zurich, Zurich, CH[3], 4. Institute of Physiology, Ruhr University, Bochum, Germany[4]

Introduction:
Heart failure with preserved ejection fraction (HFpEF) is a global public health problem with no effective treatment available. Pro-inflammatory cardiac macrophages are emerging as key determinants of adverse left ventricular remodelling; however, their role in HFpEF remains poorly understood. Mechanistically, the recruitment and activation of macrophages represent a key event in maladaptive myocardial remodelling in HFpEF patients. Evidence suggests that remodelling processes in HFpEF hearts are orchestrated and amplified by cardiac macrophages which regulate cardiomyocyte function, endothelial cell activation and fibroblast differentiation. Here we sought to determine the role of macrophage inflammation in experimental and human HFpEF

Methods:
Experiments were performed in rat cardiomyocytes (H9c2), transgenic mice, and left ventricular (LV) myocardial samples from patients with HFpEF. H9c2 treated with pro-inflammatory macrophage-like cells (RAW 264.7) conditional media in the presence or knockdown of a top-ranking activator of M1 type macrophages such as nuclear receptor corepressor 1 (NCOR1), were used to elucidate better the involvement of this gene in transcriptional regulation *in vitro*. The cardiac function of myeloid cell-specific NCOR1 knockout HFpEF mice undergoing a high-fat diet and L-NAME was investigated. LV myocardial samples were used to evaluate the pro-inflammatory activity of macrophages in human HFpEF tissues.

Results:
Macrophage marker expression in left ventricular specimens from HFpEF-patients is shifted toward enhanced pro-inflammatory (M1) and decreased regulatory (M2) macrophage markers as compared with age-matched control donors. NCOR1 - an essential co-regulator of gene transcription - was highly expressed in cultured macrophages, which is shown to drive pro-inflammatory transcriptional programs. Moreover, the depletion of the NCOR1 gene in the myeloid line contributed to an improvement in the heart function of HFpEF mice.

Conclusion:
The data strengthen the importance of immune regulation in the HFpEF and pave the way for mechanism-based therapies in this setting.

608

S. Tashi[1], M. Hermann[1]

Real-life data about lipid-lowering therapy in very elderly patients at very high cardiovascular risk

University Hospital Zurich[1]

Introduction:
With global aging, elderly patients are increasingly being diagnosed with ASCVD. The aim of this study was to assess the adherence to LDL-C targets for older patients at very high cardiovascular risk.

Methods:
For this retrospective study, we retrieved patient data (n=2'507) from the Aging Heart Zurich cohort. Adult patients, hospitalized between 2015, and 2021, were divided into "Very high ASCVD risk", and "Other ASCVD risk". Further, patients were categorized to two age groups (≥ 80 years, and 65- 79 years). Primary outcome was the degree of guideline-directed medical treatment measured by LDL concentration. Nominal logistic regression was performed with likelihood ratio test and Wald intervals. Continuous variables were compared between two groups by Mann-Whitney-U or Median test.

Results:
In total, 2'507 patients (mean age 75.8 years, 33.3% female) were included. Statin treatment was present in 69.5% of the total cohort, and in 75.6% of very high risk patients (n = 1634). Very elderly patients had 1.42 [1.16; 1.75] times higher odds not to receive indicated statin therapy compared with the 65-79 year old patients (71% [n = 487] vs. 77.7% [n = 1147]; x2= 11.4, p = 0.007: est. RR 1.30). No significant differences were found between the two age groups of very high-risk patients in achieving a LDL-C target of <1.4 mmol/l (very elderly, 18.8% [n = 86], and elderly, 17% [n = 184]; x2 = 0.70, p = 0.40).

Conclusion:
Overall, treatment with statin and achievement of the LDL-C goal in patients with very high ASCVD risk was insufficiently low. Patients aged 80 years or older were more likely not to receive statins. Our finding identifies a huge gap between the required and the actual lipid-lowering therapy in all patients demanding a better approach on achieving LDL-C levels to the given goals.

Zur Online-Teilnahme:

Organisation und Kontakt
Universitätsspital Zürich
Direktion Forschung und Lehre
Rämistrasse 100
8091 Zürich

+41 43 253 01 10
dfl@usz.ch

Das vollständige Programm und die Abstracts finden Sie unter: www.usz.ch/veranstaltung/docr

Anmeldung und Teilnahme
Es ist keine Anmeldung nötig.
Die Teilnahme ist kostenlos.

Die Veranstaltung findet vor Ort statt. Die Beiträge von 8.15 – 12.30 Uhr werden live übertragen und im Anschluss an die Veranstaltung online aufgeschaltet.

Folgen Sie dem USZ unter

05.23